UNIVERSITÀ DEGLI STUDI DI PADOVA

UNIVERSITÀ DEGLI STUDI DI PADOVA

DIPARTIMENTO DI SCIENZE CHIMICHE

SCUOLA DI DOTTORATO DI RICERCA: Scienze Molecolari

INDIRIZZO: Scienze Chimiche

CICLO: XXVIII

Synthesis of labeled peptides and study by EPR methods of their interaction with biological membranes

Direttore della Scuola: Ch.mo Prof. Antonino Polimeno

Coordinatore d'indirizzo: Ch.mo Prof. Antonino Polimeno

Supervisore: Dott.ssa Cristina Peggion

Dottoranda: Annalisa Dalzini

Index

Abstract

Antimicrobial peptides (AMPs) have been proposed as antitumor molecules since they sometimes displayed selective cytotoxicity towards cancer cells; they have the potential to bypass multi-drug resistance, as they exert their bioactivity by interacting with the membranes, without a specific target. Trichogin GA IV (TG) belongs to lipopeptaibols, a class of antimicrobial peptides characterized by the presence of tetrasubstituted α-amino acids in their sequence. Differently from other AMPs, lipopeptaibols present a significant resistance to enzyme hydrolysis. The purpose of the present Ph.D. thesis is the study of the peptide-membrane interaction in healthy and cancer cells as the membrane perturbing ability of these peptides is most likely at the basis of the selective cytotoxicity of the peptides. Working in physiological condition was of primary importance to untangle the specificity of the different peptides for the various cell lines: the membrane properties at physiological temperature are indeed among the main determinants of the peptide-membrane interaction. The study has been conducted using several techniques. Structural features of TG analogs have been quantified to rationally design new analogs with different characteristics. The results of cytotoxicity assays on cancer and healthy cells showed that it is possible to tune the toxicity of TG towards cells with different membrane composition. Fluorescence microscopy showed peptides localization on cell membranes. Electron Paramagnetic Resonance (EPR) spectroscopy is a versatile technique that has been widely exploited to determine the affinity of spin labeled peptides for model and cell membranes and their orientation in the phospholipid bilayer. The obtained results are promising, as we could relate structural modification with variations in TG analogs toxicity, an encourage further studies.

Riassunto

I peptide antimicrobici (AMPs) sono stati proposti come possibili molecole antitumorali, poiché alcuni studi hanno evidenziato la capacità di alcuni AMPs di attaccare selettivamente alcune cellule tumorali; gli AMPs sono promettenti in quanto il loro meccanismo di azione, che prevede un attacco aspecifico sulle membrane cellulari, premette di superare lo sviluppo di resistenza ai convenzionali farmaci antibiotici ed antitumorali. La Tricogina GA IV (TG) appartiene alla famiglia dei lipopeptaibolici, una classe di peptidi antimicrobici, la cui sequenza è caratterizzata dalla presenza di α-ammino acidi tetrasostituiti. Diversamente da quanto osservato per altre classi di AMPs, i lipopeptaibolici sono particolarmente resistenti all'idrolisi enzimatica. Lo scopo del presente lavoro di tesi è lo studio dell'interazione peptide-membrana nel caso di cellule sane e tumorali. Infatti, la capacità di questi peptidi di perturbare le membrane è probabilmente alla base della selettività per le cellule tumorali che alcuni di essi hanno mostrato. Di primaria importanza è stato eseguire la maggior parte degli esperimenti in condizioni fisiologiche, in quanto le proprietà delle membrane a temperatura fisiologica sono tra i principali determinanti dell'interazione peptide-membrana. In questo studio sono state utilizzate diverse tecniche. Le caratteristiche strutturali degli analoghi della TG sono state quantificate per poter sviluppare un design razionale di nuovi analoghi che presentassero caratteristiche strutturali differenti. I risultati di tossicità degli analoghi della TG su cellule sane e tumorali hanno evidenziato che è in effetti possibile modulare l'attività di questi peptidi verso cellule le cui membrane presentano diversa composizione. Tramite microscopia di fluorescenza si è osservato come questi peptidi si localizzino sulle membrane cellulari. La Risonanza Paramagnetica Elettronica (EPR) è una tecnica spettroscopia versatile che è stata utilizzata per determinare quale fosse l'affinità di peptidi marcati con sonde paramagnetiche per diversi sistemi membrano-mimetici e per membrane cellulari; inoltre è stata determinata l'orientazione che tali peptidi assumono quando immersi in un doppio strato fosfolipidico. I risultati ottenuti sono promettenti ed hanno evidenziato che è possibile correlare modifiche strutturali con variazioni nella tossicità degli analoghi della TG.

Acknowledgments

The experiments presented in this Ph.D. thesis have been conducted with the collaboration of:

Peptide synthesis and characterization: Dott.ssa Cristina Peggion, Dott.ssa Marta De Zotti and Dott.ssa Barbara Biondi, University of Padova.

Biological assays: Prof.ssa Romana Fato and Dott. Christian Bergamini, University of Bologna.

EPR spectroscopy: Prof.ssa Anna Lisa Maniero and Dott. Marco Bortolus, University of Padova.

Financial support: Fondazione Cariparo, Progetti di Eccellenza 2011-2012

1. Introduction

1.1 AntiMicrobial Peptides (AMPs)

Antimicrobial peptides, first discovered in the 1980s, are considered a fundamental part of immune system of nearly every living organism, from amoebas to humans. Their role is of key importance: they usually display a broad spectrum of activity against bacteria and fungi, and sometimes their killing potential is extended to some viruses, parasites and cancer cells. The attention on this family of peptides raised since their most common mechanism of action is to act on bacterial membranes or other generalized targets, in contrast to most antibiotics, that usually target specific proteins. This peculiar mode of action makes the development of resistance by gene mutation less likely to occur, a feature that makes AMPs promising antibacterial drugs. By now, several hundreds of AMPs have been isolated from a large variety of natural sources: plants, bacteria, fungi, fish, amphibians and mammals. The main strategy to categorize them is by their secondary structure. Indeed, the majority of AMPs adopt a stable secondary structure (the most common being helices and β-sheets) with an amphipathic character, i.e. the hydrophobic and hydrophilic residues are distributed in such a way that, when the peptide adopts its secondary conformation, they are placed at opposite sectors of the molecule. Due to the great number of peptide families, structures and modes of action, a massive work is by now needed to list and describe all the known AMPs and countless reviews have been produced in the last twenty years to keep pace with the constantly increasing knowledge about peptides. In this introductive paragraph, it will be given a brief description of some well studied peptides that are representative of different categories to show the great variety of sources, structures and modes of action of this class of molecules and to underline the reasons of the interest in the study of their bioactivity. Some comprehensive reviews on AMPs, their sources, action mechanisms, structures and application for therapeutic purposes are reported in ref [7-15].

Probably the most populated category of AMPs is the one of the α-helical peptides. An example of 3D structures of α-helical peptides is given in Figure 1.1. Although there are fully hydrophobic peptides, the ones that display the highest selectivity towards microbes are the amphipathic ones. One of the most studied α-helical peptides is alamethicin. It is produced by a fungus of the *Trichoderma* family, it is mostly hydrophobic and forms stable, organized pores on membranes made of oligomeric bundles of helices, due to the strategic location of a negatively charged Glu residue in its sequence. The fungi of the *Trichoderma* family also produce other interesting peptides, such as ampullosporin and trichogin, the latter being the focus of the present Ph.D. thesis. Like alamethicin, they have a helical secondary structure without cationic residues in their sequences, and display moderate antibacterial activity. Another famous pore-forming peptide is gramicidin A, produced by the bacterium *Bacillus brevis*; this peptide

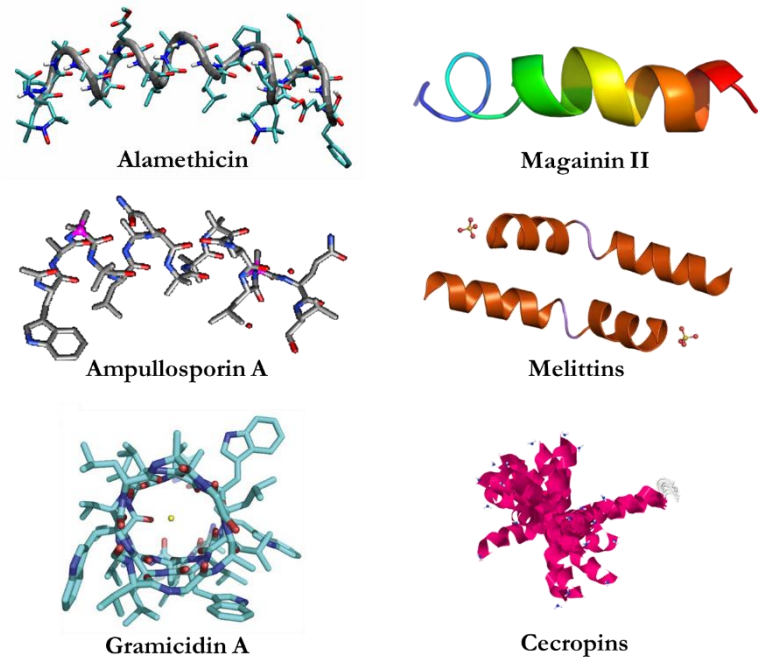

Figure 1.1 Examples of 3D structures of α-helical peptides.

locates transmembrane as a dimer with a central hole through which ions pass, destabilizing the physiological concentration gradient. Bacteria can seem unexpected sources of AMPs, but examples of peptides produced by bacteria are numerous. As an example, *Escherichia Coli* produces a series of peptides named colicins, with the purpose of reducing the competition from other bacterial strains. The bacterium *Helicobacter pilori* produces a protein, named L1, the N-terminal region of which is composed by a cationic amphipathic α-helical fragment that retains its antibacterial activity, probably against competitive bacterial strains. Among the most studied cationic α-helical peptides, there is magainin, the first peptide that was discovered to be produced by the skin of an animal, namely the frog *Xenopus laevis*. Magainin is probably the most representative peptide of the Shai-Matsuzaki-Huang mechanism: it involves the formation of transient, disordered pores, often referred as toroidal pores that induce membrane leakage and disruption. Magainins have a broad activity spectrum, from bacteria and fungi to tumor cells and viruses, and the most active peptides of this family also display a high degree of hemolysis. Another milestone in the discovery and study of AMPs is represented by cecropins, a family of helical peptides produced in the hemolymph of the moth *Hyalophora cecropia*. Differently from melittins, peptides found in bee venom, cecropins are an example of selective toxicity, since they are active against some fungi, Gram-positive and Gram-negative bacteria, but, at the same concentration, are inactive against animal cells. Interestingly, also mammals rely on peptides to defend from external pathogens; usually these peptides are called "host-defense" peptides to highlight their additional immunomodulatory activity, i.e. they usually have poor antimicrobial activity

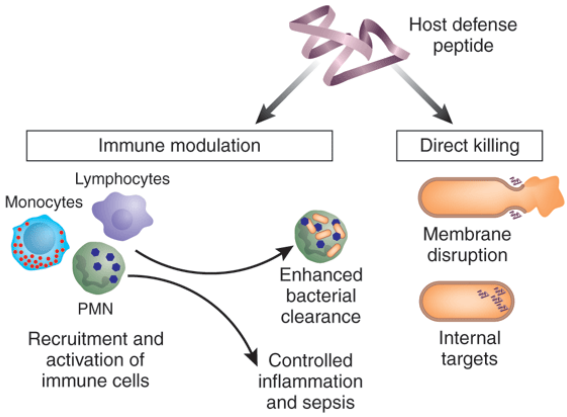

Figure 1.2 Host defense peptides act by immune modulation or by direct killing. Figure from [7].

per se, but modulate the response of the immune system (Figure 1.2). One example is represented by the large family of the cathelicidins that are produced by phagocytes of sheep, bovines, pigs, rabbits and humans. They display a variety of sequences, that is an interesting example of the so-called convergent evolution: different evolutionary pathways result in similar solutions. The differences in sequence keep the function intact while, at the same time, they ensure that peptides from different species are recognized as external by other species. For example, sheep cathelicidin SMAP-29 is lytic against human erythrocytes, but inactive against sheep erythrocytes. Another example is the pig cecropin P1. Its structure and sequence resembles those of insect cecropins, and also the activity spectrum is similar.

All the peptides presented so far share a mostly α–helical conformation. A discrete number of other peptides, instead, present different types of β-structures, an example of which is reported in Figure 1.3. To form β-structures, at least two peptides must aggregate with proper geometry; alternatively, a single peptide of sufficient length should bend to form new hydrogen bonds that sustain the β-sheet. Even in this situation, the hydrogen bonds that can be formed could be not enough to grant stability to the peptide, therefore it is more common to observe β-structures in cyclic peptides: the cyclization reduces the entropy loss after the formation of the β-structure. Examples of cyclic peptides with β-structures are protegrins, lactoferricin and gramicidin S. The most famous family of peptides with β-sheets sectors is the family of defensin. They are produced in neutrophils as part of the innate immune system and were found in mammals, insects and plants. Their structure is more complex since it comprises both β and α secondary domains. In the case of β-structured peptides, the determinants of the toxicity are usually uncertain; nevertheless, it is usually hypothesized that they act against bacteria attacking their membranes as it occurs with α-helical peptides.

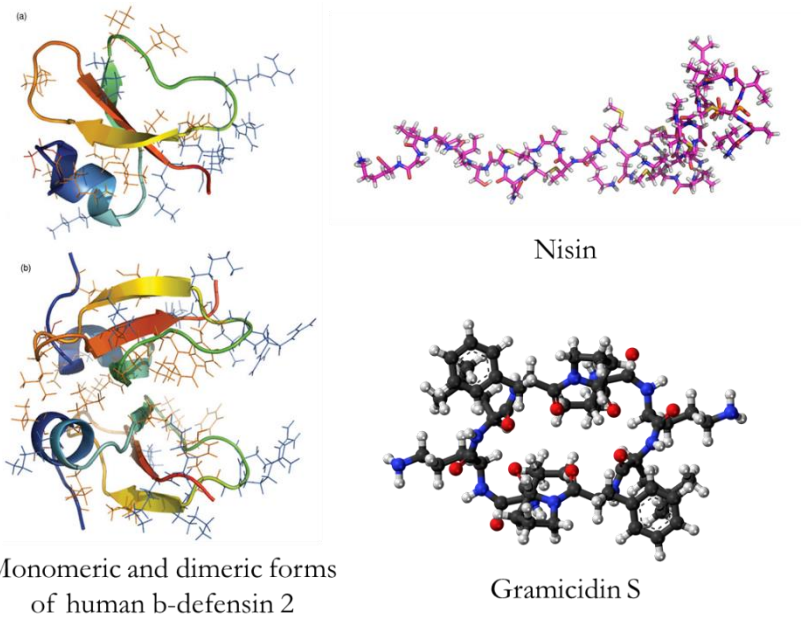

Figure 1.3 Examples of 3D structures of β-structured peptides.

After this short overview, it is clear that the potential uses of AMPs are promising. New peptides are not only discovered from natural sources, but efforts are made for a rational design of new synthetic peptides with the desired characteristics. Generally, peptides with a positive charge and amphipathic structure are the most explored to promote, at the same time, affinity for the lipid bilayers and selectivity towards negatively charged membranes. At present, many peptides reached the *in vitro* stage of study as antibiotic or anticancer drugs: among them, there are many of the peptides described before, such as some strains of cecropins, magainins, melittins, lactoferricins and human defensins. Only few of them were promoted to the *in vivo* stage of the study: some strains of magainins, human defensisn and lactoferricins. The peptide gramicidin S reached the clinical use, and nisin is being used as food additive. However, still many shortcomings must be addressed before AMPs become widely available as proper drugs. They display poor bioavailability, since they are readily degraded in the serum by proteases, limiting their pharmacokinetic properties. Moreover, the selectivity is usually a major issue both for antimicrobial and for anticancer use. The complexity of the design of new improved peptides lies in the fact that size, sequence, percentage of organized secondary structure, charge, hydrophobicity and amphipathicity are all features that are closely related to each other and influence peptides activity in an often poorly predictable manner.

1.1.1 Mechanism of action of AMPs

The broad spectrum of activity against pathogens that is usually displayed by AMPs, that extends from bacteria and fungi to viruses and cancer cells, is mainly due to their particular ability to act against a generalized target, rather than against specific proteins, as conventional antibiotics [20]. Indeed, although some AMPs actually attack key cellular processes, such as DNA synthesis, protein folding and activity [21-23], the majority of α-helical AMPs disrupt the cytoplasmic membrane in a number of different ways. Moreover, as already mentioned in the last paragraph, even when an AMP attack a specific intracellular target, the interaction of the AMP with the cell membrane remains of central importance. Usually, AMPs have the common characteristics of being positively charged, amphipathic, and with a relevant hydrophobic sector. Then, their mechanism of action should involve the binding to the membrane, mainly to negatively charged moieties, and subsequently its perturbation and eventually its disruption. Countless studies tried to categorize the mechanism of action of membrane disrupting peptides. The most common classification divides peptides that follow the barrel-stave model and peptides that follow the Shai-Matsuzaki-Huang model. In the barrel-stave model [24], peptides aggregate to form an ordered pore, exposing their hydrophobic face towards the lipid tails and the hydrophilic face toward the pore itself. One of the most famous peptides that act *via* this mechanism is the peptaibol alamethicin [24,25], along with other less famous ones [26,27]. The Shai-Matsuzaki-Huang model includes different steps of membrane perturbation [28]: first, peptides bind on the membrane surface, sometimes causing membrane thinning; when peptide concentration raises AMPs can form disordered toroidal pores that deform the membrane; finally, regardless the extent of membrane perturbation, AMPs can disrupt the membrane *via* micellization. The last step of this mechanism has sometimes been called carpet model. Along with the increasing number of discovered and studied AMPs, many variations to these two models have been proposed. A comprehensive schematic representation of the proposed modes of action is reported in Figure 1.4.

All the proposed mechanism are based on the common characteristic of α-helical AMPs to have an amphipathic secondary structure that favors the binding to the cell surface. AMPs that are long enough to span the thickness of the phospholipid bilayer, usually create pores of different geometry. Instead, shorter peptides deform the bilayer causing local perturbations in phospholipid packing. A recent review on the toroidal pore mechanism [29,30] proposes that even when the peptide concentration is low, a small number of peptides could still cause a transient disorganization of phospholipids that bend and form a temporary pore. Interestingly, it has been shown [31] that this mechanism is particularly fit to explain how AMPs with a polar or charged residue in their hydrophobic face work: the presence of a polar residue in the face that is usually bound to the lipid portion of the bilayer could pull lipid head groups into the membrane interior, inducing pore formation. In this context, the carpet model mentioned above is

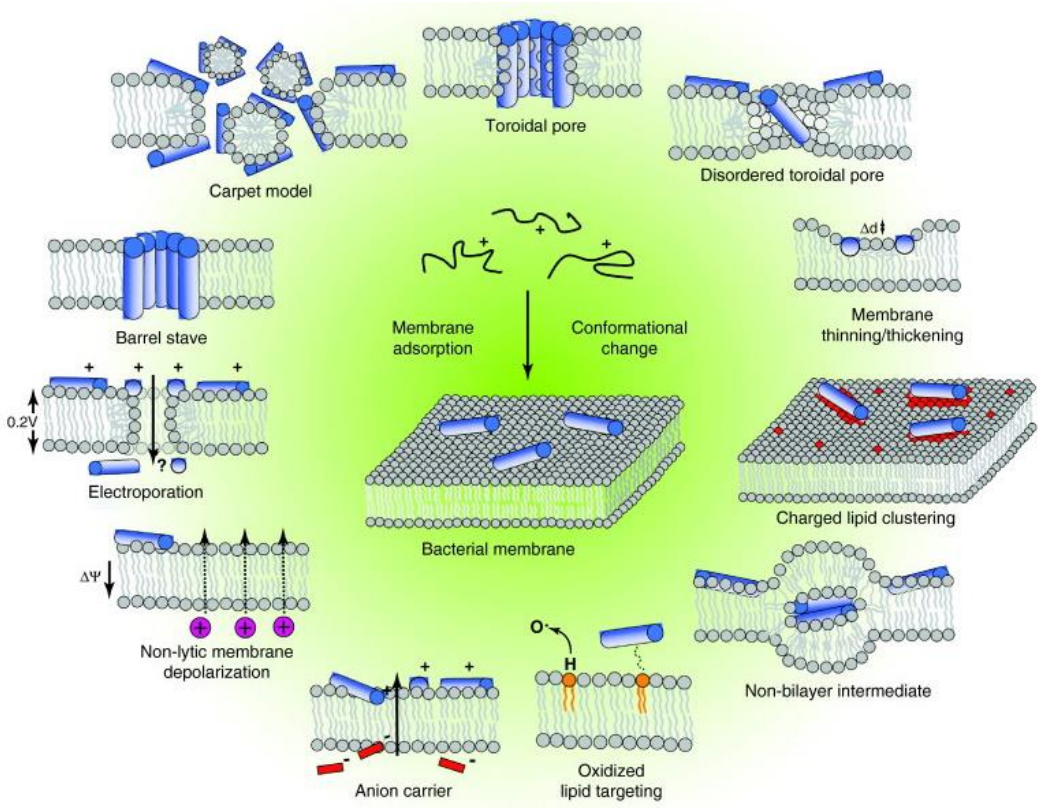

Figure 1.4 The figure shows the principal proposed mechanisms that helical peptides adopt to attack the membrane bilayer. Figure taken from ref [5].

considered as an extreme extension of the disordered torodial pores. Other α-helical AMPs are thought to cause leakage of intracellular materials or membrane depolarization because their positively charged residues compromise the membrane stability by attracting all the negatively charged head groups nearby [32]. Finally, it has to be mentioned that also some α-helical AMPs act by interfering with the activity of some proteins (as clavanin A, that inhibits the proteins involved in the maintenance of the pH gradient across the membrane [33]) or of nucleic acids (as buforin II, that intercalates between nucleic acids [34]). The description of AMPs mechanisms focused on α-helical AMPs. However, AMPs with other secondary structures sometimes share the same action mechanisms. For example, the β-hairpin structure is common among AMPs: peptides in this conformation are able to disrupt the membrane forming pores known as β-barrels, or forming β-sheet aggregates [35]. Other peptides in β-sheet conformation are, instead, active against intracellular components: they for example interfere with proteins involved in the ATP reactions, in the DNA and RNA synthesis, or directly in the synthesis of the membrane [22,36]. Moreover, bigger peptides are composed of domains in different secondary conformations. As an example, human β-defensin is has a α-helical domain and a three-stranded β-sheet [37,38].

In conclusion, it is important to remark that the great size of studies on peptides and their mechanisms of action showed that organisms developed complex pathways to defend. An organism that has to defend from an external pathogen is likely to release many isoforms of similar AMPs, each one with a different mode of action [39]. Alternatively, it has been observed that some peptides, such as magainin, work through multiple different mechanisms at the same time [40]: this strategy is actually convenient in terms of both efficiency and ability to avoid resistance mechanisms.

1.1.2 Structural parameters accounted for activity and selectivity of α-helical AMPs

Many AMPs have a stable secondary structure, the most diffuse being the α-helix. It is quite evident that the secondary structure is of paramount importance for the bioactivity of these peptides. Therefore, many studies tried to describe the influence of different structural parameters to the cytolytic effect of peptides. The most investigated parameters, are charge, helicity, hydrophobicity, hydrophobic moment, and angles subtended by domains of different polarity. Figure 1.5, from ref [1], shows an example of the parameters discussed in this paragraph, calculated for one of the most studied peptides, magainin. In figure are reported the 3D helical representation of the peptide and the helical wheel diagram, where residues with different hydrophobicity are differently colored. On the helical wheel are reported Φ, the angle subtended by the hydrophilic residues, and μ, the hydrophobic moment vector. The figure also reports the values of all the mentioned parameters: the number of residues (N), the total charge (Q), the mean hydrophobicity per residue (H) and the hydrophobicity of the domain subtended by the angle 360° - Φ (H_h), the module of the hydrophobic moment ($|\mu|$), and the angle Φ.

Many antibacterial peptides are positively charged, probably to favor the interaction with the negatively charged membranes of bacteria. Therefore, *charge* is the first

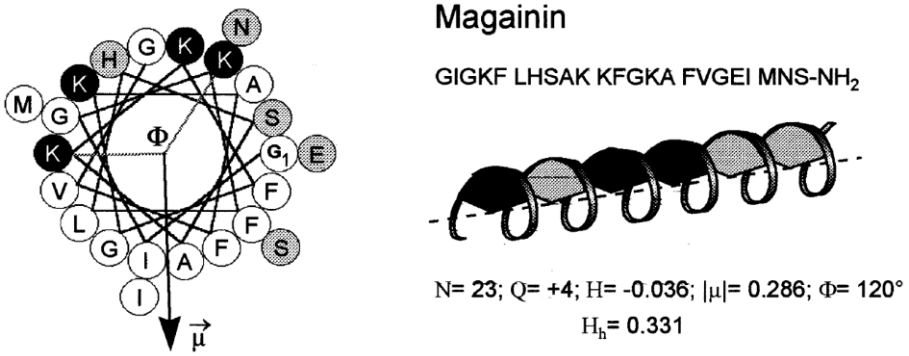

Figure 1.5 An example of a peptide in a-helical conformation, for which all the structural parameters described in this paragraph are obtained. Figure from [1].

parameter to take in consideration when trying to improve the activity of AMPs. Indeed, there are some example of peptides, like δ-hemolysin and magainin, whose antibacterial activity was greatly improved by the substitution of one or more neutral residues with positively charged ones [41-43]. Studies on model peptides [44] revealed however that it is difficult to find a simple correlation between peptide charge and antimicrobial activity. This is due to the fact that an amino-acid substitution influences not only the charge, but also other structural parameters. Subsequent studies [45] showed that peptide-membrane interaction is balanced by multiple factors, such as electrostatic and hydrophobic interactions, helicity and amphipathicity of peptides and how they relate to membrane composition.

Another feature that has been taken in consideration when trying to rationalize AMPs behavior is their *helicity*. It is nearly immediate to relate the activity of a helical peptide to the extent of its regular secondary conformation. Helicity is quite difficult to quantitatively measure for peptides. A possibility is given by ^{1}H-NMR spectroscopy that shows the correlation between nuclei depending on their distance. IR and CD spectroscopies give information on peptides secondary structures; however, they provide general information on the structure, but cannot account for small local perturbation. It is well established that certain amino-acids are helix-inducing, while others destabilize the helix [46]. Early studies showed that an enhancement of antibacterial activity of analogs of the peptides melittin and cecropin occurred when they carried substituents with increased helix inducing power and, *viceversa*, a loss of hemolytic and antimicrobial activity was displayed in analogs with substituents that prevented helical folding [47-51]. Proving that these correlations were due to the helicity and not to other properties of the substituted amino-acids, another study [52] observed the same results substituting some amino-acids with their enantiomers. Moreover, it has been observed that helicity plays a more decisive role when permeabilizing neutral membranes, while it becomes less important when attacking charged bilayers. A possible explanation is the prevalence of the electrostatic forces, when present, over hydrophobic interactions. Even encouraged by some positive results, it appears difficult to find an unambiguous relation between bioactivity and helicity alone: when studying a modified peptide, many other features may change synergically with helicity, such as the hydrophobicity of their side chain.

The *hydrophobicity* is defined as the ability of a given molecule to move from an aqueous to a hydrophobic phase. The overall hydrophobicity of a peptide depends on the hydrophobicity of the side chains of its amino-acids, and is independent from the secondary structure. Theoretical and experimental attempts to build hydrophobicity scales for amino-acids are numerous, and will be discussed diffusely in paragraph 3.4.2, along with an original proposal that is part of the present work. It is necessary for a peptide to carry hydrophobic residues, as they are needed for the binding and subsequent perturbation of the lipid bilayer; at the same time, hydrophilic residues are

required to ensure solubility in aqueous media and to prevent peptide aggregation. Some studies [53] were able to correlate a change in hydrophobicity with a change in antimicrobial properties of peptides, while some other studies [54-56] found no correlation between them. These contrasting observations can be explained since to modify hydrophobicity it is necessary to modify the primary sequence of peptides, leading to the variation of multiple parameters, such as charge, helix inducing effects, therefore, the combined effect of all these variations may not be easy to predict. Additionally, it has been verified that hydrophobic interactions are more effective on neutral membranes [57,58], thus small variations of hydrophobicity on charged peptides interacting with membranes with an excess of negative or positive charge may be negligible.

A more interesting parameter is the *hydrophobic moment*, that will be also exploited in the present work along with hydrophobicity (see paragraph 3.4.2). This parameter, strictly connected with hydrophobicity, is more informative because it includes different features of helical peptides. It is calculated as the vector sum of the hydrophobicity of each residue [59], and is strongly dependent on the secondary structure assumed by the peptide. It reflects the peptide amphipathicity, therefore it will have a high value if hydrophobic residues are located on one side of the helix and hydrophilic residues are located on the other side, while it will be very low if residues are randomly organized along the helix. It was originally intended as a parameter that could predict the affinity of helical protein domains for water or for the hydrophobic protein core, but the same principle can be used to describe the interaction between a peptide with a membrane. Indeed, it could be hypothesized that helical peptides with a strong amphipathicity are more prone to form pores that span the membrane bilayer: the hydrophobic side interacts with the lipids, while the hydrophilic side faces the aqueous phase. However, experimental evidences are more difficult to interpret, since in many peptides residues of different polarity are not regularly distributed along the helix, leading to a non-perfect amphipathicity; additionally, a secondary structure must be assumed to perform the calculation, therefore the prediction of hydrophobic moment value is inaccurate for peptides with disordered domains. Due to these issues, some studies on different peptides [60] could not find a correlation between changes in hydrophobic moment and lytic activity. As already noted for the other parameters, it is generally difficult to find direct correlations between one single parameter and peptides toxicity. A better approach is to renounce to compare peptides with very different structures, and instead to observe how small variations on a given primary structure affect these structural parameters (such as hydrophobicity and hydrophobic moment) and search for a trend that links them to peptides bioactivity. Following this method, some studies [49] actually found a correlation between a progressive loss of antimicrobial activity and the progressive reduction of hydrophobic moment of melittin.

A parameter that is, to some extent, linked to the hydrophobicity and hydrophobic moment is the *angle subtended by domains of different polarity*. It can be calculated as the angle, subtended by hydrophilic residues measured looking down along the helical axis. Evidently, such an angle can be defined only for regular amphipathic structures, while it is impossible to obtain it if the residues are randomly distributed. Some studies [61] proposed that peptides with small hydrophilic angle and a high hydrophobicity prefer to form transmembrane pores, while peptides with medium hydrophilic angle and medium hydrophobicity prefer to lie parallel to the membrane surface. Moreover, it is now well established that a large hydrophobic sector is essential for membrane binding.

It is therefore clear that the structural parameters described in this paragraph are essential to understand peptides behavior, although it is usually not easy to find a simple correlation between the variation of individual parameters with peptide activity. Even one single modification on the primary sequence can alter at the same time charge, helicity propensity, hydrophobicity and hydrophobic moment. The rational design of a peptide with an optimized balance between hemolytic and antimicrobial activity is still a challenge. It is not only essential to rationalize the combined effect of the discussed parameters, but also the characteristics of the target membranes must be taken into account.

1.1.3 Peptaibols and lipopeptaibols

Peptaibols are a particular class of antimicrobial peptides that have been isolated from the fungal families *Trichoderma* and *Gliocladium* [62-64]. The name "peptaibol" derives from the fact that they are particularly rich in the C^{α}-tetrasubstituted non coded amino acid Aib (α-aminoisobutyric acid, see Figure 1.6) and they carry an amino-alcohol at the C-terminus of the sequence; the first isolated peptaibols all carried a phenilalaninol at the C-terminus [65], but other amino-alcohols are now present in peptaibols sequences. Moreover, they are acetylated at the N-terminus. These peptides are characterized by a microheterogeneity which results in a complex mixture of closely related sequence analogs. At present, over 300 different sequences of peptaibols are known [66]. All of them are characterized by short (6-10 residues) or medium-length (11-19 residues) sequences. One of the most famous peptaibols is alamethicin [67]; other well studied long sequenced peptaibols are trichosporins and trichorzianines. Shorter sequenced peptaibols include the families of emerimicins, zervamicins and antiamoebins [68]. The presence of many Aib residues in the sequences is of particular importance. Aib is the simplest tetrasubstituted amino acid, carrying two methyl groups on the C^{α}. Since Aib is more sterically hindered than the conventional amino acids, only few torsional angles are permitted. Figure 1.6 shows the Ramachandran plot for the tripeptide Ac-Ala-Aib-Ala-OMe; differently from the quite flexible Ala residues, few torsional angles are permitted for Aib, located around -60°/-30° and +60°/+30°. Comparing them with the

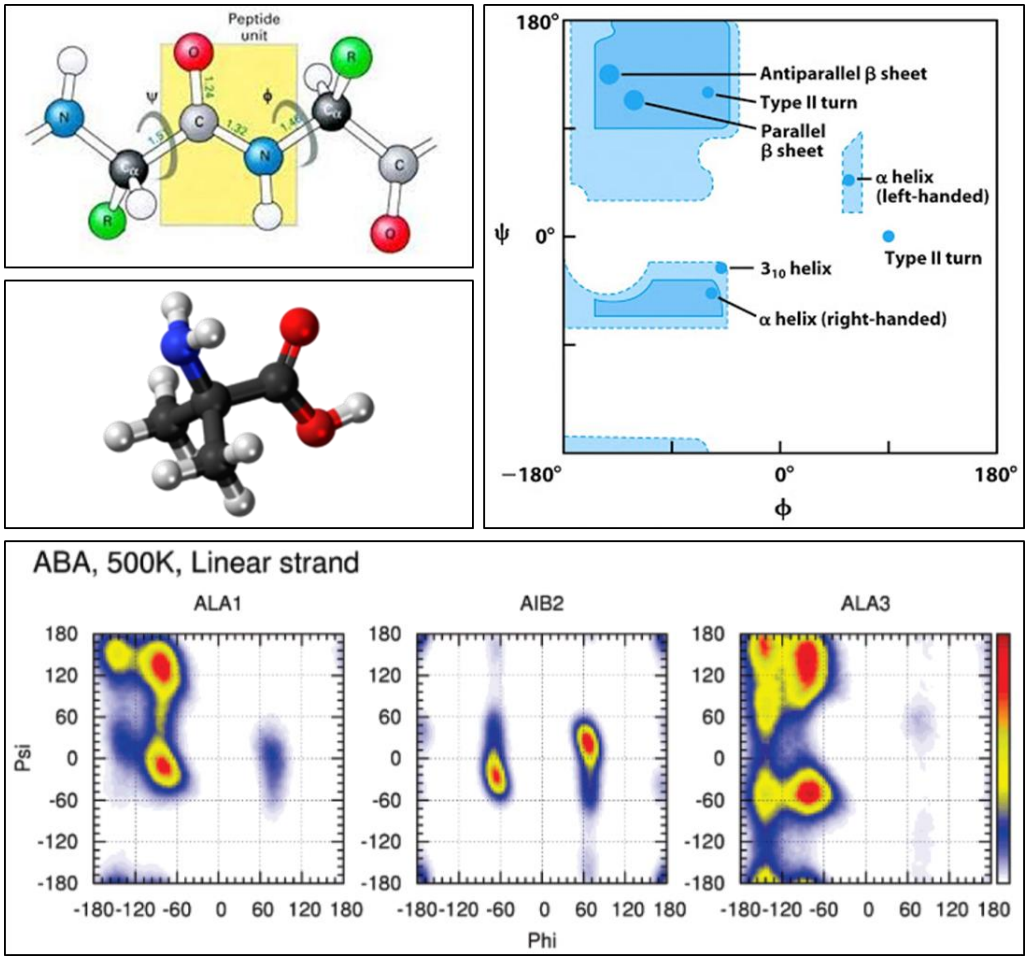

Figure 1.6 In the top left part of the figure is reported a schematic peptide bond with the torsion angles ϕ and ψ and a 3D representation of Aib. In the top right part it is shown the Ramachandran plot where torsion angles ϕ and ψ of peptide typical secondary structures are highlighted. In the bottom part, the simulated Ramachandran plot of the tripeptide Ac-Ala-Aib-Ala-OMe is reported in [18].

angles corresponding to typical secondary structures of peptides, it can be observed that Aib can only assume helical conformations, both α and 3_{10}. Since Aib is achiral, the handedness of the helix is determined by the other chiral residues in the peptide: L-amino acids induce right-handed helices, D-amino acid induce left-handed helices. There are some structural differences between α and 3_{10} helices (Figure 1.7). In the α-helix, each N-H group of the backbone donates a hydrogen bond to the C=O group four residues earlier (i+4→i). This helix is sometimes called 3.6_{13} since it has 3.6 residues per turn (an angle of 100° for each subsequent residue) and 13 atoms are involved in the ring formed by the hydrogen bonds. A more elongated and narrow helix is the 3_{10}, in which each N- H group of the backbone donates a hydrogen bond to the C=O group three residues earlier (i+3→i). It has exactly 3 residues per turn (an angle of 120° between two subsequent residues) and 10 atoms are involved in the ring formed by the

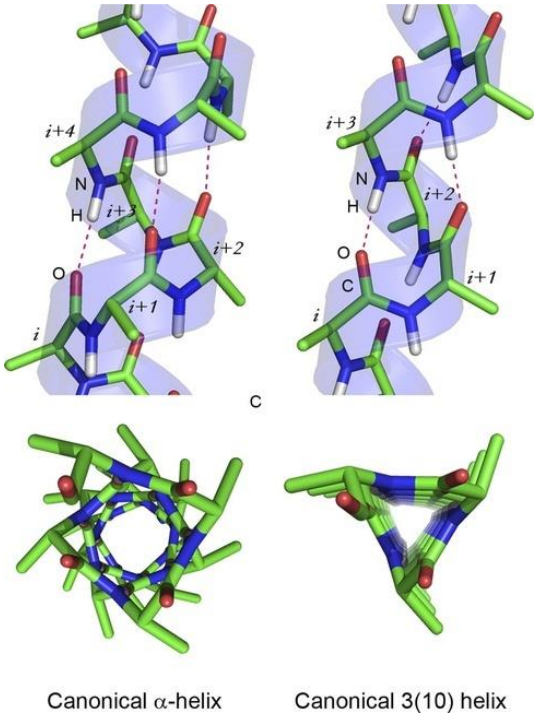

Figure 1.7 3D representations of a α-helix and a 3_{10} helix.

hydrogen bonds. The preference of peptaibols for one of these conformation is driven by different factors: usually, short peptides with a high Aib content will prefer the 3_{10} helix, while longer peptides with few Aib prefer the α-helix. It has been observed that many peptaibols adopt mixed structure, where the central part of the peptide is α-helical, while terminal domains are in 3_{10} conformation [69,70]. A more complicated role is also played by the primary sequence, since each side chain has a different helicity propensity.

The interest in peptaibols raised from their peculiar characteristics. First, they share with the other AMPs the capability of perturbing cell membranes without binding to specific receptors, with the advantage of avoiding the development of specific drug resistance. Additionally, the presence of the non-coded amino-acid Aib confers to peptaibols resistance to enzymatic degradation [71]: peptide bonds in which the sterically hindered Aib is involved cannot be lysed by proteases. Some peptaibols are also promising anticancer agents [72]: as an example, trichokonin VI was reported to inhibit the growth of hepatocellular carcinoma cells without affecting healthy liver cells [73].

A subclass of peptaibols is the family of lipopeptaibols [74]. They are characterized by the presence of a fatty acyl moiety at the N-terminus. They were isolated from cultures of different species of the fungi *Trichoderma*. They are usually short sequenced (6-11 residues) with long fatty acyl moieties (8-15 carbon atoms). They share all the characteristics typical of the peptaibols, such as a helical conformation, an abundance of Aib residues and an amino-alcohol at the C-terminus. The long saturated chain is

believed to favor the binding to lipid membranes. Many lipopeptaibols have antibacterial activity, for example trichogin GA IV is toxic against *Staphilococcus aureus*; trichoningins are selectively toxic against *Staphilococcus aureus*, while they are inactive against *Escherichia coli*. Some peptaibols also displayed other activities: trichopolyns act as immunosuppressant and inhibitors of lymphocytes proliferation; the lipopeptaibol LP 237s showed cytotoxic activity against a number of cancer cells (leukemia, lung, ovarian, colon and breast). Helioferins have a broad activity spectrum against many bacteria and fungi; additionally, they inhibit the growth of leukemia cells at concentration where they have no hemolytic effect. The first and most studied lipopeptaibol is trichogin GA IV, that is the focus of this work and will be described in the next paragraph.

1.1.3.1 Trichogin GA IV (TG)

The first lipopeptaibol discovered is trichogin. It was isolated from the first time in 1992 from the strain *Trichoderma longibrachiatum* [68] as a group of peptides with similar structure. The main isoform is trichogin GA IV, which primary sequence is as follows:

1-Oct-Aib-Gly-Leu-Aib-Gly-Gly-Leu-Aib-Gly-Ile-Lol

TG has an octanoyl chain (1-Oct) at the N-terminus and a Leucinol (Lol) at the C-terminus. It has three Aib that are able to confer a stable secondary structure even if the sequence is short. Indeed, TG conformation has been studied in methanol by ^{1}H and ^{13}C NMR and by Circular Dichroism. From these results, a predominant right-handed α-helix was proposed. Subsequent studies on the crystal structure of TG [16] (Figure 1.8) showed that this peptide, similarly to other short peptaibols rich in Aib, has a 3_{10} helical conformation for the first 2-3 residues next to the N-terminus, which is also partially disordered due to the presence of the flexible octanoyl chain. The remaining part of the sequence is in α-helical conformation. The central region, containing two Gly, is quite flexible and may create a hinge in certain TG analogs. In α-helical conformation, TG is considered an amphipathic peptide, since all the hydrophobic residues are located on one side of the helix, while the four Gly, that are slightly hydrophilic, are located on the other face. Amphipathicity seems to be a required feature to maintain, and eventually improve, TG ability to perturb phospholipids bilayers, as it was observed in a study where amphipathicity was enhanced by substituting the four Gly with Ser residues [75]. Studies have been conducted to verify the influence of the C- and N-termini on the activity of TG. Antimicrobial and hemolysis tests have been run on synthetic TG analogs varying the length of the carbon chain [76]. It was discovered that at least six carbon atoms are required for a significant activity, but a too long chain results in activity loss as well. C_2-TG and C_{16}-TG were almost completely inactive against *Staphilococcus aureus*, while C_8-TG was the most active peptide. Similar results were obtained for the hemolytic activity. Moreover, it was also observed that

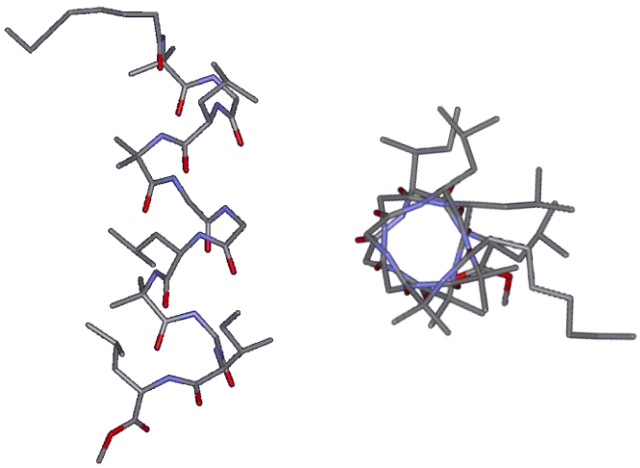

Figure 1.8 Crystal structure of Trichogin GA IV: side view and view along the helical axis.

moving the octanoyl chain at the C-terminus reduced the activity, while adding an octanoyl group both at the C- and at the N-termini improved the activity of TG [77]. Recently, also the C-terminal amino alcohol was proved to be essential for the activity of TG analogs against bacteria and tumor cells [78]. These considerations highlight the close interplay that exists between the constituents of TG: primary sequence modifications, octanoyl chain, amino alcohol, secondary structure all contribute to the behavior of TG and its analogs.

Being 11 residues long, TG is not long enough to span the membrane bilayer, as alamethicin does. Therefore, many mechanisms of action have been proposed. Initially, the X-ray studies showed that the octanoyl chain would lie perpendicular to the helical axis [16]: due to this observation, it was proposed that TG could form a barrel-stave pore made of TG dimers, in which the octanoyl chains anchored the peptide deep into the lipid bilayer, while the C-termini were facing the polar headgroups. This mechanism was proposed again more recently [79], adding the proposal that TG dimers acted as ion transporters that destabilize the ionic equilibrium of the cell. From EPR and fluorescent experiments, others proposed that, being too short, TG acts with a carpet like mechanism, thus generally perturbing the membrane [80,81]. A work that analyzed the behavior of TG analogs labeled with fluorescent probes proposed a new mechanism, according to which TG approached the membrane as a monomer and then aggregates, perturbing the membrane with a Shai-Matsuzaki-Huang model, forming pores of small dimensions [82]. Shortly after this proposal, another work [83] suggested that TG interaction with membranes is concentration dependent: at low concentration, TG lies on the membranes surface, while it aggregates and inserts into the bilayer at higher concentrations, causing leakage.

With the purpose of collecting more information on TG's behavior and elucidate the actual mechanism of action, many TG analogs have been synthesized and studied.

Recently, TG analogs lacking one or two Aib were synthesized and their antibacterial activities were tested [84]. One or two Aib were substituted with a Leu: Leu amino acids are known helix supporting residues, although less effective than Aib, and their introduction enhanced the overall amphipathicity. It was observed that all analogs have a remarkable resistance to proteolysis and are selectively toxic against *Staphilococcus aureus*, with the only exception of the analog with Leu in position 4 that completely lost its toxicity. An analysis of these peptide structures showed that they all maintain a stable α-helix, except for the non-toxic analog. The latter showed a peculiar conformation, with Gly 5 and 6 turned to form a hinge, deducing that an excessive deviation from the helical structure hinders TG activity. In the same years, another study analyzed TG analogs with different characteristics. Several analogs with one or more Gly substituted by Lys were synthesized [2] in order to confer a positive charge to TG and to enhance its amphipathicity. It was observed, for all peptides, a stable α-helical conformation that could partially switch to a 3_{10} helix at decreasing pH values. Peptides with one Lys increased their antibacterial activity with respect to the natural TG sequence, but increased their hemolytic activity as well.

From the great variety of mechanisms proposed though years of experimental observations, it is clear that elucidating the actual behavior of TG towards membranes is still an unfinished challenge. Not only modifications on even only one amino acid in the sequence can greatly change its mode of action, but also the model system used to carry out the experiments has a great influence on the results. In the present work, we will study several analogs of TG in different model membrane environments, and we will perform one of the first attempts to observe how TG interacts with viable cells.

The tetrasubstituted nitroxide amino acid TOAC

Modern spin-label techniques using the spin active 2,2,6,6-tetramethylpiperidine-1oxyl-4-amino-4-carboxylic acid (TOAC, Figure 1.9) residue have emerged as powerful tools for determination of peptides conformation, association to a bilayer, aggregation and distance between aggregated peptides. The important advantage of TOAC is that, differently from other nitroxides used in biological experiments (presented in paragraph 1.3.2), it is tightly bound to the peptide backbone and therefore its motion is directly related to the motion of the peptide [85,86]. TOAC is of primary importance in the study of the Aib-rich family of peptaibols, since it shares with Aib the characteristic of being a conformationally constrained C^{α} tetrasubstituted amino acid; they both are strong helix inducers [85,87] and many peptaibols have been modified substituting TOAC in places of the primary sequence occupied by an Aib residue. As an confirmation, conformational studies have been conducted on [Leu^{11}-OMe] TG analogs singly labeled with TOAC at positions 1, 4 or 8, or doubly labeled at positions 1 and 4,

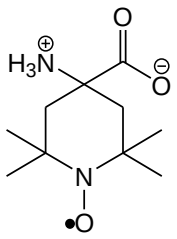

Figure 1.9 The amino acid TOAC

1 and 8, 4 and 8 [88], finding that the helix inducing properties of TOAC are equal or better than those of the Aib. Crystallographic studies on several different analogs of TG, such as [TOAC^{4,8}, Leu^{11}-OMe] TG, [Fmoc^{0}, TOAC^{4,8}, Leu^{11}-OMe] TG, [Boc-Bpa^{0}, TOAC^{8}, Leu^{11}-OMe] TG (see ref [89] for an extensive list) observed that all the studied TG analogs start with a $3_{10}/\alpha$-helix, but rapidly switch to a pure a-helix conformation, confirming that TOAC is an optimal substituent for Aib.

A study on singly labeled TG analogs ([TOAC$^{1/4/8}$, Leu^{11}-OMe] TG) showed that all these analogs have membrane permeability properties comparable to those of trichogin [80] on liposomes based on phosphatidylcholine. The same study also demonstrated, by EPR measurements, that in the absence of a transmembrane potential these analogs lie parallel to the surface of the lipid membranes, with the Gly-rich face oriented towards the aqueous phase.

Being an optimal substituent to perform EPR studies, TOAC has been widely exploited as a substituent for the peptide studied in this Ph.D. thesis, trichogin GA IV.

1.2 Hallmarks of cancer

Among diseases, cancer is one of the leading causes of mortality worldwide, with a rate of 14 million new cases each year, in a continuous increase [90]. The generic term cancer defines a number of different diseases that have the common feature of rapidly creating abnormal cells that circumvent the apoptotic system, unlimitedly grow avoiding the usual mechanisms that limit cell reproduction in confined spaces, and can invade adjoining parts of the body, spreading to other organs. Conventional treatments involve the use of radiations and chemotherapeutic drugs, including alkylating agents and antimetabolites that bind to specific targets on the membrane surface and then exert their mechanism on intracellular components, the most recurring being DNA [91]. These therapies need high doses to be successful, and the occurrence of severe side-effects often impairs the therapeutic advantage. These treatments act non-specifically against cells in rapid division, whether cancer cells or normal cells, like those of bone

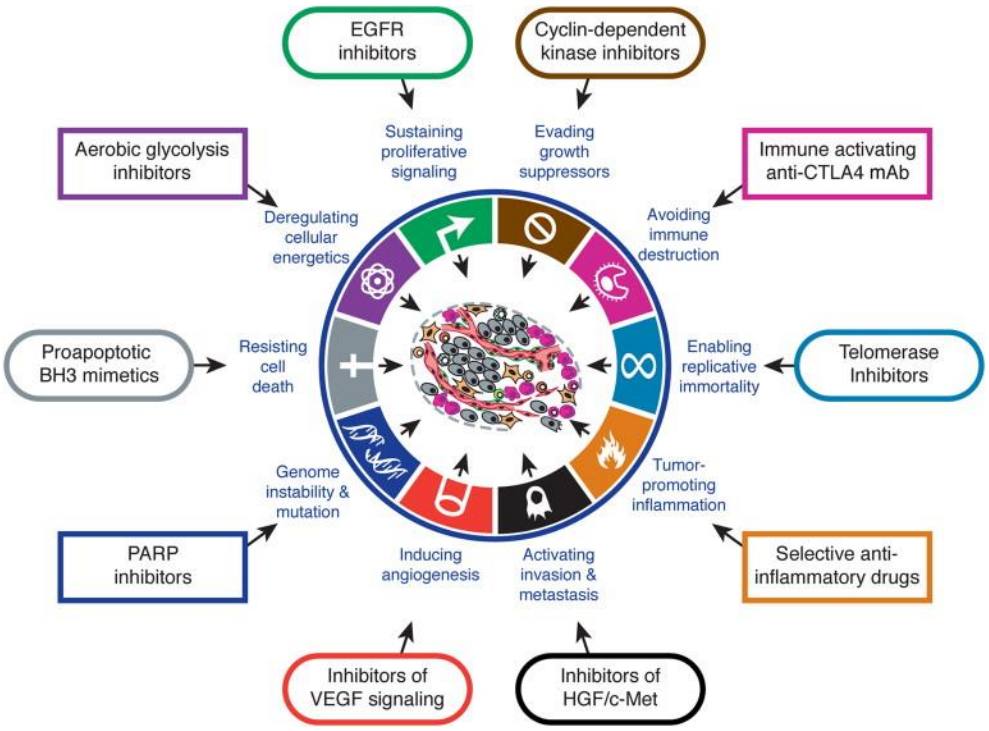

Figure 1.10 This illustration shows the six principal generalized hallmark capabilities originally proposed in [6] to characterize cancer diseases: sustaining proliferative signaling, evading growth suppressors, resisting cell death, enabling replicative immortality, inducing angiogenesis and activating invasion and metastasis. Moreover, four more hallmarks are emerging: deregulating cellular energetics, avoiding immune destruction, genome instability and mutation, tumor-promoting inflammation. Drugs that interfere with each of the acquired capabilities necessary for tumor growth and progression have been developed and are in clinical trials or in some cases approved for clinical use in treating certain forms of human cancer. The drugs developed to target each of the characteristics are listed in boxes. Figure taken from ref [19].

marrow, digestive tract and hair follicles [92-94]. In addition, the development of multidrug resistance is a major issue that further limits the efficacy of existing treatments. Resistance can vary between different patients, and involves multiple pathways [91,95,96]: for example, cancer cells may develop an efficient transport system that ejects the drug from the cytosol before it can exert its function; alternatively, they avoid apoptosis by suppressing the mechanism of Cytochrome C release; moreover, slight modifications on the active site where the drug executes its inhibition mechanism prevent the molecular recognition, inactivating the drug. Recently, several alternative and innovative cancer therapies have been developed that display a more specific action against cancer cells, reducing the damage to healthy cells and thus undesired side effects. Figure 1.10 briefly summarizes the peculiar features that can be expressed by cancer cells and treatments currently under development that exploit them [19]. Along with the six characteristics of cancer proposed in 2000 [6] (sustaining of proliferative signals; evading growth suppression; resistance to cell death; unending replication; enhanced angiogenesis; invasion of nearby tissues), four new hallmarks are rising (altered cellular energetics; resistance against immune system attack; high propensity to mutations; state of persistent inflammation). Drugs that interfere with each of these 10 hallmarks are under development (reported in Figure 1.10, boxed near the corresponding feature), and some drugs already reached the clinical stage. Although innovative, these treatments all share the same characteristic of attacking a specific receptor, thus becoming less effective, or even completely inactive, after the occurring of a mutation that modifies the moiety target of the drug. Moreover, many of the new drugs must still be used in combination with the conventional treatments, reducing the advantages in terms of minor side effects. In this context of urgent need of finding molecules that can overcome drug resistance and at the same time reduce healthy cell cytotoxicity, peptides and peptidomimetics raised attention due to their different mode of action. Indeed, many of them attack the cell membrane, disrupting it by the formation of transient pores that kill the cell in a short timespan [97,98], which would avoid the development of resistance. Therefore, host defense peptides, previously considered only for their antimicrobial activity, have been subsequently taken in consideration as anticancer agents. Currently, a relatively large group of more than a hundred AMPs has been found to have also anticancer activity [99-101]. The majority of them has common characteristics: they have low molecular weight (less than 30 amino-acids long), carry one or more cationic residues and adopt an amphipathic helical conformation in membrane systems [102,103]. These features are usually accounted for the selectivity of these peptides for cancer cells with respect to healthy cells, given the increased quantity of anionic molecules present on the outer leaflet of the bilayer of the cancer cell membrane.

1.2.1 Characteristics of the tumor cell membranes

AMPs are emerging as potential anticancer agents thanks to their peculiar behavior: as already described, they mostly attack the cell membrane itself, rather than targeting a specific receptor. Thus, it is less likely that the cell can develop resistance to the treatment: this leads to the double advantage of the possibility of faster and more efficient treatments that at the same time cause less severe side effects. In order to design and synthesize more selective peptides, it is essential to understand their exact mechanism of interaction and cell destruction. Moreover, it is important to understand the characteristics that differentiate healthy cell membranes from tumor cell membranes that determine peptides propensity to interact with tumor cells.

One of the most recurring features that differentiate healthy cells from cancer ones is the over expression of negatively charged molecules on the outer leaflet of cancer cells membranes. Many AMPs carry positively charged residues, therefore it is straightforward to correlate selectivity with promoted electrostatic interactions. Many cancer cells display an over-expression of the negatively charged lipid phosphatidilserine (PS) [104,105], while healthy cells are mostly zwitterionic, being mainly composed by phosphatidilcoline (PC) and sphingomielyn [106]. Actually, PS in healthy cells is more abundant in the inner leaflet of the cell membrane; this asymmetry is sustained by ATP-dependent mechanisms [107], that become less effective in dying cells. Therefore, a high quantity of PS on the outer leaflet of healthy cells acts like a marker that activates a series of molecular signaling responsible of the induction of apoptosis. Cancer cells, however, despite exposing high PS levels, are still able to avoid apoptosis by other mechanisms, such as escaping macrophages recognition [108,109]. For this reason, positively charged peptides that specifically bind to negatively charged membranes and rapidly provoke the lysis are suitable candidates as anticancer agents. Moreover, it is worth noting that also mitochondria membrane is rich in negatively charged lipids, the most abundant being cardiolipin [101], and some tumor cells displayed high levels of PS also on the mitochondrial membrane [105]. Therefore, even peptides that penetrate cell membranes without causing significant damage, once in the cytosol could interact with the mitochondria, causing apoptosis. Other studies [110,111] pointed out that even when the difference in PS content between cancer and healthy cells is not marked, still many AMPs are more toxic against cancer cells [112]. So, other sources responsible for the overall negative charge have been searched. Indeed, other negatively charged molecules are expressed on the surface of tumor cells. One group of them is represented

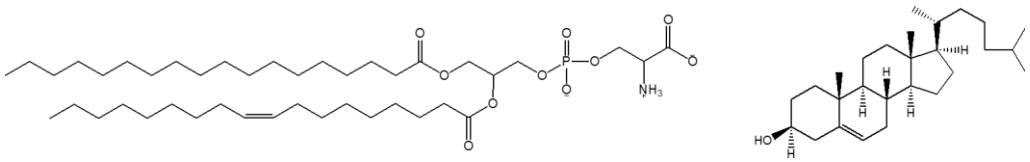

Figure 1.11 Phosphatidilserine (PS) and cholesterol.

by mucins, a family of glycoproteins rich in sialic acid residues that are overexpressed in many carcinomas [113,114] and that are correlated with the ability of the tumor cells to migrate in other regions of the body. A study pointed out that sialic acid might be a target for some anticancer AMPs such as some peptides of the cathelicidin family [115]. In contrast, other studies showed that this preference is not a general behavior of AMPs, since some peptides of the lactoferrin family do not lose cytotoxic activity after the cleavage of sialic acid from the cell membrane [116]. Another source of negative surface charges are proteoglycans, a family of membrane proteins rich in residues with negatively charged side chains [117,118] that are also susceptible to altered expression on some type of cancer cells. The role of this family of molecules as targets of AMPs is even more debated than that of mucins, since peptides have been found that are inhibited by a high expression of proteoglycans, other are not influenced by their presence, and some others seem to increase their activity [119,120]. In conclusion, many negatively charged molecules can be expressed or over expressed on cancer cell membrane; PS is certainly the most studied and it is generally accepted that it plays an important role in selectivity of cationic amphipathic peptides for cancer cells.

Another characteristic that often differentiates tumor and healthy cells is the membrane fluidity. Cancer cells often have altered fluidity: many tumor cells that affect lymph nodes, lungs and brain have an increased fluidity [121,122], while cells of other tumors, mainly solid tumors, have a decreased fluidity [123]. The rationalization of this feature, that could represent a useful characteristic to selectively target tumor cells, is complicated by the fact that even in the same cell, membrane fluidity is not uniform. Indeed, some studies [124] showed that the increased rigidity displayed by some tumors (mainly attacking breast and prostate) is due to the presence on the membrane surface of lipid-rafts that are rich in cholesterol. Additionally, cancer cells with increased rigidity may have the same total amount of cholesterol with respect to healthy cells; that implies that along with lipid rafts rich in cholesterol, other regions are, actually, poor in cholesterol and therefore more fluid. These fluid regions, mainly composed by less packed phospholipids, may be more susceptible to the attack of AMPs. Therefore, a combined presence of rigid lipid rafts, regions rich in phospholipids, and a high percentage of negatively charged PS, may be the ideal membrane composition that makes a cancer cell the preferred target of cationic helical AMPs. However, this scenario is complicated by other studies that seem to point in the opposite direction [125,126]: the high resistance to treatment displayed by some ovarian cancer cells and some leukemic cells has been linked to their remarkable rigidity, due to the high quantity of cholesterol in their membranes. It is clear, then, that fluidity is an important parameter to take into account when interpreting the interaction between cell membranes and peptides. However, it is not possible to assume *a priori* if a higher cholesterol content would lead to a more peptide-vulnerable membrane: each case should be analyzed individually.

Surface charge and fluidity are the two most important characteristics that influence the behavior of AMPs towards cell membranes. In addition to them, another common difference between cancer and healthy cells is represented by the total surface area. Indeed, many cancer cells have an increased total surface area due to the presence of microvilli [127]. Microvilli are small membrane protrusions composed of filaments linked by proteins and containing principally cytoplasm; usually no intracellular organelles. Due to their particular morphology, they are able to greatly increase the membrane surface with no increase of volume, thus increasing the ability of the cell to absorb nutrients from the extracellular environment. It is believed that AMPs can be more effective against cells rich in microvilli since a larger amount of peptides can bind to cell surface [127]. Indeed, a study [128] showed that cecropin B is more active against tumor cells with increased surface area that against healthy fibroblasts.

In summary, cancer cell membranes display various differences with respect to healthy cells that can be exploited to design selective drugs that do not undergo to the development of resistance. The ideal cancer cell to be treated with cationic helical AMPs should therefore be rich in lipid rafts alternated with fluid regions rich in phospholipids. Fluid regions should be rich in anionic phospholipid such as PS to electrostatically attract cationic AMPs. Finally, membranes rich in microvilli would have a greater surface area, where an increased number of peptides would be able to bind.

1.3 Electron Paramagnetic Resonance applied to the study of biological samples

Electron Paramagnetic Resonance (EPR) spectroscopy is a powerful tool that can provide many information on biological systems, such as peptides and proteins: it can determine the secondary, tertiary and quaternary structure of proteins and detect changes is aggregation and interactions with membranes; it is possible to describe proteins and peptides dynamics and their relative orientation in different systems. In this Ph.D. project, EPR spectroscopy has been extensively exploited to collect a variety of information on the TG analogs of our interest. In the following paragraphs, an overview of EPR theory will be given, along with how this technique is used to study biological systems. The following paragraphs, from 1.3.1 to 1.3.4, are adapted from ref [4].

1.3.1 Elements of continuous wave EPR theory

EPR spectroscopy is based on the interaction between an external magnetic field (B_0) with a dipole (μ_e) associated to the spin angular momentum of the electron. The dipole can orient itself parallel or antiparallel to the magnetic field B_0, and an oscillating magnetic field (B_1) with the proper energy can promote the transition of the electron from one orientation to another. The interaction of the dipole μ_e with the external field B_0 is called Zeeman interaction and its energy is given by:

$$E = -\overrightarrow{\mu_e}\overrightarrow{B_0} \qquad \text{Equation 1}$$

where μ_e is the magnetic moment associated to the electron spin angular momentum, $\vec{S}$:

$$\mu_e = -g\beta_e\vec{S} \qquad \text{Equation 2}$$

In equation 2, β_ε is the electron Bohr magneton. The g factor is a proportionality factor that relates the observed magnetic moment μ of a particle to its angular momentum quantum number and for the free electron its value is $g_e = 2.0023$. When the electron is located in a molecular system, the g value differs from g_e in dependence of the elctron distribution in the molecule. $\vec{S}$ is the spin angular momentum and for an electron, that has an electron spin quantum number of s=½, it can only assume the value $|S| = \sqrt{s(s+1)}\hbar = {}^{3}/_{2}\,\hbar$. Its projection on the axis parallel to the external magnetic field B_0, conventionally the z axis, can only assume two values, depending on the spin magnetic quantum number m_S: since $S_z=m_S\hbar$, then S_z can assume the values of $+1/2$ or $-1/2$ (in $\hbar$ units). Therefore two energy levels can be derived from Equation 1: $E = \pm(1/2)g\beta_eB_0$. The energy difference, in $\hbar$ units, between these two levels is therefore dependent to the external field B_0:

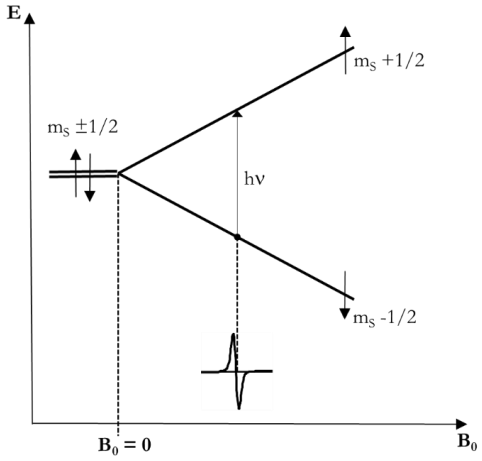

Figure 1.12 Schematic representation of the Zeeman interaction. At the proper resonance frequency hν, there is the EPR transition (one line represented as the first derivative of the signal).

$$\Delta E = h\nu = g\beta_e B_0 \qquad \text{Equation 3}$$

The dependence of ΔE on B_0 is schematized in Figure 1.12. The simplest EPR experiment is the cw EPR experiment. It consists in irradiating the sample with an oscillating magnetic field with a frequency ν that equals the energy gap (Equation 3); the strength of the magnetic field is swept to induce a transition of the unpaired electron between the two energy levels. The typical EPR signal, shown in Figure 1.12, is collected as the first derivative of the actual signal; this allows to improve the signal-to-noise ratio and to better observe scarcely resolved signals. In EPR spectroscopy at X band, the static field B_0 is about 0.3 - 0.8 mT, while the oscillating magnetic field lies in the microwave range. The intensity of the EPR signal is proportional to the microwave absorption that is dependent on the population difference between the two energy levels. The population ratio is given in equation 4, and the population difference, in the case of ΔE<<kT, is given in equation 5.

$$(N_{+1/2})/(N_{-1/2}) = \exp(-\Delta E / kT) \qquad \text{Equation 4}$$

$$(N_{-1/2} - N_{+1/2})/(N_{-1/2}) = \Delta E/kT \qquad \text{Equation 5}$$

To increase the difference of population, and therefore to improve the EPR signal, it is possible to increase the magnetic field B_0 or to lower the temperature T. To restore the Boltzmann equilibrium of the populations after the energy absorption, relaxation pathways such as the *spin-spin* relaxation and the *spin-lattice* relaxation take place. If the relaxation pathways are not efficient, the system can reach the saturation (i.e., the two energy levels are equally populated and therefore no signal can be measured). Moreover, electrons can experience a perturbation of their local environment due to the influence of magnetic nuclei. This interaction is called *hyperfine interaction* and can result in a local

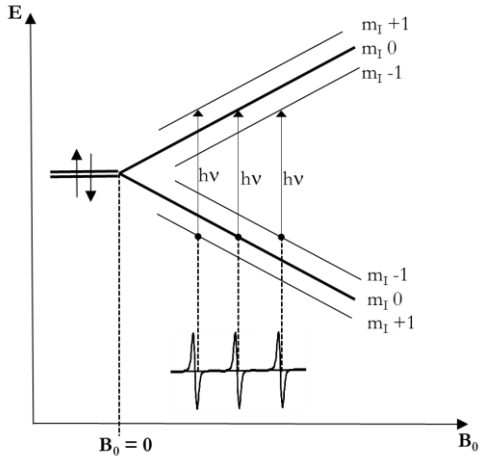

Figure 1.13 Schematic representation of the Zeeman and hyperfine interaction of a spin (S=1/2) with a nucleus with I=1. The three EPR transitions are represented as the first derivative of the signal.

enhancement or a local reduction of the external B_0. The resonance conditions in equation 3 are modified to include the hyperfine interaction A:

$$\Delta E = h\nu = g\beta_e B_0 + m_I A \qquad \text{Equation 6}$$

For a nucleus with nuclear quantum number I (characteristic of a given nuclide), m_I can assume 2I+1 values. It is then clear that the hyperfine interaction of an electron with a nucleus with nuclear spin I leads to the splitting of the electron transition into 2I+1 transitions, as represented in Figure 1.13 for the case of an hyperfine interaction of an electron (S=1/2) with a nucleus with I=1. The hyperfine interaction between an electron and a nucleus has two components, an isotropic component and a dipolar one. The isotropic splitting, defined as a_0, is proportional to the electron spin density on the nucleus, and is determined by the electronic wavefunction. The dipolar component is dependent on the spatial orientation, with respect to B_0, of the vector between the two magnetic moments. Being anisotropic, the hyperfine interactions can be described with a tensor, **A**, that in its principal axes system assumes a diagonal form:

$$\boldsymbol{A} = \begin{vmatrix} A_{xx} & 0 & 0 \\ 0 & A_{yy} & 0 \\ 0 & 0 & A_{zz} \end{vmatrix}$$

Moreover, also the Zeeman interaction of the electron spin with the external field H is anisotropic, therefore the g factor, introduced in equation 2, is a tensor that can be represented, in its principal axes system, in diagonal form as well:

$$\boldsymbol{g} = \begin{vmatrix} g_{xx} & 0 & 0 \\ 0 & g_{yy} & 0 \\ 0 & 0 & g_{zz} \end{vmatrix}$$

1.3.2 Nitroxides

Rarely biological samples are measurable with EPR spectroscopy at physiological temperature, since they do not have paramagnetic centers in their structure. With the exception of metalloproteins, biological samples as proteins and peptides must be modified with paramagnetic probes. The most commonly used probes are nitroxides, that contain an unpaired electron on the pπ orbital of the N—O bond of a nitroxide derivative; they are usually sterically hindered 5- or 6-member rings, and example is given in Figure 1.14. Nitroxides have been extensively used to label proteins at a specific site (Site Directed Spin Labeling, SDSL). The probe MTSSL (1-oxyl-2,2,5,5-tetramethylpyrroline-3-methyl) methanethiosulfonate) is covalently linked to a Cys residue of the protein. It is also possible to mutate the protein to have Cys residues available for the labeling in the desired positions. The MTSSL probe is used to study protein partition between membrane and solution, orientation and dynamics of the protein in membrane environment and solvent accessibility in different domains of the protein. To study peptides, the amino acid TOAC (2,2,6,6-tetramethylpiperidine-1oxyl-4-amino-4-carboxylic acid) has been often employed, that, differently from MTSSL, must be incorporated during the peptide synthesis and represents a direct modification on the primary sequence. TOAC is a C^{α}-tetrasubstituted, sterically hindered, amino-acid that promotes helical formation: thus, its presence could alter the secondary structure of the peptide, so its position must be chosen carefully. It is also possible to prepare β-peptides modified with a β-amino-acid, like POAC ((3R-4R)-4-amino-1-oxyl-2,2,5,5-tetramethylpirrolidine-3-carboxylic acid).

All the nitroxides used as EPR probes, some of which are described above, are based on the same principle: the unpaired electron (S=1/2) interacts with the ^{14}N nucleus (I=1). The hyperfine interaction between them generates a splitting of the electron signal into three transitions (2I+1=3, see equation 6 and Figure 1.13). The magnetically active site of these nitroxides is the N—O fragment, the structure of which is reported in Figure 1.15. The unpaired electron is localized in a 2pπ orbital on the N—O group. Typical principal values of the hyperfine tensor **A** for nitroxide spin labels are $A_{xx} \approx A_{yy} \approx 0.7$ mT and $A_{zz} \approx 3.5$ mT. Since the difference between the *x* and *y* component is

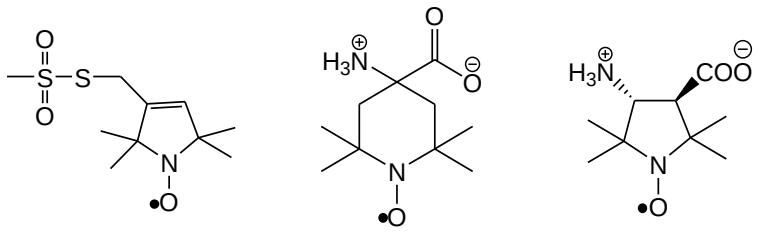

Figure 1.14 Three common EPR probes: from left, MTSSL, TOAC, POAC.

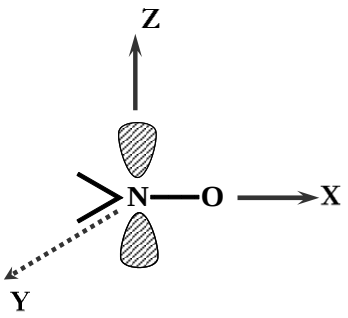

Figure 1.15 Representation of the principal axes of the N—O fragment.

usually very small, the tensor is assumed to have an axial symmetry. Instead, the **g** tensor has a rhombic symmetry, and typical values of the **g** tensor for a nitroxide spin label are $g_{xx} \approx 2.0085$, $g_{yy} \approx 2.0065$, $g_{zz} \approx 2.0027$. The fact that **A** and **g** tensors are anisotropic means that EPR spectroscopy is sensitive to changes in orientation of the nitroxide and to its rotational motion.

1.3.3 Influence of the orientation on nitroxide cw-EPR spectra

In absence of motion (on the EPR timescale), the nitroxide label has a defined orientation with respect to the magnetic field B_0. Both **g** and **A** tensors depend on the orientation of the molecule, following equations 7 and 8, respectively.

$$g(\theta,\phi) = g_{xx}\sin^2\theta\cos^2\phi + g_{yy}\sin^2\theta\sin^2\phi + g_{zz}\cos^2\theta \qquad \text{Equation 7}$$

$$A^2(\theta,\phi) = A_{xx}^2\sin^2\theta\cos^2\phi + A_{yy}^2\sin^2\theta\sin^2\phi + A_{zz}^2\cos^2\theta \qquad \text{Equation 8}$$

where θ and ϕ determine the orientation, expressed as polar angles, of the principal axes of **g** and **A** tensors with respect to the B_0 direction. This dependency is clear in the experimental spectra of Figure 1.16, where it is shown that the splitting of the three lines, determined by the hyperfine tensor, is ≈ 7 mT if the spin label *z*-axis is parallel to the magnetic field, while it is reduced to ≈ 1.4 mT if the *z*-axis is perpendicular to B_0. The center position of the spectrum is determined by the **g** tensor; assuming a given g value for a spin with the *z*-axis aligned with B_0, at X band the center of spectrum is shifted of 0.5 mT downfield if the spin is aligned with the *y*-axis and 0.9 mT downfield if the spin is aligned with the *x*-axis. If the sample is composed by many molecules, each one in a different orientation, the experimental spectrum will be the sum of each different contribution. The final intensity at each filed position is proportional to the number of spins at that specific orientation, and the resonance field for each orientation is given by equation 8.

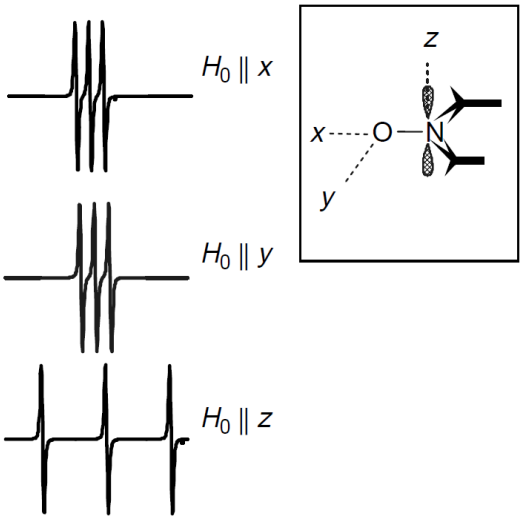

Figure 1.16 EPR spectra of a nitroxide single molecule that shows the orientational sensitivity. The splitting of the spectrum changes when the $\tilde{z}$-axis of the nitroxide rotates with respect to the magnetic field; the center of the spectrum changes when the nitroxide rotates about any axis. Figure taken from ref [4].

Figure 1.17 Broadening of the spectra with increasing disorder: a, ±1°; b, ±5°; c, isotropic distribution. Figure adapted from ref [4].

$$H_{res}(\theta, \phi, m_I) = \frac{h\nu}{\beta g(\theta, \phi)} + m_I A(\theta, \phi) \qquad \text{Equation 8}$$

Figure 1.17 shows how the spectrum changes increasing number of orientations distributed as a Gaussian distribution around a given angle. When the spins are isotropically distributed, the spectrum assumes the typical powder pattern that is the result of the contribution of all the possible orientations. The experimental features such as spectral splitting, central g value and linewidth are characteristic of the orientational distribution.

1.3.4 Influence of the dynamics on nitroxide cw EPR spectra

The sensitivity of the EPR signal to motion is due to the rotation of the molecules that modulate the anisotropic magnetic interactions. To understand the lineshape modifications due to the molecular motion, we can consider the simple exchange

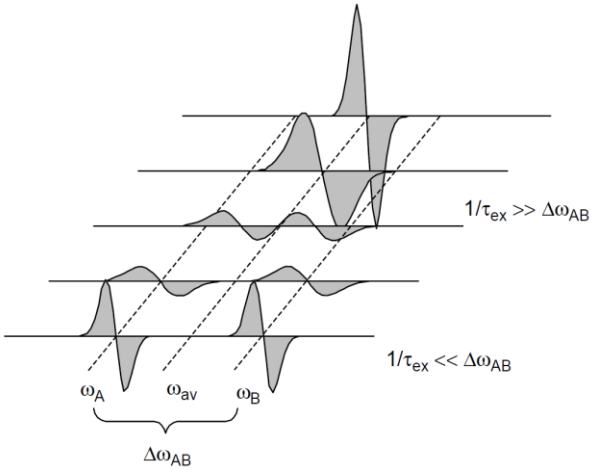

Figure 1.18 Effect on the resonance of two spins, with resonance frequencies ϖ_A and ϖ_B, of the exchange at frequency $1/\tau_{ex}$. Figure taken from ref [4].

process between two spins with different resonance frequencies, at increasing exchange frequencies, represented in Figure 1.18. Initially, the two spins A and B resonate at characteristic frequencies ϖ_A and ϖ_B and exchange their positions at a frequency of $1/\tau_{ex}$. If their exchange rate is significantly lower than $\Delta\varpi^0_{AB}$, the spectrum will be formed by two well defined signals centered at the two frequencies ϖ_A and ϖ_B, and the linewidths will be only determined by their spin-spin relaxation times, T_2. For a very fast exchange ($1/\tau_{ex} >> \Delta\varpi_{AB}$), the two peaks merge in one peak at a frequency that is the average of ϖ_A and ϖ_B. For an intermediate situation, the centers of the two EPR signals reduce their distance with respect to the slow exchange condition, and their linewidths increase, according to equations 10 and 11.

$$\Delta\omega_{AB} = \Delta\omega^0_{AB}\sqrt{1 - 8/\tau^2_{ex}\Delta\omega^0_{AB}} \qquad \text{Equation 10}$$

$$1/T_2^{eff} = 1/T_2^A + 1/T_2^B + \Delta\omega^2_{AB}\tau_{ex}/8 \qquad \text{Equation 11}$$

The reorientation of a nitroxide in a magnetic field is a form of exchange, where the exchange time τ_{ex} becomes the rotational correlation time t_R: $1/t_R$ is the exchange frequency at which the spin reorientates with respect to the magnetic field. The difference of the two resonance frequencies is determined by Zeeman and hyperfine interactions; when the molecule rotates in the magnetic field B_0, there is an exchange between different orientations, and therefore between different resonance frequencies. As in the two sites exchange model, in the EPR spectra of a rotating nitroxide the lineshape progressively broadens, as shown in Figure 1.19. Nitroxide spin labels bound to peptides and small proteins have a motion on the nanosecond timescale that is ideal to be studied with cw EPR. For a very slow motion, the typical spectrum of a rigid nitroxide (or powder spectrum) is shown. It has to be noted that the broadening of the

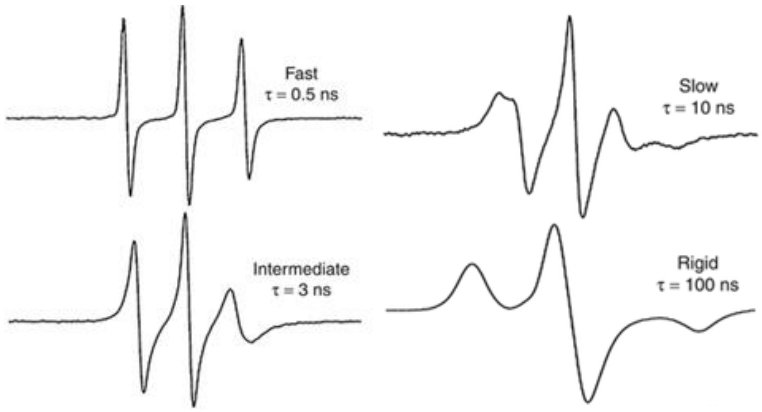

Figure 1.19 Sensitivity of the EPR spectra to different motions. Figure adapted from ref. [3]

three lines is not homogeneous, since it depends on the nuclear spin quantum number m_I relative to the ^{14}N nucleus; it is therefore minimum for the central component (m_I=0), intermediate for the low field component (m_I=+1) and maximum for the high field component (m_I=-1). It is not trivial to interpret EPR spectra in different motion regimes, however the variety of information that can be obtained encouraged the effort in the development of various computational models. Some details on the model used to simulate the EPR spectra of nitroxides interacting with lipid membranes in this Ph.D. work are reported in Appendix A.

1.3.5 Measurements of solvent accessibility

One of the more interesting information that can be obtained from EPR experiments in spin-labeled proteins or peptides is the degree of solvent accessibility of a given position labeled with the nitroxide. Solvent accessibility is a measure of the exposure of a given site to a polar (usually water) or apolar (usually the inside of a membrane) environment. Accessibility is proportional to the collision rate with diffusible paramagnetic reagents (relaxants) that are dissolved in solution of the polar or apolar solvent. For example, residues on a solvent-exposed surface or buried in the protein interior will experience high- or low-collision rates, respectively.

The determination of solvent accessibility in SDSL relies on the Heisenberg exchange mechanism [129]: an enhancement of the nitroxide relaxation due to collisions with fast-relaxing paramagnetic species in solution. For the Heisenberg exchange to be proportional to the solvent accessibility the process should be in the strong exchange limit and be diffusion-controlled, i.e. every collision must induce relaxation, a condition that is met with the relaxants that are commonly used such as oxygen, CROX or NiEDDA [130]. For a bimolecular encounter between a small nitroxide (N) in solution

and an exchange reagent *i*, the Heisenberg exchange frequency, Wex, experienced by a particular nitroxide is given by

$$W_{ex} = k_{ex}C_i \qquad \text{Equation 12}$$

where k_{ex} is the exchange rate constant and C_i is the concentration of the exchange reagent *i*. Defining T_{1i} as the longitudinal relaxation time of the reagent i and τ_c the encounter complex lifetime, for exchange reagents with $T_{1i} < \tau_c$, T_{1e} Heisenberg exchange leads to equal changes in T_{1e} and T_{2e} of the nitroxide, and

$$W_{ex} = \Delta(1/T_{1e}) = \Delta(1/T_{2e}) = k_{ex}C_i \qquad \text{Equation 13}$$

Thus, methods based on measurement of either T_{2e} or T_{1e} may be employed for experimental determination of W_{ex}. The most common EPR method for observing spin label solvent accessibility is power saturation: the intensity of the central line in the first derivative spectrum is observed as a function of the incident microwave power in the absence and in the presence of the relaxant. The saturation curves are then fitted with:

$$A = A_0\sqrt{P}/\left[1 + \left(\sqrt[\varepsilon]{2} - 1\right)\left(P/P_{1/2}\right)\right]^{\varepsilon} \qquad \text{Equation 14}$$

Where ε is a homogeneity factor dependent on the lineshape that can range from 0.5 for a Lorentzian lineshape to 1.5 for a Gaussian lineshape; A_0 is simply a scaling factor; $P_{1/2}$ is the power of the microwave field at which the signal is reduced to half with respect to the value it would have in absence of saturation. The change in $P_{1/2}$ ($\Delta P^i_{1/2}$) upon addition of the relaxant *i* is correlated with the solvent accessibility of the nitroxide. For a homogeneous Lorentzian,

$$P_{1/2} = \left(2^{2/3} - 1\right)/(\gamma^2\Lambda^2 T_{1e}T_{2e}) \qquad \text{Equation 15}$$

where $\Lambda = B_1/P_{1/2}$ is an instrumental parameter that depends on the Q factor of the used cavity and $\gamma = g\beta 2\pi/h$ is the gyromagnetic ratio. For the common case where $W_{ex} << 1/T_{2e}$, T_{2e} may be taken as a constant, and

$$\Delta P^i_{1/2} = P^i_{1/2} - P^0_{1/2} = \left(2^{2/3} - 1\right)/\left(\gamma^2\Lambda^2\right)(1/T_{2e})(1/T^i_{1e} - 1/T^0_{1e}) = \\ = ((2^{\frac{2}{3}} - 1)/(\gamma^2\Lambda^2 T_{2e}))W_{ex} \qquad \text{Equation 16}$$

where $P_{1/2}$ and $P^0_{1/2}$ are in the presence and absence of relaxant *i*, respectively, and T_{1e} and T^0_{1e} are the corresponding relaxation times. Although $\Delta P_{1/2}$ is proportional to W_{ex}, it depends on the motion of the nitroxide through T_{2e} and on properties of the resonator through Λ. Figure 1.20 shows an example of how the peak-to-peak amplitude of an experimental spectrum varies as a function of the microwave power. It can be observed that the curve profiles change for samples that have different T_1 and in the presence of different relaxants. To avoid the dependence of $P^i_{1/2}$ on experimental factors, the dimensionless quantity Π^i is used [131,132]:

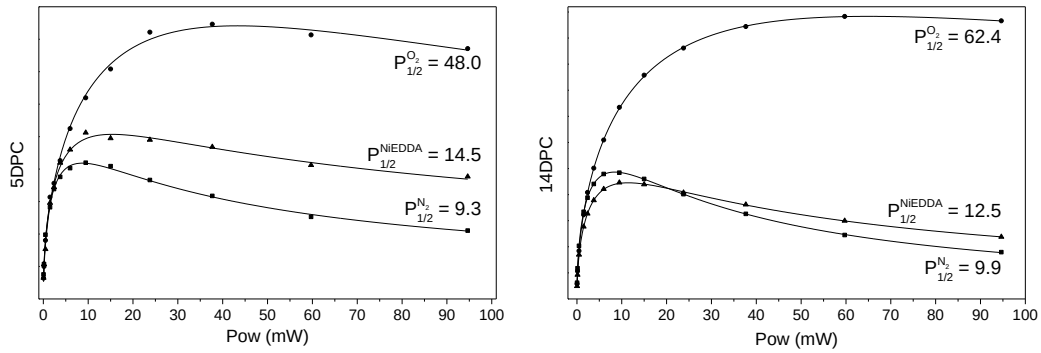

Figure 1.20 Power saturation curves of 5DPC (1-palmitoyl-2-stearoyl-(5-doxyl)-*sn*-glycero-3-phosphocholine) and 14DPC (1-palmitoyl-2-stearoyl-(14-doxyl)-*sn*-glycero-3-phosphocholine) in presence of oxygen, NiEDDA and under nitrogen flux (absence of relaxants). The peak to peak amplitude of the spectra varies as a function of the microwave power and of the accessibility of the relaxants to the nitroxides.

$$\Pi^i = \frac{\Delta P_{1/2}^i}{\Delta H_{pp}} \frac{\Delta H_{pp}^{REF}}{P_{1/2}^{REF}} = \alpha W_{ex} \qquad \text{Equation 17}$$

Division of $\Delta P_{1/2}$ by the nitroxide central linewidth, ΔH_{pp}, normalizes for the nitroxide T_{2e}, and division by the quantity $[P_{1/2}{}^{REF}/\Delta H_{pp}{}^{REF}]$ normalizes for variations in resonator efficiency. In published literature to date, a dilute DPPH (2,2-diphenyl-1-picrylhydrazyl) powder in KCl was selected as the reference, and the reported Π values depend on this choice.

An application of solvent accessibility measurements: membrane immersion depth of a nitroxide

Measurements of accessibility to a certain relaxant are extensively applied to scan the secondary conformation of selected domains of proteins and to determine the penetration depth of a nitroxide bound to a peptide in a membrane bilayer. These experiments are based on the different solubility of polar and non-polar relaxing agents in the aqueous and in the lipid phase of a phospholipid bilayer [17]. Indeed, if a spin labeled amino acid has a high frequency collision, i.e. has a high accessibility, with a water soluble relaxant, such as NiAA (nickel(II) acetylacetonate) or NiEDDA (nickel(II) ethylenediaminediaceate), then that amino acid is facing the aqueous environment. Conversely, if the nitroxide has a high accessibility to a nonpolar relaxant, the most used being O_2, then it can be concluded that the amino acid is facing the hydrophobic lipid tails of the bilayer. Additionally, oxygen has a concentration gradient that increases towards the center of the bilayer, thereby solutes that are located more deeply in the membrane have a higher collision frequency than those located just below the polar headgroup region. In the case of a helical peptide, it is possible to obtain information

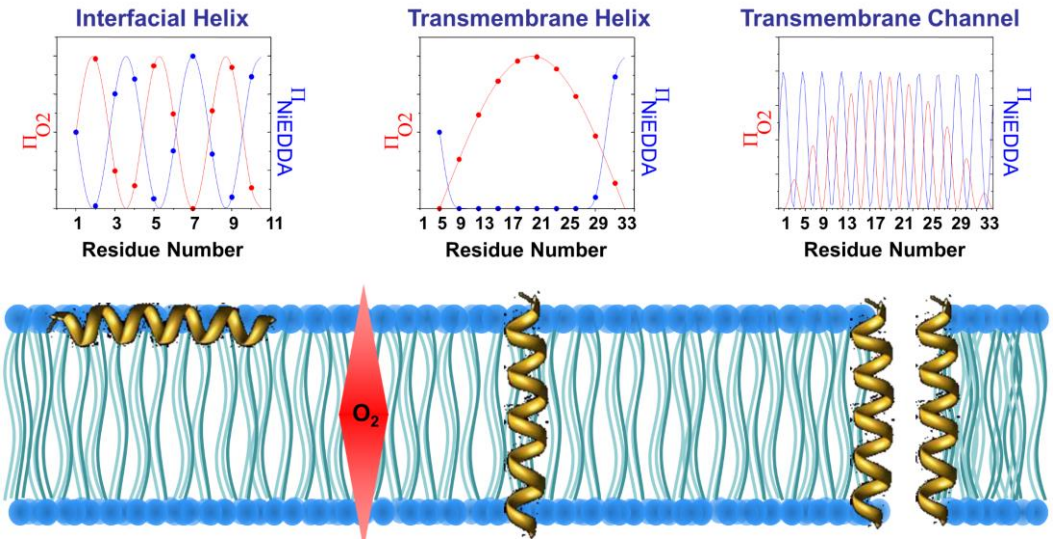

Figure 1.21 Scanning of accessibility Π of helices labeled in different positions. The accessibility profile varies depending on the orientation of the helix with respect to the membrane bilayer. Π profile of the transmembrane helix is directly proportional to the solubility of the two different relaxants (NiEDDA and O_2) in water and in hydrophobic environment.

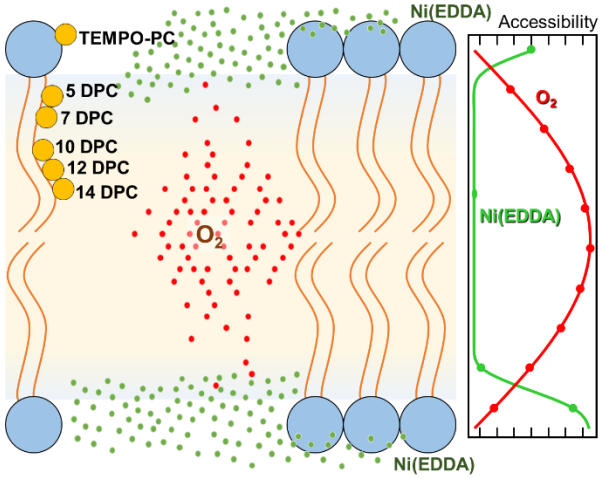

Figure 1.22 Schematic representation of a phospholipid bilayer of POPC doped with *X*-DPC (1-palmitoyl-2-stearoyl-(*X*-doxyl)-*sn*-glycero-3-phosphocholine), labelled at different position (yellow circles). It is also represented the concentration at different depths of the bilayer of the two used relaxants: O_2 (red dots) is more soluble in the lipid phase, NiEDDA (green dots) is more soluble in aqueous phase.

on its position relatively to a membrane bilayer by labeling the sequence in different positions and measuring the accessibility Π^i for all the analogs. Figure 1.21 shows how Π varies in presence of NiEDDA or in presence of O_2 for peptides with different orientation in the membrane. To obtain a correlation between accessibilities of a label and its actual depth of insertion into the phospholipid bilayer, it is necessary to first build the so called "molecular ruler", using vesicles doped with a phospholipid carrying a spin label at different positions of the lipid tails. In this way, the values obtained for the reference system (the labeled phospholipids) can be used as a comparison for solutes of unknown depth. A schematic representation of the ruler is reported in Figure 1.22. The results of the accessibilities to oxygen and NiEDDA are generally combined in the dimensionless depth parameter Φ, given in equation 18.

$$\Phi = ln \frac{\Delta P_{1/2}^{O_2}}{\Delta P_{1/2}^{NiEDDA}} \qquad \text{Equation 18}$$

$\Delta P_{1/2}$ is defined in equation 16. Φ values obtained for the reference system are then used as a comparison for solutes of unknown depth. The advantage of Φ is that, being a ratio of two experiments, all the dependencies on the experimental setup are canceled out and it does not depend on the choice of reference as Π does.

2. Aim of the work

In this Ph.D. thesis, the antimicrobial lipopeptaibol trichogin GA IV (TG) and several of its analogs are studied. The main goal is to determine, with several techniques, key features of peptides structure that influence peptide behavior towards cancer and healthy cell membranes in physiological conditions.

A series of TG analogs have been designed to vary some key structural parameters of the peptide: helicity, hydrophobicity, hydrophobic moment, charge. All peptides were synthesized by Solid Phase Peptide Synthesis. Then, the toxicity of all the peptides has been tested against three healthy and cancer cell lines, the membranes of which have a significantly different composition.

Peptides secondary structure has been extensively characterized: Circular Dichroism spectra have been performed in membrane mimicking environment and in model membranes. A hydrophobicity scale has been developed extended to quantify the hydrophobicity and hydrophobic moment of the peptides. Through this work, it was possible to shed light on the interaction between structure and activity of these TG analogs.

Many experiments have been performed to observe the interaction between peptides and membranes. Fluorescence microscopy allowed to directly observe the localization of TG analogs on cell membranes. EPR experiments gave information on the binding propensity and on the dynamics of spin labeled TG analogs interacting with model membranes composed of synthetic phospholipids, with reconstituted cell membranes from healthy and cancer cell lines, and, finally, with viable cells.

Important information on the orientation of spin labeled TG analogs in membranes came from the immersion depth measurements that have been performed in model membranes and in viable cells.

3. Results and discussion

3.1 Design of TG analogs

The native sequence of TG is shown in the helical wheel representation in Figure 3.1. TG is normally considered a hydrophobic peptide due to the presence of many hydrophobic amino-acids and also owing to the lipidic octanoyl chain at the N-terminus. It has a slightly amphipathic character since it presents a lipophilic face made of hydrophobic residues and a slightly hydrophilic face composed by Gly residues. The helix can be divided into three sectors: a slightly hydrophilic sector of ~140° entirely made of glycine residues (red), a highly hydrophobic sector of ~130° (blue), and a structural/hydrophobic sector (green) of ~90° made of the octanoyl fatty chain and three Aib residues that have a helix-promoting function. When designing TG analogs, we didn't alter the hydrophobic sector for two reasons: a strong hydrophobic sector is a prerequisite for effective membrane perturbation [1]; the hydrophobic sector of TG is the only one that contains chiral amino acids, that are essential to induce TG to prefer a right handed helix over the left handed helix. Then, we focused our attention on the hydrophilic (red) and structural (green) sectors. In order to enhance the mild amphipathic character of TG, we introduced the positively charged Lys or Arg in place of Gly. These substitutions should not preclude helical formation, but aim at introducing charges on the hydrophilic side of the helix. The occurrence of these two amino acids in natural peptides and proteins is dependent on the particular biological function [133] and arginine-rich peptides are known for their cell-penetrating properties [134]. For example, in previous works [$Lys^{5,6}$] TG showed a remarkably increased activity against *S. aureus* bacterial strain [2]. Here, TG analogs containing either Lys or Arg have been prepared to assess whether the type of charged residue influences the toxicity of the peptide towards the cells. The enhancement of the overall hydrophobicity was achieved by Aib-to-Leu substitutions. Leu is a known helix-supporting residue; although it is less effective than Aib, Leu in position 4 or 8 should not heavily perturb

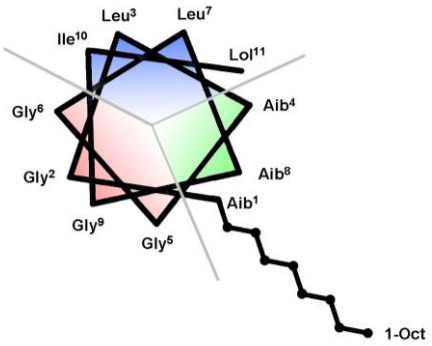

Figure 3.1 Helical wheel representation of TG. The octanoyl tail present at the N-terminus is shown in the bottom right part. The grey lines divide the peptide in three sectors.

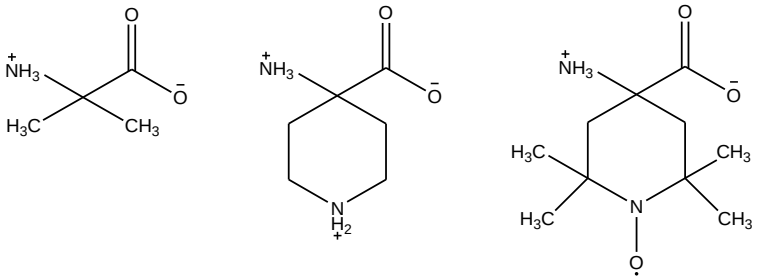

Figure 3.2 The three non-standard residues used in the syntheses. From left, Aib, Api, TOAC.

the helicity and stability of the helix. Perturbation of the hydrophobic/hydrophilic balance in TG has been achieved by inserting an Api residue, a positively charged C^{α}-tetrasubstituted amino acid. This substitution was chosen since it has been previously reported that a slight perturbation of amphipathicity, via the introduction of a charged residue in the hydrophobic sector, leads to an improvement in the selectivity of peptides [135]. It has been placed in positions naturally occupied by Aib so to guarantee the maintenance of helicity in TG analogs. Several analogues carry the paramagnetic amino-acid TOAC in position 1 were synthesized. Additionally, few analogs carrying TOAC in positions 4 or 8 have been synthesized to carry out the immersion depth measurements (see paragraph 3.5.2.4). With this modification we do not significantly impact the helical formation, although TOAC is quite big and sterically hindered. Indeed, it has already been published that TOAC is able to reinforce helical conformation and impart good

Table 3.1 Short name and primary sequence of the studied peptides.

Peptide	Primary sequence	Peptide	Primary sequence
TG	*Oct*-UGLUGGLUGI-Lol	[Arg^{2}] TG	*Oct*-U**R**LUGGLUGI-Lol
[TOAC^{1}] TG	*Oct*-**X**GLUGGLUGI-Lol	[TOAC^{1}, Arg^{2}] TG	*Oct*-**XR**LUGGLUGI-Lol
[TOAC^{4}] TG	*Oct*-UGL**X**GGLUGI-Lol	[TOAC^{1}, Arg^{9}] TG	*Oct*-**X**GLUGGLU**R**I-Lol
[TOAC^{8}] TG	*Oct*-UGLUGGL**X**GI-Lol	[Api^{8}] TG	*Oct*-U**R**LUGGLUGI-Lol
[Lys^{6}] TG	*Oct*-UGLUG**K**LUGI-Lol	[TOAC^{1}, Api^{4}] TG	*Oct*-**X**GL**Z**GGLUGI-Lol
[TOAC^{1}, Lys^{6}] TG	*Oct*-**X**GLUG**K**LUGI-Lol	[Leu^{4}] TG	*Oct*-**XR**LUGGLUGI-Lol
[TOAC^{4}, Lys^{6}] TG	*Oct*-UGL**X**G**K**LUGI-Lol	[TOAC^{1}, Leu^{4}] TG	*Oct*-**X**GLUGGLU**R**I-Lol
[TOAC^{8}, Lys^{6}] TG	*Oct*-UGLUG**K**L**X**GI-Lol	[TOAC^{1}, Leu^{8}] TG	*Oct*-**X**GLUGGL**L**GI-Lol
[Lys^{5,6}] TG	*Oct*-UGLU**KK**LUGI-Lol	TG-FITC	*Oct*-UGLUGGLUGIL-**FITC**
[TOAC^{1}, Lys^{5,6}] TG	*Oct*-UGLU**KK**LUGI-Lol	[Lys^{6}] TG-FITC	*Oct*-UGLUG**K**LUGIL-**FITC**

biological properties to peptides [88]. Moreover, two additional analogues with the C-terminus modified with the fluorescent probe fluorescein isothiocyanate (FITC) were used for the fluorescence microscopy experiments. A summary of all the studied analogs is reported in Table 3.1. Finally, some peptides were synthesized in the first stages of this project, but measurements on them were subsequently discontinued: they were TG analogs with TOAC positions 1, 4 and 8 or Lys in position 6, all lacking the C-terminal amino-alcohol and carrying a methyl ester instead. The toxicity data obtained for these peptides were in agreement with recently published data [78] that underlined the importance of the terminal amino-alcohol for the bioactivity of TG analogs. Therefore, we decided to focus only on TG analogs that kept both the C- and N-termini intact.

3.2 Peptide synthesis

All the TG analogs studied in this work were synthesized by Solid Phase Peptide Synthesis (SPPS). SPPS was developed in the middle 60s by Merrifield [136-139] and it brought a significant improvement with respect to the synthesis in solution, leading to the win of the Noble Prize in 1985 [140]. In the SPPS, the C-terminal amino-acid of the desired peptide is covalently linked to an insoluble resin, from which it is cleaved only when the synthesis is completed. The solid support allows to use reagents in large excess to drive the reactions to completion and to wash the resin effectively, obtaining the final peptide in a relatively pure form. The SPPS can also be conducted as an automated synthesis, further reducing the synthetic time and solvent consumption. The general process to synthesize peptides on a resin is schematized in Figure 3.3. It starts by loading the resin with the C-terminal amino-acid. The residue, as well as all the other residues that will be added in the subsequent passages, are protected at the alpha amino group with a protecting group, to avoid polymerization. Moreover, also the reactive side chains are kept protected with an orthogonal protecting group until the synthesis is complete. The next step is the removal of the protecting group at the N-terminal; then, the next amino-acid, protected at the N-alpha, is coupled to the N-terminal amino-acid on the resin. After the coupling, it is possible to remove the protection at the new N-terminal residue and repeat the deprotection-coupling cycle until the sequence is complete. All the protecting groups at the side chains are removed in one

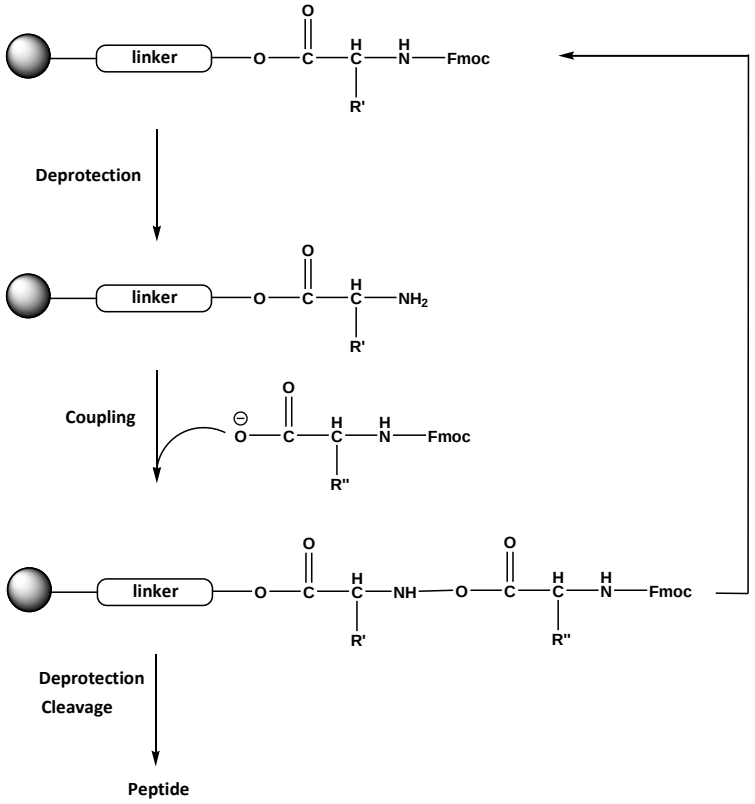

Figure 3.3 Schematic representation of the SPPS process.

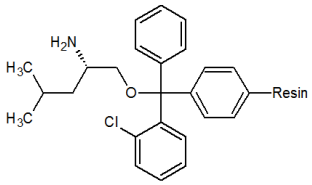

Figure 3.4 2-chlorotrytil resin linked to Leucinol.

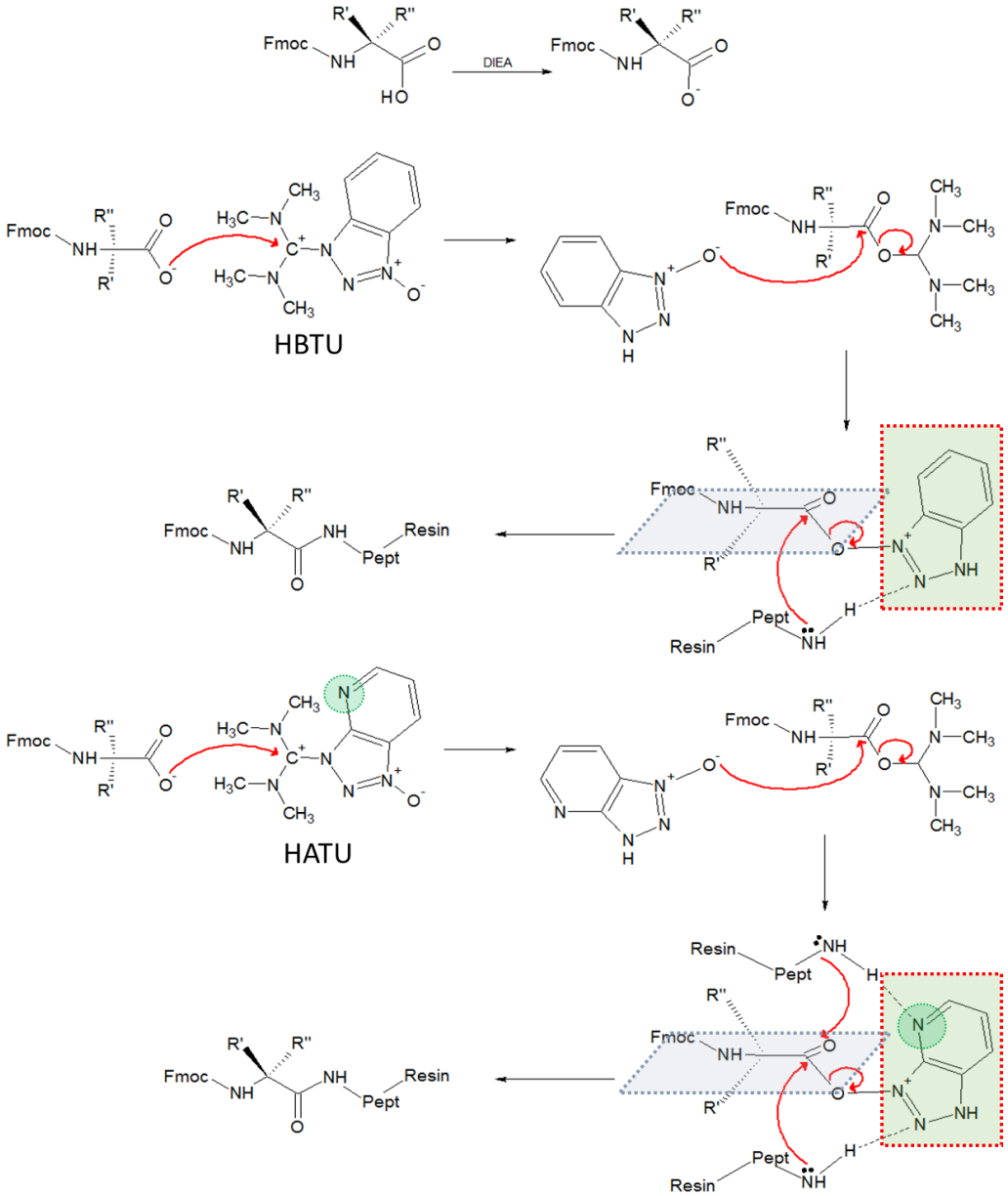

Figure 3.5 Mechanism of the coupling reaction. After deprotonation by means of a base, the deprotonated, protected, residue is activated by reacting with HBTU that induces a favorable orientation of the growing peptide for the coupling with the desired residues thanks to a hydrogen bond with a nitrogen on the HBTU ring. The HATU ring has an additional nitrogen that enables one additional coupling geometry.

step before the peptide is cleaved from the resin. For the synthesis of the TG analogs, a protocol was developed and optimized [2,141] in the research group of Prof. C. Toniolo and Prof. F. Formaggio, University of Padova. The used resin is a styrene copolymer containing 1-2% of divynilbenzene, acting as a cross-linker. The C-terminal is separated from the resin by 2-chlorotrytil [142-144], that is optimal for the synthesis of TOAC-labeled peptides since it is removable in mild acidic conditions (see below). The Lol residue is already linked to the resin (Figure 3.4). The coupling procedure involves the activation of the N^{α} protected amino-acid *via* the uronium salt HBTU ([2-(1*H*-1,2,3-benzotriazol-1-yl)-1,1,3,3-tetramethyl uronium hexafluorophosphate]) for the standard residues, while for the less reactive C^{α}-tetrasubstituted residues (Aib, TOAC, Api) it is required a strong activant [145,146], i.e. HATU ([2-(1*H*-7-aza-1,2,3-benzotriazol-1-yl)-1,1,3,3-tetramethyl uronium hexafluorophosphate]). Figure 3.5 schematizes the reaction mechanism for both activation pathways [147-149], that enhance the electrophilic propensity of the carbonyl group; an activated ester is formed, that reacts quickly with the N-terminal of the peptide. Both HBTU and HATU lead to the formation of the ester that perform its catalytic effect promoting an optimal geometry between the peptide on the resin and the coupling amino-acid. As shown in the figure, HATU has a higher activating capability since it has two nitrogens that can form hydrogen bonds with the N-terminus of the peptide, favoring the attack of the new residue. After the coupling, the Fmoc (9-fluorenylmethyloxycarbonyl) group that protects the N-terminal part of the peptide is removed with a basic treatment with a secondary amine that attacks the acidic proton of the fluorenyl ring. The chosen base is piperidine, since it has the double purpose: it removes the Fmoc group from the peptide sequence *via* a β-elimination and it scavenges the byproduct dibenzofulvene that would form a covalent bond with the N-terminal part of the peptide if not readily removed from the solution. The β-elimination reaction is schematized in Figure 3.6. At the end of the coupling steps, the completed peptide is cleaved from the resin in mild acidic conditions using HFIP (1,1,1,3,3,3,-hexafluoropropan-2-ol), that are appropriate to preserve the radical function of the paramagnetic amino acid TOAC, present in most of the peptide sequences. The mechanism of reaction involved in the resin cleavage is shown in Figure 3.7. However, some amino-acids had reactive side-chains that were

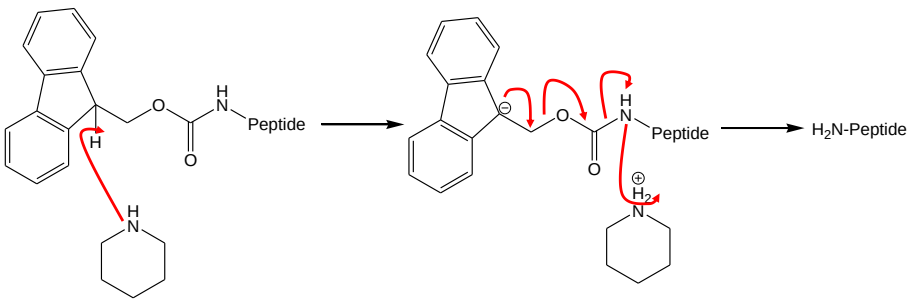

Figure 3.6 Mechanism of the elimination reaction.

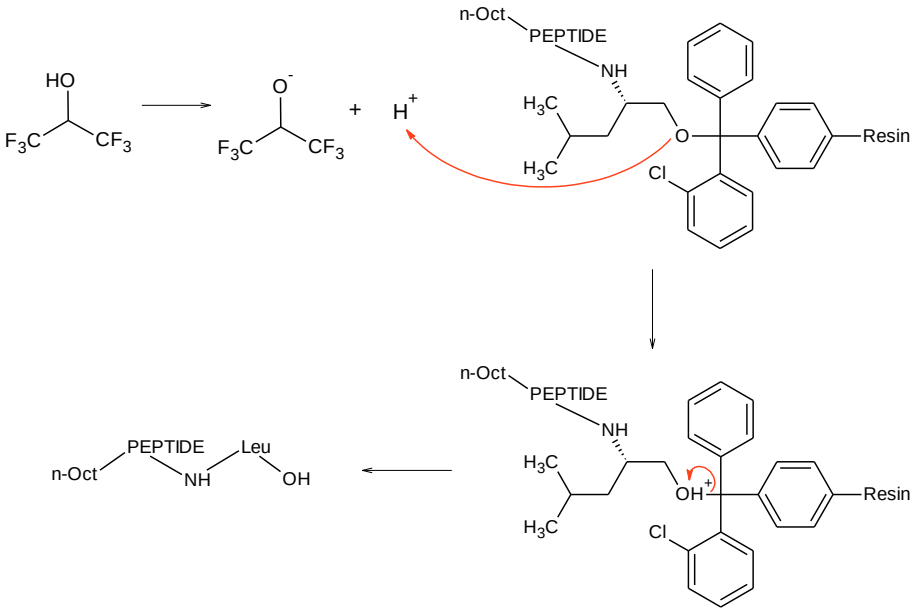

Figure 3.7 Mechanism of the reaction of cleavage of the peptide from the resin.

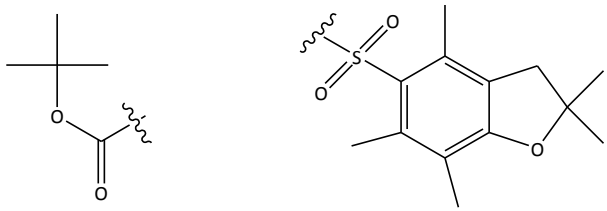

Figure 3.8 The two protecting groups Boc (left) e Pbf (right).

protected during the coupling reactions. In particular, Lys and Api side-chains were protected with Boc (t-Butyloxycarbonyl) group and Arg was protected with Pbf (2,2,4,6,7-pentamethyldihydrobenzofuran-5-sulphonyl), see Figure 3.8. All these protecting groups are acid labile, so it was chosen to remove them as a single step with the cleavage of the peptide from the resin. This required stronger acidic conditions (TFA or HCl) that cause the partial TOAC disproportion to an oxoammonium cation and hydroxylamine [150] (see figure 3.9). The regeneration of the TOAC radical moiety was achieved with a basic treatment with ammonia and followed with reverse phase HPLC. All the peptides were, subsequently to the cleavage, purified by reverse phase liquid chromatography and characterized by ESI-MS and, for peptides without the TOAC residue, ^{1}H-NMR. All the peptides were purified until a purity >98% was obtained.

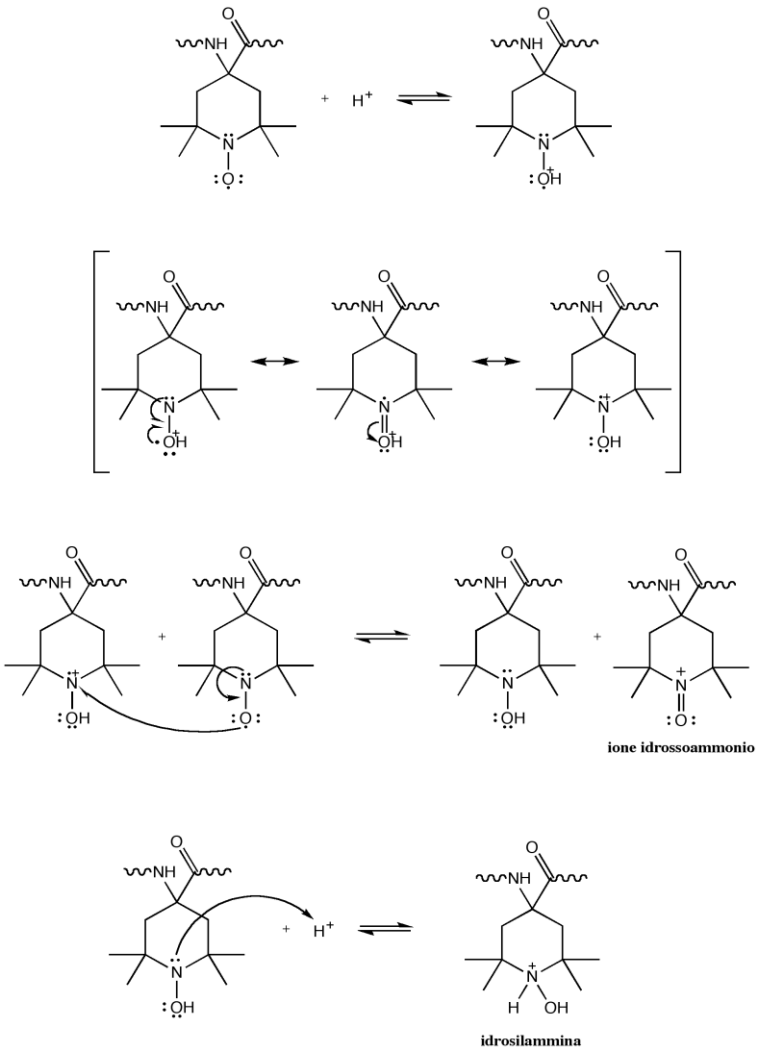

Figure 3.9 Disproportion reaction that can happen on TOAC in acidic environment.

3.3 Biological assays

3.3.1 Cytotoxicity assay

We studied the effect of TG and its analogues on normal (HDF) and transformed (T67 and HeLa) cells. The cellular viability was assessed after 24 hours of exposure to the peptides by the MTT (3-(4,5-dimethylthiazol-2-yl)-2,5-diphenyltetrazolium bromide) assay. The MTT assay is a standard colorimetric assay that measures the activity of the enzymes that transform MTT to formazan. The enzymes, that are only active in viable cells, exert their activity cleaving the tetrazolium ring of the MTT, that has a light yellow color, forming formazan, an insoluble salt with an intense violet color (see Figure 3.10 and [151]). After the treatment, viable cells are quantified by measuring the absorbance of the formazan at λ=570 nm. To perform the assay, the desired cell line is cultured in plates or flasks with the proper culture medium in controlled atmosphere and at constant temperature (T=37°C, 5% CO_2). The cells are seeded in a multiwell plate so to have ~ 30000-50000 cells per well. Then, different amounts of peptide are added to the different wells. A typical treatment scheme is represented in Figure 3.11. After 24 hours of treatment, the culture medium is removed and each well is treated with a solution of MTT. Only the viable cell are able to transform the MTT to formazan, thanks to the succinate dehydrogenase enzyme. After 1 hour of treatment, the solution with the unreacted MTT is removed and each well is filled with DMSO, which has the

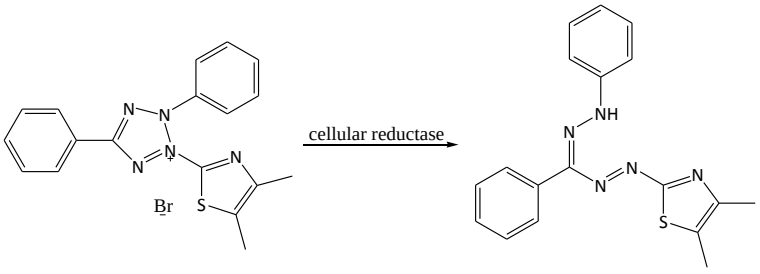

Figure 3.10 The reaction the leads to the formation of the violet formazan salt from the MTT molecule.

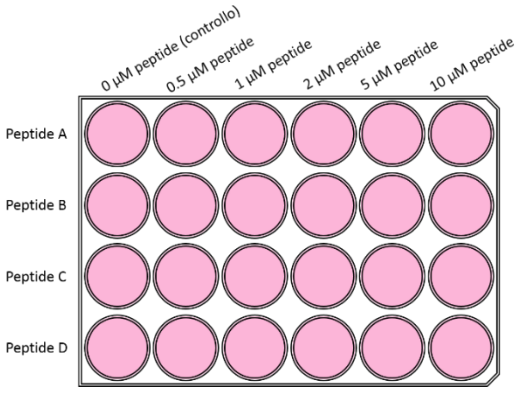

Figure 3.11 An example of the usage of a multiwell plate for a MTT assay.

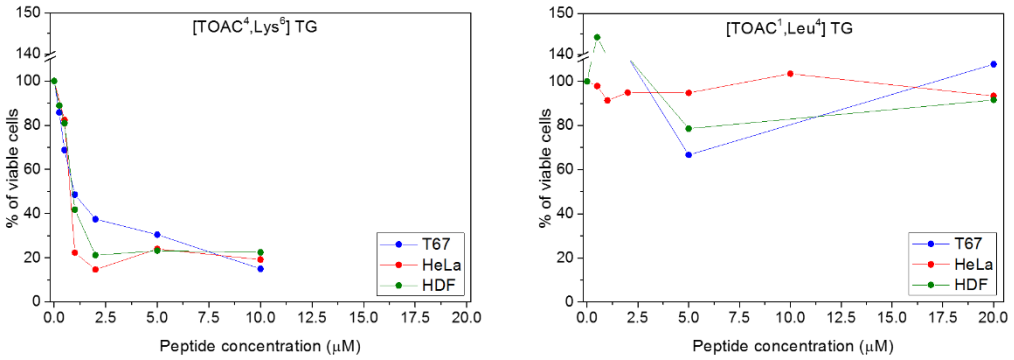

Figure 3.12 Two MTT toxicity curves of two peptides against three cell lines. [TOAC^4, Lys^6] TG is highly toxic against all cell lines, while [TOAC^1, Leu^4] TG is always non-toxic.

double function of solubilizing the formazan salts and killing all residual viable cells to avoid any further reaction. Finally, the absorbance at λ=570 nm is measured: it is directly proportional to the quantity of formazan, i.e. directly related to the viable cells present in the well. Then, the results are weighted to consider the absorbance of DMSO and normalized so the absorbance of the control wells is set to 100%. From the percentages of absorbance it is possible to draw toxicity curves, from which the EC_{50} is calculated; an example of the curves is reported in Figure 3.12. The EC_{50} is representative of the toxicity of the peptide: it is the concentration at which the measured absorbance is 50% of the absorbance measured in the control wells. In Table 3.2 the EC_{50} of all the studied TG analogs is reported. The sequence of the main isoform of trichogin GA IV showed moderate toxicity with EC_{50} values of 2, 8 and 4 μM for T67, HeLa and HDF cells, respectively. Surprisingly, the enhancement of the amphipathic character of the peptide with the introduction of charged residues in the hydrophilic face does not improve the toxicity significantly. The introduction of a single Lys at position 6 slightly improved the toxicity, while the introduction of two Lys at positions 5 and 6, or of a single Arg in positions 2 or 9, slightly lowered it. The substitutions in the structural/hydrophobic face of the peptide, introducing a Leu in place of an Aib in position 4 or 8, had a more dramatic effect, completely abolishing the cytotoxic activity of the peptides up to 20 μM. From the point of view of selectivity, the best results were obtained with the introduction of the charged amino acid Api at position 4 or 8. Api conferred to the TG sequence a selective toxicity against T67 cells, in fact no cytotoxic effects were observed on the other two lines.

Concerning the influence of TOAC on TG analogs toxicity, we observe that the radicalic amino acid TOAC in position 1 is an optimal probe since its insertion has almost no influence on the toxicity of the TG analogs. TOAC in position 8 also did not alter the toxicity of the corresponding analog without the sin label. [TOAC^4] TG represents the only exception since it is completely non-toxic. As can be easily observed,

Table 3.2 Toxicity of all the studied peptides, expressed as EC_{50} (μM). Peptides that were non-toxic at up to 20 μM are reported as n.t. (non-toxic). The EC_{50} values have an average error of about ±2 μM.

Peptide	EC_{50} (μM)			Peptide	EC_{50} (μM)		
	T67	HeLa	HDF		T67	HeLa	HDF
TG	2	8	4	[TOAC^1, Arg^9] TG	8	5	8
[TOAC^1] TG	1	3	5	[Lys^{5,6}] TG	7	10	15
[TOAC^8] TG	4	4	7	[TOAC^1, Lys^{5,6}] TG	10	6	15
[Lys^6] TG	4	2	2	[TOAC^1, Api^4] TG	8	n.t.	n.t.
[TOAC^1, Lys^6] TG	1	3	5	[Api^8] TG	13	n.t.	n.t.
[TOAC^4, Lys^6] TG	2	3	6	[TOAC^4] TG	n.t.	n.t.	n.t.
[TOAC^8, Lys^6] TG	2	3	5	[Leu^4] TG	n.t.	n.t.	n.t.
[Arg^2] TG	8	4	8	[TOAC^1, Leu^4] TG	n.t.	n.t.	n.t.
[TOAC^1, Arg^2] TG	8	9	15	[TOAC^1, Leu^8] TG	n.t.	n.t.	n.t.

position 4 is a key position to influence the behavior of TG and its analogs; this aspect will be discussed more extensively later. We chose to use mainly the analogues bearing the TOAC residue at position 1 for both CD and EPR experiments, since the insertion of the spin labelled amino acid TOAC at position 1 did not significantly influence the cytotoxicity in any of the analogs with respect to the same analogs without the spin label, as previously observed for the bioactivity of other peptides [88]. In light of the MTT assay results, we decided to focus our attention, for the spectroscopic studies, on four peptides that are representative of the different behaviors displayed by the peptides towards the cells. [TOAC^1] TG as the reference peptide. [TOAC^1, Leu^4] TG that shows no toxicity. [TOAC^1, Lys^6] TG that is the most toxic peptide on all the cell lines. [TOAC^1, Api^4] TG that has a selective toxicity. Finally, the analogues labelled with FITC could not be reliably tested on cell viability since the label interferes with the MTT assay.

3.3.2 Quantification of cell membrane constituents

As described in paragraph 1.2.1, membrane composition is an important aspect to take into account to understand the binding propensity and behavior of peptides. We focused on two components that are most extensively considered to influence peptide-membrane relationship, phosphatidylserine (PS) and cholesterol. Indeed, the amount of PS and cholesterol in the plasma membrane has been suggested to partake in the selectivity of AMPs towards tumor cells [116]. The negative charge of PS exposed on the outer leaflet favors the binding of positively charged peptides to the membrane,

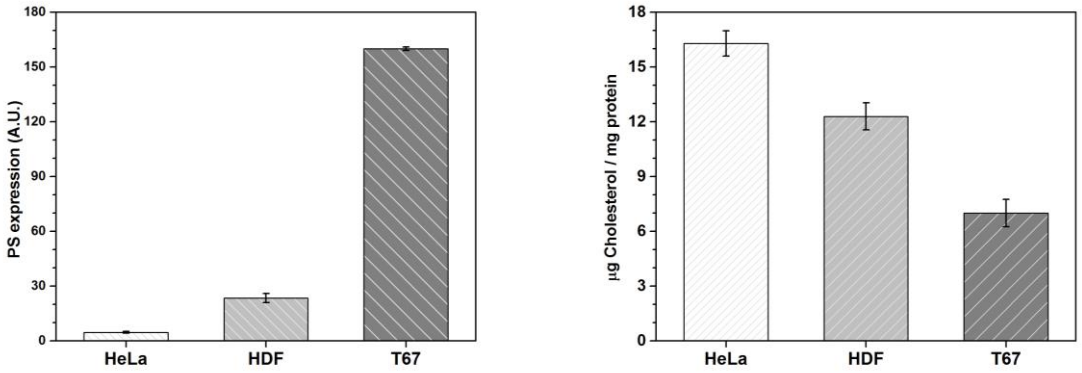

Figure 3.13 Left, Annexin V assay to quantify the amount of PS exposed on the outer cell membrane. Right, cholesterol content assay, quantifying the total cellular cholesterol. The error bars are relative to the standard deviation of three repeated experiments.

while cholesterol, altering the membrane fluidity, can interfere with the peptide binding. In particular, regions rich in cholesterol, such as lipid rafts, are more rigid, with the lipids being in a liquid-ordered phase rather than in the liquid crystalline (fluid) phase [152-154]. We tested the different cell lines for the exposition of phosphatidylserine (PS) on the membrane surface and for their total amount of cholesterol. It has to be noted that the ratio between intracellular and membrane cholesterol levels do not vary significantly between cell lines [155], therefore the total amount of cholesterol reflects directly its abundance on the membrane surface. The details of both assays are reported in the *Experimental details* section.

As shown in Figure 3.13, the three cell lines are characterized by significantly different compositions of the outer surface of the plasma membrane. T67 cells have high negative surface charge (high PS expression on the outer membrane leaflet) and low cholesterol levels, a composition that is typical of tumor cells. HeLa, although transformed cell line, have high cholesterol levels and low negative charge. HDF has an in-between profile. A fourth cell line, 769P (a kidney tumor), was acquired and MTT assays started also on this cell line. It displayed in-between values for PS expression and cholesterol quantity; moreover, the MTT assays of some peptides on 769P showed no difference in toxicity with respect to the other three cell lines. Therefore, we decided to focus the experimental efforts only on the three cell lines that are reported in Figure 3.13.

3.4 Structural characterization

3.4.1 Circular Dichroism

The secondary structure of all the peptides have been studied by far-UV CD in methanol and in SDS micellar environment. CD is based on the interaction of a chiral sample with a linearly polarized light. A linearly polarized light can be expressed as the vector sum of a right-handed and a left-handed component of a circularly polarized light; these two components (E_R and E_L) have the same amplitude and are in-phase. Being itself chiral, the circularly polarized light interacts with optically active chiral molecules. The two components E_R and E_L are absorbed differently, E_R and E_L after interacting with a chiral sample have different amplitudes, and the light becomes elliptically polarized. The measure of this difference in absorbance (ΔA) is expressed as degree of ellipticity, that is related to the difference of absorbance with the relation $\theta = 33 \cdot \Delta A$. θ has positive values if $E_R > E_L$, while it has negative values for $E_R < E_L$. The molar ellipticity $[\theta]$ is the ellipticity normalized for the sample concentration (c, in mol/L) and the cell optical path (l, in cm): $[\theta] = \theta/(c \cdot l)$. The variation of $[\theta]$ varying the incident wavelength λ, caused by the variation of ΔA, gives the CD spectrum. CD is often used to investigate the secondary structure of proteins and peptides. Indeed, the far-UV spectrum of a polypeptide chain has a typical fingerprint lineshape that allows to distinguish helices, β sheets and random coils [156]. The random coil conformation has a negative maximum at $\approx$ 200 nm and a weak maximum at $\approx$ 220 nm. β structures present an intense

Table 3.3 R value of peptides in MeOH and SDS environment. The symbol – indicates that measurements are still in progress due to experimental issues. Peptides concentration 10^{-4} M. SDS concentration 0.1 M. ([a]) data taken from [2]. (--) experimental data not available / still in progress.

Peptide	$R = [\theta]_{222}/[\theta]_{208}$		Peptide	$R = [\theta]_{222}/[\theta]_{208}$	
	MeOH	**SDS**		**MeOH**	**SDS**
TG	0.2	0.5	[TOAC^1, Arg^9] TG	0.4	0.6
[TOAC^1] TG	0.3	0.6	[Lys^{5,6}] TG	0.5	0.5
[TOAC^8] TG	0.5	0.7	[TOAC^1, Lys^{5,6}] TG	0.6	0.8
[Lys^6] TG	0.5[a]	0.5[a]	[TOAC^1, Api^4] TG	0.5	0.6
[TOAC^1, Lys^6] TG	--	--	[Api^8] TG	0.4	0.4
[TOAC^4, Lys^6] TG	0.5	0.7	[TOAC^4] TG	--	--
[TOAC^8, Lys^6] TG	--	--	[Leu^4] TG	0.3	0.6
[Arg^2] TG	0.4	0.6	[TOAC^1, Leu^4] TG	0.4	0.7
[TOAC^1, Arg^2] TG	0.3	--	[TOAC^1, Leu^8] TG	0.2	0.7

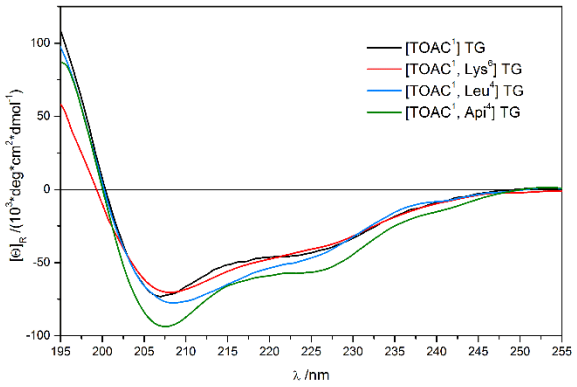

Figure 3.14. Far-UV CD spectra of [TOAC^1] TG, [TOAC^1, Api^4] TG, [TOAC^1, Lys^6] TG and [TOAC^1, Leu^4] TG in $2 \cdot 10^{-4}$ M POPC SUV. Peptide concentration, 10^{-4} M.

maximum at ≈ 195 nm and a negative maximum of medium intensity at ≈ 218 nm. α-helices have an extremely intense maximum at ≈ 192 nm and two negative maxima at ≈ 208 and 222 nm of about the same intensity. For all the analogues, in the CD spectra we can observe two negative Cotton effects at 204-206 nm and 220-224 nm and a positive Cotton effect at about 195 nm, features typical of right-handed helix conformations. The first two negative maxima are related to the parallel component of the π⟶π* transition and to the n⟶π* transition of the peptide chromophore, while the positive maximum is related to the perpendicular component of the π⟶ π* transition [157]. An estimation of the helical type (whether 3_{10} or α) can be achieved by the measurement of the ratio of the two negative maxima [157-159] of the ellipticity, R= $[\theta]_{222}/[\theta]_{208}$. In the spectra registered in methanol this parameter ranges from 0.2 to 0.6, indicating that the peptides adopt mostly a well-established 3_{10}-helix. In SDS solution, the experimental R value increases for almost all of the peptides, ranging from 0.4 to 0.8. These values are consistent with the presence of a prevalent α-helical conformation. Moreover, a large change in R upon changing the solvent indicates that the structure of the peptide is able to flip from 3_{10} to α helix. The values of R calculated for all peptides in the two environments are reported in Table 3.3.

In addition the CD spectra of four analogs (see paragraph 3.3.1) were recorded in a model membrane composed by 1-palmitoyl-2-oleoyl-*sn*-glycero-3-phosphocholine (POPC) at a peptide/lipid ratio of 1/20 (Figure 3.14). The shape of the CD spectra are all consistent with the presence of a well-developed, right-handed, mixed 3_{10}/α-helical conformation in membrane (R≈0.6). Therefore, it can be safely concluded that the helical conformation is conserved in phospholipid bilayers. This result will be exploited to interpret some of the findings of the EPR spectroscopy (see paragraph 3.5.2) and to perform the calculation of the amphipathic moment of the TG analogs, as will be discussed in the next section.

3.4.2 Hydrophobicity ‹H› and hydrophobic moment μ

Useful structural parameters to understand the peptide-membrane interaction are the mean hydrophobicity (‹H›) and hydrophobic moment (μ). They are widely used to characterize peptide sequences [1,10]. ‹H› depends only on the primary sequence and is higher for more hydrophobic peptides, while μ depends on the peptide secondary structure and is directly proportional to the amphipathicity.

From the individual H values, the mean hydrophobicity per residue is calculated as the mediated hydrophobicity of all the amino acids of a peptide sequence:

$$\langle H \rangle = \left(\sum_{i=1}^{N} H_i \right) \Big/ N \qquad \text{Equation 19}$$

where H_i is the hydrophobicity of the amino acid and N the number of the residues of the peptide. Since amphipathicity and helical secondary structure are considered of primary importance to predict the behavior of AMPs, the hydrophobic moment μ was introduced to rationalize and quantify the amphipathicity of peptides. Assuming a helical secondary structure, μ is defined by following the relationship [59]:

$$\mu = \left\{ \left[\sum_{i=1}^{N} H_i sin(\delta_i) \right]^2 + \left[\sum_{i=1}^{N} H_i cos(\delta_i) \right]^2 \right\}^{1/2} \Big/ N \qquad \text{Equation 20}$$

where H_i is the hydrophobicity of the amino acid n and δ_i is the angle at which successive side chains emerge from the backbone when the helix is viewed down its axis. A geometric representation of μ is given in Figure 3.15, where each H value is represented as a red vector pointing in the direction of the corresponding side chain, and the vector sum of all H vectors, represented as a blue arrow, is the final μ value.

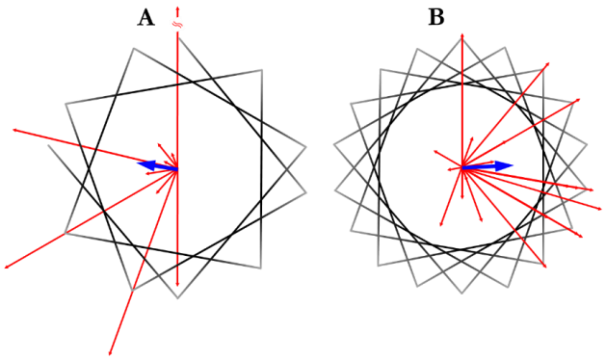

Figure 3.15 Schematic representation of the helical wheel of trichogin (A) and magainin 2 (B). For each residue is reported the vector associated to its hydrophobicity. Their vector sum is the hydrophobic moment, represented as a blue arrow.

Hydrophobic interactions play an important role in the affinity of peptides for the phospholipid bilayer of biological membranes, so it is reasonable to seek correlations between the mean hydrophobicity of a peptide and its activity towards membranes and cells. However, the estimation of the propensity of peptides and protein to move to a hydrophobic phase is not trivial, and since the middle 1980s nearly two hundred t heoretical or experimental hydrophobicity scales of coded amino-acids have been developed, each one considering different peculiar characteristics. In 1984, D. Eisenberg reviewed the existing hydrophobicity scales [160], pointing out the difficulty to make a rational comparison between them. He then proposed a new scale, called Normalized Consensus Scale (NCS), that was designed to mitigate the effect of the outlier values of four different existing scales: (1) von Heijne scale [161], that performed a theoretical calculation on the octanol-water partition coefficient; (2) Janin scale [162], that measured the insertion depth of the residues in globular proteins; (3) Chothia scale [163], that, similarly to Janin scale, observed the distribution of amino-acids side chains between the surface and the interior of a protein; (4) Wolfenden scale [164], that is an experimental measure of the ΔG of transfer of an amino-acid from water to a hydrophobic phase. The NCS became one of the most exploited to calculate the mean hydrophobicity of peptides. Lately, an extensive work by Tossi & Sandri [10,165,166] developed the new Combined Consensus hydrophobicity Scale (CCS) based on a set of 195 scales present in the literature, determined with theoretical, statistical and experimental methods. CCS defines the hydrophobicity of the amino acids in a scale from -10 (Arg, considered the most hydrophilic among standard amino-acids) to +10 (Phe, considered the most hydrophobic amino-acid) and it has been widely used [167,168] to calculate the hydrophobicity of antimicrobial peptides because it firstly included non proteinogenic amino acids, as the frequently occurring Aib. However, the CCS scale does not include the amino acids Api and TOAC, present in our analogs. Additionally, TG and its derivatives are characterized by peculiar N- and C-terminal groups (1-Oct and Lol, respectively) that are fundamental for the cytotoxic effect and are also not included in the list. Therefore, in order to exploit this tool for the TG analogs synthesized during this project, it was necessary to calculate the hydrophobicity values for the missing residues. Exploiting the good correlation [166] of the CCS scale

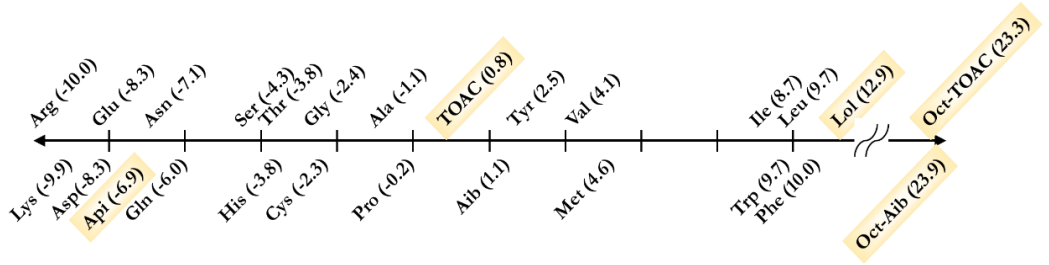

Figure 3.16 The hydrophobicity scale used in this work (see text). Values highlighted in yellow have been calculated in this work for the first time.

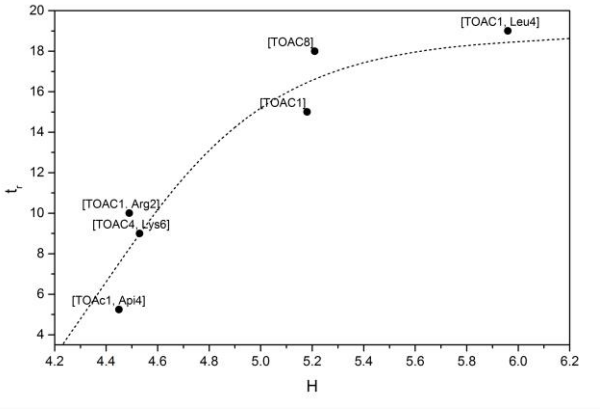

Figure 3.17. Calculated H of some TG analogs plotted against their retention times on reverse phase HPLC. Eluant system: solvent A, H_2O/CH_3CN 9:1 + 0.05% TFA; solvent B, CH_3CN/H_2O 9:1 + 0.05% TFA; gradient 60-100% B in 30 mins; Phenomenex C18 Jupiter 300A column.

with the octanol/water partition coefficient (logP) for N-acetylated and C-amidated residues, we calculated logP as the average of the slightly different values obtained from different software (Kowwin v. 1.68 and ChemDraw v. 9.0) and extrapolated H values on the CCS scale (for the details, see *Experimental details* section). The obtained values, along with the H values of the residues already present in the original work, are reported in Figure 3.16. Given the extremely high hydrophobicity of the alkylic chains, the residues that include the octanoyl chain at the N-terminus have H values that widely exceed the value +10 of Phe. The obtained ‹H› values for the peptides are reported in Table 3.4 together with the values of their hydrophobic moment. The validity of the calculated ‹H› values has been confirmed by comparison with the retention times in reverse phase HPLC of a selection of peptides (see Figure 3.17). It should be stressed

Table 3.4 H and μ values for all the studied TG analogs.

Peptide	‹H›	μ	Peptide	‹H›	μ
TG	5.23	3.09	[TOAC^1, Arg^9] TG	4.49	3.75
[TOAC^1] TG	5.18	3.08	[Lys^{5,6}] TG	3.87	3.96
[TOAC^8] TG	5.21	3.08	[TOAC^1, Lys^{5,6}] TG	3.81	3.95
[Lys^6] TG	4.55	3.63	[TOAC^1, Api^4] TG	4.45	2.43
[TOAC^1, Lys^6] TG	4.49	3.61	[Api^8] TG	4.50	2.82
[TOAC^4, Lys^6] TG	4.53	3.60	[TOAC^4] TG	5.21	3.07
[TOAC^8, Lys^6] TG	4.53	3.61	[Leu^4] TG	6.01	3.83
[Arg^2] TG	4.54	3.78	[TOAC^1, Leu^4] TG	5.96	3.82
[TOAC^1, Arg^2] TG	4.49	3.77	[TOAC^1, Leu^8] TG	5.96	3.51

that the retention times of the peptides in closely linked to the elution conditions that have been properly chosen in order to elute peptides with very different hydrophobicity with the same column in the same conditions. Therefore, a linear correlation between ‹H› and retention times should not be expected: it is sufficient that peptides with increasing hydrophobicity display higher retention times. In the calculation of μ, given the results of CD spectra in SUV (Figure 3.14), we used an angle of 100°, typical of an α-helical structure, for all the peptides. Indeed, it was previously reported [16] that the 3_{10} portion of the TG helix is confined to the 1-3 resides at the N terminus. Using an angle δ_n of 120° (typical of the 3_{10} helix) for those amino acids leads to no significant difference in the final value of μ. The values of μ are reported in Table 3.4. TG analogs with hydrophobic substituents (Leu in position 4 or 8) are more hydrophobic than TG, while all the other analogs, carrying one or two positive charges, have a minor H value. All the analogs with an enhanced amphipathicity have a higher μ value than TG. The only analogs with a minor hydrophobic moment are Api-bearing analogs, since they have a charged residue in the hydrophobic face.

3.4.3 Structure-activity relationship

The overall results of the MTT assay (Table 3.2) made clear that a subtle equilibrium exists between the physico-chemical and structural parameters of the analogues and their cytotoxicity. To investigate and rationalize, we plotted ‹H› against μ in the so-called Eisenberg plot (Figure 3.18) for all the analogues. This plot has been created in the middle 1980s to categorize proteins depending on their surface-seeking propensity [160]: indeed, it was observed that proteins or peptides from fragments of proteins have different combinations of ‹H› and μ values depending on their propensity to seek the aqueous phase, to assume a globular structure, or to locate transmembrane. Since then, parameters as ‹H›, μ, amphipathic angle, net charge, secondary conformation have been studied in detail in search of a correlation between at least some of them and peptide activity [1]. One graphical tool that was often employed to seek these correlations is the Eisenberg plot. Unfortunately, cytotoxic peptides can be hardly distinguished from inactive ones only on the basis of their plot localization [1,169] due to the complex interplay between the many structural and chemical parameters that govern their behavior. This may be due to the fact that the Eisenberg plot has been generally used to seek correlations between a large variety of peptides with very different structures, lengths etc.; therefore, small, but significant, variations may be hard to detect. On the contrary, our TG analogs are similar to each other, and the small variations in ‹H› and μ become readily visible. Indeed, for our TG analogues, the plot clearly shows that there is a good linear correlation (R=0.94) between ‹H› and μ for all the cytotoxic peptides, while the other peptides fall in other regions of the plot. An exception is represented by

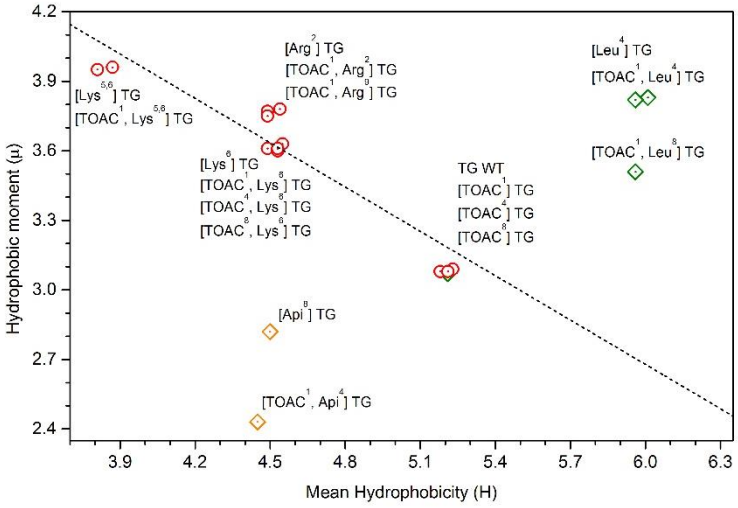

Figure 3.18. Eisenberg plot for the TG analogues studied in this work. Cytotoxic peptides are represented in red circles; non-toxic peptides in green diamonds and selective peptides in yellow triangles. The dashed line indicates the linear correlation between μ and ‹H› of the toxic TG analogues.

[TOAC^4] TG, since it is non-toxic but has the same ‹H› and μ values as [TOAC^1] TG and [TOAC^8] TG. It is interesting to note that the peptides carrying the Aib-to-Api substitutions (the selective peptides) are out from the linear correlation of the plot and fall in a region that is diametrically opposed to that occupied by the inactive Aib-to-Leu substituted analogues. This observation suggests that only particular pairs of ‹H› and μ values result in fully active peptides. In particular, the substitutions that overly enhance the total hydrophobicity result in activity loss, while substitutions that only decrease the hydrophobic moment, perturbing the hydrophilic-hydrophobic balance, induce a selective toxicity towards a specific cell line. It is important to note that both selective peptides have positive charge in the hydrophobic side of the helix; they are only toxic towards T67 cancer cells, i.e. the cell line that showed the highest quantity of the negatively charged PS in the surface. Moreover, non-toxic peptides carry hydrophobic substitutions in the same positions of the sequence. Then, it may be deduced that charges act as leading force for the activity of these peptides; additionally, the structural sector appears to be remarkably important, as small variations on it result in great modification in peptides activity. These aspect will be studied in more details in the next sections.

Thereby, we observed that modifications, especially those occurring on the structural sector, might have a strong impact on both toxicity and selectivity of the different peptides. Moreover, the Eisenberg plot revealed to be a useful tool that highlighted a correlation between structural parameters and TG analogs activity. Thus, even though it cannot provide alone a quantitative explanation for peptides cytotoxicity, it can be exploited for the design of the modification of new analogs.

3.5 Characterization of the peptide-membrane interaction

3.5.1 Fluorescence microscopy

Two TG analogs were modified at position 11 with the fluorescent probe FITC (TG-FITC and [Lys^6] TG-FITC). These peptide are used to observe the localization in HeLa cells. The cells were treated for 3 hours with the peptides at a final concentration of 0.5 μM; the green signal of the FITC, at λ = 545 nm, was observed with a fluorescence microscope, further details are described in the *Experimental details* section. The micrographs reported in Figure 3.19 show that the fluorescence is mainly located in the outer plasma membrane, accordingly to the hydrophobic nature of the TG analogs. Cells treated with TG-FITC appear mostly intact, as could be expected since the TG analog lacks of the C-terminal amino alcohol, that is required for the cytotoxicity [78]. On the other hand, [Lys^6] TG-FITC induces a visible membrane lysis; we speculate that, since TG analogs with lysine in position 6 are the most toxic, this modification is able to counterbalance the lack of the C-terminal alcohol. Cells treated with TG-FITC and [Lys^6] TG-FITC were also stained with rhodamine that is known to localize in

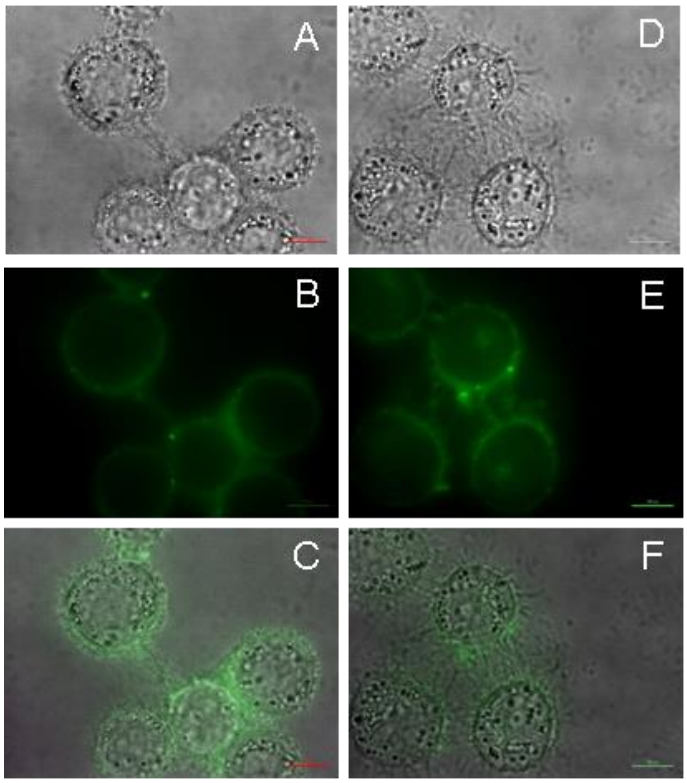

Figure 3.19 Fluorescence microscopy of HeLa cells treated with 0.5 μM of TG-FITC conjugate analogs for 3 hours. Panels A and D refer to the bright field images in the presence of [FITC^{11}] TG and [Lys^6, FITC^{11}] TG respectively. Panels B and E refer to the green fluorescence images in the presence of [FITC^{11}] TG and [Lys^6, FITC^{11}] TG respectively. Panels C and F refer to the merging of bright and fluorescence fields.

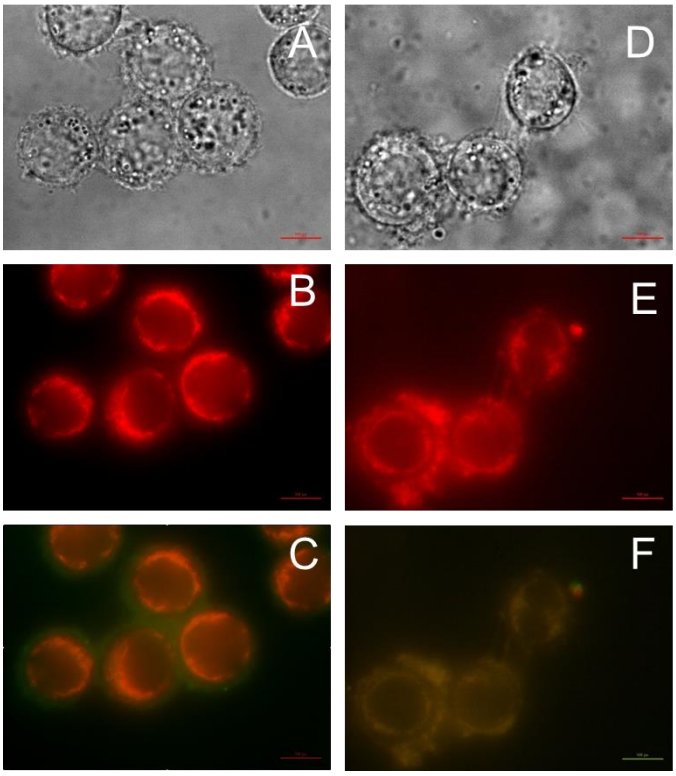

Figure 3.20 Fluorescence microscopy of HeLa cells treated with 0.5 μM of TG-FITC conjugate analogs for 3 hours and, subsequently, with rhodamine. Panels A and D refer to the bright field images in the presence of [FITC[11]] TG and [Lys[6], FITC[11]] TG respectively. Panels B and E refer to the red fluorescence images in the presence of [FITC[11]] TG and [Lys[6], FITC[11]] TG respectively. Panels C and F refer to the merging of red and green fluorescence fields.

mitochondria. The micrographs, shown in Figure 3.20, confirm that in the case of treatment with TG-FITC, that does not damage the cell membrane, there is no colocalization of the two fluorescent probes: FITC is located only on the outer cell membrane, while rhodamine in located only in mitochondria. Conversely, since HeLa cells membranes are severely damaged by [Lys[6]] TG-FITC, the intracellular material leaks outside the cells and the two probes are dispersed in the same areas.

3.5.2 Electron Paramagnetic Resonance

3.5.2.1 TG analogs in model membrane systems

We recorded cw EPR spectra of all the spin labeled analogs in POPC (1-palmitoyl-2-oleoyl-sn-glycero-3-phosphocholine) model membranes in HEPES buffer at pH=7.0, at a P/L of 1/100. The SUV diameter has been checked for different samples by dynamic light scattering measurements and has always found to be 40-60 nm. These conditions were chosen to resemble the conditions used to perform the CD

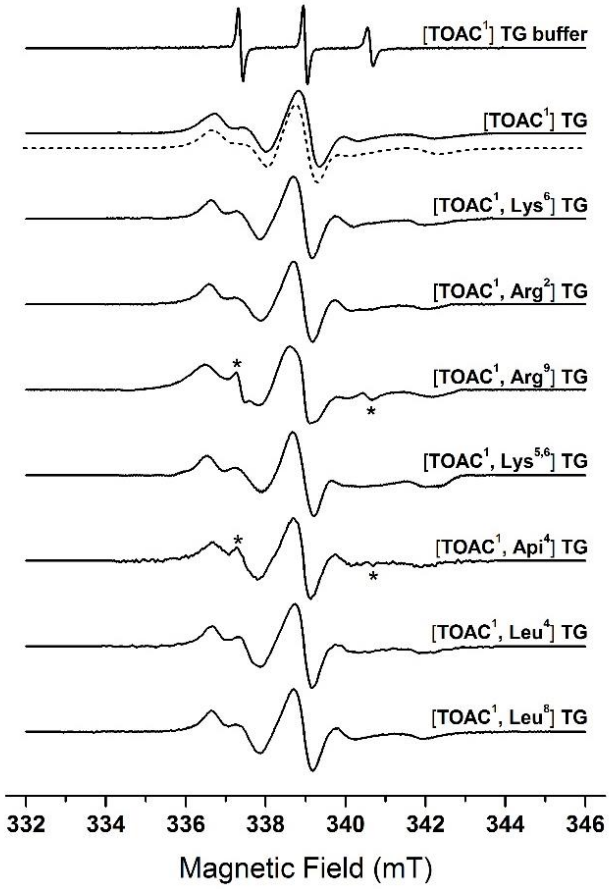

Figure 3.21 EPR spectra of the TOAC-labeled TG analogs interacting with POPC SUV. In dashed line the simulation of the spectrum of [TOAC^1] TG. P/L ratio 1/100, HEPES buffer pH=7.0. All spectra have been normalized to unit intensity for convenience. The asterisks indicate the spectral contributions of the small fraction of peptides in solution.

experiments. The EPR spectra of all the labeled peptides recorded at these conditions are reported in Figure 3.21. All spectra exhibit a broad lineshape, indicative of the slow motion (on the EPR timescale) of the nitroxide bound to a peptide that is located almost 100% in the membrane. For comparison, the top part of Figure 3.21 reports the spectrum of [TOAC^1] TG in buffer: it shows three sharp lines typical of a fast-moving peptide in aqueous solution. The EPR spectra of [TOAC^1, Api^4] TG and [TOAC^1, Arg^9] TG show additional contributions indicative of the presence of fast moving peptides (less than 1% of the total spins). It has previously been explained that the mobility of the nitroxide strongly influences the spectral lineshape: since all spectra have almost the same lineshape, there are no variation in the dynamics of the different analogs when bound to the membrane. Then, only the spectrum of [TOAC^1] TG was simulated to determine the peptide dynamics that is quantitatively expressed by the isotropic rotational correlation time, τ. A τ value of $\approx$ 9 ns was obtained. The details of the simulations are reported in the *Experimental details* section.

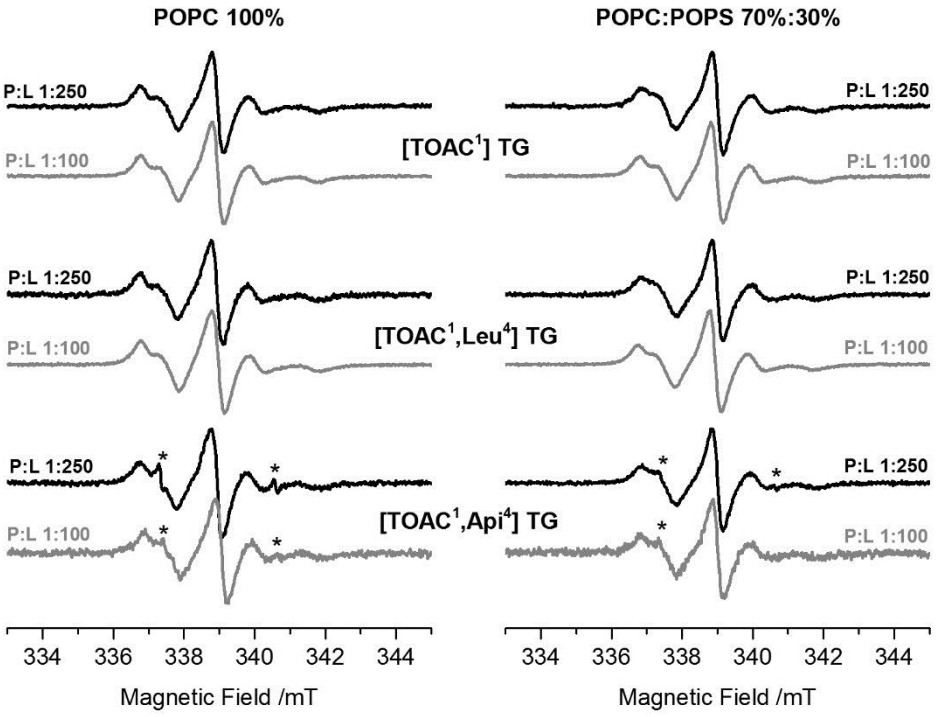

Figure 3.22 EPR spectra of the three tested peptides in POPC vesicles (left) and POCP/POPS 7/3 vesicles (right) at two different peptide/lipid ratio (black lines, 1/250; grey lines, 1/100). Buffer HEPES, pH = 7.0, T = 308 K.

We then performed further measurements with some spin labeled TG analogs with significantly different activity ([TOAC^1]TG is the reference peptide, [TOAC^1, Leu^4]TG is non-toxic, and [TOAC^1, Api^4]TG is the only labeled peptide with selective toxicity). Their binding and mobility were tested on model membranes of different compositions and in different solvent conditions to verify if these parameters can influence the binding propensity of different peptides. We used SUV of POPC as a model membrane for zwitterionic eukaryotic cells, and POPC/POPS (1-palmitoyl-2-oleoyl-sn-glycero-3-phospho-L-serine) in 7/3 molar ratio as a model for the negatively charged bacterial and cancer cells such as the T67 cell line. The SUV diameter has been checked also for POPC/POPS vesicles and has been found equal to that of POPC vesicles. The three peptides were added to SUV in a peptide/lipide (P/L) ratio of 1/100 and 1/250; the complete set of measurements was performed in both HEPES (4-(2-hydroxyethyl)-1-piperazineethanesulfonic acid) buffer with zero salts at pH=7.0 and in PBS (phosphate buffered saline) buffer at pH=7.4. The EPR spectra, recorded at a constant temperature of 308 K in HEPES buffer, are shown in Figure 3.22. All peptides bind with high affinity (>99%) to both types of membranes and in each buffer, and the slight differences shown by some spectra are negligible.

3.5.2.2 TG analogs in reconstituted cell membranes

We performed EPR measurements in conditions similar to the physiological environment has been the preparation of reconstituted cell membranes. These systems are prepared by centrifuging the cells at proper experimental conditions to isolate a fraction containing mainly the plasma membrane and some intracellular material, such as nuclei; the fraction is mechanically stressed and resuspended in the desired buffer. The details of the preparation of these samples are reported in the *Experimental Details* section. The EPR experiments were performed on reconstituted membranes, the diameter of which was checked with dynamic light scattering, obtaining a mean diameter of ≈ 400 nm with a broad distribution for reconstituted membranes derived from T67 and HeLa cell lines. Some samples were also sonicated, obtaining a smaller, more homogeneous diameter of ≈ 100 nm. We did not observe any difference in the EPR spectra depending on the diameter of the reconstituted membranes, therefore we focused our experiments on the samples without sonication.

First, four peptides were chosen to observe their interaction in reconstituted T67 membranes at the two P/L ratio that were used also in the SUV experiments. The four chosen peptides were [TOAC^1] TG as the reference peptide, [TOAC^1, Leu^4] TG as a non-toxic peptide, [TOAC^1, Api^4] TG since it is the labeled peptide that displayed selective toxicity, and [TOAC^4, Lys^6] TG as a highly cytotoxic peptide. For these samples, the P/L ratio must be estimated from the lipid content of the reconstituted membranes. The lipid content is estimated from the protein count, assuming a fixed protein/lipid ratio for the cell lines. The spectra of all peptides interacting with the membranes, along with their simulations, are reported in Figure 3.23. The amounts of peptide in the two phases (membrane and solution) are obtained from the relative contribution of each spectral component to the total area of the simulated spectrum. All of them show two spectral components, indicating that the TOAC-labelled peptides are only partially bound to the cell membrane. A P/L ratio of 1/250 is generally enough

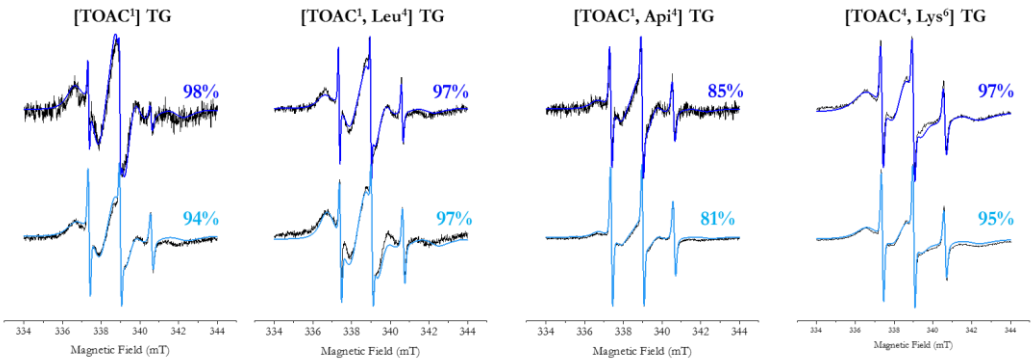

Figure 3.23 Simulation (colored lines) of the EPR spectra (black lines) of TG analogs interacting with reconstituted cell membranes from T67 cells at a P/L of 1/250 (blue lines) and 1/100 (light blue lines)

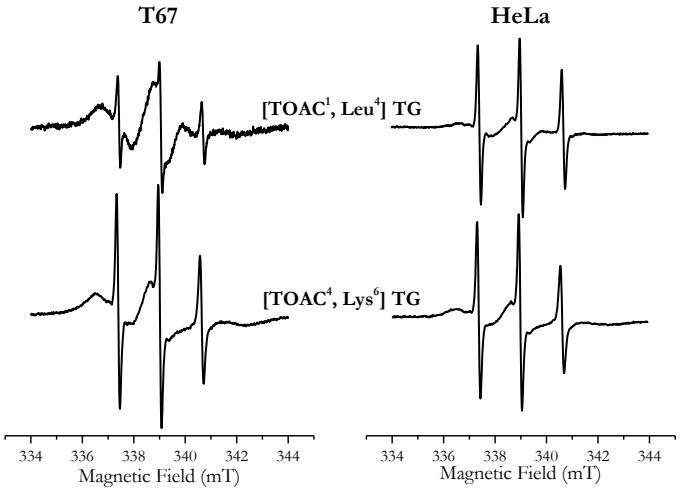

Figure 3.24 EPR spectra of TG analogs interacting with reconstituted cell membranes from T67 and HeLa cells at a P/L of 1/100.

to saturate the membrane, and the addition of more peptide to reach a P/L of 1/100 only leads to finding more peptides in solution. It can be noted that, in this case, [TOAC^1, Api^4] TG exhibits a lower affinity than the other TG analogs. While the other three peptides have binding percentages higher than 94%, only 85% of [TOAC^1, Api^4] TG is bound at P/L 1/250, and the value reduces to 81% at P/L 1/100.

We then performed the experiments on two peptides, one completely hydrophobic ([TOAC^1, Leu^4] TG), and one highly toxic and positively charged ([TOAC^4, Lys^6] TG), interacting with reconstituted membranes of HeLa cells, that have a considerably lower amount of exposed PS (see paragraph 3.3.2). The experimental spectra, shown in Figure 3.24, show that [TOAC^4, Lys^6] TG has almost the same affinity for the HeLa and T67 cells, while [TOAC^1, Leu^4] TG has a considerably minor affinity for HeLa cells relative to T67 cells. These differences are difficult to interpret, and cannot be directly correlated to the different charge exposed on the membranes surfaces, because the procedures of isolation of the membrane material and the subsequent sonication, may have led to membranes with very different composition with respect to the membranes of the corresponding viable cells. Indeed, often membranes are asymmetric, i.e. they have different composition on the inner leaflet with respect to the outer leaflet; an example is PS content, since it is usually over expressed on the outer leaflet of many cancer cells. With the membrane breaking and reconstitution, this asymmetry is lost. Therefore, although interesting, these experiments present the main disadvantage that the sample preparation leads to vesicles, the composition of which is not precisely determined, and could be altered by the presence of intracellular material. Therefore, we did not further pursue the experiments on these systems and preferred to develop an experimental procedure that allowed us to work directly with viable cells.

3.5.2.3 TG analogs in viable cells

We performed EPR experiments in viable cells of the three cell lines used for the MTT toxicity assay to assess the peptide dynamics and peptide binding to the cell membrane. We chose to use the four labeled TG analogs that were chosen also for CD measurements in model membranes: [TOAC^1] TG as the reference peptide; [TOAC^1, Leu^4] TG that shows no toxicity; [TOAC^1, Lys^6] TG that is the most toxic peptide on all the cell lines; [TOAC^1, Api^4] TG that has a selective toxicity.

We decided to perform EPR experiments in cells in the same experimental conditions of the MTT toxicity assays. The samples contain 25 nmol of peptides per million cells: this peptide-to-cell ratio is comparable to 2 μM concentration in the MTT assay. The spectra were recorded after 15-20 minutes of incubation of the peptide to the cell suspension. For further details on the preparation of the samples, see *Experimental Details* section. As for the experiments with reconstituted cell membranes, we faced the issue of estimating the P/L ratio to see whether the EPR experiments in viable cells can be compared to those in model membranes. The estimate was made for the HeLa cell line for which the cell volume has been measured, V~2.4·10^{-15} m^3 [170]. The average

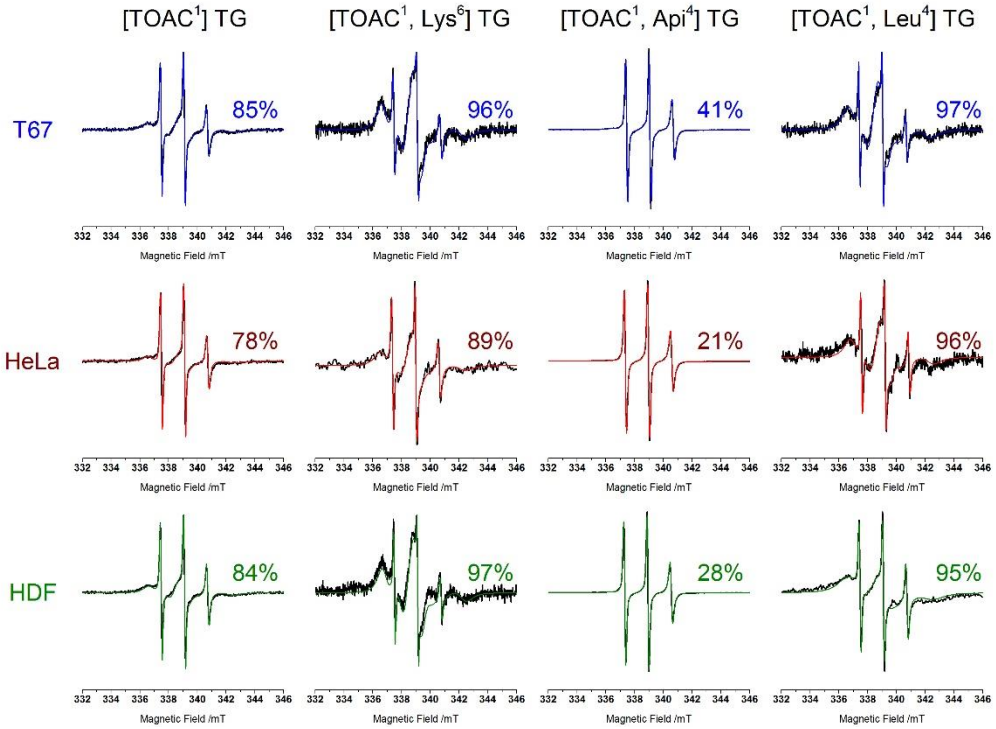

Figure 3.25 EPR spectra of selected TOAC-labeled TG analogs interacting with the different cell lines. Experimental spectra in black, simulations in colored lines. From left to right the different analogs; from top to bottom the different cell lines. For each spectrum is reported the percentage of the membrane-bound peptide as obtained from the simulations. Temperature 293 K, peptide to cell ratio: 25 nmol/10^6 cells. All spectra have been normalized to unit intensity.

area per lipid at 30 °C for choline headgroups (PC) is ~$6.5 \cdot 10^{-19}$ m^2 [171]. The cell number in each well of the MTT assay is ~40000 cells for 500 μL of buffer. Considering a spherical cell and a double layer of phospholipids and ignoring the protein content to get an upper limit of the estimate, there are ~$2.7 \cdot 10^9$ lipid molecules per each cell. Then the P/L ratio for the 1 μM concentration in the MTT assay is 3/1. This ratio is extremely high, and raises doubts on the reliability of the estimate. Nevertheless, it is clear that the experiments in cells and in model system cannot be directly compared. The concentration range to prepare a sample of a peptide with viable cells is extremely limited due to the concentration and time limits over which cells begin to precipitate; thus experiments with much lower P/L ratios (such as 1/100 or 1/250) are impossible to perform since the signal is below the detection limit of our instrument.

The spectra of all peptides interacting with the three cell lines, along with their simulations, are reported in Figure 3.25. All of them show two spectral components, indicating that the TOAC-labelled peptides are only partially bound to the cell membrane. The amounts of peptide in the two phases (membrane and solution) are obtained from the relative contribution of each spectral component to the total area of the simulated spectrum. Among the analogues, [TOAC^1, Lys^6] TG and [TOAC^1, Leu^4] TG show the largest percentages of bound peptide (≥90%), [TOAC^1] TG is slightly less bound to the cells (~80%), while [TOAC^1, Api^4] TG is mostly free in solution (<40% bound). Moreover, from the simulation was also obtained the rotational correlation time that for all spectra has a similar value of $\tau \approx 10$ ns, suggesting that there are no significant differences in dynamics neither between different analogues nor between different cell lines.

Considerations on the binding of peptides to model and cell membranes

EPR experiments in model and cell membranes were made after verifying by fluorescence microscopy that peptides locate in the cell membrane, without affecting nuclei or mitochondria, differently from the experimental evidence found on other AMPs [116].

The binding percentages of peptides towards HeLa cells are generally slightly lower than towards the other cell lines. This could be related to the membrane composition of HeLa cells, particularly rich in cholesterol, which is supposed to interfere with the peptide binding [153].

[TOAC^1, Api^4] TG displayed a very low level of binding for all the cell membranes, regardless its toxicity to them: this could be explained considering that it carries a positive charge in the structural region of the helix; this perturbation destabilizes the favorable interaction between the hydrophobic side of the peptide and the hydrocarbon region of the bilayer. Moreover, [TOAC^1, Api^4] TG is selectively toxic towards T67 cells,

where the binding is higher with respect to the other two cell lines. This higher binding can be explained by the higher negative charge on the membrane surface of T67 cells, that electrostatically interact with the positively charged Api.

The dynamics of all peptides bound to the different membranes are similar, as confirmed by the correlation times ($\tau \approx 8$-12 ns). The values of τ are almost identical in cells and POPC SUV, where the lipids are in the liquid crystalline phase. These results suggest that all peptides bind to zones of the plasma membrane having a high fluidity, thereby it is highly unlikely that they are embedded in lipid rafts, regions rich in cholesterol that are in a liquid-ordered phase [153,172].

The EPR results both in model and in cell membranes show that there is no apparent correlation between the amount of peptide binding and cytotoxicity since three of the four analogs (a non-toxic and two toxic analogs) show very high binding to the three cell lines, the exception being [TOAC^1, Api^4] TG. However, the results obtained for [TOAC^1, Api^4] TG suggest that even if the cytotoxicity cannot be directly related to the affinity of the peptide for the membrane surface, that regulates the level of binding, nevertheless a critical peptide concentration in the membrane must be reached to trigger toxicity and membrane lysis. Therefore, it can be deduced that a certain level of binding is required for peptides to exert their toxicity, but is not sufficient. Other factor must play a role, such as peptides penetration depth, that has been measured for our labeled TG analogs and will be discussed further below.

Evolution of EPR spectra of TG analogs in viable cells over 24 hours

The time evolution of some EPR spectra of peptides interacting with viable cells has been followed, to verify the lifetime of the nitroxide moiety in the cell suspension. Indeed, EPR experiments with cells are sometimes difficult to perform since nitroxides are quickly reduced to diamagnetic hydroxylamines by antioxidants present in the cytoplasm [173]. Then, if the nitroxides enters in contact with the cytoplasm, whether the peptides enter the cell or the cytoplasm leaks out, the EPR signal is expected to decay with time. Indeed, it has been previously reported [174] that when the TOAC amino acid is incubated with cell extracts under nearly "in-cell" conditions, it displays a half-life of only few minutes because it is quickly reduced by enzyme-mediated reactions. Figure 3.26 reports the evolution over time of two peptides ([TOAC^1, Leu^4] TG and [TOAC^1, Lys^6] TG) interacting with viable cells for over 24 hours, together with the total area of the spectra, expressed as a percentage of the area of the first collected spectrum.

All nitroxides consumed very slowly, with more than 80% of the spins still present after roughly 2 hours (see the inset in Figure 3.26). This confirms that the EPR signal of peptides in cells (as those reported in Figure 3.25) can be accumulated for several

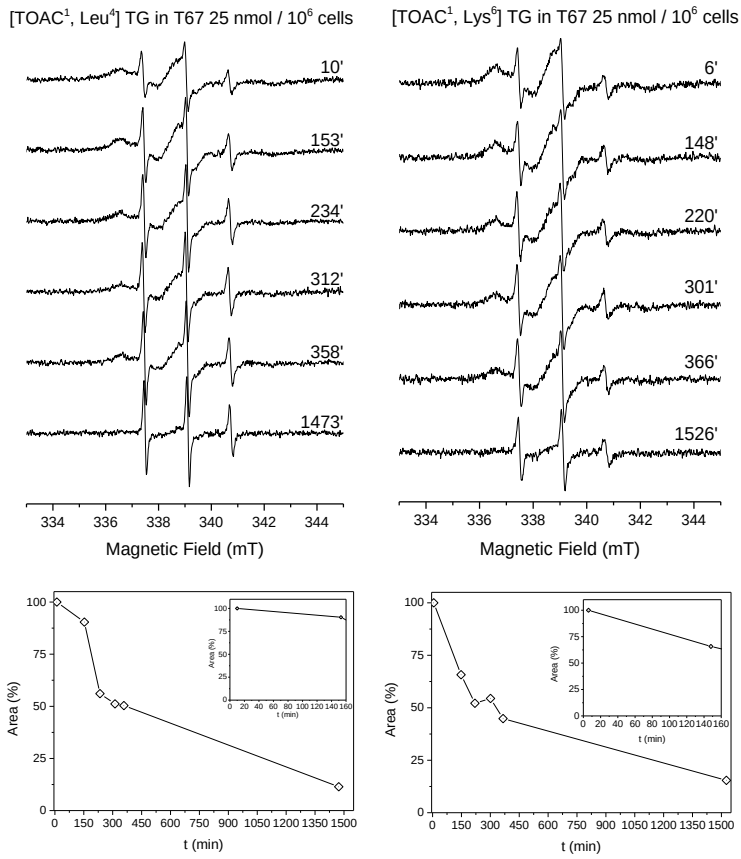

Figure 3.26 EPR spectra over time of three peptides interacting with T67 cells. On the top part, the spectra with the time, in minutes, at which the signals are collected after the addition of the peptide to the cell suspension. On the bottom part, the area of the spectra, expressed as the percentage with respect to the first collected spectrum; for each graph, it is also reported a zoom of the areas of the spectra collected in the first 160 minutes.

minutes after the addition to peptide into the cell suspension to improve S/N ratio without causing distortions due to nitroxide consumption.

After 24 hours, when the cells are certainly dead, the nitroxide is almost completely consumed (10-15%) for both peptides: this suggests that both toxic and non-toxic peptides are exposed to the cell antioxidants. The amount of residual signal after 24 hours is probably tied to the overall amount of antioxidants in the samples.

The rate of consumption is comparable for both peptides, a result that is puzzling considering that 1) [TOAC^1, Leu^4] TG is non-toxic while [TOAC^1, Lys^6] TG is above its EC50 value in the conditions of this experiment; 2) toxic peptides disgregate the cell membrane (see paragraph 3.5.1) releasing the antioxidant in solutions. We suggest that in both cases the TOAC labels in the peptides are protected from the action of the cytosolic antioxidants by being buried in the membrane (see the next paragraph). Nevertheless, further experiments need to be devised to further explore this aspect.

3.5.2.4 Immersion depth of TG analogs in model and cell membranes

The insertion depth of spin labeled TG analogs was measured to understand their exact location in model membrane of POPC SUV. We followed two approaches: 1) we measured all analogs labeled at position 1 to evaluate whether there are differences in insertion depth between them; 2) we chose two analogs and labeled all TOAC positions to determine the orientation of the helix in the membrane. We also started to perform the penetration depth experiments in viable cells.

The method for the measurement of the insertion depths, described in paragraph 1.3.5, is based on the dipolar interaction of a nitroxide with paramagnetic reagents that are differently soluble in aqueous and in lipid phase [17]. The measurements were conducted loading the sample in a gas-permeable TPX capillary first under oxygen flow, then under nitrogen flow, and finally adding a Ni(EDDA) solution to the sample under nitrogen flow. The samples are composed of TG analogs in POPC vesicles at a P/L ratio of 1/100, in consistency with the CD and the CW EPR experiments. The obtained depth parameters are reported in Table 3.5, along with those of the molecular ruler, for comparison.

Table 3.5 Depth parameters of the spin labelled TG analogs interacting with POPC SUV and, for comparison, of the spin labelled phospholipids used as reference. POPC vesicles concentration, 10 mM, P/L ratio 1/100. ([a]) Repeated measurements of TempoPC showed a large variability in Φ, but always lower than 0.3. ([b]) The apparent inversion of Φ is present also in the original paper [17].

Labelled peptides	Depth parameter Φ	Labelled phospholipids	Depth parameter Φ
[TOAC^{1}] TG	0.9	TEMPO PC	-0.1[a]
[TOAC^{4}] TG	2.9	5DPC	1.4
[TOAC^{8}] TG	1.4	7DPC	1.2[b]
[TOAC^{1}, Lys^{6}] TG	1.0	10DPC	2.1
[TOAC^{4}, Lys^{6}] TG	2.7	12DPC	2.4
[TOAC^{8}, Lys^{6}] TG	1.8	14DPC	3.0
[TOAC^{1}, Lys^{5,6}] TG	0.9		
[TOAC^{1}, Arg^{2}] TG	0.4		
[TOAC^{1}, Arg^{9}] TG	0.6		
[TOAC^{1}, Api^{4}] TG	1.3		
[TOAC^{1}, Leu^{4}] TG	1.3		
[TOAC^{1}, Leu^{8}] TG	0.9		

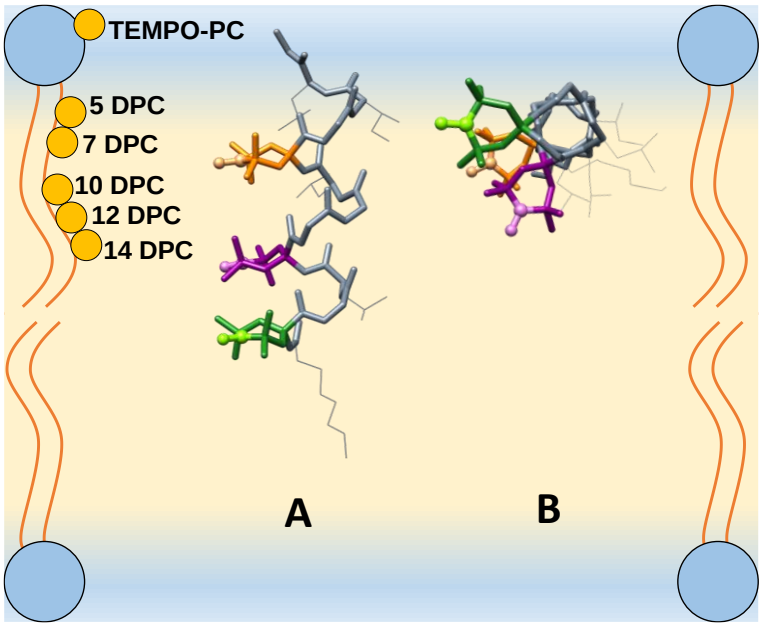

Figure 3.27 In-scale cartoon of two possible orientations of TG in a POPC bilayer at P/L ratio of 1/100: (A) TG inserted into the membrane; (B) TG parallel to the membrane. The peptide secondary structure is in agreement with crystallographic data [16], with the three TOAC labels added in positions 1 (green), 4 (purple) and 8 (orange). The other side chains are represented as thin sticks for clarity.

A first observation of the depth parameters Φ allows to note that for almost all the TG analogs, the TOAC in position 1 locates at the same depth. The only exception is represented by analogs with an Arg residue, whose nitroxide is closer to the aqueous phase with respect to the other analogs. This is probably due to the combined effect of the positive charge and the position of the Arg residues, that are able to strongly interact with the hydrophilic phase. This experimental values alone already give a hint on the most probable orientation of the peptide: indeed, the TG analogs must lie parallel to the membrane surface in order to expose both residues 2 and 9 to the aqueous phase.

Two series of TG analogs with the TOAC in the three positions originally occupied by the Aib ([TOAC$^{1/4/8}$] TG and [TOAC$^{1/4/8}$, Lys^{6}] TG) were measured to obtain the orientation of the peptide in the bilayer. For both analogs, the depth parameters increase in the order TOAC^{1}<TOAC^{8}<TOAC^{4}. In general, helical AMPs adopt two main orientations: they lie parallel to the membrane surface or adopt a largely transmembrane orientation. We modeled the TOAC labels into the crystal structure of the TG helix and built an in-scale cartoon to distinguish, on the basis of the depth parameters, the most probable orientation of TG: the results are shown in Figure 3.27. The transmembrane orientation (Figure 3.27A) can be promoted by the octanoyl chain that anchors the peptide to the lipid tails, if the N-terminus is inserted first. This orientation implies that the TOAC moiety in position 1 is the most buried, the one in position 8 is the closest

Table 3.6 Depth parameters of spin labelled TG interacting with whole cells. Cells concentration, $5 \cdot 10^6$ cells/mL; peptide/cell ratio, 125 nmol/10^6 cells.

Labelled peptides	Depth parameter Φ	Cell line
[TOAC^1] TG	1.4	HeLa
[TOAC^1, Leu^4] TG	0.9	T67
[TOAC^1, Lys^6] TG	1.8	HeLa

to the aqueous phase, and the TOAC in position 4 lies in the middle. Comparing the depth parameters Φ of [TOAC$^{1/4/8}$] TG and their analogs with Lys in position 6, it is clear that this orientation is not supported by the data collected in our experimental conditions. The other possible orientation is represented by TG that lies parallel to the membrane surface (Figure 3.27B). In this case, the hydrophobic side chains and the octanoyl moiety are in contact with the hydrophobic bilayer, while the Gly residues (that are eventually substituted by hydrophilic amino acids like Lys or Arg) are facing the polar headgroups. This orientation is optimal to match the calculated depth parameters: TOAC in position 4 is located between carbon 12 and carbon 14 of the lipid chain, TOAC in position 8 is located between carbon 5 and carbon 7, and, finally, TOAC in position 1 is next to the polar headgroups.

We started to perform the insertion depth measurements in viable cells, but the work has encountered several difficulties that are still being solved at the time of this writing, among which the peptide-cells system stability over time and the lower sensitivity limit of the instrument, that is critical for these samples.

As yet, three peptides have been tested with T67 or HeLa cells and the depth parameters are reported in Table 3.6. The samples contain 125 nmol of peptides per million cells: this peptide-to- cell ratio is comparable to a 10 μM concentration in the MTT assay. It can be observed that the toxic peptide, [TOAC^1, Lys^6] TG, has the TOAC spin label positioned deeper than the other two non-toxic peptides. This difference could be significant, however further experiments in all cell lines need to be performed. Moreover, it should be kept in mind that the molecular ruler was built for a POPC SUV system; therefore it cannot be considered valid for the cells a priori. A new molecular ruler should be created doping the cells with a small amount of phospholipids labeled in different positions before deducing the actual depth of the labeled peptides in the cell membranes.

4. Conclusions

In this Ph.D. thesis, a rational search for TG analogs with different substitution has been performed. The goal was to synthesize and characterize different analogs to understand the key features that regulate the behavior of this family of lipopeptaibols towards the cell membranes.

The cell lines were chosen to have different level of exposed phosphatidilserine (PS, that negatively charges the outer leaflet of the membranes) and cholesterol (that reduces the membranes fluidity), two components that proved to influence the selectivity of cationic α-helical peptides towards membranes of bacteria and cancer cells.

We synthesized, via solid phase peptide synthesis, a wide number of helical peptides that had different charge, hydrophobicity and hydrophobic moment. The Gly-to-Arg and Gly-to-Lys substitutions enhanced the amphipathicity of the natural sequence with the introduction of one or two positively charged amino-acids. All these peptides displayed a non-selective toxicity, tested with the MTT assay, comparable to that of the native TG. The perturbation of the hydrophobic/structural sector caused significant modification to the analogs behavior. Aib-to-Leu substitutions completely abolished toxicity, while, interestingly, Aib-to-Api substitution conferred selectivity towards the T67 cell line to the peptides. Many analogs carried the spin labeled TOAC amino acid, that was inserted to perform EPR experiments and that, in the majority of the cases, did not alter the peptides toxicity; only one exception has been found, [TOAC^4] TG that lost its toxicity.

The interpretation of the Eisenberg plot (that relates the mean hydrophobicity per residue, ‹H›, with hydrophobic moment, μ) in light of the toxicity results, highlights that a defined ratio between ‹H› and μ is required to retain toxicity. Strong deviations from this balance result in activity dramatic lowering or complete loss. Therefore, ‹H› and μ appear to be key feature to predict toxicity in this family of peptides, so this correlation can be exploited in the design of future TG analogs. [TOAC^4] TG, that was an exception since it is the only case where the introduction of TOAC led to toxicity loss, has the same ‹H› and μ values of [TOAC^1] TG and [TOAC^8] TG. These observations highlight the position 4 as particularly sensitive to amino acids substitutions.

Further experiments were carried out to examine in depth the interaction of the peptides with model and cell membranes and to understand peptides localization and affinity for the membranes, and in particular to understand the selectivity of the Api-derivatives. Fluorescence microscopy and EPR spectra on model membranes of POPC confirmed that peptides have a strong affinity for the lipid phase and locate on the outer membrane leaflet. Moreover, the similarity of the correlation times calculated by simulations of the EPR spectra of the peptides interacting both with model and cell membranes led to the

conclusion that peptides likely locate in regions with the same fluidity and composition. From the calculated binding percentages of the peptides interacting with cells, we observed that a lower membrane fluidity, caused by high cholesterol content, such as that of HeLa cells, slightly hinders the binding of the peptides to the surface. Moreover, the overall high affinities displayed by both toxic and non-toxic peptides suggest that binding is a required stage, but not sufficient, for the peptides action. Finally, we observe a singular low affinity of the selective Api-bearing analog for the membranes, with an even lower affinity for those cells against which it is not active. The reason for this behavior resides in the perturbation of the hydrophobic/structural sector with a positive charge that lowers the affinity of the peptide helix for the lipid bilayer. At the same time, the electrostatic interaction between the positive charge and the highly negative surface of T67 cells acts as a driving force that lets the local peptide concentration reach a critical limit after which it becomes toxic.

Immersion depth measurements on spin labeled TG analogs showed that, in model membranes TG and [Lys^6] TG lie parallel to the membrane surface. The hydrophobic side chains and the octanoyl moiety are in contact with the hydrophobic bilayer, while the hydrophilic residues are facing the polar headgroups. First attempts to perform these experiments in viable cells were encouraging. Although they still need to be perfected, they showed significantly differences in the depth of toxic and non-toxic TG analogs.

Overall, this work studied promising TG analogs, characterizing their structural features and their biological activity. We found that TG is very sensitive to amino acids substitutions, since even one single modification can significantly alter the peptide behavior. The EPR spectroscopy represented an unconventional tool in the study of peptides and gave important information on the binding of peptides to different membranes (model and cell membranes). It was possible to work often in physiological conditions, a task of primary importance for this project. The results obtained so far are promising and encourage further studies.

5. Experimental details

Instrumentation for peptide characterization

UV-Vis spectroscopy. UV measurements were performed by means of a Shimadzu UV-2501PC spectrometer using quartz reduced optical path cell.

FT-IT spectroscopy. The FT-IR absorption spectra of peptides dissolved in deuterated chloroform were recorded with a spectrophotometer Perkin-Elmer model 1720X operating in the Fourier transform, using cells with pathway length of 0.1 cm with CaF_2 windows. The room that houses the sample is maintained under constant flow of nitrogen in order to minimize the contributions due to water vapor.

Mass spectroscopy. To record the mass spectra, a mass spectrometer was used, TOF (time Of Flight) and as ESI ionization technique was used, positive ions formed were accelerated to 10, 15,20 or 30 keV and analyzed linearly. The ESI generates the spray from an aqueous medium acidified with formic acid to improve the ionization of the molecules.

HPLC analysis. The HPLC measurements were performed using an Agilent 1200 series apparatus, equipped with a UV detector at variable wavelengths. The used wavelength is 226 nm. Eluents: solvent A, H_2O/CH_3CN 9:1 + 0.05% TFA; solvent B, CH_3CN/H_2O 9:1 + 0.05% TFA. Column: C18 Phenomenex Jupiter 300A.

Peptide Synthesis

All the peptides have been synthesized by Solid Phase Peptide Synthesis (SPPS). The employed resin is H-L-Leu-ol-2-chloro-trytil, which has a loading of 0.62 mmol/g (i.e., number of active sites per grams of resins. Amino acids are protected at the α-NH with the Fmoc protecting group. Side chains of the amino acids Api and Lys were protected with Boc protecting group, while the side chain of Arg was protected with Pbf. The general synthesis method is as follows:

- The desired quantity of resin in put in a plastic syringe of proper size; the resin is mixed for 60 minutes with dimethylformamide (DMF) to solvate it to obtain a "gel" in which penetration and removal of reagents is favorable.
- The coupling reaction is carried out adding to the resin 2 equivalents of Fmoc-AA-OH, 2 equivalents of the proper activating agent (HBTU/HOBt or HATU), 4 equivalents of base (N,N-diisopropyltehylamine, DIPEA), using anhydrous DMF as solvent. The solution is mixed for 60 minutes.
- The excess of reagents is removed by filtration and the resin is washed 5 times with DMF.

- The Fmoc protecting group is removed with a 20% solution of piperidine mixed with the resin for about 10 minutes; the operation is repeated again and then the resin is then washed with DMF.
- The coupling of the subsequent amino acids is carried out as described above, until the end of the desired sequence.
- The N-terminus of the TG analogs is capped by reaction with the n-octanoic acid: 2 equivalents of n-octanoic acid and 2 equivalents of HATU are mixed with the resin for 60 minutes.
- In the end, the peptide is cleaved from the resin with a solution of 30% hexafluoroisopropanol (HFIP) in dichloromethane. the resin is washed with this solution several times: first, the solutions are collected separately after 1 hour of mixing, then, a cleavage is conducted overnight.

Regarding the synthesis, it has to be added that:

- The coupling of Aib, Api, TOAC and of the amino acids that follow them in the sequence, is repeated twice due to the scarce reactivity of the C^{α}-tetrasubstituted amino acid.
- During the synthesis, it is possible to perform a "small cleavage" of a small portion of the resin to check, via mass spectrometry, that the coupling is proceeding as desired.

After the cleavage of all the peptide from the resin, the collected fractions of peptides are characterized by mass spectrometry (ESI/TOF) and HPLC. Then, it is necessary to purify the products using reverse phase HPLC.

Two peptides were synthesized by me during the Ph.D. project; the synthesis of [$TOAC^1$, Leu^4] TG ad [$TOAC^1$, Leu^8] TG is reported here. The other peptides were synthesized in the group of Dott. C. Peggion, University of Padova. The detailed synthesis of them can be found in [175,176].

[$TOAC^1$, Leu^4]TG. The peptide has been synthesized using the general method that is described in this paragraph, starting from 106.9 mg of resin (0.0535 mmol). For each step, 1 ml of DMF containing 0.107 mmol of Fmoc-AA-OH amino acid, 0.107 mmol of HBTU, 0.107 mmol of HOBt (or 0.107 mmol of HATU for C^{α}-tetrasubstituted amino acids) and 0.214 mmol of DIPEA is added to the resin and mixed for 60 minutes. Then the resin is washed 5 times with 1 ml of DMF. 1 ml of solution of DMF containing 20% of piperidine is mixed for 5 minutes with the resin, then another ml of the same solution is mixed for 10 minutes. Finally, the resin is washed 8 times with 1 ml of DMF. The coupling proceeded with the same steps for all the amino acids and the n-octanoic acid. The cleavage is performed in multiple steps, each one of them carried out mixing 3 ml of DCM containing 30% of HFIP for 1 hour. 27.4 mg of crude peptide are isolated.

They are then purified with a column Sep-Pak C18 35cc Vac Cartridge, 10 g, 55-105 μm Particle Size, using the following elution method: 100 ml H_20 100%; 100 ml H_20 90% and MeCN 10%; 100 ml H_20 70% and MeCN 30%; 200 ml H_20 50% and MeCN 50%; 200 ml H_20 30% and MeCN 70%; 200 ml H_20 10% and MeCN 90%; 100 ml MeCN 100%; 100 ml MeOH 100%. The fractions are checked by HPLC using a C18 Phenomenex Jupiter 300A reverse phase column with the following eluant system: solvent A, H_2O/CH_3CN 9:1 + 0.05% TFA; solvent B, CH_3CN/H_2O 9:1 + 0.05% TFA; gradient 70-90% B in 20 mins. The fractions containing the pure product were concentrated in vacuum, freeze-dried and characterized.

Yield: 27%.

Purity: 98.8%.

IR: 3314 cm^{-1} (Amide A: stretching of the N-H bonds of peptides in helical conformation); 1656 cm^{-1} (Amide I: stretching of the C=O group, bending of the N-H and stretching of the C-N typical of peptides in helical conformation); 1538 cm^{-1} (Amide II: stretching of the C-N and bending of the N-H). [177-179]

MS (ESI-TOF): $[M+H]^+_{calc}$ = 1206.80; $[M+H]^+_{sper}$ = 1206.79; $[M+H]^{++}_{sper}$ = 603.91.

HPLC gradient 70-90% B in 20 mins, flux 1 mL/min; reverse phase column C18 Phenomenex Jupiter 300A: retention time = 17.77 min.

[TOAC^1, Leu^8]TG. The peptide has been synthesized using the general method that is described in this paragraph, starting from 108.7 mg of resin (0.0544 mmol). For each step, 1 ml of DMF containing 0.109 mmol of Fmoc-AA-OH amino acid, 0.109 mmol of HBTU, 0.109 mmol of HOBt (or 0.109 mmol of HATU for C^α-tetrasubstituted amino acids) and 0.218 mmol of DIPEA is added to the resin and mixed for 60 minutes. Then the resin is washed 5 times with 1 ml of DMF. 1 ml of solution of DMF containing 20% of piperidine is mixed for 5 minutes with the resin, then another ml of the same solution is mixed for 10 minutes. Finally, the resin is washed 8 times with 1 ml of DMF. The coupling proceeded with the same steps for all the amino acids and the n-octanoic acid. The cleavage is performed in multiple steps, each one of them carried out mixing 3 ml of DCM containing 30% of HFIP for 1 hour. 27.0 mg of crude peptide are isolated. They are then purified with a column Sep-Pak C18 35cc Vac Cartridge, 10 g, 55-105 μm Particle Size, using the following elution method: 100 ml H_20 100%; 100 ml H_20 90% and MeCN 10%; 100 ml H_20 70% and MeCN 30%; 200 ml H_20 50% and MeCN 50%; 200 ml H_20 30% and MeCN 70%; 200 ml H_20 10% and MeCN 90%; 100 ml MeCN 100%; 100 ml MeOH 100%. The fractions are checked by HPLC using a C18 Phenomenex Jupiter 300A reverse phase column with the following (eluant system: solvent A, H_2O/CH_3CN 9:1 + 0.05% TFA; solvent B, CH_3CN/H_2O 9:1 + 0.05% TFA;

gradient 70-90% B in 20 mins. The fractions containing the pure product were concentrated in vacuum, freeze-dried and characterized.

Yield: 43%.

Purity: 95.5%.

IR: 3307 cm^{-1} (Amide A: stretching of the N-H bonds of peptides in helical conformation); 1656 cm^{-1} (Amide I: stretching of the C=O group, bending of the N-H and stretching of the C-N typical of peptides in helical conformation); 1540 cm^{-1} (Amide II: stretching of the C-N and bending of the N-H).

MS (ESI-TOF): $[M+H]^{+}_{calc}$ = 1206.80; $[M+H]^{+}_{sper}$ = 1206.75; $[M+H]^{++}_{sper}$ = 603.41.

HPLC gradient 70-90% B in 20 mins, flux 1 mL/min; reverse phase column C18 Phenomenex Jupiter 300A: retention time = 14.02 min.

Cell culture

Culture media, fetal bovine serum (FBS) and antibiotics were purchased from Carlo Erba Dasit Group. The T67 human glioma cell line was derived by Lauro et al. [180] from a World Health Organization (WHO) Grade III gemistocytic astrocytoma. Human dermal fibroblasts (HDF) were obtained by ATCC. HDF were cultured in Fibroblast Basal Medium (ATCC) supplemented with 10% FBS. T67 and HeLa cells were cultured in Dulbecco's modified Eagle's medium (MMedical) supplemented with 10% FBS, 100 UI/ml penicillin, 100 μg/ml streptomycin, and 40 μg/ml gentamycin, and kept in a 5% CO_2 atmosphere at 37 °C, with saturating humidity. Cell viability and number were measured by trypan blue exclusion method [181].

Cytotoxicity assay

Cytotoxicity of peptides was estimated using a MTT assay. All the chemicals used for this assay have been purchased by sigma Aldrich and used without further purification. T67, HeLa and HDF cells were seeded in 24-well plates at 1 × 105 cells/well. Experiments were performed after 24 h of incubation at 37 °C in 5% CO_2. After this time cells were washed and treated for 24 h with different concentrations of peptides; the cells are then incubated for 60 mins with 300 μM of MTT in culture medium. The absorbance of each well was measured at 450 nm with a spectrofluorometer (Wallac Victor multilabel counter; Perkin-Elmer Inc., Boston, MA, USA). Data are reported as the mean ± standard deviation of at least three independent experiments.

Cholesterol quantification

The cholesterol content of cultured cells was determined using the cholesterol oxidase method with minor modifications [182]. Pelleted cells were treated with lysis buffer (0.1% Triton X-100 v/v) to a final protein concentration of 0.5 mg/ml. Then, 10 microliters of reaction mix (500 mM $MgCl_2$, 500 mM Tris buffer (pH 7.4), 10 mM ditiotreitol, 5% sodium cholate (w/v), 0.1% Triton X-100 (w/v), 0.8 U/ml cholesterol oxidase and 0.8U/ml cholesterol esterase) were added to 100µL of cell suspension. The solution was incubated at 37°C for 30 minutes and was stopped by adding 100µl of a 1:1 methanol/ethanol (v/v) solution and incubated at 0°C for 30 min. After 10 min of centrifugation at 10000 x g, 10µL of the supernatant was analyzed by HPLC. The oxidized cholesterol was separated on a Kinetex C18 column (100 x 4.6 mm, 2.6 µm; Phenomenex, CA, USA) using a mobile phase consisting in 1:99 acetic acid/methanol (v/v) at a flow rate of 0.4 ml/min with a Agilent 1100 HPLC system. Absorbance at λ 240 nm was monitored by a photodiode array detector. To quantitate the amount of cholesterol, external cholesterol calibration standards were used.

Annexin V assay

The phosphatidylserine (PS) located on the outer leaflet of the plasma membrane was measured using Alexa Fluor® 488 Annexin V Kit (Molecular Probes, Invitrogen) following manufacturer instruction. The fluorescent signal was detected by flow cytometry using a Beckman-Coulter Epics XL-MCL cytofluorimeter at λ_{exc} 488 nm, λ_{em} 525 nm.

Circular Dichroism

Spectrograde MeOH (Acros) and 100 mM SDS were used as solvents. The small unilamellar vesicles (SUV) used in this study were prepared from POPC. The lipids were dissolved in chloroform and a homogeneous lipid film was obtained by drying the solution under a gentle dry nitrogen stream; the film was left overnight under vacuum in a desiccator to remove any trace of solvent. The following day the film was resuspended in HEPES buffer (5mM, pH 7.4) to obtain a lipid concentration of 2 mM. SUV in the 30-50 nm diameter range were prepared by sonication: the lipid suspension was immersed in a water bath and sonicated until the solution started to clear. Vesicle dimensions were checked during preparation by dynamic light scattering using a NICOMP Model 370 Submicron Particle Sizer by Pacific Scientific. The peptides were incorporated in the liposomes as follows: a methanol solution of the peptide was evaporated in an Eppendorf tube. The pre-formed liposomes were added and the solution was then sonicated for 3 min. Vesicles were used fresh after preparation. CD recordings were carried out on a JASCO J-715 (Tokyo, Japan) spectropolarimeter. The

CD spectra were acquired and processed using the J-700 program for Windows. All spectra were recorded at r.t., using Hellma (Müllheim, Germany) cylindrical quartz cells with Suprasil windows, optical path-lengths of 0.01 cm, a bandwidth of 2 nm, and a time constant of 2 s at a scan speed of 20 nm/min. The signal-to-noise ratio was improved by accumulating 36 scans. The values are expressed in terms of $[\theta]_R$, the total molar ellipticity [deg·cm^2·dmol^{-1}].

Determination of the hydrophobicity values for new residues

The CCS scale (see paragraph 3.4.2) has been correlated with literature experimental LogP values, finding an excellent correlation (Figure 5.1A). Then, the H values on the CCS scale for many N-acetylated and C-amidated residues has been related to the estimated value obtained for those residues from two different software (Figure 5.1B and 5.1C). The linear fit of these data showed a good correlation and led to the equations: $y = 0.13x - 1.34$ (5.1B) and $y = 0.12x - 1.43$ (5.1C), where y is the estimated H value on each scale and x is the H value on the CCS scale. From these equation, the estimated values of Api (and Api linked to the octanoyl chain), TOAC (and TOAC linked to the octanoyl chain) and Lol have been reported on the CCS scale. All the values are reported in Table 5.1 and Table 5.2.

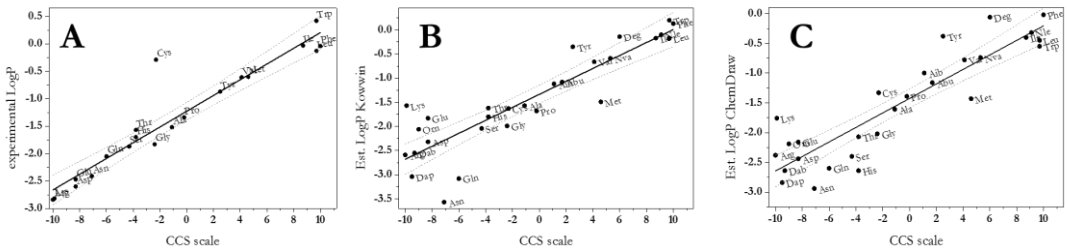

Figure 5.1 Correlation between the CCS scale with the experimental LogP (A), the estimated LogP from Kowwin (B) and the estimated LogP from ChemDraw (C).

Table 5.1 H values of different residues on the CCS scale relate to the experimental values, and the estimated LogP with the two used software.

Residue	H (CCS scale)	Experimental LogP	Estimated LogP from Kowwin	Estimated LogP from ChemDraw
Phe	10.0	-0.04	+0.13	-0.02
Trp	9.7	+0.42	+0.20	-0.55
Leu	9.7	-0.13	-0.17	-0.45
Ile	8.7	-0.03	-0.17	-0.4
Met	4.6	-0.60	-1.49	-1.43
Val	4.1	-0.61	-0.66	-0.78
Tyr	2.5	-0.87	-0.35	-0.38
Pro	-0.2	-1.34	-1.68	-1.39
Ala	-1.1	-1.52	-1.57	-1.6
Cys	-2.3	-0.29	-1.63	-1.33
Gly	-2.4	-1.83	-1.99	-2.02
Thr	-3.8	-1.57	-1.62	-2.07
His	-3.8	-1.70	-1.80	-2.64
Ser	-4.3	-1.87	-2.04	-2.40
Gln	-6.0	-2.05	-3.08	-2.60
Asn	-7.1	-2.41	-3.57	-2.94
Asp	-8.3	-2.60	-2.32	-2.44
Glu	-8.3	-2.47	-1.83	-2.16
Lys	-9.9	-2.82	-1.57	-1.76
Arg	-10.0	-2.84	-2.59	-2.38
Nle	9.1	--	-0.10	-0.32
Deg	6.0	--	-0.14	-0.06
Nva	5.3	-0.45	-0.59	-0.74
Abu	1.7	--	-1.08	-1.16
Aib	1.1	-0.87	-1.12	-1.00
Orn	-9.0	--	-2.06	-2.19
Dab	-9.3	--	-2.55	-2.64
Dap	-9.5		-3.04	-2.84

Table 5.2 H values estimated with the two software and reported on the CCS scale.

Residue	Est LogP (Kowwin)	H value on CCS scale	Est LogP (ChemDraw)	H value on CCS scale	Mean of the two H values on the CCS
Api	-2.45	-8.54	-2.06	-5.25	-6.9
TOAC	-1.53	-1.46	-1.06	3.08	0.81
Lol	0.15	11.46	0.30	14.42	12.94
Oct-Aib	1.83	24.38	1.38	23.42	23.90
Oct-TOAC	1.41	21.15	1.62	25.42	23.29

Fluorescence Microscopy

HeLa cells were washed with PBS (NaCl 137 mM, KCl 2.7 mM, Na_2HPO_4 10 mM, KH_2PO_4 1.8 mM, pH 7.4), detached with 0.05% trypsin–EDTA solution and centrifuged for 3 min at 300×g. The pellet was resuspended in DMEM medium and cells were counted by using trypan blue exclusion method. Then, 5×10^3 cells were seeded on custom chambers [183] with glass bottom, in 100 µL of complete DMEM medium and incubated at 37 °C in a humidified atmosphere with 5% CO_2. After 24 h, cells were washed with PBS and incubated for 3 hours with 10µM of [FITC^{11}] TG and [Lys^6, FITC^{11}] TG dissolved in DMEM. After this time, cells were carefully washed with PBS, then 50 µL of PBS supplemented with calcium and magnesium (NaCl 137 mM, KCl 2.7 mM, Na_2HPO_4 10 mM, KH_2PO_4 1.8 mM, $CaCl_2$ 1 mM, $MgCl_2$ 0.5 mM, pH 7.4) was added to each chamber. Finally, chambers were mounted on the microscope stage for analysis. Micrographs were acquired on a Zeiss Axiovert 200 inverted microscope equipped with XBO xenon 75W short arc lamp and a Photometrics Coolsnap FX CCD camera (Roper Scientific) with Metafluor Imaging Software version 6.1r6 (Universal Imaging Inc.) at λ_{exc} 500 nm, λ_{em} 545 nm.

EPR in membranes: model membranes, reconstituted cell membranes and viable cells

Methanol, 99.9%, spectrophotometric grade, [4-(2-hydroxyethyl)-1-piperazinyl] ethanesulfonic acid (HEPES), and PBS buffer (NaCl 137 mM, KCl 2.7 mM, Na_2HPO_4 10 mM, KH_2PO_4 1.8 mM, pH 7.4) were purchased from Sigma-Aldrich. A 50 mM, pH 7.0, HEPES buffer solution was prepared to be used for liposomes. 1-palmitoyl-2-oleoyl-*sn*-glycero-3-phosphocholine (POPC) was purchased from Avanti Polar Lipids, Alabaster (AL) as chloroform solution. For the EPR experiments in liposomes, POPC liposomes preparation and peptide incorporation were carried out in the same way as for CD experiments. Reconstituted cell membranes are prepared by culturing the cells as already described. Cells are centrifuged for 5 minutes at 800 g with a Eppendorf Centrifuge 5810; the supernatant is removed and the pellet is resuspended in the desired buffer. The pellet is kept at 0°C and homogenized by mechanical friction; after this operation the pellet is ready to be stored until use. For the EPR experiments in cells, T67, HeLa and HDF cells were cultured as described above and then stored in liquid nitrogen as a $5 \cdot 10^6$ cells/mL suspension in PBS buffer until use. The frozen suspension was quickly warmed in a 37°C water bath and washed twice with PBS. The peptides were incorporated in the cells as described in the CD section; the 3 min sonication was avoided to prevent damages to the cells. CW-EPR spectra were performed using a Bruker ER200D spectrometer operating at X-band (~9.5 GHz), equipped with a rectangular cavity, ER4102ST, fitted with a cryostat, and a variable-temperature controller, Bruker ER4111VT. The microwave frequency was measured by

a frequency counter, HP5342A. All spectra were obtained using the following parameters: microwave power 2.1 mW; modulation amplitude 0.10 mT; modulation frequency 100 kHz; time constant 41 ms; conversion time 82 ms; scan width 12 mT; 1024 points; temperature 293 K. The spectra were obtained as the average of 16 or 25 scans. The spectra of the TOAC-labeled peptides were simulated with a program based on the stochastic Liouville equation [184], that is extensively used to simulate the EPR spectra of spin-labeled peptides, proteins and lipids [185-189]. The simulation method relies on several reference systems: the **g** and ^{14}N hyperfine (**A**) tensors of the TOAC label are considered collinear and their orientation relative to the rotational diffusion reference frame is determined by a set of Euler angles. The simulation approach was simplified, using a single isotropic value (D_{iso}) for the diffusion tensor, and the rotational correlation times τ are related to D_{iso} via the classic equation $\tau=1/6D_{iso}$. The principal values of the **g** (g_{xx}=2.0096, g_{yy}=2.0064, g_{zz}=2.0027) and **A** tensors were obtained from the literature [190], except for the value of the A_{zz} component. Since the values of the A_{zz} hyperfine component depend strongly on the polarity of the environment, its value has been optimized: $A_{xx} = A_{yy} = 0.56$ mT in all environments, while $A_{zz} = 3.27$ mT for peptides bound to SUV, $A_{zz} = 3.35$ mT for peptides bound to cells, $A_{zz} = 3.47$ mT for peptides bound to reconstituted cell membranes and $A_{zz} = 3.75$ mT for peptides in solution.

Immersion depth measurements

Power saturation experiments were performed in POPC liposomes prepared in the same way as those used for CD experiments. The peptides were incorporated into liposomes as follows: a methanol solution of the peptide was evaporated in an Eppendorf tube. The pre-formed liposomes were added and the tube was repeatedly vortexed. The solution was then sonicated for 3 min. The EPR experiments were performed using a Bruker ESP380 spectrometer operating at the X-band (B9.5 GHz), equipped with a room temperature dielectric resonator, ER4123D. The microwave frequency was measured using a frequency counter, HP5342A. All spectra were obtained using the following parameters: a modulation amplitude of 0.16 mT; a modulation frequency of 100 kHz; a time constant of 41 ms; a conversion time of 82 ms; a scan width of 1.25 mT; 512 points; a temperature of 298 K. The microwave power was ramped down automatically from 95 mW to 0.05 mW (the attenuation ramp in dB units was 2.0, 4.0, 6.0, 8.0, 10.0, 12.0, 14.0, 16.0, 18.0, 20.0, 25.0, 30.0, 35.0). The spectra at each power were averaged 3 times. The experimental protocol for the insertion depth measurements is as follows: approximately 5 mL of the sample were loaded into a gas-permeable TPX capillary (L&M EPR Supplies, Inc., Milwaukee, WI, USA) and 3 saturation experiments were performed. The first experiment was done on the sample in equilibrium with air to saturate the membrane with oxygen. The second experiment was performed on the same sample after de-oxygenation under a dry nitrogen flow for 20 min. The third

experiment was carried out on a new sample to which NiEDDA was added to a final concentration of 50 mM; the sample was then de-oxygenated as above. All experiments were performed at least in duplicate. The power saturation data were obtained using a home-written program in Matlab that measures the peak-to-peak amplitudes of the central line of the spectra. The saturation curves were obtained by plotting the amplitude data *vs.* the microwave power, and fitted using equation 14. The dimensionless immersion depth parameter Φ is calculated from the ratio of the $P_{1/2}$ parameters obtained from the fitting of the three experiments described above, using equation 18.

6. References

1 M. Dathe et al. Structural features of helical antimicrobial peptides: Their potential to modulate activity on model membranes and biological cells. *Bba-Biomembranes* **1462**, 71-87 (1999).

2 M. De Zotti et al. Trichogin ga iv: A versatile template for the synthesis of novel peptaibiotics. *Organic & biomolecular chemistry* **10**, 1285-1299 (2012).

3 J.L. Kear, Fanucci G. E. in *Encyclopedia of Biophysics* 1994-1999 (2013).

4 P.G. Fajer. in *Encyclopedia of analytical chemistry* (ed R. A. Meyers) 5725–5761 (John Wiley & Sons Ltd, Chichester, 2000).

5 L.T. Nguyen et al. The expanding scope of antimicrobial peptide structures and their modes of action. *Trends in biotechnology* **29**, 464-472 (2011).

6 D. Hanahan et al. The hallmarks of cancer. *Cell* **100**, 57-70 (2000).

7 R.E.W. Hancock et al. Antimicrobial and host-defense peptides as new anti-infective therapeutic strategies. *Nature biotechnology* **24**, 1551-1557 (2006).

8 R.M. Epand et al. Diversity of antimicrobial peptides and their mechanisms of action. *Bba-Biomembranes* **1462**, 11-28 (1999).

9 L.T. Nguyen et al. The expanding scope of antimicrobial peptide structures and their modes of action. *Trends in biotechnology* **29**, 464-472 (2011).

10 A. Tossi et al. Amphipathic, alpha-helical antimicrobial peptides. *Biopolymers* **55**, 4-30 (2000).

11 M. Zasloff. Antimicrobial peptides of multicellular organisms. *Nature* **415**, 389-395 (2002).

12 M.D. Seo et al. Antimicrobial peptides for therapeutic applications: A review. *Molecules* **17**, 12276-12286 (2012).

13 R.E.W. Hancock et al. Cationic peptides: A new source of antibiotics. *Trends in biotechnology* **16**, 82-88 (1998).

14 D.M.E. Bowdish et al. A re-evaluation of the role of host defence peptides in mammalian immunity. *Curr Protein Pept Sc* **6**, 35-51 (2005).

15 M.D. Seo et al. Antimicrobial peptides for therapeutic applications: A review. *Molecules* **17**, 12276-12286 (2012).

16 C. Toniolo et al. Structure determination of racemic trichogin a iv using centrosymmetric crystals. *Nature structural biology* **1**, 908-914 (1994).

17 C. Altenbach et al. A collision gradient method to determine the immersion depth of nitroxides in lipid bilayers: Application to spin-labeled mutants of bacteriorhodopsin. *Proc Natl Acad Sci U S A* **91**, 1667-1671 (1994).

18 R. Schweitzer-Stenner et al. Conformational manifold of alpha-aminoisobutyric acid (aib) containing alanine-based tripeptides in aqueous solution explored by vibrational spectroscopy, electronic circular dichroism spectroscopy, and molecular dynamics simulations. *J Am Chem Soc* **129**, 13095-13109 (2007).

19 D. Hanahan et al. Hallmarks of cancer: The next generation. *Cell* **144**, 646-674 (2011).

20 R.E. Hancock et al. Antimicrobial and host-defense peptides as new anti-infective therapeutic strategies. *Nature biotechnology* **24**, 1551-1557 (2006).

21 P. Nicolas. Multifunctional host defense peptides: Intracellular-targeting antimicrobial peptides. *The FEBS journal* **276**, 6483-6496 (2009).

22 K.A. Brogden. Antimicrobial peptides: Pore formers or metabolic inhibitors in bacteria? *Nature reviews. Microbiology* **3**, 238-250 (2005).

23 N. Papo et al. Can we predict biological activity of antimicrobial peptides from their interactions with model phospholipid membranes? *Peptides* **24**, 1693-1703 (2003).

24 R.O. Fox, Jr. et al. A voltage-gated ion channel model inferred from the crystal structure of alamethicin at 1.5-a resolution. *Nature* **300**, 325-330 (1982).

25 K. He et al. Neutron scattering in the plane of membranes: Structure of alamethicin pores. *Biophysical journal* **70**, 2659-2666 (1996).

26 G. Molle et al. Voltage-dependent and multi-state ionic channels induced by trichorzianines, anti-fungal peptides related to alamethicin. *FEBS letters* **224**, 208-212 (1987).
27 G. Molle et al. Design and conformation of non-aib synthetic peptides enjoying alamethicin-like ionophore activity. *Biopolymers* **28**, 273-283 (1989).
28 M. Zasloff. Antimicrobial peptides of multicellular organisms. *Nature* **415**, 389-395 (2002).
29 D. Sengupta et al. Toroidal pores formed by antimicrobial peptides show significant disorder. *Biochimica et biophysica acta* **1778**, 2308-2317 (2008).
30 H. Leontiadou et al. Antimicrobial peptides in action. *J Am Chem Soc* **128**, 12156-12161 (2006).
31 M. Mihajlovic et al. Antimicrobial peptides bind more strongly to membrane pores. *Biochimica et biophysica acta* **1798**, 1494-1502 (2010).
32 R.M. Epand et al. Bacterial membrane lipids in the action of antimicrobial agents. *J Pept Sci* **17**, 298-305 (2011).
33 E.J. van Kan et al. Clavanin permeabilizes target membranes via two distinctly different ph-dependent mechanisms. *Biochemistry-Us* **41**, 7529-7539 (2002).
34 Y. Lan et al. Structural contributions to the intracellular targeting strategies of antimicrobial peptides. *Biochimica et biophysica acta* **1798**, 1934-1943 (2010).
35 M. Tang et al. Structure and mechanism of beta-hairpin antimicrobial peptides in lipid bilayers from solid-state nmr spectroscopy. *Molecular bioSystems* **5**, 317-322 (2009).
36 J.L. Gifford et al. Lactoferricin: A lactoferrin-derived peptide with antimicrobial, antiviral, antitumor and immunological properties. *Cellular and molecular life sciences : CMLS* **62**, 2588-2598 (2005).
37 Z. Wu et al. Engineering disulfide bridges to dissect antimicrobial and chemotactic activities of human beta-defensin 3. *Proc Natl Acad Sci U S A* **100**, 8880-8885 (2003).
38 E. Kluver et al. Structure-activity relation of human beta-defensin 3: Influence of disulfide bonds and cysteine substitution on antimicrobial activity and cytotoxicity. *Biochemistry-Us* **44**, 9804-9816 (2005).
39 M.L. Mangoni et al. Temporins and their synergism against gram-negative bacteria and in lipopolysaccharide detoxification. *Biochimica et biophysica acta* **1788**, 1610-1619 (2009).
40 A. Peschel et al. The co-evolution of host cationic antimicrobial peptides and microbial resistance. *Nature reviews. Microbiology* **4**, 529-536 (2006).
41 V.M. Dhople et al. Generation of analogs having potent antimicrobial and hemolytic activities with minimal changes from an inactive 16-residue peptide corresponding to the helical region of staphylococcus aureus delta-toxin. *Protein engineering* **8**, 315-318 (1995).
42 R. Bessalle et al. Augmentation of the antibacterial activity of magainin by positive-charge chain extension. *Antimicrobial agents and chemotherapy* **36**, 313-317 (1992).
43 K. Matsuzaki et al. Interactions of an antimicrobial peptide, magainin 2, with outer and inner membranes of gram-negative bacteria. *Biochimica et biophysica acta* **1327**, 119-130 (1997).
44 T. Kiyota et al. Design and synthesis of amphiphilic alpha-helical model peptides with systematically varied hydrophobic-hydrophilic balance and their interaction with lipid- and bio-membranes. *Biochemistry-Us* **35**, 13196-13204 (1996).
45 M. Dathe et al. Hydrophobicity, hydrophobic moment and angle subtended by charged residues modulate antibacterial and haemolytic activity of amphipathic helical peptides. *FEBS letters* **403**, 208-212 (1997).
46 P.Y. Chou et al. Empirical predictions of protein conformation. *Annual review of biochemistry* **47**, 251-276 (1978).
47 S.E. Blondelle et al. Hemolytic and antimicrobial activities of the twenty-four individual omission analogues of melittin. *Biochemistry-Us* **30**, 4671-4678 (1991).

48 S.E. Blondelle et al. Probing the relationships between the structure and hemolytic activity of melittin with a complete set of leucine substitution analogs. *Peptide research* **4**, 12-18 (1991).
49 E. Perez-Paya et al. The role of amphipathicity in the folding, self-association and biological activity of multiple subunit small proteins. *The Journal of biological chemistry* **270**, 1048-1056 (1995).
50 D. Andreu et al. N-terminal analogues of cecropin a: Synthesis, antibacterial activity, and conformational properties. *Biochemistry-Us* **24**, 1683-1688 (1985).
51 E. Gazit et al. Interaction of the mammalian antibacterial peptide cecropin p1 with phospholipid vesicles. *Biochemistry-Us* **34**, 11479-11488 (1995).
52 Y. Pouny et al. Interaction of antimicrobial dermaseptin and its fluorescently labeled analogues with phospholipid membranes. *Biochemistry-Us* **31**, 12416-12423 (1992).
53 P. Juvvadi et al. Hydrophobic effects on antibacterial and channel-forming properties of cecropin a-melittin hybrids. *J Pept Sci* **2**, 223-232 (1996).
54 S.E. Blondelle et al. Design of model amphipathic peptides having potent antimicrobial activities. *Biochemistry-Us* **31**, 12688-12694 (1992).
55 R. Bessalle et al. Structure-function studies of amphiphilic antibacterial peptides. *Journal of medicinal chemistry* **36**, 1203-1209 (1993).
56 N. Ohmori et al. Interaction of alpha-helical peptides with phospholipid membrane: Effects of chain length and hydrophobicity of peptides. *The journal of peptide research : official journal of the American Peptide Society* **51**, 103-109 (1998).
57 M. Dathe et al. Peptide helicity and membrane surface charge modulate the balance of electrostatic and hydrophobic interactions with lipid bilayers and biological membranes. *Biochemistry-Us* **35**, 12612-12622 (1996).
58 T. Wieprecht et al. Peptide hydrophobicity controls the activity and selectivity of magainin 2 amide in interaction with membranes. *Biochemistry-Us* **36**, 6124-6132 (1997).
59 D. Eisenberg et al. The helical hydrophobic moment: A measure of the amphiphilicity of a helix. *Nature* **299**, 371-374 (1982).
60 K. Matsuzaki et al. Molecular basis for membrane selectivity of an antimicrobial peptide, magainin 2. *Biochemistry-Us* **34**, 3423-3429 (1995).
61 R. Brasseur et al. Peptides in membranes: Tipping the balance of membrane stability. *Trends in biochemical sciences* **22**, 167-171 (1997).
62 E. Benedetti et al. Peptaibol antibiotics: A study on the helical structure of the 2-9 sequence of emerimicins iii and iv. *Proc Natl Acad Sci U S A* **79**, 7951-7954 (1982).
63 H. Bruckner et al. Paracelsin, a peptide antibiotic containing alpha-aminoisobutyric acid, isolated from trichoderma reesei simmons. Part a. *Experientia* **39**, 528-530 (1983).
64 M.R. Hermosa. Molecular characterization and indentification of biocontrol isolates of trichoderma spp. *Appl Environ Microbiol* **66**, 1890-1898 (2002).
65 R.C. Pandey et al. Structure of antiamoebin i from high resolution field desorption and gas chromatographic mass spectrometry studies. *J Am Chem Soc* **99**, 5203-5205 (1977).
66 M. Shi et al. Antimicrobial peptaibols, novel suppressors of tumor cells, targeted calcium-mediated apoptosis and autophagy in human hepatocellular carcinoma cells. *Mol Cancer* **9** (2010).
67 R.C. Pandey, Cook, J. C., Jr.; Rinehart, K. L., Jr. *J Am Chem Soc* **99**, 8469-8483 (1977).
68 C. Auvinguette et al. Trichogin-a-iv, an 11-residue lipopeptaibol from trichoderma-longibrachiatum. *J Am Chem Soc* **114**, 2170-2174 (1992).
69 C. Toniolo et al. Control of peptide conformation by the thorpe-ingold effect (c alpha-tetrasubstitution). *Biopolymers* **60**, 396-419 (2001).
70 I.L. Karle et al. Structural characteristics of alpha-helical peptide molecules containing aib residues. *Biochemistry-Us* **29**, 6747-6756 (1990).
71 M. De Zotti et al. Trichogin ga iv: An antibacterial and protease-resistant peptide. *J Pept Sci* **15**, 615-619 (2009).

72 S. Ayers et al. Peptaibols from two unidentified fungi of the order hypocreales with cytotoxic, antibiotic, and anthelmintic activities. *J Pept Sci* **18**, 500-510 (2012).
73 M. Shi et al. Antimicrobial peptaibols, novel suppressors of tumor cells, targeted calcium-mediated apoptosis and autophagy in human hepatocellular carcinoma cells. *Mol Cancer* **9**, 26 (2010).
74 S.R. C. Auvin-Guette, Y. Prigent, B. Bodo. Trichogin a iv, an 11-residue lipopeptaibol from trichoderma longibrachiatum. *Journal of American Chemical Society* **114**, 2170-2174 (1992).
75 R.F. Epand et al. Analogs of the antimicrobial peptide trichogin having opposite membrane properties. *European journal of biochemistry / FEBS* **268**, 703-712 (2001).
76 C. Toniolo et al. Effect of n-alpha-acyl chain length on the membrane-modifying properties of synthetic analogs of the lipopeptaibol trichogin ga iv. *J Am Chem Soc* **118**, 4952-4958 (1996).
77 C. Piazza et al. Total synthesis and membrane modifying properties of the lipopeptaibol trikoningin kb ii and its analogues with acyl chains of different length at the n- and c-termini. *J Pept Sci* **5**, 96-102 (1999).
78 R. Tavano et al. The peculiar n- and c-termini of trichogin ga iv are needed for membrane interaction and human cell death induction at doses lacking antibiotic activity. *Bba-Biomembranes* **1848**, 134-144 (2015).
79 V.N. Syryamina et al. Small-amplitude backbone motions of the spin-labeled lipopeptide trichogin ga iv in a lipid membrane as revealed by electron spin echo. *J Phys Chem B* **114**, 12277-12283 (2010).
80 V. Monaco et al. Orientation and immersion depth of a helical lipopeptaibol in membranes using toac as an esr probe. *Biopolymers* **50**, 239-253 (1999).
81 R.F. Epand et al. The antimicrobial peptide trichogin and its interaction with phospholipid membranes. *European Journal of Biochemistry* **266**, 1021-1028 (1999).
82 L. Stella et al. Aggregation and water-membrane partition as major determinants of the activity of the antibiotic peptide trichogin ga iv. *Biophysical journal* **86**, 936-945 (2004).
83 C. Mazzuca et al. Mechanism of membrane activity of the antibiotic trichogin ga iv: A two-state transition controlled by peptide concentration. *Biophysical journal* **88**, 3411-3421 (2005).
84 M. De Zotti et al. Antimicrobial lipopeptaibol trichogin ga iv: Role of the three aib residues on conformation and bioactivity. *Amino acids* **43**, 1761-1777 (2012).
85 C. Toniolo et al. Toac, a nitroxide spin-labeled, achiral c(alpha)-tetrasubstituted alpha-amino acid, is an excellent tool in material science and biochemistry. *Biopolymers* **47**, 153-158 (1998).
86 R. Bartucci et al. Backbone dynamics of alamethicin bound to lipid membranes: Spin-echo electron paramagnetic resonance of toac-spin labels. *Biophysical journal* **94**, 2698-2705 (2008).
87 C. Toniolo et al. Synthesis and conformational studies of peptides containing toac, a spin-labelled c alpha, alpha-disubstituted glycine. *J Pept Sci* **1**, 45-57 (1995).
88 T.T.T. Bui et al. Toac: A useful c-alpha-tetrasubstituted alpha-amino acid for peptide conformational analysis by cd spectroscopy in the visible region. Part i. *J Chem Soc Perk T 2* **5**, 1043-1046 (2000).
89 C. Peggion et al. Trichogin: A paradigm for lipopeptaibols. *J Pept Sci* **9**, 679-689 (2003).
90 B.W. Stewart, Wild, C. P. *World cancer report 2014*. (IARC Nonserial Publication, 2014).
91 R. Perez-Tomas. Multidrug resistance: Retrospect and prospects in anti-cancer drug treatment. *Curr Med Chem* **13**, 1859-1876 (2006).
92 J. Cassidy et al. Oxaliplatin-related side effects: Characteristics and management. *Semin Oncol* **29**, 11-20 (2002).
93 B. Kalyanaraman et al. Doxorubicin-induced apoptosis: Implications in cardiotoxicity. *Mol Cell Biochem* **234**, 119-124 (2002).

94 L.L. Smith et al. Chemoprevention of breast cancer by tamoxifen: Risks and opportunities. *Crit Rev Toxicol* **30**, 571-594 (2000).
95 M.M. Gottesman. Mechanisms of cancer drug resistance. *Annual review of medicine* **53**, 615-627 (2002).
96 J.P. Gillet et al. Mechanisms of multidrug resistance in cancer. *Methods in molecular biology* **596**, 47-76 (2010).
97 R.A. Cruciani et al. Antibiotic magainins exert cytolytic activity against transformed-cell lines through channel formation. *P Natl Acad Sci USA* **88**, 3792-3796 (1991).
98 N. Papo et al. New lytic peptides based on the d,l-amphipathic helix motif preferentially kill tumor cells compared to normal cells. *Biochemistry-Us* **42**, 9346-9354 (2003).
99 G.S. Wang et al. Apd2: The updated antimicrobial peptide database and its application in peptide design. *Nucleic Acids Res* **37**, D933-D937 (2009).
100 Z. Wang et al. Apd: The antimicrobial peptide database. *Nucleic Acids Res* **32**, D590-D592 (2004).
101 D.W. Hoskin et al. Studies on anticancer activities of antimicrobial peptides. *Bba-Biomembranes* **1778**, 357-375 (2008).
102 K. Lohner et al. Molecular mechanisms of membrane perturbation by antimicrobial peptides and the use of biophysical studies in the design of novel peptide antibiotics. *Comb Chem High T Scr* **8**, 241-256 (2005).
103 K. Lohner. New strategies for novel antibiotics: Peptides targeting bacterial cell membranes. *Gen Physiol Biophys* **28**, 105-116 (2009).
104 T. Utsugi et al. Elevated expression of phosphatidylserine in the outer-membrane leaflet of human tumor-cells and recognition by activated human blood monocytes. *Cancer Res* **51**, 3062-3066 (1991).
105 F. Schroeder et al. Membrane lipids and enzymes of cultured high- and low-metastatic b16 melanoma variants. *Cancer Res* **44**, 3262-3269 (1984).
106 E.M. Bevers et al. Regulatory mechanisms of transmembrane phospholipid distributions and pathophysiological implications of transbilayer lipid scrambling. *Lupus* **7 Suppl 2**, S126-131 (1998).
107 M. Seigneuret et al. Atp-dependent asymmetric distribution of spin-labeled phospholipids in the erythrocyte membrane: Relation to shape changes. *Proc Natl Acad Sci U S A* **81**, 3751-3755 (1984).
108 M.S. Soengas et al. Inactivation of the apoptosis effector apaf-1 in malignant melanoma. *Nature* **409**, 207-211 (2001).
109 T. Miyashita et al. Bcl-2 oncoprotein blocks chemotherapy-induced apoptosis in a human leukemia cell line. *Blood* **81**, 151-157 (1993).
110 H.M. Chen et al. Effects of the anti-bacterial peptide cecropin b and its analogs, cecropins b-1 and b-2, on liposomes, bacteria, and cancer cells. *Bba-Gen Subjects* **1336**, 171-179 (1997).
111 A.J. Verkleij et al. The asymmetric distribution of phospholipids in the human red cell membrane. A combined study using phospholipases and freeze-etch electron microscopy. *Biochimica et biophysica acta* **323**, 178-193 (1973).
112 R.F. Zwaal et al. Pathophysiologic implications of membrane phospholipid asymmetry in blood cells. *Blood* **89**, 1121-1132 (1997).
113 D.W. Kufe. Mucins in cancer: Function, prognosis and therapy. *Nature reviews. Cancer* **9**, 874-885 (2009).
114 K.L. Carraway et al. Membrane mucins and breast cancer. *Cancer control : journal of the Moffitt Cancer Center* **6**, 613-614 (1999).
115 A. Risso et al. Cytotoxicity and apoptosis mediated by two peptides of innate immunity. *Cellular immunology* **189**, 107-115 (1998).
116 S. Riedl et al. Membrane-active host defense peptides - challenges and perspectives for the development of novel anticancer drugs. *Chem Phys Lipids* **164**, 766-781 (2011).

117 L. Kjellen et al. Proteoglycans: Structures and interactions. *Annual review of biochemistry* **60**, 443-475 (1991).
118 D.L. Rabenstein. Heparin and heparan sulfate: Structure and function. *Natural product reports* **19**, 312-331 (2002).
119 B. Fadnes et al. The anticancer activity of lytic peptides is inhibited by heparan sulfate on the surface of the tumor cells. *BMC cancer* **9**, 183 (2009).
120 B. Fadnes et al. Small lytic peptides escape the inhibitory effect of heparan sulfate on the surface of cancer cells. *BMC cancer* **11**, 116 (2011).
121 C.M.P. Rodrigues et al. Perturbation of membrane dynamics in nerve cells as an early event during bilirubin-induced apoptosis. *J Lipid Res* **43**, 885-894 (2002).
122 M. Sok et al. Cell membrane fluidity and prognosis of lung cancer. *The Annals of thoracic surgery* **73**, 1567-1571 (2002).
123 W.J. van Blitterswijk. in *Physiology of membrane fluidity.* (ed Shinitzky. M.) 53-84 (CRC Press, 1984).
124 Y.C. Li et al. Elevated levels of cholesterol-rich lipid rafts in cancer cells are correlated with apoptosis sensitivity induced by cholesterol-depleting agents. *Am J Pathol* **168**, 1107-1118; quiz 1404-1105 (2006).
125 G.L. May et al. Plasma membrane lipid composition of vinblastine sensitive and resistant human leukaemic lymphoblasts. *International journal of cancer. Journal international du cancer* **42**, 728-733 (1988).
126 A. Mazzoni et al. Cytoplasmic membrane cholesterol and doxorubicin cytotoxicity in drug-sensitive and multidrug-resistant human ovarian cancer cells. *Oncology research* **5**, 75-82 (1993).
127 N. Papo et al. Host defense peptides as new weapons in cancer treatment. *Cellular and molecular life sciences : CMLS* **62**, 784-790 (2005).
128 S.C. Chan et al. Enhancement of the cytolytic effect of anti-bacterial cecropin by the microvilli of cancer cells. *Anticancer research* **18**, 4467-4474 (1998).
129 M.L.L. M. T. Watts, M. P. Eastman. Electron spin resonance studies of heisenberg spin exchange. Effect of macrocyclic polyethers on the spin exchange rate for ion pairs. *J. Phys. Chem.* **77**, 625-628 (1973).
130 C. Altenbach et al. Accessibility of nitroxide side chains: Absolute heisenberg exchange rates from power saturation epr. *Biophysical journal* **89**, 2103-2112 (2005).
131 Z.T. Farahbakhsh et al. Spin labeled cysteines as sensors for protein-lipid interaction and conformation in rhodopsin. *Photochemistry and photobiology* **56**, 1019-1033 (1992).
132 K.J. Oh et al. Site-directed spin labeling of proteins. Applications to diphtheria toxin. *Methods in molecular biology* **145**, 147-169 (2000).
133 D. Gilis et al. Optimality of the genetic code with respect to protein stability and amino-acid frequencies. *Genome Biol* **2** (2001).
134 D. Oh et al. Enhanced cellular uptake of short polyarginine peptides through fatty acylation and cyclization. *Mol Pharmaceut* **11**, 2845-2854 (2014).
135 J. Hu et al. Designed antimicrobial and antitumor peptides with high selectivity. *Biomacromolecules* **12**, 3839-3843 (2011).
136 B. Merrifield. Concept and early development of solid-phase peptide synthesis. *Method Enzymol* **289**, 3-13 (1997).
137 B. Merrifield. Solid-phase synthesis. *Science* **232**, 341-347 (1986).
138 B. Merrifield. Solid-phase synthesis. *Chem Scripta* **25**, 121-131 (1985).
139 B. Merrifield. Solid-phase synthesis. *Bioscience Rep* **5**, 353-376 (1985).
140 R.B. Merrifield. Solid-phase synthesis (nobel lecture). *Angew Chem Int Edit* **24**, 799-810 (1985).
141 M. De Zotti et al. Synthesis, preferred conformation, protease stability, and membrane activity of heptaibin, a medium-length peptaibiotic. *J Pept Sci* **17**, 585-594 (2011).
142 K. Barlos et al. 2-chlorotrityl chloride resin - studies on anchoring of fmoc-amino acids and peptide cleavage. *Int J Pept Prot Res* **37**, 513-520 (1991).

143 R. Bollhagen et al. A new reagent for the cleavage of fully protected peptides synthesized on 2-chlorotrityl chloride resin. *J Chem Soc Chem Comm*, 2559-2560 (1994).
144 L. Kocsis et al. The effect of peptide length on the cleavage kinetics of 2-chlorotrityl resin-bound ethers. *J Pept Sci* **12**, 428-436 (2006).
145 L.A. Carpino et al. Advantageous applications of azabenzotriazole (triazolopyridine)-based coupling reagents to solid-phase peptide-synthesis. *J Chem Soc Chem Comm*, 201-203 (1994).
146 L.A. Carpino. 1-hydroxy-7-azabenzotriazole - an efficient peptide coupling additive. *J Am Chem Soc* **115**, 4397-4398 (1993).
147 J. Rebek et al. Mechanism of the carbodiimide reaction. Ii. Peptide synthesis on the solid phase. *J Am Chem Soc* **96**, 1606-1607 (1974).
148 N.L. Benoiton et al. Studies on racemization during couplings using a series of model tripeptides involving activated residues with unfunctionalized side chains. *Int J Pept Protein Res* **17**, 197-204 (1981).
149 W. Konig et al. [a new method for synthesis of peptides: Activation of the carboxyl group with dicyclohexylcarbodiimide using 1-hydroxybenzotriazoles as additives]. *Chemische Berichte* **103**, 788-798 (1970).
150 V.A. Golubev, Sen, V. D., Kulyk, I. V., Aleksandrov, A. L. Mechanism of the oxygen disproportionation of ditert-alkylnitroxyl radicals. *Bull. Acad. Sci. URRS, Chem. Sect.*, 2235-2243 (1975).
151 T. Mosmann. Rapid colorimetric assay for cellular growth and survival: Application to proliferation and cytotoxicity assays. *Journal of immunological methods* **65**, 55-63 (1983).
152 L.J. Pike. Rafts defined: A report on the keystone symposium on lipid rafts and cell function. *J Lipid Res* **47**, 1597-1598 (2006).
153 P.J. Quinn. A lipid matrix model of membrane raft structure. *Prog Lipid Res* **49**, 390-406 (2010).
154 A. Cambi et al. Nanoscale membrane organization: Where biochemistry meets advanced microscopy. *Acs Chem Biol* **7**, 139-149 (2012).
155 Y.C. Li et al. Elevated levels of cholesterol-rich lipid rafts in cancer cells are correlated with apoptosis sensitivity induced by cholesterol-depleting agents. *Am J Pathol* **168**, 1107-1118 (2006).
156 N. Greenfield et al. Computed circular dichroism spectra for the evaluation of protein conformation. *Biochemistry-Us* **8**, 4108-4116 (1969).
157 M.C. Manning et al. Theoretical cd studies of polypeptide helices - examination of important electronic and geometric factors. *Biopolymers* **31**, 569-586 (1991).
158 C. Toniolo et al. Circular dichroism spectrum of a peptide 3(10)-helix. *J Am Chem Soc* **118**, 2744-2745 (1996).
159 F. Formaggio et al. The first water-soluble 3(10)-helical peptides. *Chem-Eur J* **6**, 4498-4504 (2000).
160 D. Eisenberg. Three-dimensional structure of membrane and surface proteins. *Annual review of biochemistry* **53**, 595-623 (1984).
161 G. von Heijne et al. Trans-membrane translocation of proteins. The direct transfer model. *European journal of biochemistry / FEBS* **97**, 175-181 (1979).
162 J. Janin. Surface and inside volumes in globular proteins. *Nature* **277**, 491-492 (1979).
163 C. Chothia. The nature of the accessible and buried surfaces in proteins. *Journal of molecular biology* **105**, 1-12 (1976).
164 R. Wolfenden et al. Affinities of amino acid side chains for solvent water. *Biochemistry-Us* **20**, 849-855 (1981).
165 A. Giangaspero et al. Amphipathic alpha helical antimicrobial peptides. *European journal of biochemistry / FEBS* **268**, 5589-5600 (2001).
166 A. Tossi, Sandri, L.G.A. in *Peptides 2000: 27th European Peptide Symposium.* 416–417.
167 M. Bortolus et al. Interaction of hydrophobic and amphipathic antimicrobial peptides with lipid bicelles. *J Pept Sci* **20**, 517-525 (2014).

168 K.H. Lee et al. Interactions between the plasma membrane and the antimicrobial peptide hp (2-20) and its analogues derived from helicobacter pylori. *The Biochemical journal* **394**, 105-114 (2006).
169 S.R. Dennison et al. A theoretical analysis of secondary structural characteristics of anticancer peptides. *Mol Cell Biochem* **333**, 129-135 (2010).
170 L. Zhao et al. Intracellular water-specific mr of microbead-adherent cells: The hela cell intracellular water exchange lifetime. *NMR in biomedicine* **21**, 159-164 (2008).
171 H.I. Petrache et al. Area per lipid and acyl length distributions in fluid phosphatidylcholines determined by (2)h nmr spectroscopy. *Biophysical journal* **79**, 3172-3192 (2000).
172 D. Kurad et al. Spin-label hf-epr of lipid ordering in cholesterol-containing membranes. *Appl Magn Reson* **21**, 469-481 (2001).
173 H.M. Swartz et al. Cellular metabolism of water-soluble nitroxides: Effect on rate of reduction of cell/nitroxide ratio, oxygen concentrations and permeability of nitroxides. *Biochimica et biophysica acta* **888**, 82-90 (1986).
174 M. Azarkh et al. Evaluation of spin labels for in-cell epr by analysis of nitroxide reduction in cell extract of xenopus laevis oocytes. *Journal of magnetic resonance* **212**, 450-454 (2011).
175 G. Panighel. *Sintesi, studi spettroscopici e interazioni con membrane di analoghi del peptaibiotico tricogina ga iv* Master Degree thesis, University of Padova, (2014).
176 M. Fiscato. *Sintesi e studi conformazionali di analoghi del peptaibiotico tricogina ga iv, contenenti api e toac* Master Degree thesis, University of Padova, (2013).
177 C.P. Rao et al. Infrared spectroscopy as a probe for the development of secondary structure in the amino-terminal segment of alamethicin. *FEBS letters* **100**, 244-248 (1979).
178 G.M. Bonora et al. Folded and extended structures of homooligopeptides from .Alpha.,.Alpha.-dialkylated .Alpha.-amino acids. An infrared absorption and proton nuclear magnetic resonance study. *J Am Chem Soc* **106**, 8152-8156 (1984).
179 M. Tanaka et al. Helical versus planar conformation of homooligopeptides prepared from diethylglycine (= 2-amino-2-ethylbutanoic acid). *Helv Chim Acta* **82**, 494-510 (1999).
180 G.M. Lauro et al. Prostaglandin-e2 as an immunomodulating factor released invitro by human glioma-cells. *Acta Neuropathol* **69**, 278-282 (1986).
181 A. Gorman, McCarthy, J., Finucane, D., Reville, W., Cotter, T. in *Techniques in apoptosis, a users guide* (ed T. G. Cotter, and Martin, S. J., Eds.) 6-7 (1996).
182 J.A. Contreras et al. Combination of an enzymatic method and hplc for the quantitation of cholesterol in cultured cells. *J Lipid Res* **33**, 931-936 (1992).
183 C. Bergamini et al. A practical approach for the detection of DNA nanostructures in single live human cells by fluorescence microscopy. *Methods* **67**, 185-192 (2014).
184 D.E. Budil et al. Nonlinear-least-squares analysis of slow-motion epr spectra in one and two dimensions using a modified levenberg-marquardt algorithm. *Journal of Magnetic Resonance, Series A* **120**, 155-189 (1996).
185 J.J. Inbaraj et al. Determining the topology of integral membrane peptides using epr spectroscopy. *J Am Chem Soc* **128**, 9549-9554 (2006).
186 M. Bortolus et al. Alamethicin in bicelles: Orientation, aggregation, and bilayer modification as a function of peptide concentration. *Bba-Biomembranes* **1828**, 2620-2627 (2013).
187 M. Bortolus et al. Self-association of an enantiopure beta-pentapeptide in nematic liquid crystals. *Chem-Eur J* **19**, 17963-17968 (2013).
188 M. Bortolus et al. Interaction of hydrophobic and amphipathic antimicrobial peptides with lipid bicelles. *J Pept Sci* **20**, 517-525 (2014).
189 L. Hoffman et al. Conformational changes underlying calcium/calmodulin-dependent protein kinase ii activation. *Embo J* **30**, 1251-1262 (2011).

190 J.J. Inbaraj et al. Determining the topology of integral membrane peptides using epr spectroscopy. *J Am Chem Soc* **128**, 9549-9554 (2006).

7. Appendices

7.1 Appendix A

As observed in the EPR spectra reported in paragraph 3.5.2, the signal of a nitroxide depends on its dynamics, and therefore it closely reflect the dynamic of the molecule at which the nitroxide is bound. A fast moving spectrum is determined by the mean values of the isotropic magnetic tensors. A slow moving spectrum is observed when the motion rate equals the rate of the magnetic interactions of the studied system. The interpretation of the experimental spectra requires complex models. A general model has been developed by J. Freed in collaboration with the Theoretical Chemistry group of the University of Padova, which allows to calculate the EPR spectrum for any motion regimen of the nitroxide and, moreover, it allows to consider the effect of anisotropic motions and orienting phases. The method is based on the Stochastic Liouville Equation (SLE), which combines the quantomechanic description of the energy of the system with the stochastic approach for the description of the microscopic dynamics. The program used for the EPR spectra simulation is based on this model. It requires a limited number of parameters and a deep knowledge of the theory is not necessary. The main parameters required for the simulation of an EPR spectrum in a slow motion regimen are:

- The principal values of the tensors **g** (g_{xx}, g_{yy}, g_{zz}) and **A** (A_{xx}, A_{yy}, A_{zz}).
- The reciprocal orientation of the two principal tensors and their orientation with respect to the molecule, for a case in which the motion is not considered isotropic.
- The linewidths.
- In the case of anisotropic motion, the principal values of the tensor **R**, which represents the motion frequency along the principal axes of the molecule (R_{xx}, R_{yy}, R_{zz}).

7.2 Appendix B

In Appendix B are reported the three papers that have been published during my Ph.D. period. They concern side projects that are at some extent correlated with the main topic of the thesis and with work that was useful to learn and develop experimental procedures that have been exploited also in the study of TG analogs.

- Bortolus Marco, Dalzini Annalisa, Toniolo Claudio, Hahm Kyung-Soo, Maniero Anna Lisa. Interaction of hydrophobic and amphipathic antimicrobial peptides with lipid bicelles, *Journal of Peptide Science*, **2014**, 20, 7, 517-525. In this paper, EPR spectroscopy is exploited to study how AMPs with different composition and amphipathicity perturb spin labeled bicelles, a model membrane system that can be macroscopically oriented in a magnetic field at physiological temperature. We observe that peptides that are known to disrupt the membrane by different mechanisms show very distinct trends of the order parameter (the parameter that describes the degree of perturbation of the bicelles) as a function of the peptide concentration. So, it was possible to exploit these differences to evaluate the mechanism of membrane disruption of new peptides.
- Mobbili Giovanna, Crucianelli Emanuela, Barbon Antonio, Marcaccio Massimo, Pisani Michela, Dalzini Annalisa, Ussano Eleonora, Bortolus Marco, Stipa Pierluigi, Astolfi Paola. Liponitroxides: EPR study and their efficacy as antioxidants in lipid membranes, *RSC Advances*, **2015**, 5, 98955-98966. In this paper the inclusion of a series of lipid-functionalized nitroxides in phospholipids bilayer has been studied by EPR spectroscopy. The molecular ruler, i.e. the immersion depth of nitroxides bound at different positions of the lipid tail of a doxyl-PC, has been developed and then exploited to determine the immersion depth of the studied compounds. Thanks to these measurements, it was possible to correlate the antioxidant activity and the mode of action of the liponitroxides with their penetration into the phospholipid bilayer.
- Bortolus Marco, Dalzini Annalisa, Formaggio Fermando, Toniolo Claudio, Gobbo Marina, Maniero Anna Lisa. An EPR study of ampullosporin A, a medium-length peptaibiotic, in bicelles and vesicles, *PCCP*, **2016**, 18, 749-760. In this paper, EPR spectroscopy has been exploited for various experiments. From immersion depth measurements of peptides labeled in different positions and at different concentration, we observed that the peptide orientation in the bilayer is dependent on its concentration. We also obtained information of the secondary conformation, orientation and aggregation of ampullosporin in different model membrane systems.

Special Issue Article

Journal of PeptideScience

Received: 28 February 2014 Accepted: 10 April 2014 Published online in Wiley Online Library

(wileyonlinelibrary.com) DOI 10.1002/psc.2645

Interaction of hydrophobic and amphipathic antimicrobial peptides with lipid bicelles‡

Marco Bortolus,[a] Annalisa Dalzini,[a] Claudio Toniolo,[a] Kyung-Soo Hahm[b] and Anna Lisa Maniero[a]*

Bicelles are model membrane systems that can be macroscopically oriented in a magnetic field at physiological temperature. The macroscopic orientation of bicelles allows to detect, by means of magnetic resonance spectroscopies, small changes in the order of the bilayer caused by solutes interacting with the membrane. These changes would be hardly detectable in isotropic systems such as vesicles or micelles. The aim of this work is to show that bicelles represent a convenient tool to investigate the behavior of antimicrobial peptides (AMPs) interacting with membranes, using electron paramagnetic resonance (EPR) spectroscopy. We performed the EPR experiments on spin-labeled bicelles using various AMPs of different length, charge, and amphipathicity: alamethicin, trichogin GA IV, magainin 2, HP(2–20), and HPA3. We evaluated the changes in the order parameter of the spin-labeled lipids as a function of the peptide-to-lipid ratio. We show that bicelles labeled at position 5 of the lipid chains are very sensitive to the perturbation induced by the AMPs even at low peptide concentrations. Our study indicates that peptides that are known to disrupt the membrane by different mechanisms (i.e., alamethicin vs magainin 2) show very distinct trends of the order parameter as a function of peptide concentration. Therefore, spin-labeled bicelles proved to be a good system to evaluate the membrane disruption mechanism of new AMPs. Copyright © 2014 European Peptide Society and John Wiley & Sons, Ltd.

Keywords: antimicrobial peptides; bicelles; EPR; order parameter; membrane interaction; peptaibiotics

Introduction

Antimicrobial peptides (AMPs) play an important role in the host defense mechanism of most living organisms and they are known to possess antibiotic activity against bacteria and fungi [1–3]. These peptides usually interact with the lipid bilayer of microbial cell membranes, causing an increase in permeability and cell disruption. As a consequence, they possess a great potential as therapeutic agents that can overcome the increasing resistance of bacteria to common antibiotics [4]. The large amount of data collected so far indicate that the strength and mechanisms of interaction of AMPs with membranes strongly depend on the combination of several features including main-chain length, secondary structure, charge, hydrophobicity, and amphipathic character [2,5,6]. Understanding the structure–activity relationships of AMPs appears essential for the development of antimicrobial agents with improved properties [1].

Several mechanisms of membrane disruption have been hypothesized, but all of them can be reconducted to two main categories: the barrel-stave model [7], characterized by AMPs self-assembly governed by the peptide–peptide hydrophobic interactions and the Shai–Matsuzaki–Huang model [8], dominated by the peptide–lipid interaction. In the barrel–stave model, AMPs generate a pore structure where the peptides form the walls and expose their hydrophilic face toward the inner part [9]. The barrel–stave model has been closely associated with the peptaibiotic alamethicin that forms voltage-dependent pores [7,9,10] and has been also invoked for other hydrophobic peptides [11,12]. The Shai–Matsuzaki–Huang mechanism involves several levels of membrane disruption that can be caused by AMPs depending on their strength and effective concentration as follows: (i) AMPs can be absorbed parallel to the membrane surface, causing membrane thinning, (ii) AMPs can form disordered pores where peptides and lipids are mixed (called toroidal pores), (iii) AMPs can act as detergents micellizing the membrane [1,13]. The Shai–Matsuzaki–Huang mechanism is usually invoked for cationic amphipathic AMPs, the hydrophilic or positively charged side of which promotes the binding to the surface of negatively charged bacterial membranes, whereas the hydrophobic side is responsible for the interaction with the lipid components.

Model membrane systems play a key role to dissect the different aspects of the peptide–membrane interaction. Among model membranes, bicelles have one unique advantage over micelles or vesicles that makes them an ideal system for magnetic spectroscopies [14]: they can be macroscopically oriented in solution (no solid support is needed) at physiological temperature under a magnetic field. Additionally, bicelles are in the fluid phase at physiological temperature, the curvature stress of the bilayer is negligible, and the membrane is fully hydrated. A schematic representation of a bicelle is shown in Figure 1. The system is

* *Correspondence to: Anna Lisa Maniero, Department of Chemistry, University of Padova, via Marzolo 1, Padova, 35131, Italy. E-mail: annalisa.maniero@unipd.it*

‡ *This article is published in Journal of Peptide Science as part of the Special Issue devoted to contributions presented at the 1st International Conference on Peptide Materials for Biomedicine and Nanotechnology, Sorrento, October 28-31, 2013, edited by Professor Mariano Venanzi, Professor Claudio Toniolo and Professor Giancarlo Morelli.*

a *Department of Chemistry, University of Padova, via Marzolo 1, Padova, 35131, Italy*

b *BioLeaders Corp., 559 Yongsan-Dong, Yuseong-Ku, Daejeon, 305-500, Korea*

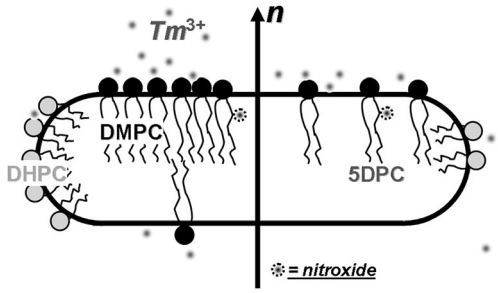

Figure 1. Schematic representation of a bicelle. The cartoon shows the long-chain phospholipids (DMPC), the short-chain phospholipids (DHPC), the spin-labeled phospholipids (5DPC), and the lanthanide ions (Tm^{3+}) used to align the membrane normal parallel to an external magnetic field. For the abbreviations see Materials and Methods.

composed of planar regions, made primarily of long-chain phospholipids, and curved edge regions, composed essentially of short-chain phospholipids. Normally, bicelles align in a strong magnetic field with the membrane normal ***n*** perpendicular to the field, but, in the presence of paramagnetic lanthanide ions, bicelles can be aligned, even at low magnetic fields (less than 1 T), with the membrane normal parallel or perpendicular to the external field, depending on the chosen lanthanide [14].

Magnetic spectroscopies, such as NMR and electron paramagnetic resonance (EPR) can take advantage of the high spectral resolution afforded by the macroscopic orientation of bicelles to characterize the interaction of solutes with the bilayers. Spin-labeling EPR spectroscopy is a well-proven technique for studying the interactions of peptides and other solutes with lipid membranes: the spin label, usually a nitroxide, can be placed either on the lipids or on the solute [15–18]. EPR experiments performed using bicelles can provide a wealth of information both on the effects of solutes on the lipid packing and on solute characteristics, as orientation, dynamics, and aggregation [17–19].

In this work, using bicelles and EPR spectroscopy, we investigated the membrane disruption mechanisms of several AMPs having different length, hydrophobicity, hydrophobic moment, and charge. These parameters have been shown to influence the activity of AMPs in different ways [6]. The peptides studied are listed in Table 1: despite the different lengths, all these AMPs adopt a mostly helical conformation in membrane or membrane-like environments. For this reason, they are shown in Figure 2 in the helical wheel representation. We studied two peptides that are archetypical of the two principal mechanisms of pore formation, namely, alamethicin (barrel–stave) [9,20–22] and magainin 2 (Shai–Matsuzaki–Huang) [22–26] and three peptides the mechanism of action of which is currently under debate, trichogin GA IV, HP(2–20), and HPA3. Alamethicin and trichogin GA IV are peptaibiotics, a family of AMPs rich in hydrophobic residues and characterized by the presence of an alcoholic function at the C-terminus and an acyl group at the *N*-terminus [27]. The formation of a helical secondary structure in both peptides is promoted by the presence of several C^{α}-tetrasubstituted Aib residues. Alamethicin, the most studied peptaibiotic, is composed of 19 amino acids [28]. Trichogin GA IV is a shorter peptaibiotic formed by ten residues, none of which is charged. Moreover, it carries 1-octanoyl fatty acyl chain at the *N*-terminus [29,30], which likely plays a role in the antimicrobial activity of this peptide [31]. Magainin 2, the first AMP that has been discovered, is a positively charged peptide composed of 23 residues that shows strong bactericidal, fungicidal, and virucidal activities [32,33]. HP(2–20), derived from the *N*-terminal region of the *Helicobacter pylori* ribosomal protein L1, is a positively charged peptide composed of 19 amino acids. Its central portion (residues 4–16) is arranged in an amphipathic helical structure [34,35]. Several analogs of HP(2–20) have been synthesized, the most promising of which is HPA3 [34]. It is characterized by an increase of amphipathicity combined with a limited extension of the helical region (residues 4–18).

Materials and Methods

Materials

Alamethicin from *T. viride* (mixture of the natural isomorphs) was purchased from Sigma-Aldrich, Saint Louis, MO, USA. Magainin 2 was purchased from Bachem AG, Bubendorf, Switzerland. The synthesis of HP(2–20) [34], HPA3 [34], and trichogin GA IV [37] has all been previously reported. 1,2-Dihexanoyl-*sn*-glycero-3-phosphocholine (DHPC), 1,2-dimyristoyl-*sn*-glycero-3-phosphocholine (DMPC), and 1-palmitoyl-2-stearoyl-(5-doxyl)-*sn*-glycero-3-phos phocholine (5DPC) were purchased as chloroform solutions from Avanti Polar Lipids, Alabaster, AL, USA. 2-[4-(2-Hydroxyethyl)-1-piperazinyl]ethanesulfonic acid (HEPES) and the lanthanide salt $TmCl_3\,6H_2O$ were purchased from Sigma-Aldrich. A 50 mM, pH 7.0, HEPES buffer solution was used for bicelle preparation and for the stock solutions of Tm^{3+}.

Table 1. The peptides studied in this work. The common name, sequence, hydrophobicity, hydrophobic moment, overall and net charges, and the organism that produces them are reported

Peptide	Sequence[a]	Hydrophobicity	Hydrophobic moment	Overall charges	Net charge	Origin
Alamethicin (main isomorph)	Ac–UPUAUAQ UVUGLUPVUUEQ–Phol	0.57	1.70	0/−1	−1	Fungus (*Trichoderma viride*)
Trichogin GA IV	1-Oct-UGLUGGLUGI-Lol	2.86[b]	3.30[b]	0/0	0	Fungus (*Trichoderma longibrachiatum*)
Magainin 2	GIGKFLHSAKKFGKAFVGEIMNS	−0.58	3.28	+5/−1	+4	Frog (*Xenopus laevis*)
HP(2–20)	AKKVFKRLEKLFSKIQNDK	−2.75	3.98	+7/−2	+5	Bacterium (*Helicobacter pylori*)
HPA3	AKKVFKRLEKLFSKIWNWK	−0.98	4.07	+7/−1	+6	Synthetic analog of HP(2–20)

[a]Ac, acetyl; Phol, phenylalaninol; U, α-aminoisobutyric acid (Aib); 1-Oct, 1-octanoyl; Lol, leucinol.
[b]Hydrophobicity and hydrophobic moment for trichogin GA IV are not easily comparable with those of other peptides because it is much shorter and the 1-Oct group cannot be taken into account in the calculations.

Journal of PeptideScience

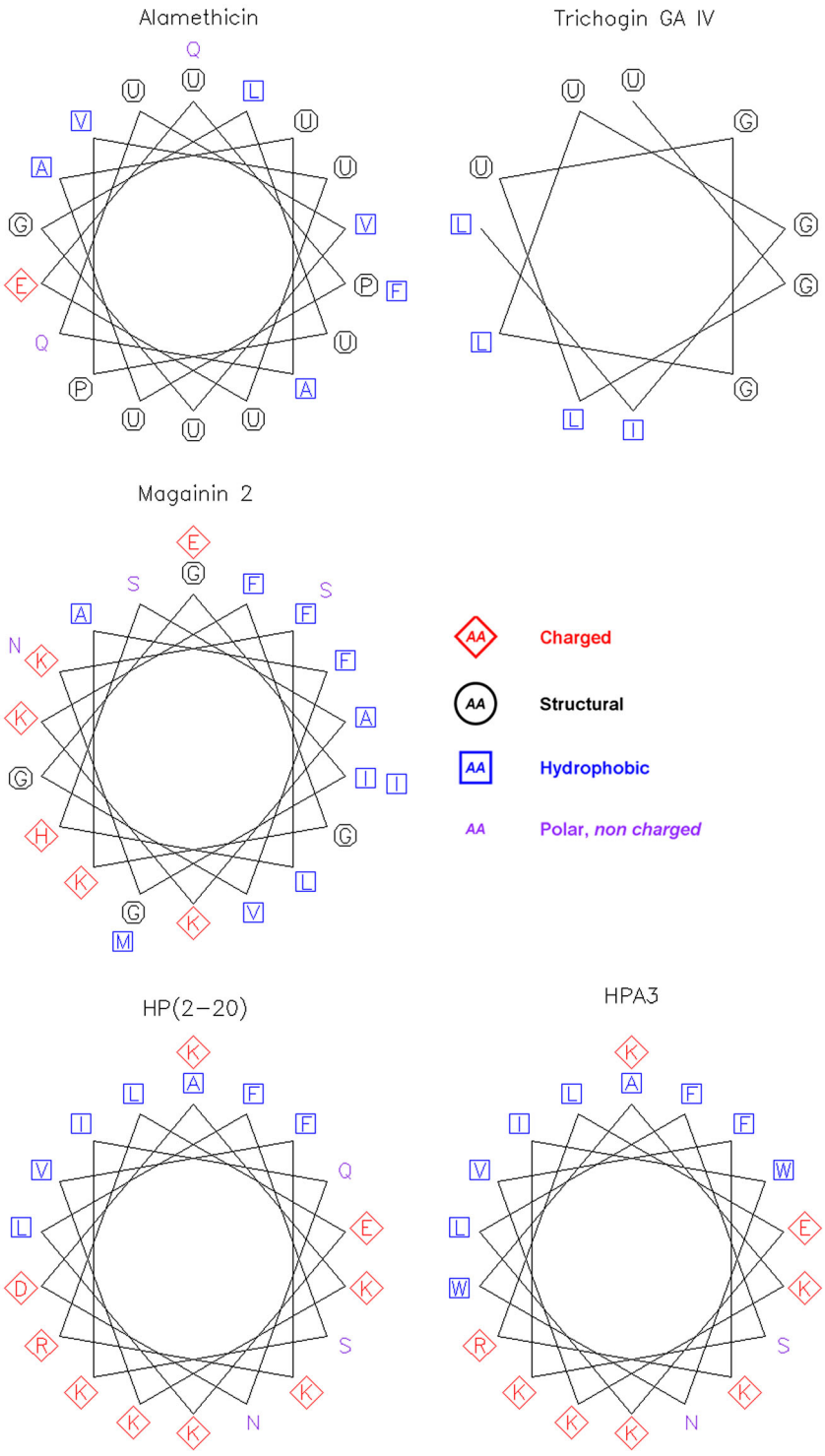

Figure 2. Helical wheel representations of the peptides studied in this work. The colors follow the convention given in Ref. [36]. U is α-aminoisobutyric acid (Aib).

Helical Wheels and Hydrophobic Moment Calculation

The helical wheels in Figure 2 were drawn using the program Pepwheel of the EMBOSS suite [38] that can be found at http://emboss.bioinformatics.nl. The hydrophobic moments given in Table 1 were calculated with the formula reported by Eisenberg [39], using the new consensus hydrophobicity scale reported by Tossi [40].

Bicelle Stock Preparation

The chloroform solutions of the phospholipids and a methanol solution of the peptides were mixed in a glass test tube. Samples at different peptide concentrations were prepared keeping the lipid content constant and varying the amount of peptide to obtain the desired peptide-to-lipid (P/L) ratio. The P/L ratios reported in this work refer to DMPC only. The final lipid

composition of each solution was 11.2 μmol of DMPC, 3.1 μmol of DHPC, and, where present, 25 nmol of 5DPC spin label (~0.2% of the total lipids). The q = (DMPC)/(DHPC) ratio was therefore ~3.5. A thick film, containing the lipids and the peptide, was produced by evaporation of the solvent under a stream of dry nitrogen gas. The film was dried under vacuum overnight and then scratched off the glass tube and placed into an Eppendorf tube. Then 33 μL of buffer was added, obtaining a solution of 25% (w/w) lipid concentration. The resulting suspension was vortexed until it appeared homogeneous. The sample was then placed in a bath sonicator filled with an ice/water mixture and sonicated for 30 min. Finally, the solution was subjected to four freeze/thaw cycles: 30 min in a 328 K water bath was followed by a quick freeze in liquid nitrogen (vortexing of the sample at each step was performed to insure perfect homogeneity). This procedure yielded a clear, viscous, stock of bicelles with the peptide incorporated in the bilayers.

EPR Sample Preparation

The samples for EPR experiments were prepared as follows: 15 μL of bicelles was added to 10 μL of a buffered lanthanide solution of Tm^{3+} [corresponding to a final (Tm^{3+})/(DHPC) ratio of 0.1]. The final concentration of the phospholipids was 17% (w/w). The resulting solution (25 μL) was transferred to a 1-mm inner diameter EPR quartz tube. Given the experimental conditions (lipid concentration, q ratio, temperature), the bicelles used in this work are not ideal disks but rather stacks of almost planar phospholipid bilayers dotted with DHPC pores and separated by buffer regions ~15-nm wide [41].

A literature procedure [14] was used to obtain aligned samples: the sample tube was placed at room temperature (~298 K) in the EPR cavity, and the magnetic field was set to 800 mT. Then, the temperature was slowly raised to 318 K and subsequently lowered to the selected temperature of 308 K (35 °C). The magnetic field was set to ~350 mT, and the spectrum was recorded immediately. Loss of order in the sample during the measurement time (~40 s) is negligible as a result of the high viscosity of the bicelle solution, which prevents membrane reorientation.

EPR Experiments

Electron paramagnetic resonance spectra were performed using a ER200D spectrometer operating at X-band (~9.5 GHz), equipped with a rectangular cavity, ER4102ST, fitted with a cryostat, and a variable-temperature controller, ER4111VT, all from Bruker BioSpin GmbH, Rheinstetten, Germany. The microwave frequency was measured by a frequency counter, HP5342A. All spectra were obtained using the following parameters: microwave power, 2.1 mW; modulation amplitude, 0.16 mT; modulation frequency, 100 kHz; time constant, 20 ms; conversion time, 41 ms; scan width, 15 mT; 1024 points; and temperature, 308 K. All spectra were obtained in a single scan.

EPR Spectral Simulations

We performed simulations of 5DPC spectra with a program based on the stochastic Liouville equation [42] that is extensively used to simulate EPR spectra of spin-labeled systems [19,43–47]. The simulation method relies on several reference systems, the relative orientation of which is defined by different sets of Euler angles [42]. The simulation strategy has been previously given in detail [18]: the experimental spectra could be precisely simulated by keeping all the magnetic and motional parameters of the nitroxide constant, while changing the order parameter S. The principal values of g and ^{14}N hyperfine (A) tensors, the principal values of the diffusion tensor (D), and the relative orientation of its principal axes relative to the g tensor reference frame (Ω_D), reported in Table 2, were taken from the literature [18,48]. The $\beta = 33°$ value has been attributed to the presence of a lipid mismatch between the DMPC chains (14 carbons) and those of 5DPC (18 carbons) [18].

Results

Hydrophobic Peptides: Alamethicin, Trichogin GA IV

In a previous report [18], we have shown that alamethicin progressively perturbed the bilayer upon increasing its concentration. The order parameter of 5DPC decreases exponentially with the P/L ratio, but the membrane is not completely destroyed even at a P/L ratio of 1 : 20.

The experimental spectra of 5DPC in bicelles in the absence and in the presence of trichogin GA IV and the corresponding simulations are illustrated in Figure 3. The spectrum in the absence of peptide [Figure 3(A)] shows a simple three-line structure typical of a partially oriented nitroxide. Macroscopically, the membrane normal ***n*** (Figure 1) lies parallel to the magnetic field of the spectrometer; from a microscopic point of view, the plane of the 5DPC nitroxide ring is roughly perpendicular to the membrane normal. Therefore, the average direction of the nitrogen p_z orbital (corresponding to the A_{zz} and g_{zz} tensor components) is parallel to the external magnetic field. Then, the spectral width of 5DPC in the partially oriented bicelles is dominated by the largest hyperfine tensor component (A_{zz}), partially averaged because of the complex motions of the lipid side chains [49].

The lineshape does not change in the presence of trichogin GA IV up to a P/L ratio of 1 : 300 [Figure 3(B–D)]. Trichogin GA IV is a hydrophobic peptaibiotic as alamethicin and it is fully bound to the membrane at these P/L ratios [50]. Thus, our results suggest that at low P/L ratio, where the peptide is likely to be monomeric, trichogin GA IV does not perturb the bilayer structure [50]. At higher P/L ratios [Figure 3(E–H)], the spectra change in a remarkable way as evident from the 'kinks' (see the arrows in Figure 3) and the general broadening observed.

Table 2. Parameters used for fitting the spectra of 5DPC at all P/L ratios: g and A tensors, diffusion tensor (D), angles between the magnetic and the diffusion frame (Ω_D), angle between the diffusion frame and the membrane normal (Ψ)

					Ω_D[a]			
		g	A/mT	$D/10^6\ s^{-1}$	α	β	γ	Ψ
5DPC[b]	x	2.0088	0.65	8	0°	33°	0°	0°
	y	2.0061	0.58	8				
	z	2.0027	3.35	500				

[a]For an axial diffusion tensor, the angle α is irrelevant [42].
[b]g and A tensors were taken from Ref. [48].

Journal of PeptideScience

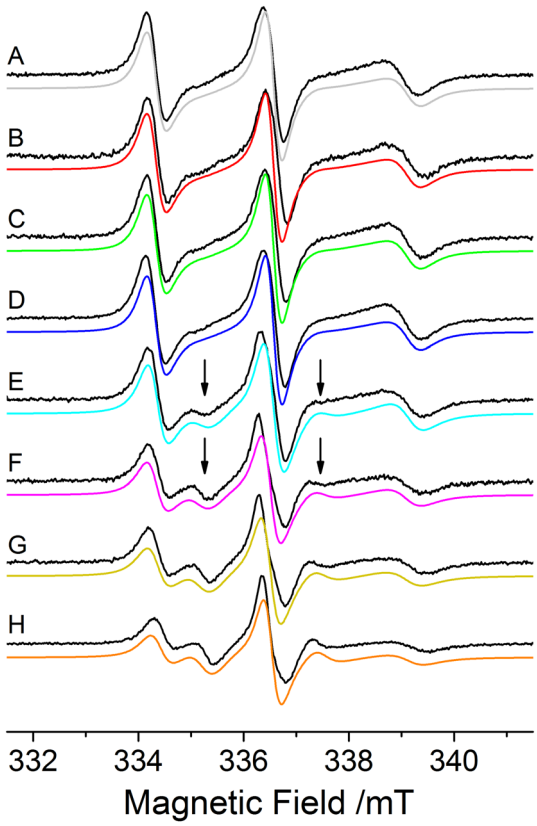

Figure 3. Simulated (colored lines) and experimental (black lines) EPR spectra of DMPC/DHPC bicelles labeled with 5DPC and oriented with the magnetic field parallel to the bilayer normal, $T = 308$ K. The bicelles incorporate trichogin GA IV at increasing P/L ratios: (A) no peptide; (B) 1 : 1000; (C) 1 : 500; (D) 1 : 300; (E) 1 : 200; (F) 1 : 100; (G) 1 : 50; and (H) 1 : 25. The arrows indicate the most significant changes in the lineshape induced by the peptide.

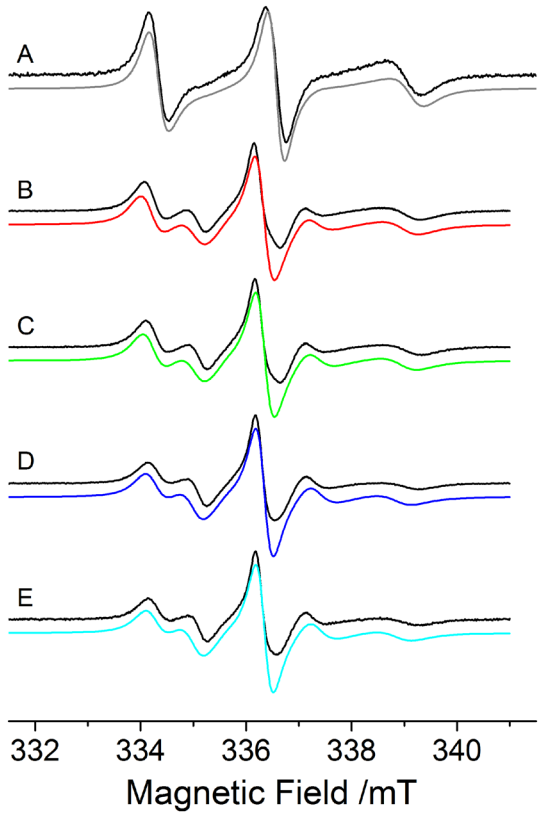

Figure 4. Simulated (colored lines) and experimental (black lines) EPR spectra of DMPC/DHPC bicelles labeled with 5DPC and oriented with the magnetic field parallel to the bilayer normal, $T = 308$ K. The bicelles incorporate magainin 2 at increasing P/L ratios: (A) no peptide; (B) 1 : 500; (C) 1 : 400; (D) 1 : 300; and (E) 1 : 100.

The changes in lineshape induced by increasing amounts of peptide have been rationalized using the easily interpretable order parameter of the spin label, S [18]. S decreases upon increasing the peptide concentration as the spin labels, and therefore the phospholipid chains, experience a progressive loss of order. The graph of the order parameters as a function of the P/L ratio, which collects the data for all peptides, is shown in the Discussion section. Overall, the changes in lineshape for trichogin GA IV as a function of the P/L ratio are very similar to those of alamethicin [18]. Trichogin GA IV shows an exponential decrease of the order parameter and a non-vanishing order parameter even at a P/L ratio of 1 : 25 [Figure 3(H)].

Amphipathic Peptides: Magainin 2, HP(2–20), and HPA3

The experimental spectra of 5DPC in bicelles in the presence of magainin 2 and the corresponding simulations are reported in Figure 4. The spectra exhibit a dramatic alteration of the lineshape when magainin 2 is present, relative to the one observed in the absence of peptide [reported for convenience in Figure 4(A)]. This alteration is evident at a P/L ratio of 1 : 500. Moreover, the overall spectral lineshape indicates that magainin 2 induces a much more severe disordering effect on the membrane than alamethicin and trichogin GA IV. Indeed, the lineshape observed for magainin 2 at a P/L ratio of 1 : 500 is very similar to that observed for trichogin GA IV only at a P/L ratio of 1 : 50.

The experimental spectra and the corresponding simulations for the two peptides derived from *Helicobacter pylori,* HP(2–20) and HPA3, are illustrated in Figure 5. The two peptides, with the same length but different net charge and amphipathicity, show remarkably different effects on the lineshape of the 5DPC spectra as a function of the P/L ratio. HP(2–20) has no effect on the bilayer up to a P/L ratio of 1 : 75 [Figure 5(A–C)]. Changes in lineshape begin at P/L ratios of 1 : 70 and continue up to the maximum concentration explored in this study at a P/L ratio of 1 : 25 [Figure 5(D–F)]. On the other hand, HPA3 shows strong alterations of the lineshape at P/L ratios as low as 1 : 375. At P/L ratios of 1 : 190 and lower, the spectra exhibit an almost isotropic lineshape.

Discussion

The lipid order alterations caused by AMPs can be studied by different techniques, among others NMR [51–54] and EPR spectroscopies [18,55], or X-ray diffraction [22]. The experimental data are typically analyzed in terms of order parameters that provide information on the average orientation of chemical bonds, molecular segments, molecules, or assembly of molecules [56]. In this work, we quantitatively express the bilayer

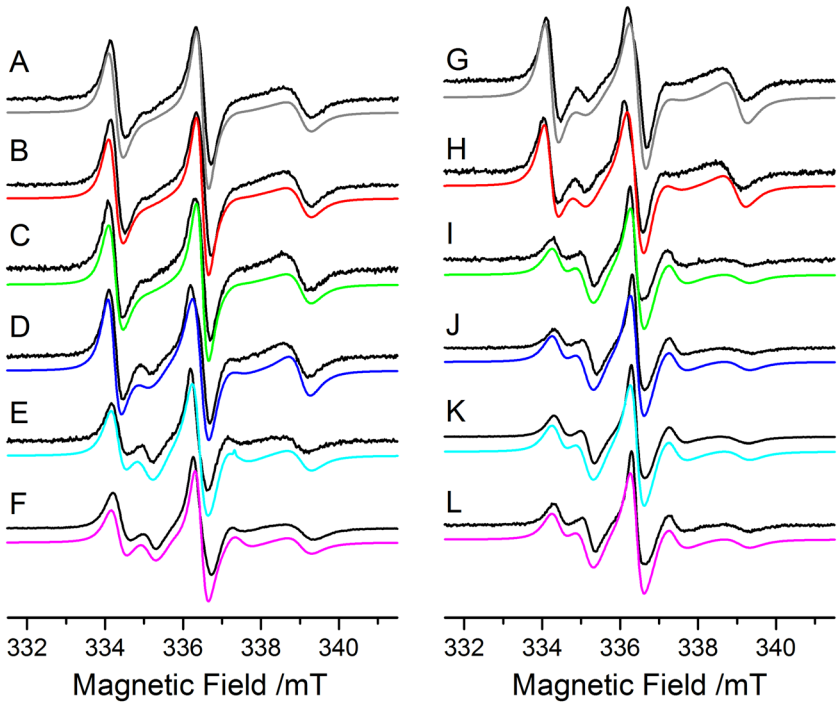

Figure 5. Simulated (colored lines) and experimental (black lines) EPR spectra of DMPC/DHPC bicelles labeled with 5DPC and oriented with the magnetic field parallel to the bilayer normal, $T = 308$ K. The bicelles incorporate HP(2–20), left, or HPA3, right, at increasing P/L ratios: HP(2–20), (A) 1 : 255; (B) 1 : 100; (C) 1 : 75; (D) 1 : 70; (E) 1 : 50; (F) 1 : 25. HPA3, (G) 1 : 375; (H) 1 : 310; (I) 1 : 190; (J) 1 : 100; (K) 1 : 70; and (L) 1 : 50.

perturbation caused by AMPs through *S*, the order parameter of the nitroxide moiety in 5DPC, determined from the simulation of the EPR spectra. In Figure 6, we summarize the results obtained for all of the peptides at increasing P/L ratios at near physiological temperature (308 K). As evident from Figure 6, *S* is very sensitive to the perturbation induced by AMPs even at low P/L ratios. Instead, ^{2}H-NMR spectroscopic studies reveal a chain order profile in which bonds close to the head group region are almost unaffected [57,58]. The order parameters obtained by EPR and NMR are not directly comparable because they refer to different molecular segments and are calculated from different magnetic interactions. The order parameters obtained by ^{2}H-NMR experiments are determined from the quadrupolar splittings for the different C–D bonds of the lipid chains (and extended to the different C–C segments) [54,59], whereas the order parameters obtained by EPR are calculated from the hyperfine interaction of the nitroxide moiety.

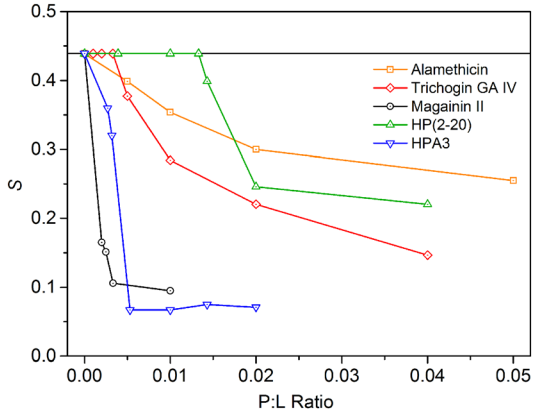

Figure 6. Plot of the 5DPC order parameter *S* as a function of the P/L ratio. The order parameter has been obtained from the simulations of the EPR spectra of DMPC/DHPC bicelles at 308 K. The horizontal black line at $S = 0.44$ represents the order parameter observed in the absence of peptides.

In Figure 6, the first point at $S = 0.44$ corresponds to the order parameter observed in the absence of peptides [Figure 3(A)]. This value is the upper limit observed in the spectra of oriented bicelles. When the peptides bind to the bicelles, the order parameter decreases with the P/L ratio. This trend, however, is not identical for all peptides, and some important differences can be observed. Two main groups can be identified: alamethicin and trichogin GA IV, hydrophobic peptaibiotics, show an exponential decrease of the order parameter that never approaches the isotropic limit. Magainin 2 and HPA3, amphipathic cationic peptides, exhibit a very steep decrease of *S* at very low P/L ratios; then, *S* quickly reaches a plateau at values close to the isotropic limit ($S = 0$). The behavior of HP(2–20) is different from those of both hydrophobic and amphipathic peptides; an initial extended plateau, where *S* is at its maximum value, is followed by a sudden drop to an almost constant value of *S* (≈0.25).

The AMPs under study are characterized by different length, hydrophobicity, hydrophobic moment, and charge (Table 1). These parameters are known to influence binding and activity of AMPs toward membranes [6]. For zwitterionic membranes, such as the DMPC/DHPC bicelles, hydrophobic rather than electrostatic interactions were shown to affect the AMPs behavior [6,57]. Thereby, the effects on the order parameter shown in Figure 6 are not expected to be critically dependent on the net charge. Our results can be rationalized starting from the observation that the loss of order in the lipid chains induced by helical AMPs depends on their insertion depth and on their orientation

Journal of PeptideScience

relative to the membrane normal ***n*** [57], which in turn are tied to the mechanism of membrane disruption. Peptides that absorb parallel to the membrane surface can have very different effects on the lipid packing (and consequently on the order parameter) depending on their insertion depth. Peptides that intercalate in the polar headgroup region cause a large alteration of the lipid packing, resulting in a strong decrease of the order parameter [57]. Peptides that penetrate deeper into the membrane should minimally perturb the bilayer because the mass density and lateral pressure profile of the bilayer have a local minimum below the headgroup region [60]. On the other hand, a transmembrane orientation always leads to a modest decrease of the order parameter, because the perturbation of the membrane packing is minimal [57].

We will first discuss alamethicin and magainin 2, the mechanism of action of which is well-known. Alamethicin interacts with the membrane through formation of concentration-dependent and voltage-dependent barrel–stave pores that do not involve a strong deformation of the bilayer. Additionally, we have shown that alamethicin adopts a transmembrane orientation in bicelles at all P/L ratios [18]. Overall, the gradual and modest decrease of the order parameter shown in Figure 6 is in excellent agreement with the behavior of alamethicin. Magainin 2, a cationic and amphipathic AMP, is the first AMP that has been shown to form the so-called toroidal pores. These are disordered pores where the peptides and the polar lipid headgroups are mixed [23–26]. Toroidal pores are now recognized as one aspect of the more general Shai–Matsuzaki–Huang mechanism that is usually invoked for cationic amphipathic AMPs. In this model, the peptides bind parallel to the headgroup region close to the membrane-water interface. At higher concentrations, they bend the lipids, forming toroidal pores, and eventually they could micellize the membrane. Thus, magainin 2 is expected to strongly disrupt the lipid packing even at low P/L ratio, leading to the steep and marked decrease of the order parameter shown in Figure 6.

In this framework, we discuss the effect of the other AMPs on the bilayer order. Trichogin GA IV is another hydrophobic peptaibiotic, like alamethicin. Its location in the bilayer and its mechanism of action have been studied by EPR and several other spectroscopic and theoretical methods [50,61–68]. Although the detailed mechanism is still under debate, there is a general consensus that at low P/L ratios, the peptide is monomeric and absorbed parallel to the membrane surface below the polar headgroups. It becomes oligomeric and adopts a transmembrane orientation at high P/L ratios [66–68]. The insertion depth of trichogin GA IV at low P/L ratios explains the plateau of the order parameter that we observe for P/L ratio up to 1 : 300. At higher P/L ratios, the trend of the order parameter is very similar to that of alamethicin, indicating a transmembrane insertion. The curve of trichogin GA IV is shifted to lower values of *S* than that of alamethicin, indicating a slightly greater disrupting effect on the membrane. Alamethicin is long enough to span the whole bicelle, and tilts its helical axis to minimize the lipid mismatch, allowing a stable insertion [18]. On the contrary, trichogin GA IV is too short to span the membrane. We can speculate that the orientation of its helical axis would be subjected to large fluctuations because the peptide cannot be anchored to the membrane surfaces. Moreover, the peptide has a very flexible linear octanoyl chain at the *N*-terminus. Both factors can explain the greater decrease of the order parameter with respect to alamethicin.

Both HP(2–20) and its synthetic analog HPA3 are amphipathic and cationic: HPA3 is characterized by two pinpoint substitutions at the hydrophobic/hydrophilic interface of the helix i.e. two Trp residues substituted for Gln and Asp (Figure 2). HPA3 was designed to have higher hydrophobicity and amphipathicity than HP(2–20), because it was suggested that for good activity AMPs should possess a high hydrophobic moment coupled to a moderate hydrophobicity [6]. In agreement with the predictions, HPA3 has improved activity against bacteria and fungi relative to HP(2–20) [34]. Its mechanism of action has been studied using a combination of fluorescence, electron microscopy, and cross-linking experiments [35]. The experimental data suggest that HPA3 acts as oligomeric species with formation of discrete toroidal pores (≈4 nm in diameter) [35]. Our data fully support the formation of toroidal pores for HPA3, because the curve of the order parameter shows the same trend as that of magainin 2, characterized by a steep decrease of the order parameter at very low P/L ratios and a final value of *S* close to the isotropic limit.

For HP(2–20), no conclusive evidence for a specific mechanism can be found in the literature [35,69–71]. The peptide was shown to bind as a monomer causing membrane thinning and to create small pores (2 nm in diameter) in the oligomeric form. In agreement with the complex picture described in the literature, the trend of *S* for HP(2–20) is different from that of the other peptides. There is an initial plateau where no membrane perturbation takes place, which extends to a P/L ratio of 1 : 75. Then, *S* rapidly drops and stabilizes at intermediate values, in between those shown by alamethicin and trichogin GA IV. These results can be discussed in light of the much lower hydrophobicity of HP(2–20) relative to that of HPA3. We calculated that although the difference in the hydrophobic moment is modest, 3.98 for HP(2–20) *versus* 4.07 for HPA3, there is a great variation in the hydrophobicity, −2.75 for HP(2–20) *versus* −0.98 for HPA3 (Table 1). The very low hydrophobicity, compared with those of the other peptides, implies that the affinity of HP(2–20) for the zwitterionic lipid bilayer is limited, and the binding constant is probably low. The initial plateau of the order parameter is the result of extremely low concentrations of membrane-bound peptide. Once a critical concentration is reached, the peptide binds to the membrane and causes the observed decrease of the order parameter. Given its high hydrophobic moment, it is reasonable to hypothesize that the peptide is bound parallel to the surface. However, because the angle formed by the hydrophilic sector of HP(2–20) is very high (~220°), much higher than those of HPA3 (~180°) or magainin 2 (~120°), HP(2–20) probably resides closer to the surface as compared with the other two peptides. The limited decrease of the order parameter seems to indicate that HP(2–20) saturates the membrane at low concentrations of bound peptide. Overall, our data suggest that the behavior of HP(2–20) cannot be simply reconducted to either of the two mechanisms of membrane disruption discussed earlier. More probably, this peptide induces the formation of transient openings in the membrane when the regions of irregular lipid packing surrounding each monomer overlap.

Conclusions

In this work, we studied the interaction of macroscopically oriented DMPC/DHPC bicelles, doped with the spin-labeled phospholipid 5DPC, with several AMPs at physiological temperature

and at different P/L ratios using EPR spectroscopy. The lineshape of 5DPC proved to be very sensitive to the presence of the peptides, even at very low P/L ratios. The simulation of the EPR spectra allowed us to determine the variation of *S*, the order parameter of 5DPC, as a function of the P/L ratio.

We compared the EPR spectra obtained for three peptides for which the mechanism of action is not well-defined, HP2-20, HPA3, trichogin GA IV, with the results on two peptides that are prototypes of the principal mechanisms of pore formation, magainin 2 (toroidal pores) and alamethicin (barrel-stave pores). In our experiments, magainin 2 shows a strong perturbation of the order parameter at very low P/L ratios and leads to a steep decrease of the lipid order parameter that almost reaches the isotropic limit as the peptide concentration is increased. On the contrary, alamethicin displays a gradual lowering of the order parameter, moderate even at high P/L ratios. On the basis of the results for the two archetypical peptides, we conclude that trichogin GA IV, a hydrophobic lipopeptide, inserts deeply below the lipid head groups and acts in a similar way as alamethicin. HPA3, a cationic, amphipathic peptide, shows the same behavior of magainin 2 and thus likely forms toroidal pores. Finally, HP(2–20), also a cationic, amphipathic peptide, but much more hydrophilic than HPA3, does not follow simply one of the two classic mechanisms of membrane disruption.

In conclusion, we have shown that AMPs with different mechanisms of action show very different trends of the order parameter as a function of peptide concentration. Therefore, we suggest that bicelles, in combination with EPR spectroscopy, represent a valuable tool to evaluate how the membranes are disrupted by new AMPs.

Acknowledgement

This work was supported by Fondazione CARIPARO (Progetti Eccellenza 2011/2012) and MIUR (PRIN 2010–2011, prot. 2010NRREPL).

References

1 Fjell CD, Hiss JA, Hancock REW, Schneider G. Designing antimicrobial peptides: form follows function. *Nat. Rev. Drug Discovery* 2012; **11**: 37–51.
2 Bechinger B, Aisenbrey C. The polymorphic nature of membrane-active peptides from biophysical and structural investigations. *Curr. Protein Pept. Sci.* 2012; **13**: 602–610.
3 Vila-Farres X, Giralt E, Vila J. Update of peptides with antibacterial activity. *Curr. Med. Chem.* 2012; **19**: 6188–6198.
4 Seo MD, Won HS, Kim JH, Mishig-Ochir T, Lee BJ. Antimicrobial peptides for therapeutic applications: a review. *Molecules* 2012; **17**: 12276–12286.
5 Scheller A, Oehlke J, Wiesner B, Dathe M, Krause E, Beyermann M, Melzig M, Bienert M. Structural requirements for cellular uptake of α-helical amphipathic peptides. *J. Pept. Sci.* 1999; **5**: 185–194.
6 Dathe M, Wieprecht T. Structural features of helical antimicrobial peptides: their potential to modulate activity on model membranes and biological cells. *Biochim. Biophys. Acta, Biomembr.* 1999; **1462**: 71–87.
7 Fox RO, Richards FM. A voltage-gated ion channel model inferred from the crystal structure of alamethicin at 1.5-Å resolution. *Nature* 1982; **300**: 325–330.
8 Zasloff M. Antimicrobial peptides of multicellular organisms. *Nature* 2002; **415**: 389–395.
9 He K, Ludtke SJ, Worcester DL, Huang HW. Neutron scattering in the plane of membranes: structure of alamethicin pores. *Biophys. J.* 1996; **70**: 2659–2666.
10 Boheim G, Kolb HA. Analysis of the multi-pore system of alamethicin in a lipid membrane. I. Voltage-jump current relaxation measurements. *J. Membr. Biol.* 1978; **38**: 99–150.
11 Molle G, Duclohier H, Spach G. Voltage-dependent and multistate ionic channels induced by trichorzianines, antifungal peptides related to alamethicin. *FEBS Lett.* 1987; **224**: 208–212.
12 Molle G, Duclohier H, Dugast JY, Spach G. Design and conformation of non-Aib synthetic peptides enjoying alamethicin-like ionophore activity. *Biopolymers* 1989; **28**: 273–283.
13 Bobone S, Roversi D, Giordano L, De Zotti M, Formaggio F, Toniolo C, Park Y, Stella L. The lipid dependence of antimicrobial peptide activity is an unreliable experimental test for different pore models. *Biochemistry* 2012; **51**: 10124–10126.
14 Cardon TB, Tiburu EK, Lorigan GA. Magnetically aligned phospholipid bilayers in weak magnetic fields: optimization, mechanism, and advantages for X-band EPR studies. *J. Magn. Reson.* 2003; **161**: 77–90.
15 Berliner LJ. (Ed). *Spin Labeling the Next Millennium*, New York: Plenum Press,1998.
16 Bortolus M, Tombolato F, Tessari I, Bisaglia M, Mammi S, Bubacco L, Ferrarini A, Maniero AL. Broken helix in vesicle and micelle-bound a-synuclein: insights from site-directed spin labeling-EPR experiments and md simulations. *J. Am. Chem. Soc.* 2008; **130**: 6690–6691.
17 Bortolus M, Parisio G, Maniero AL, Ferrarini A. Monomeric fullerenes in lipid membranes: effects of molecular shape and polarity. *Langmuir* 2011; **27**: 12560–12568.
18 Bortolus M, De Zotti M, Formaggio F, Maniero AL. Alamethicin in bicelles: orientation, aggregation, and bilayer modification as a function of peptide concentration. *Biochim. Biophys. Acta, Biomembr.* 2013; **1828**: 2620–2627.
19 Inbaraj JJ, Cardon TB, Laryukhin M, Grosser SM, Lorigan GA. Determining the topology of integral membrane peptides using EPR spectroscopy. *J. Am. Chem. Soc.* 2006; **128**: 9549–9554.
20 He K, Ludtke SJ, Huang HW, Worcester DL. Antimicrobial peptide pores in membranes detected by neutron inplane scattering. *Biochemistry* 1995; **34**: 15614–15618.
21 Salditt T, Li CH, Spaar A. Structure of antimicrobial peptides and lipid membranes probed by interface-sensitive X-ray scattering. *Biochim. Biophys. Acta, Biomembr.* 2006; **1758**: 1483–1498.
22 Li C, Salditt T. Structure of magainin and alamethicin in model membranes studied by X-ray reflectivity. *Biophys. J.* 2006; **91**: 3285–3300.
23 Matsuzaki K. Magainins as paradigm for the mode of action of pore forming polypeptides. *Biochim. Biophys. Acta, Rev. Biomembr.* 1998; **1376**: 391–400.
24 Papo N, Shai Y. Exploring peptide membrane interaction using surface plasmon resonance: differentiation between pore formation *versus* membrane disruption by lytic peptides. *Biochemistry* 2003; **42**: 458–466.
25 Ludtke SJ, He K, Heller WT, Harroun TA, Yang L, Huang HW. Membrane pores induced by magainin. *Biochemistry* 1996; **35**: 13723–13728.
26 Nguyen KT, Le Clair SV, Ye SJ, Chen Z. Molecular interactions between magainin 2 and model membranes *in situ*. *J. Phys. Chem. B* 2009; **113**: 12358–12363.
27 Toniolo C, Brückner H. (Eds). *Peptaibiotics*, Wiley-VCH: Weinheim, Germany, 2009.
28 Leitgeb B, Szekeres A, Manczinger L, Vagvolgyi C, Kredics L. The history of alamethicin: a review of the most extensively studied peptaibol. *Chem. Biodivers.* 2007; **4**: 1027–1051.
29 De Zotti M, Biondi B, Peggion C, Formaggio F, Park Y, Hahm KS, Toniolo C. Trichogin GA IV: a versatile template for the synthesis of novel peptaibiotics. *Org. Biomol. Chem.* 2012; **10**: 1285–1299.
30 De Zotti M, Biondi B, Formaggio F, Toniolo C, Stella L, Park Y, Hahm KS. Trichogin GA IV: an antibacterial and protease-resistant peptide. *J. Pept. Sci.* 2009; **15**: 615–619.
31 Toniolo C, Crisma M, Formaggio F, Peggion C, Monaco V, Goulard C, Rebuffat S, Bodo B. Effect of N-α-acyl chain length on the membrane-modifying properties of synthetic analogs of the lipopeptaibol trichogin GA IV. *J. Am. Chem. Soc.* 1996; **118**: 4952–4958.
32 Bechinger B. Detergent-like properties of magainin antibiotic peptides: a P-31 solid-state NMR spectroscopy study. *Biochim. Biophys. Acta, Biomembr.* 2005; **1712**: 101–108.
33 Imura Y, Choda N, Matsuzaki K. Magainin 2 in action: distinct modes of membrane permeabilization in living bacterial and mammalian cells. *Biophys. J.* 2008; **95**: 5757–5765.
34 Lee KH, Lee DG, Park Y, Kang DI, Shin SY, Hahm KS, Kim Y. Interactions between the plasma membrane and the antimicrobial peptide HP (2–20) and its analogues derived from *Helicobacter pylori*. *Biochem. J.* 2006; **394**: 105–114.
35 Park SC, Kim MH, Hossain MA, Shin SY, Kim Y, Stella L, Wade JD, Park Y, Hahm KS. Amphipathic a-helical peptide, HP (2–20), and its analogues derived from *Helicobacter pylori*: pore formation mechanism in various lipid compositions. *Biochim. Biophys. Acta, Biomembr.* 2008; **1778**: 229–241.

36 Tossi A, Sandri L, Giangaspero A. Amphipathic, a-helical antimicrobial peptides. *Biopolymers* 2000; **55**: 4–30.
37 Peggion C, Formaggio F, Crisma M, Epand RF, Epand RM, Toniolo C. Trichogin: a paradigm for lipopeptaibols. *J. Pept. Sci.* 2003; **9**: 679–689.
38 Rice P, Longden I, Bleasby A. Emboss: the European molecular biology open software suite. *Trends Genet.* 2000; **16**: 276–277.
39 Eisenberg D. Three-dimensional structure of membrane and surface proteins. *Annu. Rev. Biochem.* 1984; **53**: 595–623.
40 Tossi A, Sandri L, Giangaspero A. New consensus hydrophobicity scale extended to non-proteinogenic amino acids. In *Peptides 2002: Proceedings of the Twenty-Seventh European Peptide Symposium*, Edizioni Ziino: Napoli, Italy, 2002; 416–417.
41 Nieh MP, Glinka CJ, Krueger S, Prosser RS, Katsaras J. SANS study of the structural phases of magnetically alignable lanthanide-doped phospholipid mixtures. *Langmuir* 2001; **17**: 2629–2638.
42 Budil DE, Lee S, Saxena S, Freed JH. Nonlinear-least-squares analysis of slow-motion EPR spectra in one and two dimensions using a modified Levenberg-Marquardt algorithm. *J. Magn. Reson., Ser. A* 1996; **120**: 155–189.
43 Liang ZC, Lou Y, Freed JH, Columbus L, Hubbell WL. A multifrequency electron spin resonance study of T4 lysozyme dynamics using the slowly relaxing local structure model. *J. Phys. Chem. B.* 2004; **108**: 17649–17659.
44 Kroncke BM, Horanyi PS, Columbus L. Structural origins of nitroxide side chain dynamics on membrane protein a-helical sites. *Biochemistry* 2010; **49**: 10045–10060.
45 Xu DJ, Crepeau RH, Ober CK, Freed JH. Molecular dynamics of a liquid crystalline polymer studied by two-dimensional Fourier transform and CW ESR. *J. Phys. Chem.* 1996; **100**: 15873–15885.
46 Hoffman L, Stein RA, Colbran RJ, Mchaourab HS. Conformational changes underlying calcium/calmodulin-dependent protein kinase II activation. *EMBO J.* 2011; **30**: 1251–1262.
47 Barnes JP, Liang ZC, Mchaourab HS, Freed JH, Hubbell WL. A multifrequency electron spin resonance study of T4 lysozyme dynamics. *Biophys. J.* 1999; **76**: 3298–3306.
48 Kurad D, Jeschke G, Marsh D. Spin-label HF-EPR of lipid ordering in cholesterol-containing membranes. *Appl. Magn. Reson.* 2001; **21**: 469–481.
49 Cassol R, Ge MT, Ferrarini A, Freed JH. Chain dynamics and the simulation of electron spin resonance spectra from oriented phospholipid membranes. *J. Phys. Chem. B.* 1997; **101**: 8782–8789.
50 Bocchinfuso G, Bobone S, Mazzuca C, Palleschi A, Stella L. Fluorescence spectroscopy and molecular dynamics simulations in studies on the mechanism of membrane destabilization by antimicrobial peptides. *Cell. Mol. Life Sci.* 2011; **68**: 2281–2301.
51 Mason AJ, Chotimah INH, Bertani P, Bechinger B. A spectroscopic study of the membrane interaction of the antimicrobial peptide pleurocidin. *Mol. Membr. Biol.* 2006; **23**: 185–194.
52 Mason AJ, Gasnier C, Kichler A, Prevost G, Aunis D, Metz-Boutigue MH, Bechinger B. Enhanced membrane disruption and antibiotic action against pathogenic bacteria by designed histidine-rich peptides at acidic pH. *Antimicrob. Agents Chemother.* 2006; **50**: 3305–3311.
53 Bechinger B, Salnikov ES. The membrane interactions of antimicrobial peptides revealed by solid-state NMR spectroscopy. *Chem. Phys. Lipids* 2012; **165**: 282–301.
54 Seelig A, Seelig J. The dynamic structure of fatty acyl chains in a phosphatidylcholine bilayer measured by deuterium magnetic resonance. *Biochemistry* 1974; **13**: 4839–4845.
55 Subczynski WK, Wisniewska A, Kusumi A, McElhaney RN. Effects of pH-induced variations of the charge of the transmembrane α-helical peptide Ac-K-2(LA)(12)K-2-amide on the organization and dynamics of the host dimyristoylphosphatidylcholine bilayer membrane. *Biochim. Biophys. Acta, Biomembr.* 2005; **1720**: 99–109.
56 Yeagle P. *The Structure of Biological Membranes*, CRC Press: Boca Raton, FL,2005.
57 Bechinger B. Rationalizing the membrane interactions of cationic amphipathic antimicrobial peptides by their molecular shape. *Curr. Opin. Colloid Interface Sci.* 2009; **14**: 349–355.
58 Mason AJ, Martinez A, Glaubitz C, Danos O, Kichler A, Bechinger B. The antibiotic and DNA-transfecting peptide LAH4 selectively associates with, and disorders, anionic lipids in mixed membranes. *FASEB J* 2006; **20**: 320–322.
59 Douliez JP, Leonard A, Dufourc EJ. Restatement of order parameters in biomembranes: calculation of C-C bond order parameters from C-D quadrupolar splittings. *Biophys. J.* 1995; **68**: 1727–1739.
60 Parisio G, Ferrarini A. Solute partitioning into lipid bilayers: an implicit model for nonuniform and ordered environment. *J. Chem. Theory Comput.* 2010; **6**: 2267–2280.
61 Heuber C, Formaggio F, Baldini C, Toniolo C, Müller K. Multinuclear solid-state-NMR and FT-IR-absorption investigations on lipid/trichogin bilayers. *Chem. Biodivers.* 2007; **4**: 1200–1218.
62 Milov AD, Samoilova RI, Tsvetkov YD, Formaggio F, Toniolo C, Raap J. Membrane-peptide interaction studied by PELDOR and CW ESR: peptide conformations and cholesterol effect on the spatial peptide distribution in the membrane. *Appl. Magn. Reson.* 2005; **29**: 703–716.
63 Dzuba SA. Structural studies of biological membranes using ESEEM spectroscopy of spin labels and deuterium substitution. *J. Struct. Chem.* 2013; **54**: S1–S15.
64 Dzuba SA, Raap J. Spin-echo electron paramagnetic resonance (EPR) spectroscopy of a pore-forming (lipo)peptaibol in model and bacterial membranes. *Chem. Biodivers.* 2013; **10**: 864–875.
65 Mazzuca C, Stella L, Venanzi M, Formaggio F, Toniolo C, Pispisa B. Mechanism of membrane activity of the antibiotic trichogin GA IV: a two-state transition controlled by peptide concentration. *Biophys. J.* 2005; **88**: 3411–3421.
66 Bocchinfuso G, Palleschi A, Orioni B, Grande G, Formaggio F, Toniolo C, Park Y, Hahm KS, Stella L. Different mechanisms of action of antimicrobial peptides: insights from fluorescence spectroscopy experiments and molecular dynamics simulations. *J. Pept. Sci.* 2009; **15**: 550–558.
67 Syryamina VN, De Zotti M, Peggion C, Formaggio F, Toniolo C, Raap J, Dzuba SA. A molecular view on the role of cholesterol upon membrane insertion, aggregation, and water accessibility of the antibiotic lipopeptide trichogin GA IV as revealed by EPR. *J. Phys. Chem. B* 2012; **116**: 5653–5660.
68 Salnikov ES, Erilov DA, Milov AD, Tsvetkov YD, Peggion C, Formaggio F, Toniolo C, Raap J, Dzuba SA. Location and aggregation of the spin-labeled peptide trichogin GA IV in a phospholipid membrane as revealed by pulsed EPR. *Biophys. J.* 2006; **91**: 1532–1540.
69 Jang SH, Park Y, Park SC, Kim PI, Lee DG, Hahm KS. Antinematodal activity and the mechanism of the antimicrobial peptide, HP (2–20), against *Caenorhabditis elegans*. *Biotechnol. Lett.* 2004; **26**: 287–291.
70 Lee DG, Kim PI, Park Y, Jang SH, Park SC, Woo ER, Hahm KS. HP (2–20) derived from the amino terminal region of *Helicobacter pylori* ribosomal protein L1 exerts its antifungal effects by damaging the plasma membranes of *Candida albicans*. *J. Pept. Sci.* 2002; **8**: 453–460.
71 Lee DG, Park Y, Kim HN, Kim HK, Kim PI, Choi BH, Hahm KS. Antifungal mechanism of an antimicrobial peptide, HP (2–20), derived from N-terminus of *Helicobacter pylori* ribosomal protein L1 against *Candida albicans*. *Biochem Biophys. Res. Commun.* 2002; **291**: 1006–1013.

RSC Advances

PAPER

Cite this: *RSC Adv.*, 2015, **5**, 98955

Liponitroxides: EPR study and their efficacy as antioxidants in lipid membranes†

Giovanna Mobbili,[a] Emanuela Crucianelli,[a] Antonio Barbon,[c] Massimo Marcaccio,[d] Michela Pisani,[b] Annalisa Dalzini,[c] Eleonora Ussano,[d] Marco Bortolus,*[ce] Pierluigi Stipa*[b] and Paola Astolfi*[b]

Received 15th September 2015
Accepted 3rd November 2015

DOI: 10.1039/c5ra18963b

www.rsc.org/advances

A series of lipid-functionalized nitroxides having a pyrroline nitroxide moiety linked either to a glycerol or to a steroid unit has been synthesized, and their inclusion inside phospholipid bilayers has been investigated by Electron Paramagnetic Resonance (EPR) spectroscopy. The antioxidant behavior of these nitroxides has been studied in azo-initiator induced lipid peroxidation by means of the Thiobarbituric Acid Reactive Species (TBARS) assay; a correlation with their penetration depth within the bilayer has been found. The possible mechanisms involved in the antioxidant action have been considered, discussed and alternative pathways have been suggested for the synthesized liponitroxides due to their different localization. The steroid derivative is limited to scavenging radicals that are generated in the aqueous phase, while the glycerolipids can also act as chain breaking antioxidants.

Introduction

Lipid peroxidation (LP) is a critical and common damaging process in biological membranes and liposomial dispersion containing polyunsaturated fatty acids (PUFAs). The associated damage is highly detrimental to the functioning of the cell and its survival, since membranes form the basis of many cellular organelles like mitochondria, plasma membranes, lysosomes, peroxisomes, *etc.* Thus, prevention of LP represents an interesting therapy in many diseases and pathologies involving free radicals[1] and is also an important aspect in the preparation and preservation of liposomes to be used as carriers for several agents in medicinal, pharmaceutical, cosmetic and food industry applications.

In this context cyclic nitroxides (aminoxyls), stable compounds with an unpaired electron on the N–O function included in an aliphatic or aromatic ring system, have gained popularity as a distinct class of antioxidants thanks to their protective effects against oxidative stress in a multiplicity of biological systems.[2] It has been shown that nitroxides effectively protect cells, tissues, organs, and animals from radical-induced damage and that these antioxidant activities derive from their abilities to scavenge radicals,[3] catalyze superoxide dismutation,[4] facilitate catalase-like activity of heme-proteins,[5] detoxify hypervalent metals, and oxidize reduced transition metals ions.[6] The antioxidant activity of both aliphatic[7] and aromatic[8] nitroxides against radical-induced LP has been extensively studied due to the importance and seriousness of this phenomenon. In fact, their reactivity toward lipid derived radicals ($L^{\bullet}$) *via* radical–radical coupling is well known and documented, whereas more controversial is that toward oxygen-centred radicals (ROS, reactive oxygen species)[9] which is still debated.[10] However, it has been shown that nitroxides are able to reduce alkylperoxyl radicals forming the corresponding oxoammonium cations ($>N^{+}=O$) and that a relationship between the oxidation potentials of nitroxides and their peroxyl radicals scavenging abilities exists.[10a] Since peroxyl radicals are important intermediates in LP, it follows that the antioxidant power of a nitroxide against lipid peroxidation should be determined by its radical scavenging ability as well as its redox potential. However, these are not the only aspects that demand consideration, given the complexity of biological lipid membranes and of LP, a process in which the formation of the damaging species is not uniform across the membrane. Since the peroxidation normally takes places at the fatty acids double bonds, which are located at specific positions in the bilayers, the structure of the nitroxide, its penetration as well as its

[a]*Department of Life and Environmental Sciences, Università Politecnica delle Marche, Via Brecce Bianche 12, I-60131 Ancona, Italy*

[b]*Department of Materials, Environmental Sciences and Urban Planning, Università Politecnica delle Marche, Via Brecce Bianche 12, I-60131 Ancona, Italy. E-mail: p.stipa@univpm.it; p.astolfi@univpm.it*

[c]*Department of Chemical Sciences, Università di Padova, Via Marzolo 1, I-35131 Padova, Italy. E-mail: marco.bortolus@unipd.it*

[d]*Department of Chemistry "G. Ciamician", Università di Bologna, Via Selmi 2, I-40126 Bologna, Italy*

[e]*Department of Material Sciences, Università degli Studi di Milano Bicocca, Via Roberto Cozzi 55, I-20125 Milano, Italy*

† Electronic supplementary information (ESI) available: Spectroscopic characterization of liponitroxides. Cyclic voltammetric curves of **Chol-NO** at low temperature in THF; background cyclic voltammetric curves for 0.08 M $NaBF_4$ aqueous electrolyte solution with PBS buffer at pH = 7.4. Accessibility parameters Π_i to oxygen and to NiEDDA. See DOI: 10.1039/c5ra18963b

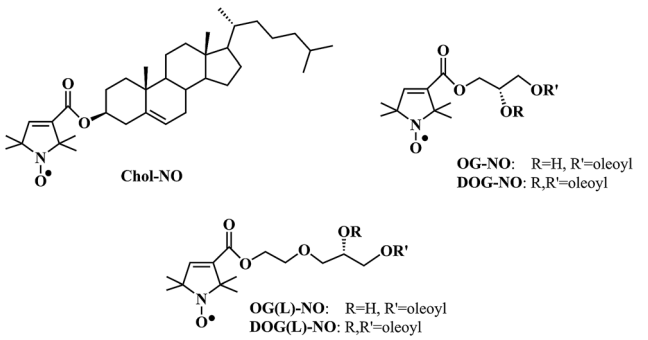

Chart 1 Lipid-functionalized nitroxides **NOXs** synthesized and tested for their antioxidant activity.

Table 1 Half-wave ($E_{1/2}$) redox potentials (*vs.* NHE) of studied species at 298 K

Species[a]	(Red) – $E_{1/2}$/V	(Ox) – $E_{1/2}$/V
DOG-NO[a]	−1.58[b,c]	1.33
OG(L)-NO[a]	−1.57[b,c]	1.31
OG(L)-NO(ads)	—	1.12
Chol-NO[a]	−1.59[b,c]	1.32
Chol-NO(ads)[d]	−1.07[c]	1.16

[a] In a 0.08 M $TBAPF_6$/THF solution. [b] Sluggish electrochemical process. [c] Irreversible process, peak potential. [d] Drop casted species on GC electrode in a 0.08 M $NaBF_4$ aqueous solution buffered (pH = 7.4) with phosphate buffer.

mobility in the membrane interior have also to be taken into account. For these reasons, lipid-functionalized nitroxides that have a good affinity for lipid bilayer are attractive molecules to be used as antioxidants, but so far, they have been synthesized mainly as potential spin probes for Electron Paramagnetic Resonance (EPR) spectroscopy[11] in the context of membrane structure studies.[12] Only in one case the antioxidant activity of two steroidic nitroxyl radicals has been also studied.[7a]

In this work, a series of lipid-functionalized nitroxides (**NOXs**) has been synthesized (Chart 1) with the double aim of locating the nitroxide at different depths inside the lipid membrane, and to look for relationships between their location and antioxidant activity. These compounds have a pyrroline nitroxide linked to a cholesterol unit or to glycerol esterified with one or two oleoyl moieties. In particular, the glycerol-functionalized nitroxides contain one (**OG-NO**/**OG(L)-NO**) or two (**DOG-NO**/**DOG(L)-NO**) oleic acid chains, which may differently anchor the molecule into the lipid bilayer. Moreover, two of the **NOXs** have a polar spacer group in the headgroup region (**OG(L)-NO** and **DOG(L)-NO**), which is expected to push the pyrroline nitroxide toward the lipid–water interface. The electrochemical behaviour of the synthesized compounds has been studied both in THF solution and in an aqueous environment to evaluate their oxidation potential. The position, orientation and dynamics of the **NOXs** inside the bilayer have been determined using different EPR techniques both in liposomes (small unilamellar vesicles, SUV) and in bicelles.[13] Finally, the antioxidant activity of the synthesized **NOXs** has been studied during radical-induced peroxidation of egg-yolk L-α-phosphatidylcholine (Egg-PC) liposomes, chosen as model membranes, and discussed on the basis of their position inside the lipid.

Results

Redox properties

The electrochemical investigation of the nitroxide species was carried out by cyclic voltammetry (CV) in tetrahydrofuran (THF) and in solid state as film in aqueous electrolyte solution (drop-casting the nitroxide lipid onto glassy carbon (GC) disk electrode surface) in aqueous electrolyte solution, at room temperature, using platinum and GC disk as working electrode. THF was chosen as it has a relatively low dielectric constant and so the species are in an environment more similar to that inside a bilayer. The redox potentials of three among the synthesized compounds are collected in Table 1 which are representative for all the others. In fact, it is reasonable to admit that the structure of the lipid portion of the molecule does not substantially affect the redox activity centred on the nitroxide unit.

The cyclic voltammetric curves of **Chol-NO**, in THF and in buffered aqueous solution (drop casted film onto a CG disk electrode) are reported in Fig. 1 (see also Fig. S1† for the electrochemical behaviour at 213 K and Fig. S2† for the background curves in aqueous electrolyte, in the ESI†). In both cases, it is possible to observe a reversible one-electron oxidation process with a half-wave potential of 1.32 V (THF) and 1.16 V (PBS) *vs.* NHE. This can be safely attributed[14] to the oxidation of the nitroxide moiety to form the oxoammonium cation $\rangle N{=}O^+$. On the negative potential side, a one-electron chemically irreversible reduction process can be observed with a cathodic peak potential of −1.59 V (THF) and −1.06 V (PB) *vs.* NHE.

As expected, no substantial differences were found between the redox potentials of the various **NOXs** since the portion of the molecule involved in the redox processes (the pyrroline moiety) is the same in all cases.

Penetration depth

The dimensionless immersion depth parameter Φ was obtained by measuring the enhancement of the relaxation properties (which are related to the saturation of the EPR transitions) for the different **NOXs** generated by the collision of the radicals with paramagnetic relaxing agents having a different distribution inside and outside the membrane. By using either a lipophilic or a hydrophilic agent, respectively oxygen or the complex nickel-ethylenediamine-*N*,*N*′-diacetic acid (NiEDDA),[15] the relaxation properties of **NOXs** will be affected differently, depending on the localization of the nitroxide with respect to the plane of the phosphate groups of the bilayer. The position of the nitroxide relative to such a plane was obtained by comparing the results on the **NOXs** with those of nitroxide-labeled phospholipids (**SLs**)[15] used as standards: 1-palmitoyl-2-stearoyl-(*n*-doxyl)-sn-glycero-3-phosphocholine (*n*DPC) and 1-palmitoyl-2-oleoyl-sn-glycero-3-phospho(tempo)choline (TempoPC).

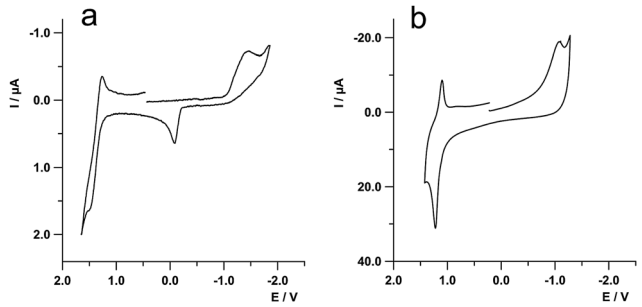

Fig. 1 Cyclic voltammetric curves of species **Chol-NO**. (a) 1 mM in 0.08 M TBAH/THF solution. Sweep rate 1 V s^{-1}, working electrode: Pt (125 μm, diameter), $T = 298$ K; (b) COL-NO drop-casted onto a GC disk electrode (3 mm, diameter), 0.08 M $NaBF_4$ aqueous solution with PB buffer at pH = 7.4, sweep rate 0.2 V s^{-1}, $T = 298$ K.

EPR spectra of **NOXs** in 1-palmitoyl-2-oleoyl-sn-glycero-3-phosphocholine (POPC) small unilamellar vesicles (SUV) at room temperature (298 K) at low microwave power (2 mW) are reported in Fig. 2, panel (f). These spectra have a lineshape much broader than that of **NOXs** in buffer solution (the spectrum of OG in buffer is reported for comparison). The broad lines are indicative of the damping of the nitroxide motion caused by its incorporation in the liposomes. **NOXs** spectra in membranes are discussed in detail in the next section.

In Fig. 2, panels (a)–(e), the saturation curves (and the corresponding fitting) for each sample in the presence of either oxygen or NiEDDA are also shown.

All the experimental details, the fitting procedure, and the used formulas are described in the Experimental section. From the fitting, the saturation parameters, $p^{i}_{1/2}$ were obtained allowing the determination of immersion depth parameters Φ (the accessibility parameters Π_i, to oxygen and to NiEDDA, were determined and reported in ESI, Table S1†). The results of the analysis are summarized in Table 2, where the reported data are the average of experiments performed at least in duplicate. The table reports the adimensional parameters Φ for standard nitroxide-labeled lipids (**SL**) and for our **NOXs** ordered by the increasing penetration depth. Overall, the data show that the water accessibility of **NOXs** decreases in the order: **Chol-NO** ≫ **DOG(L)-NO** > **DOG-NO** ≈ **OG(L)-NO** ≈ **OG-NO**.

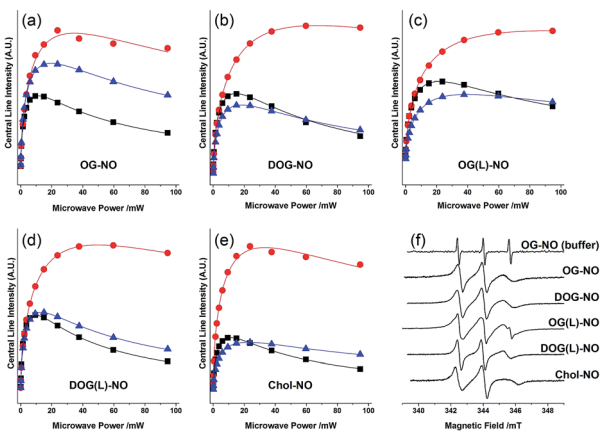

Fig. 2 Power saturation curves (dots), their fitting (lines) and EPR spectra of the **NOXs** in POPC small unilamellar vesicles acquired at room temperature (298 K) in different conditions: black squares, purged with nitrogen; red dots, in equilibrium with air (oxygen); blue triangles, 50 mM NiEDDA and purged with nitrogen. The EPR spectra are relative to the nitrogen purged samples and are taken at low microwave power. For comparison we report the spectrum of OG in buffer.

Liponitroxides in bicelles

To fully understand, at a molecular level, the motion and orientation of **NOXs** in the bilayer, we recorded and simulated their EPR spectra in oriented lipid bicelles at near physiological temperature (308 K), Fig. 3. Bicelles have the peculiarity, with respect to micelles or vesicles, to be macroscopically oriented in solution at physiological temperature under a magnetic field, a property that makes them invaluable for the determination of

Table 2 Penetration depth parameter (Φ) of the different reference spin labels (**SL**) and of the **NOXs** in POPC small unilamellar vesicles obtained at room temperature. The reported uncertainty is a rough estimate based on repeated experiments

SL	Φ (±0.1)	NOX	Φ (±0.1)
TempoPC	<0.3[a]	**Chol-NO**	0.7
5DPC	1.4[b]	**DOG(L)-NO**	1.4
7DPC	1.2[b]	**DOG-NO**	1.8
10DPC	2.1	**OG(L)-NO**	1.9
12DPC	2.4	**OG-NO**	2.1
14DPC	3.0		

[a] Repeated measurements of TempoPC showed a large variability in Φ, but always lower than 0.3. [b] The apparent inversion of Φ is present also in the original paper.[15]

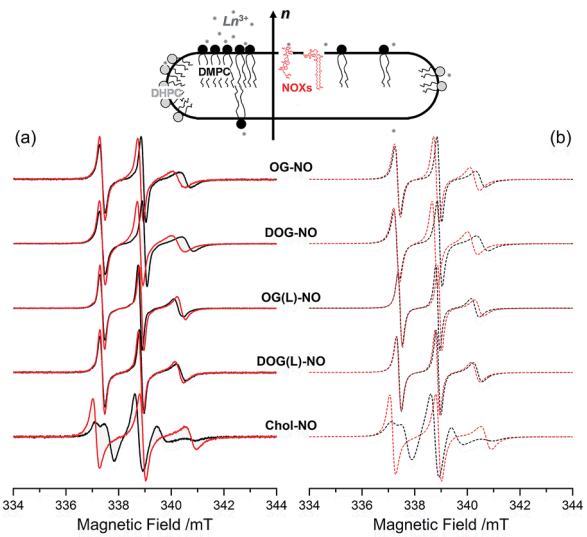

Fig. 3 Top, schematic representation of a bicelle. Panel (a), EPR spectra of **NOX** in DMPC/DHPC bicelles at 308 K. In black the spectra recorded with $B_0 \| \boldsymbol{n}$, in red the spectra recorded with $B_0 \perp \boldsymbol{n}$. Panel (b), spectral simulations (black $B_0 \| \boldsymbol{n}$; red $B_0 \perp \boldsymbol{n}$).

the order and dynamics of solutes and biological molecules in bilayers.[13,16]

These systems are composed of planar regions, made primarily by long chain phospholipids 1,2-dimyristoyl-sn-glycero-3-phosphocholine (DMPC), and of curved edge regions, composed by short-chain phospholipids, 1,2-dihexanoyl-sn-glycero-3-phosphocholine (DHPC). EPR spectra of **NOXs** in bicelles, oriented with the magnetic field (B_0) parallel (black line) and perpendicular (red line) to the membrane normal ($\boldsymbol{n}$), are reported in Fig. 3, panel (a). The spectral simulations, shown in dotted lines in panel (b), are in a rather good agreement with experimental data and offer some insight on the motional parameters of **NOXs** as well as on the orientation of the nitroxide moiety relative to the membrane normal; the simulation parameters are reported in Table 3. The orientation procedure and the simulation details are described in detail in the Experimental section.

The spectra show a single species in slow-motion régime, characteristic of the inclusion of the pyrroline group inside the high-viscosity membrane region. The principal values of the axial rotational diffusion tensor **D** ($\boldsymbol{D}_{\parallel} \approx \boldsymbol{D}_{\perp}$)[18] are in the order of 10^8 s^{-1}, typically 1–2 order of magnitudes lower than in water and this is a clear indication that **NOXs** are fully incorporated in the bicelles. The motion of the nitroxide unit in the glycerolipids is strongly affected by the presence of the additional ethylene glycol unit. The lipids with the ethylene glycol linker (**OG(L)-NO**, **DOG(L)-NO**) have an almost isotropic motion ($\boldsymbol{D}_{\parallel} \approx \boldsymbol{D}_{\perp}$), indicating that the rotational motion of the nitroxide is almost independent from the motion of the lipid tail. On the contrary, when the nitroxide is directly attached to the glycerol unit (**OG-NO**, **DOG-NO**) the diffusion tensor is axial and typical of a molecule with a prolate shape ($\boldsymbol{D}_{\parallel} > \boldsymbol{D}_{\perp}$). The cholesterol derivative **Chol-NO** undergoes a slower and more axial motion than the glycerolipids, as expected from its bulky anisotropic shape.

A further confirmation of the inclusion of the pyrroline group inside the membrane is given by the $\boldsymbol{g}_{xx}$ and A_{zz} values obtained from the simulations. These values are sensitive to the polarity of the environment and, as found by M. Plato *et al*,[17] they range from *ca.* $\boldsymbol{g}_{xx} = 2.0090$ and $A_{zz} = 3.35$ mT in an apolar environment to *ca.* $\boldsymbol{g}_{xx} = 2.0083$ and $A_{zz} = 3.65$ mT in a highly polar environment. As shown in Table 3, the obtained values clearly indicate that all **NOXs** are in an apolar environment; the A_{zz} value for **Chol-NO** is larger than the others (3.45 mT *vs.* 3.35 mT, respectively), suggesting that the pyrroline moiety of this nitroxide is located in a slightly more polar environment.

The linewidths (Gaussian linewidths $\leq$0.1 mT for all spectra) are such to exclude **NOXs** clusterization that would have generated significant Lorentzian line broadening by spin–spin interaction.

As shown in Fig. 3, different spectra were recorded when bicelle planes were parallel or perpendicular to the magnetic field. This means that **NOXs** are oriented with respect to the membrane surface; with the exception of **DOG(L)-NO** which has almost completely overlapping spectra. The differences in the spectra between the two orientations depend on the degree of order experienced by the nitroxide in the bilayer: this is quantitatively expressed in Table 3 by the principal values of the adimensional, traceless, order parameter matrix S, in particular by the S_{zz} componenent. **OG(L)-NO** and **DOG(L)-NO** have a smaller degree of order than **OG-NO** and **DOG-NO**. These results, together with the observed values for the rotational diffusion tensors, further confirm that the ethylene glycol unit decouples the motion of the pyrroline unit from that of the lipid chains. In particular, **DOG(L)-NO** has almost a negligible degree of order. On the other hand, the cholesterol derivative **Chol-NO** has a much larger degree of order than the glycerolipids and, interestingly, it displays a biaxial orientation ($S_{xx} \neq S_{yy} \neq S_{zz}$), which is typical for molecules having a strongly anisotropic shape.

EPR spectra simulations also give information about the orientation (given by the Euler angles Ω_D) of the nitroxide ring relative to the principal diffusion axis (Ω_D) and hence of the chain bearing the pyrroline group relative to the membrane normal. For all glycerolipids, the plane of the nitroxide ring is tilted relative to the membrane normal ($\beta_D \neq 0°$, Table 3), suggesting that the headgroup is not in a fully extended conformation. **OG(L)-NO** shows a significantly larger tilt ($\beta_D = 65°$) than the other glycerolipids ($\beta_D \sim 40°$) and this is evident in the spectra with a narrower width for the $B_0 \| \boldsymbol{n}$ orientation than for the $B_0 \perp \boldsymbol{n}$ one. The larger tilt for **OG(L)-NO** suggests that the low water accessibility of this **NOXs** (if compared with that of

Table 3 Parameters used for the fitting of the spectra of **NOXs** in bicelles. Rotational diffusion tensor (D), Euler angles between the magnetic and the diffusion frame (Ω_D), order parameter (S). The $\boldsymbol{g}$ tensor for all **NOXs** is $\boldsymbol{g}_{xx} = 2.0088$; $\boldsymbol{g}_{yyx} = 2.0061$; $\boldsymbol{g}_{zz} = 2.0027$. The hyperfine tensor is $A_{xx} =$ 0.60 mT; $A_{yy} = 0.5$ mT; $A_{zz} = 3.35$ mT for all glycerolipids $A_{xx} = 0.60$ mT; $A_{yy} = 0.5$ mT; $A_{zz} = 3.45$ mT for **Chol-NO**

		OG-NO	**DOG-NO**	**OG(L)-NO**	**DOG(L)-NO**	**Chol-NO**
$\boldsymbol{D}/s^{-1}$	$\boldsymbol{D}_{\parallel}$	3.16×10^8	3.16×10^8	1.94×10^8	1.94×10^8	4.20×10^8
	$\boldsymbol{D}_{\perp}$	0.79×10^8	0.79×10^8	1.54×10^8	1.54×10^8	0.08×10^8
Ω_D[a]	β	42°	40°	65°	40°	90°
	γ	90°	90°	90°	90°	48°
S	S_{xx}	−0.08	−0.10	−0.05	−0.015	−0.19
	S_{yy}	−0.08	−0.10	−0.05	−0.015	−0.22
	S_{zz}	+0.16	+0.20	+0.10	+0.03	+0.41

[a] For an axial diffusion tensor the angle α is irrelevant.[18]

DOG(L)-NO which has the same ethylene glycol unit) is the result of the nitroxide ring folding back on the lipid chain towards the bilayer interior. For **Chol-NO**, the plane of the nitroxide ring lies perpendicular to the membrane normal ($\beta_D = 90°$) and, by considering the shape of the molecule, this suggests that the nitroxide ring is coplanar with the cholesterol rings.

Antioxidant activity

The antioxidant activity of the synthesized **NOXs** against radical-induced lipid peroxidation was evaluated in SUV of Egg-PC containing poly-unsaturated chains susceptible of oxidation. The water-soluble azo-initiator 2,2′-azobis(2-amidinopropane) dihydrochloride (AAPH) was used as the radical generating system since it thermally decomposes at a constant rate producing a continuous flux of radicals.[19]

The water soluble nitroxide, 3-carboxy-2,2,5,5-tetramethyl-pyrroline-1-oxyl (Pyrr-NO) was included in the study for comparison.

The antioxidant activity of the synthesized lipo-nitroxides **NOXs**, and of Pyrr-NO, was evaluated by measuring the percentage inhibition of aldehydic breakdown products (Thio-barbituric Reactive Species, TBARS) formed during the peroxidation process and shown in Fig. 4. Even if TBARS assay is not so specific and may give overestimated results, it remains however the simplest, cheapest and widely used method for identifying the presence of lipid peroxide products (malondialdehyde and other aldehydes).

All synthesized compounds are able to inhibit lipid peroxidation in a percentage range 40–70%, with glycerolipid derivatives being more active than the cholesterol-functionalized analogue. A good antioxidant activity was observed also for Pyrr-NO.

EPR signal decay

The EPR signal decay of the functionalized nitroxides incorporated in liposomes, or added to liposome suspensions as for the pyrroline nitroxide, was followed by EPR spectroscopy during incubation with AAPH at 310 K. The results are given as h/h_0, where h is the total peak to peak intensity of the lowest line of the EPR signal at time t and h_0 is the total peak to peak intensity of the same line at the initial time. The signal intensity decreased during incubation time as shown in Fig. 5, where typical decays are shown for **OG(L)-NO**, **Chol-NO** and Pyrr-NO nitroxides. All the glycerolipid-derivatives have a gradual decay similar to **OG(L)-NO** with the almost complete disappearance of the signal after *ca.* 1 hour without a clear delay (data not shown). The same trend was observed for the decay of **Chol-NO** EPR signal, but in this case the decay was slower and the signal disappeared in almost 2 hours.

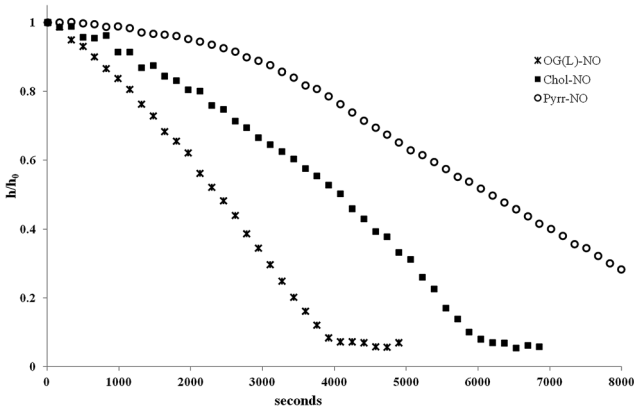

Fig. 5 Relative EPR signal intensities (h/h_0) *versus* time in Egg-PC liposomes loaded with nitroxides upon incubation with AAPH at 310 K. The nitroxide radical EPR signal intensity was measured as the total peak to peak intensity of the lower field peak.

On the other hand, Pyrr-NO behaved in a different way, showing a delay in the EPR signal decay. The same experiment was carried out in the absence of oxygen by degassing with argon the sample before incubation at 310 K and a gradual and more rapid decay without any delay (data not shown) was observed. For comparison, also lipid-functionalized nitroxides were incubated with AAPH in the absence of oxygen, but no differences in their EPR behaviour were observed.

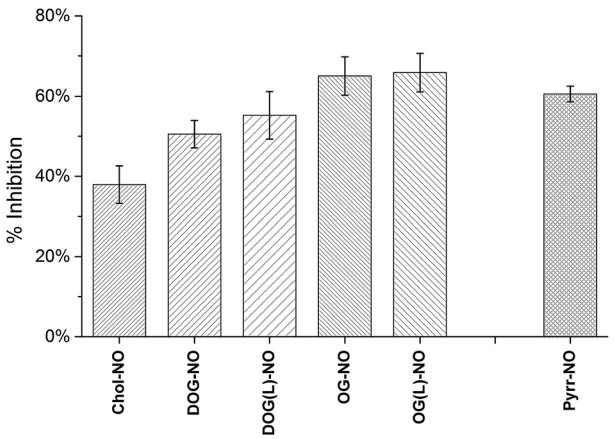

Fig. 4 % Inhibition of TBARS formation in PC (3 mM) liposomes peroxidation by **NOXs** or Pyrr-NO (0.06 mM) induced by thermal decomposition (310 K, 2 h) of AAPH (5 mM).

Discussion

OG-NO, **DOG-NO**, and **OG(L)-NO** have a similar penetration depth ($\Phi \approx 2.0$) and, by comparing this value with those obtained for the **SLs**, it can be deduced that the nitroxide function in these derivatives is located between the seventh and tenth carbon of the lipid tails, well inside the bilayer. **DOG-(L)** has instead a Φ comparable to that of 5DPC, suggesting that the combination of two lipid tails with the flexible ethylene glycol unit allows it to point towards the aqueous phase. The nitroxide group of **Chol-NO** is located in the headgroup region: it has a low Φ and has a A_{zz} value of 3.45 mT (Table 3), close to a typical value for a polar environment.

The different position/penetration of nitroxides can be correlated with their antioxidant activity: in Fig. 6, the %

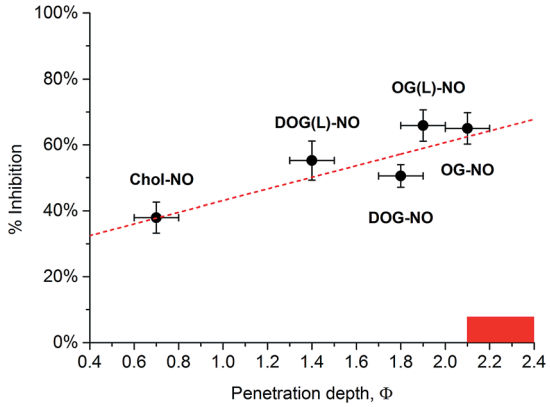

Fig. 6 Linear correlation between the % inhibition of the **NOXs** and the penetration depth. The red bar indicates the Φ value of the region C10–C12 that includes the bis-allylic carbon (C11) of PUFAs.

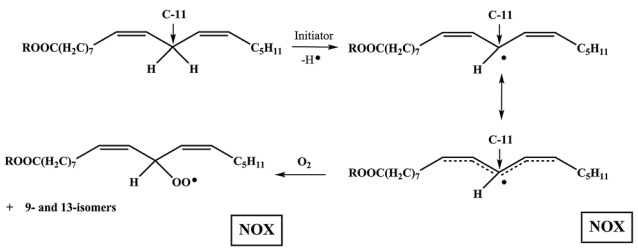

Scheme 1 Initiating steps of Egg-PC lipid peroxidation.

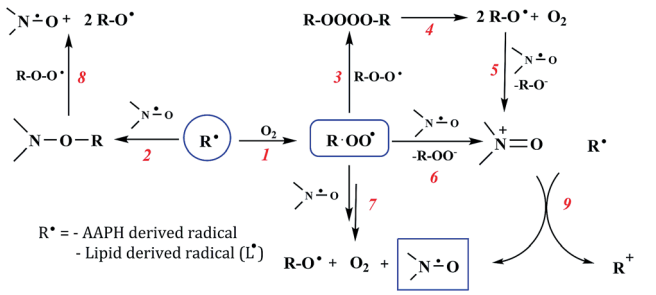

Scheme 2 Possible mechanisms of action of NOXs towards radical species involved in the process (initiation in the aqueous phase and propagation in the lipid bilayer).

inhibition of lipid peroxidation obtained in the TBARS assay is plotted as a function of the penetration depth parameter Φ.

The figure shows that the antioxidant activity increases linearly with the penetration depth. The maximal activity is reached when **NOXs** are close to the most common position of the double bonds in PUFAs (red rectangle in the figure). In fact, the most active **NOXs** are located in the proximity of the bis-allylic hydrogen atoms of the linoleic chain (15% of the fatty acid residues of PC are represented by polyunsaturated linoleic acid), which are preferentially abstracted by radical initiators (peroxyls, alkoxyls, *etc.*) in the first step of LP (Scheme 1). This is in agreement with data reported in the literature according to which nitroxides work as better inhibitors in the peroxidation of rat liver microsomes[7c] if they are at the same depth of the generated radicals in the bilayer.

Peroxyl radicals are usually considered as initiators of LP. In the present work, they are initially formed in the aqueous phase by the rapid reaction between AAPH-derived C-centred radicals and oxygen (the coupling is nearly diffusion controlled, $k \simeq 10^9$ M^{-1} s^{-1}). They are able to cross the lipid membrane and to abstract a labile hydrogen atom from a lipid chain giving the corresponding C-centred radical L$^\bullet$ in the propagation step ($k =$ 16 M^{-1} s^{-1}).[20] Alternatively, alkylperoxyl radicals may also dimerize to give the corresponding unstable tetraoxide which, in turn, decomposes with formation of molecular oxygen and of the corresponding alkoxyls ($k \simeq 10^5$ M^{-1} s^{-1} in water), as evidenced by spin trapping experiments,[21] (reactions 3 and 4 in Scheme 2), able to initiate lipid peroxidation and to generate L$^\bullet$ radicals, as well. LP process has thus been triggered and **NOXs**, being incorporated in the membrane interior, might act as chain-breaking antioxidants by reacting with the lipid-derived C-radicals (L$^\bullet$) through a fast radical coupling[22] or with the corresponding O-centred radicals (peroxyls LOO$^\bullet$ and alkoxyls LO$^\bullet$ formed in the bilayer from the reaction of L$^\bullet$ with oxygen) though an electron transfer process.[10a] At physiological temperature and pO_2, the concentration of L$^\bullet$ should be lower than that of LOO$^\bullet$, hence the reaction between **NOXs** and alkyl radicals should be disfavoured with respect to that with oxygen-centred ones. However, a competition between nitroxides and oxygen towards L$^\bullet$ radicals cannot be ruled out, although oxygen is about four times more concentrated in membranes than in aqueous phases.[23] In fact, the reaction rate between L$^\bullet$ and O_2 to yield LOO$^\bullet$ does not depend only on oxygen partition but also on its diffusion, which is *ca.* 10 times slower in lipid bilayer than in water.

Lipid-functionalized nitroxides could in principle react both with C-centred radicals (L$^\bullet$) and O-centred radicals derived from AAPH, or generated from the lipid chains (LO$^\bullet$ and LOO$^\bullet$), but all these reactions have to be considered on the basis of the redox potentials of the **NOXs**.

Focusing on the oxidation potentials listed in Table 1 for **NOXs** and the redox potentials reported for peroxyl radicals,[24] an electron transfer process[25] (reaction 6, Scheme 2) is rather unlikely to occur in a lipidic environment especially if an "outer sphere" single electron transfer mechanism is considered. More favorable is the reaction when the oxidizing species are alkoxyl radicals (reaction 5, Scheme 2) instead of peroxyls due to their higher reduction potentials.[24] However, it cannot be excluded that the reaction between **NOXs** and O-centred radicals (peroxyls and alkoxyls) proceeds according to an inner-sphere electron transfer mechanism.[10a]

On the other hand, if the reactions reported in Scheme 2 are considered from a kinetic point of view, we can observe that once the initiating C-centred radicals are formed (R$^\bullet$ could derive from AAPH in the aqueous phase or from the lipid chains inside the membrane), they may react either with molecular oxygen or with **NOXs** (reactions 1 and 2, respectively). A competition between the two reactions is possible, both processes being characterized by very high rate constants near

to the diffusion control limit in liquid solutions. However, it has been reported that in the system under investigation, water-soluble peroxyl radicals are generated from AAPH decomposition approximately at a rate of 10^{-8}–10^{-9} M s^{-1},[26] thus representing the rate determining step for the whole process. In fact, all the rate constants for the reactions reported in the scheme should be 3–4 order of magnitude higher and very close to each other,[27] and could occur with the same probability. The formed peroxyls may thus undergo self-decomposition (reactions 3 and 4) to give the corresponding alkoxyls, able to propagate the oxidative process by a H-abstraction from lipid chains ($k_{abs} \approx 10^5$ M^{-1} s^{-1}), or to be reduced by nitroxides (reaction 5). In this latter reaction, as well in reaction 6, oxoammonium cations are formed which are known to be strong oxidants, able to react with alkyl radicals as indicated in reaction 9.[28]

The minor protection effect against lipid peroxidation observed for the cholesterol-derivative may be likely explained considering its location close to the membrane surface, far away from the site of generation of L$^{\bullet}$ radicals. **Chol-NO** could thus react with the initiators radicals (O-centred ones) formed by AAPH, before they reach the oxidable lipid chain. Moreover, **Chol-NO** has a reduced mobility inside the membrane due to its rigid structure and liposomes viscosity as well. As a consequence, the initiating radicals generated in the aqueous phase are only partially intercepted by the antioxidant and can thus propagate the peroxidation of the lipid bilayers. In fact, only a small fraction of attacking radicals is sufficient to induce chain oxidation of many lipid molecules.

The good antioxidant activity of Pyrr-NO, comparable with those of the glycerolipid functionalized nitroxides and better than that of **Chol-NO**, may be explained considering its location in the water phase, where the initiating radicals are generated and where the reaction (electron transfer) is expected to occur. In fact, as shown in Table 1 or reported in the literature,[14] the pyrroline moiety is more easily oxidized in an aqueous environment even by peroxyl radicals: a rate constant of 8.1×10^5 M^{-1} s^{-1} has been reported[10a] for the reaction between 3-carbamoylproxyl nitroxide and *t*-butylperoxyl radicals in aqueous solution. Similar or even higher rate constants (according to their reduction potentials[24]) are expected for the reduction of an alkoxy radical by a nitroxide.

EPR measurements of **NOXs** signal decay indicate that the disappearance of the signal is gradual, with no delay, and rather slow likely because of the occurrence of reactions 7, 8 and 9 (Scheme 2).[9,29] The even slower decay observed with **Chol-NO** compared to that of the other glycerolipid nitroxides can be justified by its localization and lower mobility within the bilayer[30] and is in agreement with its lower antioxidant activity. The presence of a delay in the Pyrr-NO signal decay indicates that during this time interval it reacts very slowly with O-centred radicals[7e,31] generated from AAPH and, once the oxygen dissolved in solution has been consumed, Pyrr-NO reacts with AAPH derived C-centred radicals (reaction 1, Scheme 2). This latter reaction accounts also for the fact that the signal decay was faster in the absence of oxygen and with no delay. On the other hand, since no differences were observed with **NOXs**, in the presence or in the absence of oxygen, it could be hypothesized that with these derivatives the coupling of the nitroxide with C-centred radicals formed from AAPH and from the lipid chains represents the main reaction.

According to the TBARS assay, glycerolipid nitroxides and Pyrr-NO seem to have the same antioxidant activity, whereas EPR signal decays are rather different. This could be explained by considering the differences between the two kinds of experiments. As already said, TBARS assays allow the determination of the final aldehydic products of LP without considering the fate of the antioxidant, *i.e.* the nitroxide in the present work. On the other hand, when EPR measurements are performed, the disappearance of the nitroxide is monitored and hence we have direct information on the nitroxide, on its reactivity and on its fate. **NOXs** in liposomes are consumed faster than Pyrr-NO in the water phase and this may likely be due to the fact that Pyrr-NO may react only with O-centred radicals, whereas **NOXs** react both with C- and O-centred radicals. Moreover, the radicals present in the aqueous phase are those deriving from the slow decomposition of the azo-initiator, while in the lipid environment where peroxidation, a radical chain process, is occurring we can expect that the number of radical species should be higher.

Conclusions

The antioxidant activity of nitroxides functionalized with cholesterol or glycerol units **NOXs** has been studied and correlated with their penetration into POPC liposomes chosen as model membranes. **NOXs** are selectively incorporated at different depths in the bilayer in close proximity to the site of damage during lipid peroxidation. Those derivatives which are closer to the oxidable carbon atoms of the lipid chains are better inhibitors of lipid peroxidation.

Moreover, the obtained results indicate that nitroxides may behave differently according to their localization. In particular, they can be seen as preventive or chain-breaking antioxidants according to their environment and to their penetration attitude within the bilayer. **Chol-NO**, which is inserted in the membrane but close to the surface, can scavenge initiating radicals but not the lipophilic radicals formed during the propagation steps and hence is not able to break the chain propagation. On the other hand, the glycerol nitroxides residing deeper in the membrane interior may not only block the initiating radicals but may also be regarded as chain-breaking antioxidants, being able to intercept the radicals responsible for the propagation of the lipid peroxidation. This is of particular interest since the antioxidant activity often depends more on the localization than on the chemical reactivity.

As a concluding remark, we point out that our approach is based on the combination of advanced experimental techniques that allowed us to probe the properties of these system in-depth. Nevertheless, in modern EPR spectroscopy, there is not only a trend towards to the use of DFT methods for the evaluation of the EPR parameters,[32] but also to the integration of spectroscopic data, DFT and molecular dynamics to better characterize the effects of the molecular motions in different environments.[33] Despite the availability of these methods, they

have not been applied yet to refine the interpretation of EPR data in complex environments such as biological membranes, and we think that this approach could represent an interesting development in this field.

Experimental section

All materials and reagents used in the synthesis of **NOXs** were purchased from Sigma-Aldrich and used without purification. 2,2,5,5-Tetramethyl-3-pyrrolin-1-oxyl-3-carboxilic acid (Pyrr-NO) was prepared according to the method of Rozanstev.[34]

^{1}H NMR spectra and ^{13}C NMR spectra were recorded on a Varian Mercury 400 (400 MHz and 100 MHz, respectively) at 25 °C after *in situ* reduction with hydrazobenzene. Chemical shifts (δ) are given in ppm and residual solvent signals for $CHCl_3$ (δ_H 7.26 ppm and δ_C 77.0 ppm) were used as internal references. Coupling constants (J) are given in Hertz. Electron spray ionization mass spectrometry (ESI-MS) was performed on an Agilent Series 1100 MSD Mass Spectrometer. High resolution mass spectrometry was performed on a Xeno G2-S QTof Waters spectrometer. Elemental analysis was performed on a Thermo Fischer Scientific FLASH 2000 Organic Elemental Analyzer. FTIR spectra were acquired using DRIFT technique on a Perkin Elmer Spectrum GX1 and are expressed in wave number (cm^{-1}).

Tetrabutylammonium hexafluorophosphate (TBAH), sodium tetrafluoborate ($NaBF_4$) and phosphate buffer solution (PB) were used as received as supporting electrolyte, and all were electrochemical or analytical grade from Sigma-Aldrich. Water was milliQ grade. Dry tetrahydrofuran (THF) was purified and dried as previously reported,[35] stored in a specially designed Schlenk flask and protected from light.

Shortly before performing the electrochemical measurements, the solvent was distilled *via* a closed system into an electrochemical cell containing the supporting electrolyte and the species under examination.

1-Palmitoyl-2-oleoyl-sn-glycero-3-phosphocholine (POPC), 1,2-dihexanoyl-sn-glycero-3-phosphocholine (DHPC), 1,2-dimyristoyl-sn-glycero-3-phosphocholine (DMPC) and all nitroxide-labeled phospholipids (**SLs**): 1-palmitoyl-2-stearoyl-(*n*-doxyl)-sn-glycero-3-phosphocholines (5DPC, 7DPC, 10DPC, 12DPC and 14DPC) and 1-palmitoyl-2-oleoyl-sn-glycero-3-phospho(tempo)-choline (TempoPC) were purchased from Avanti Polar Lipids (Alabaster, AL, USA) as chloroform solutions. Nickel(II)-ethylene-*N*,*N*′ diaminediacetic acid (NiEDDA) was prepared from ethylenediamine-*N*,*N*′-diacetic acid (EDDA) and nickel(II) hydroxide [$Ni(OH)_2$] according to published procedures.[15] These reagents, 2-[4-(2-hydroxyethyl)-1-piperazinyl] ethanesulfonic acid (HEPES), and the lanthanide salts $TmCl_3 \cdot 6H_2O$ and $DyCl_3 \cdot 6H_2O$ were purchased from Sigma-Aldrich. A 50 mM, pH 7.0, HEPES buffer solution was prepared to be used for the preparation of POPC small unilamellar vesicles (SUV) and bicelles, and for the stock solutions of Tm^{3+} and Dy^{3+}.

Egg-yolk L-α-phosphatidylcholine (Egg-PC) as chloroform solution for liposomes preparation was purchased from Sigma-Aldrich and used without purification. A 5 mM phosphate buffer (PB) solution was prepared to be used for PC liposomes, for Pyrr-NO and AAPH solutions.

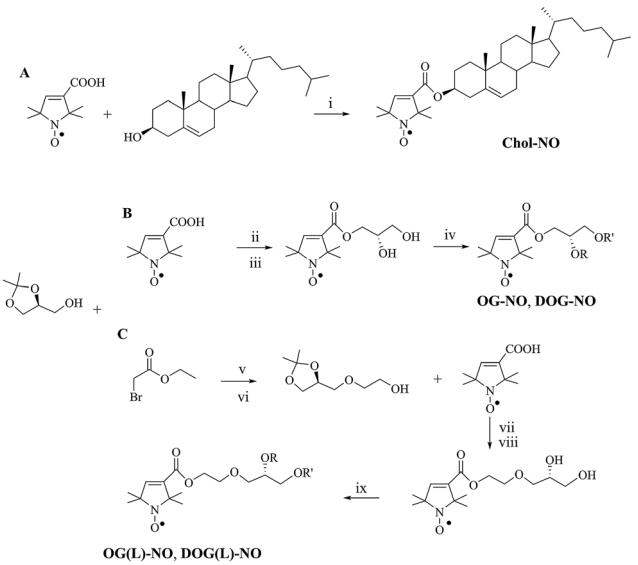

Scheme 3 Reagents and conditions: (A) (i) DCC, DMAP, dry DCM, rt, on, 63%. (B) (ii) DCC, DMAP, DCM, rt, on, 51%. (iii) *p*-TsOH, CH_3OH, rt, on, 72%. (iv) Oleic acid (1 or 2 eq.), DCC, DMAP, DCM, rt, on, 50% (**OG-NO**), 88% (**DOG-NO**). (C) (v) NaH (60%), dry THF, 0 °C then rt, on, 40%. (vi) $LiAlH_4$, dry THF, 0 °C, 83%. (vii) DCC, DMAP, DCM, rt, on, 62%. (viii) *p*-TsOH, CH_3OH, rt, on, 72%, 98%. (ix) Oleic acid (1 or 2 eq.), DCC, DMAP, DCM, rt, on, 40% (**OG-(L)-NO**), 67% (**DOG(L)-NO**).

Synthesis

Chol-NO was synthesized by *N*,*N*-dicyclohexylcarbodiimide (DCC) coupling of a cholesterol molecule with 2,2,5,5-tetramethyl-3-pyrrolin-1-oxyl-3-carboxylic acid Pyrr-NO (Scheme 3A). Glycerolipid nitroxides were synthesized following a synthetic procedure already reported in the literature.[36] (Scheme 3B and C), starting from 1,2-isopropyliden-3-*O*-sn-glycerol.

For **OG-NO** and **DOG-NO**, it was condensed with Pyrr-NO and, after removal of the isopropylidene protecting, was esterified with one (**OG-NO**) or two equivalents of oleic acid (**DOG-NO**). **OG(L)-NO** and **DOG(L)-NO** were prepared with the same reactions, but in these cases 1,2-isopropyliden-3-*O*-sn-glycerol was first reacted with ethyl bromoacetate in order to introduce the oxyethylene linker.

Spectroscopic characterization of the synthesized **NOXs** can be found in the ESI.†

Electrochemical measurements

Electrochemical experiments were carried out in an airtight single-compartment cell described elsewhere[37] by using platinum and glassy carbon (GC) as working electrode, a platinum spiral as counter electrode and a silver spiral as a quasi-reference electrode. For the measurements in aprotic solvent, the cell containing the supporting electrolyte and the electroactive compound was dried under vacuum at about 110 °C for at least 48 h before each experiment. All the $E_{1/2}$ potentials have been directly obtained from CV curves as averages of the cathodic and anodic peak potentials for one-electron peaks and by digital simulation for those processes closely spaced in

multielectron voltammetric peaks. The $E_{1/2}$ values are referred to a normal hydrogen electrode (NHE) and have been determined by adding, at the end of each experiment, ferrocene as an internal standard and measuring them with respect to the ferrocenium/ferrocene couple standard potential. The potentials thus obtained were not corrected for the two unknown contribution of the liquid junction potential between the organic phase and the aqueous NHE solution. Experiments in aqueous solution of the species immobilized as film, onto the electrode surface, have been carried out in the same cell described above. The species were immobilized on the GC working electrode (3 mm diameter disk) as thin film by drop-casting 100 μL of a 0.1 mM chloroform solution of the compounds investigated.

Voltammograms were recorded with an AMEL Mod. 552 potentiostat or a custom made fast potentiostat[38] controlled by an AMEL Mod. 568 programmable function generator. The potentiostat was interfaced to a Nicolet Mod. 3091 digital oscilloscope and the data transferred to a personal computer by the program Antigona.[39] Minimization of the uncompensated resistance effect in the voltammetric measurements was achieved by the positive-feedback circuit of the potentiostat. Digital simulations of the cyclic voltammetric curves were carried out either by Antigona or DigiSim 3.0.

Penetration depth measurements

Penetration depth experiments were performed in POPC SUV prepared by mixing the chloroform stock solutions of POPC and NOXs or SLs in a 100 : 1 ratio. The mixed solutions were evaporated in a glass test tube under a stream of dry nitrogen gas and the resulting film was dried overnight under vacuum. The lipid film was hydrated for 30 minutes with HEPES buffer to a final concentration of 10 mM for the lipid and 100 μM for NOX or SL. Lipid suspensions were sonicated in a water bath until they started to clear. SUV in the 30–50 nm diameter range were obtained and their dimensions were checked during preparation by Dynamic Light Scattering (DLS) using a NICOMP Model 370 Submicron Particle Sizer by Pacific Scientific. Vesicles were used fresh after preparation.

The EPR experiments were performed using a Bruker ESP380 spectrometer operating at X-band (~9.5 GHz), equipped with a room-temperature dielectric resonator, ER4123D. The microwave frequency was measured by a frequency counter, HP5342A. All spectra were obtained using the following parameters: modulation amplitude 0.16 mT; modulation frequency 100 kHz; time constant 41 ms; conversion time 82 ms; scan width 1.25 mT; 512 points; temperature 298 K. The microwave power was ramped down automatically from 95 mW to 0.05 mW (the attenuation ramp in dB units was 2.0, 4.0, 6.0, 8.0, 10.0, 12.0, 14.0, 16.0, 18.0, 20.0, 25.0, 30.0, 35.0). The spectra were acquired in a single scan. The experimental protocol for the insertion depth measurements is as follows. Approximately 5 μL of sample were loaded into a gas-permeable TPX capillary (L&M EPR Supplies, Inc., Milwaukee, WI, USA) and three saturation experiments were performed. The first experiment was done on the sample in equilibrium with air to saturate the membrane with oxygen. The second experiment was performed on the same sample after de-oxygenation under a dry nitrogen flow for twenty minutes. The third experiment was performed on a new sample to which NiEDDA was added to a final concentration of 50 mM; the sample was then de-oxygenated as above. All experiments were performed at least in duplicate. The power saturation data were obtained using a home-written program in Matlab that calculates the peak-to-peak amplitudes of the central line of the spectra. The saturation curves were obtained plotting the amplitude data *vs.* the microwave power, and fitted using the standard equation:[15]

$$y = Ap_{1/2}[1 + (2^{1/h} - 1)x/p_{1/2}]^{-h}$$

$p_{1/2}$ is the saturation parameter, namely the power where the first derivative amplitude is reduced to half of its unsaturated value, h is the homogeneity parameter, indicating the homogeneity of saturation of the resonance line, (ranging between $h = 1.5$ for a fully homogeneously-broaden line and $h = 0.5$ for a fully inhomogeneously-broaden line), and A is a scaling factor that accounts for the absolute signal intensity. The saturation profile and the saturation parameter were obtained also for DPPH (2,2-diphenyl-1-picrylhydrazyl).[40] The best-fit $p_{1/2}$ parameters of the three experiments described above were used to calculate the dimensionless immersion depth parameter (Φ) as

$$\Phi = \ln \frac{p_{1/2}^{\text{oxygen}} - p_{1/2}^{\text{nitrogen}}}{p_{1/2}^{\text{NiEDDA}} - p_{1/2}^{\text{nitrogen}}}$$

Bicelle stock preparation and EPR experiments

Chloroform solutions of the phospholipids (DMPC and DHPC) and a methanol solution of the **NOX** were mixed in a glass test tube in a 1 : 100 **NOX** to DMPC ratio. The obtained solutions contained 11.2 μmol of DMPC, 3.1 μmol of DHPC, and, where present, 25 nmol of **NOX** (~0.2% of the total lipids); the q = [DMPC]/[DHPC] ratio was therefore $q \sim 3.5$. A thick lipid film was produced by evaporation of the solvent under a stream of dry nitrogen gas which was then dried under vacuum overnight. The following day the lipids were scratched off the glass tube and placed into an Eppendorf tube, to which 33 μL of buffer were added, obtaining a 25% (w/w) lipid concentration. The resulting suspension was vortexed until it appeared homogeneous. The sample was then placed in a bath sonicator that was filled with an ice/water mixture and sonicated for 30 minutes. Finally, the solution was subjected to four freeze/thaw cycles: 30 minutes in a 328 K water bath followed by a quick freeze in liquid nitrogen; vortexing of the sample at each step was performed to insure perfect homogeneity. The procedure yielded a clear, viscous, stock of bicelles with the **NOX** incorporated in the bilayers. Starting from the stock solution, 25 μL were prepared as follows: 15 μL of bicelles were added to 10 μL of buffer (for isotropic samples), or, for oriented samples, to 10 μL of buffered lanthanide solution of Tm^{3+} or Dy^{3+} (corresponding to a final $[Ln^{3+}]$/[DHPC] ratio of 0.1). The resulting solution was transferred to a 1 mm inner diameter EPR quartz tube. The final concentration of the phospholipids was 17% (w/w). Given the

experimental conditions (lipid concentration, q ratio, temperature), the bicelles used in this work are not ideal disks, but rather stacks of almost planar phospholipid bilayers dotted with DHPC pores and separated by buffer regions ~15 nm wide.[41]

Samples with $\boldsymbol{n}$ oriented along and perpendicular to the magnetic field can be obtained in two ways: (a) by preparing two samples doped with lanthanide salts that yield bicelles with different orientation in a strong magnetic field (B_0), Tm^{3+} for $\boldsymbol{n} \| B_0$ or Dy^{3+} for $\boldsymbol{n} \perp B_0$; (b) by preparing a single sample doped with Tm^{3+} and taking the spectra before and after a rotation of the sample tube by 90° inside the cavity of the spectrometer. This latter method exploits the extremely high viscosity of the bicelle solution at 308 K and the slow relaxation of the oriented phase at the magnetic field of the experiment (350 mT) which prevents the lipid reorientation within the timeframe of the EPR experiments (3 minutes). After having verified the equivalence of the procedures, the second method was adopted in this work since it requires a single sample.

A literature procedure[13] was used to obtain aligned samples: the sample tube was placed at room temperature (~298 K) in the EPR cavity and the magnetic field was set to 800 mT; then the temperature was slowly raised to 318 K and subsequently lowered to the temperature of choice, 308 K (35 °C). The magnetic field was set to ~350 mT and the spectrum was recorded immediately: loss of order in the sample during the measurement time (~40 s) is negligible as a result of the high viscosity of the bicelle solution and slow relaxation of the oriented phase at the magnetic field of the experiment (350 mT) which prevents the lipid reorientation.

EPR spectra were performed using a Bruker ER200D spectrometer operating at X-band (~9.5 GHz), equipped with a rectangular cavity, ER4102ST, fitted with a cryostat, and a variable-temperature controller, Bruker ER4111VT; the microwave frequency was measured by a frequency counter, HP5342A. All spectra were obtained using the following parameters: microwave power 2.1 mW; modulation amplitude 0.16 mT; modulation frequency 100 kHz; time constant 20 ms; conversion time 41 ms; scan width 15 mT; 1024 points; temperature 308 K; all spectra were obtained in a single scan.

EPR spectral simulations

We performed simulations of the **NOX** spectra with a program based on the stochastic Liouville equation,[18] that is extensively used to simulate EPR spectra of spin-labeled systems.[16d,42] The simulation method relies on several reference systems whose relative orientation is defined by different sets of Euler angles.[18] The simulation parameters are listed in Table 3. The principal values of the $\boldsymbol{g}$ and ^{14}N hyperfine (A) tensors were obtained from the literature;[16d,43] the principal values of the rotational diffusion tensor ($\boldsymbol{D}$), the relative orientation of its principal axes relative to the $\boldsymbol{g}$ tensor reference frame (Ω_D), the adimensional and traceless order parameter matrix (S, expressing the degree of order), and the angle (Ψ) defining the orientation of the magnetic field relative to the average long diffusion axis were obtained from the simulation.

Peroxidation of Egg-PC liposomes and assessment of nitroxides % inhibition (TBARS assay): oxidation induced by 2,2′-azobis(2-amidinopropane) dihydrochloride (AAPH)

Liposomes were prepared by the "thin film hydration" method. Chloroform stock solutions (2 mM) were prepared for each tested compound except for 2,2,5,5-tetramethyl-3-pyrrolin-1-oxyl-3-carboxilic acid (Pyrr-NO), whose 2 mM solution was prepared in phosphate buffer PB. Appropriate amounts of chloroform solutions of PC (100 mg mL^{-1}) and tested compound (2 mM in $CHCl_3$) were mixed in a 50 : 1 molar ratio. The solvent was slowly evaporated with a stream of nitrogen and the thin film obtained was dried for at least 2 h under reduced pressure. This dried film was then resuspended by vortex agitation in the required amount of 5 mM PB (pH 7.4) to a 3 mM Egg-PC and 0.06 mM antioxidant final concentration and incubated overnight to swell and stabilize. The same procedure was used to prepare a suspension of Egg-PC liposomes (3 mM final concentration) without tested nitroxides to be used as the control in the evaluation of the percentage of inhibition of nitroxides on the basis of the equation below. Samples containing Pyrr-NO were obtained by hydrating the Egg-PC film with a PB- solution containing the proper volume of the 2 mM stock solution in PB in order to have 0.06 mM final concentration of nitroxide. The resulting MLV (Multi Lamellar Vesicles) were sonicated for 12 min with a Sonic Vibracell sonicator to obtain SUV (Small Unilamellar Vesicles) and the size distribution (mean diameter) was verified by Dynamic Light Scattering (DLS) using a Nanosizer (Nano-ZS, Nanoseries, Malvern) and found to be in the range 89–105 nm. Oxidized samples were obtained by taking up 300 μL portions of each dispersion, adding 25 μL AAPH 65 mM (5 mM final concentration) and incubating for 2 h at 310 K. Addition of 10 μL of 20 mM methanolic BHT to the oxidized liposomes stopped the reaction and prevented further Egg-PC peroxidation during the TBARS assay. Other 300 μL of the liposome dispersions were added with 25 μL of PBS (instead of AAPH) and 10 μL of 20 mM methanolic BHT to make sure that during incubation, also in the absence of radical initiator, no oxidation occurs and incubated at 310 K for the same time. 0.9 mL of TBA–TCA–HCl reagent (0.375% w/v TBA, 15% w/v TCA, 0.2 M HCl) were added to all samples, oxidized and non-oxidized, which were then heated for 15 min at 368 K, cooled and centrifugated at 5000 rpm for 10 min. A pink chromophore developed after the reaction between the thiobarbituric acid and malondialdehyde and other aldehydes formed from the degradation of lipid peroxides. Its absorbance was measured at 532 nm on a microplate reader (Biotek, Synergy HT) for the determination of the aldehydic breakdown products of lipid peroxidation (TBARS).[44] The antioxidant activity of the studied compounds was expressed as % inhibition according to the following equation:

$$\%\ \text{Inhibition} = (1 - \Delta A_{\text{sample}}/\Delta A_{\text{PC}}) \times 100$$

where ΔA_{sample} is the difference of the absorbance between the oxidized and non-oxidized sample containing nitroxide and ΔA_{PC} is the difference of the absorbance between the oxidized

and non-oxidized Egg-PC. All experiments were run in triplicate and repeated at least four times.

EPR signal decay

SUV were prepared from PC and **NOX** (2 mM in $CHCl_3$) or Pyrr-NO (2 mM in PB) following the same procedure described for AAPH experiments. 25 μL of AAPH (final concentration 5 mM) were added to 300 μL of each suspension in an Eppendorf tube, mixed and transferred into a glass capillary tube which was then put inside the EPR cavity. Each sample was incubated for 2 h at 310 K following the decay of the nitroxide three lines signal upon heating. EPR spectra were recorded using a Bruker EMX spectrometer operating at X-band (~9.5 GHz), equipped with a rectangular cavity, ER4102ST, fitted with a variable-temperature controller, a microwave frequency counter and an NMR gaussmeter for field calibration. Spectra were recorded using the following parameters: microwave power 20 mW; modulation amplitude 0.2 mT; modulation frequency 100 kHz; time constant 0.32 ms; conversion time 41 ms; scan width 10 mT; number of scans 50; delay after each measurement 120 s.

Acknowledgements

We thank Dr Barbara Biondi for ESI-MS spectra. This work was supported by MIUR (PRIN 2010–2011) [2010PFLRJR(PROxi); 2010NRREPL; 2010A2FSS9] and by Fondazione CARIPARO (Progetti Eccellenza 2011/2012).

References

1 A. Negre-Salvayre, N. Auge, V. Ayala, H. Basaga, J. Boada, R. Brenke, S. Chapple, G. Cohen, J. Feher, T. Grune, G. Lengyel, G. E. Mann, R. Pamplona, G. Poli, M. Portero-Otin, Y. Riahi, R. Salvayre, S. Sasson, J. Serrano, O. Shamni, W. Siems, R. C. M. Siow, I. Wiswedel, K. Zarkovic and N. Zarkovic, *Free Radical Res.*, 2010, **44**, 1125.

2 M. C. Krishna and A. Samuni, *Methods Enzymol.*, 1994, **234**, 580.

3 (*a*) V. W. Bowry and K. U. Ingold, *J. Am. Chem. Soc.*, 1992, **114**, 4992; (*b*) A. Samuni, S. Goldstein, A. Russo, J. B. Mitchell, M. C. Krishna and P. Neta, *J. Am. Chem. Soc.*, 2002, **124**, 8719; (*c*) S. Goldstein, A. Samuni and A. Russo, *J. Am. Chem. Soc.*, 2003, **125**, 8364.

4 (*a*) M. C. Krishna, D. A. Grahame, A. Samuni, J. B. Mitchell and A. Russo, *Proc. Natl. Acad. Sci. U. S. A.*, 1992, **89**, 5537; (*b*) M. C. Krishna, A. Russo, J. B. Mitchell, S. Goldstein, H. Dafni and A. Samuni, *J. Biol. Chem.*, 1996, **271**, 26026.

5 M. C. Krishna, A. Samuni, J. Taira, S. Goldstein, J. B. Mitchell and A. Russo, *J. Biol. Chem.*, 1996, **271**, 26018.

6 P. Bar-On, M. Mohsen, R. Zhang, E. Feigin, M. Chevion and A. Samuni, *J. Am. Chem. Soc.*, 1999, **121**, 8070.

7 (*a*) G. Cighetti, P. Allevi, S. Debiasi and R. Paroni, *Chem. Phys. Lipids*, 1997, **88**, 97; (*b*) A. N. Cimato, L. L. Piehl, G. B. Facorro, H. B. Torti and A. A. Hager, *Free Radicals Biol. Med.*, 2004, **37**, 2042; (*c*) Y. Miura, H. Utsumi and A. Hamada, *Arch. Biochem. Biophys.*, 1993, **300**, 148; (*d*) U. A. Nilsson, L. I. Olsson, G. Carlin and A. C. Bylund-Fellenius, *J. Biol. Chem.*, 1989, **264**, 11131; (*e*) A. M. Samuni and Y. Barenholz, *Free Radicals Biol. Med.*, 1997, **22**, 1165; (*f*) A. M. Samuni and Y. Barenholz, *Free Radicals Biol. Med.*, 2003, **34**, 177; (*g*) T. Yamasaki, Y. Ito, F. Mito, K. Kitagawa, Y. Matsuoka, M. Yamato and K. Yamada, *J. Org. Chem.*, 2011, **76**, 4144.

8 (*a*) J. Antosiewicz, E. Damiani, W. Jassem, M. Wozniak, M. Orena and L. Greci, *Free Radicals Biol. Med.*, 1997, **22**, 249; (*b*) E. Damiani, R. Castagna and L. Greci, *Free Radicals Biol. Med.*, 2002, **33**, 128.

9 P. Stipa, *J. Chem. Soc., Perkin Trans. 2*, 2001, 1793.

10 (*a*) S. Goldstein and A. Samuni, *J. Phys. Chem. A*, 2007, **111**, 1066; (*b*) D. H. R. Barton, V. N. le Gloahec and J. Smith, *Tetrahedron Lett.*, 1998, **39**, 7483.

11 B. P. Soule, F. Hyodo, K.-I. Matsumoto, N. L. Simone, J. A. Cook, M. C. Krishna and J. B. Mitchell, *Free Radicals Biol. Med.*, 2007, **42**, 1632.

12 (*a*) S. Banerjee, U. R. Desai and G. K. Trivedi, *Tetrahedron*, 1992, **48**, 133; (*b*) S. Banerjee and G. K. Trivedi, *Tetrahedron*, 1992, **48**, 9939; (*c*) S. Banerjee, G. K. Trivedi, S. Srivastava and R. S. Phadke, *Bioorg. Med. Chem.*, 1993, **1**, 341; (*d*) S. Banerjee, G. K. Trivedi, S. Srivastava and R. S. Phadke, *Steroids*, 1994, **59**, 377–382; (*e*) R. Katoch, G. K. Trivedi and R. S. Phadke, *Bioorg. Med. Chem.*, 1999, **7**, 2753; (*f*) S. Pajk and S. Pečar, *Tetrahedron*, 2009, **65**, 659.

13 T. B. Cardon, E. K. Tiburu and G. A. Lorigan, *J. Magn. Reson.*, 2003, **161**, 77.

14 P. Carloni, E. Damiani, L. Greci, P. Stipa, G. Marrosu, R. Petrucci and A. Trazza, *Tetrahedron*, 1996, **52**, 11257.

15 C. Altenbach, D. A. Greenhalgh, H. G. Khorana and W. L. Hubbell, *Proc. Natl. Acad. Sci. U. S. A.*, 1994, **91**, 1667.

16 (*a*) M. Bortolus, A. Dalzini, C. Toniolo, K. S. Hahm and A. L. Maniero, *J. Pept. Sci.*, 2014, **20**, 517; (*b*) M. Bortolus, M. de Zotti, F. Formaggio and A. L. Maniero, *Biochim. Biophys. Acta, Biomembr.*, 2013, **1828**, 2620; (*c*) M. Bortolus, G. Parisio, A. L. Maniero and A. Ferrarini, *Langmuir*, 2011, **27**, 12560; (*d*) J. J. Inbaraj, T. B. Cardon, M. Laryukhin, S. M. Grosser and G. A. Lorigan, *J. Am. Chem. Soc.*, 2006, **128**, 9549.

17 M. Plato, H. J. Steinhoff, C. Wegener, J. T. Torring, A. Savitsky and K. Mobius, *Mol. Phys.*, 2002, **100**, 3711.

18 D. E. Budil, S. Lee, S. Saxena and J. H. Freed, *J. Magn. Reson., Ser. A*, 1996, **120**, 155.

19 E. Niki, *Methods Enzymol.*, 1990, **186**, 100.

20 F. Antunes, L. R. C. Barclay, M. R. Vinqvist and R. E. Pinto, *Int. J. Chem. Kinet.*, 1998, **30**, 753.

21 (*a*) A. G. Krainev and D. J. Bigelow, *J. Chem. Soc., Perkin Trans. 2*, 1996, 747; (*b*) R. U. Rojas Wahl, L. Zeng, S. A. Madison, R. L. de Pinto and B. J. Shay, *J. Chem. Soc., Perkin Trans. 2*, 1998, 2009.

22 A. L. J. Beckwith, V. W. Bowry and K. U. Ingold, *J. Am. Chem. Soc.*, 1992, **114**, 4983.

23 M. Moller, H. Botti, C. Batthyany, H. Rubbo, R. Radi and A. Denicola, *J. Biol. Chem.*, 2005, **280**, 8850.

24 G. Merenyi, J. Lind and L. Engman, *J. Chem. Soc., Perkin Trans. 2*, 1994, 2551.

25 L. Eberson, *Electron Transfer Reactions in Organic Chemistry*, Springer-Verlag, Berlin, 1987.
26 L. R. C. Barclay, S. J. Locke, J. M. MacNeil, J. vanKessel, G. W. Burton and K. U. Ingold, *J. Am. Chem. Soc.*, 1984, **106**, 2479.
27 (*a*) P. Neta, R. E. Huie and A. B. Ross, *J. Phys. Chem. Ref. Data*, 1990, **19**, 413; (*b*) E. T. Denisov and T. G. Denisova, *Handbook of Antioxidants*, CRC Press, Boca Raton, Florida, 2000.
28 K. U. Ingold and D. A. Pratt, *Chem. Rev.*, 2014, **114**, 9022.
29 J. L. Hodgson and M. L. Coote, *Macromolecules*, 2010, **43**, 4573.
30 K. Krumova, S. Friedland and G. Cosa, *J. Am. Chem. Soc.*, 2012, **134**, 10102.
31 A. M. Samuni, A. Lipman and Y. Barenholz, *Chem. Phys. Lipids*, 2000, **105**, 121.
32 (*a*) P. Stipa, *Chem. Phys.*, 2006, **323**, 501; (*b*) P. Stipa, *Tetrahedron*, 2013, **69**, 4591; (*c*) F. Neese, *Wiley Interdiscip. Rev.: Comput. Mol. Sci.*, 2012, **2**, 73.
33 (*a*) A. Collauto, A. Barbon, M. Zerbetto and M. Brustolon, *Mol. Phys.*, 2013, **111**, 2933; (*b*) V. Barone, M. Brustolon, P. Cimino, A. Polimeno, M. Zerbetto and A. Zoleo, *J. Am. Chem. Soc.*, 2006, **128**, 15865.
34 E. G. Rozantsev, *Free Nitroxyl Radicals*, Plenum, 1970, p. 249.
35 (*a*) C. Bruno, R. Benassi, A. Passalacqua, F. Paolucci, C. Fontanesi, M. Marcaccio, E. A. Jackson and L. T. Scott, *J. Phys. Chem. B*, 2009, **113**, 1954; (*b*) A. A. La Pensee, J. Bickley, S. J. Higgins, M. Marcaccio, F. Paolucci, S. Roffia and J. M. Charnock, *J. Chem. Soc., Dalton Trans.*, 2002, 4095.
36 G. Angelini, M. Pisani, G. Mobbili, M. Marini and C. Gasbarri, *Biochim. Biophys. Acta, Biomembr.*, 2013, **1828**, 2506.
37 M. Marcaccio, F. Paolucci, C. Paradisi, M. Carano, S. Roffia, C. Fontanesi, L. J. Yellowlees, S. Serroni, S. Campagna and V. Balzani, *J. Electroanal. Chem.*, 2002, **532**, 99.
38 C. Amatore and C. Lefrou, *J. Electroanal. Chem.*, 1992, **324**, 33.
39 L. Mottier, in *Antigona*, University of Bologna, Bologna, Italy, 1999.
40 C. Altenbach, W. Froncisz, R. Hemker, H. McHaourab and W. L. Hubbell, *Biophys. J.*, 2005, **89**, 2103.
41 M. P. Nieh, C. J. Glinka, S. Krueger, R. S. Prosser and J. Katsaras, *Langmuir*, 2001, **17**, 2629.
42 (*a*) Z. C. Liang, Y. Lou, J. H. Freed, L. Columbus and W. L. Hubbell, *J. Phys. Chem. B*, 2004, **108**, 17649; (*b*) B. M. Kroncke, P. S. Horanyi and L. Columbus, *Biochemistry*, 2010, **49**, 10045; (*c*) D. J. Xu, R. H. Crepeau, C. K. Ober and J. H. Freed, *J. Phys. Chem.*, 1996, **100**, 15873; (*d*) L. Hoffman, R. A. Stein, R. J. Colbran and H. S. Mchaourab, *EMBO J.*, 2011, **30**, 1251; (*e*) J. P. Barnes, Z. C. Liang, H. S. Mchaourab, J. H. Freed and W. L. Hubbell, *Biophys. J.*, 1999, **76**, 3298.
43 D. Kurad, G. Jeschke and D. Marsh, *Appl. Magn. Reson.*, 2001, **21**, 469.
44 J. A. Buege and S. D. Aust, *Methods Enzymol.*, 1978, **52**, 302.

PCCP

PAPER

View Article Online
View Journal | View Issue

Cite this: *Phys. Chem. Chem. Phys.*, 2016, **18**, 749

An EPR study of ampullosporin A, a medium-length peptaibiotic, in bicelles and vesicles†

Marco Bortolus,[ab] Annalisa Dalzini,[a] Fernando Formaggio,[a] Claudio Toniolo,[a] Marina Gobbo*[a] and Anna Lisa Maniero*[a]

Received 15th July 2015,
Accepted 17th November 2015

DOI: 10.1039/c5cp04136h

www.rsc.org/pccp

Ampullosporin A is a medium-length (14-amino acid long) hydrophobic peptide of the peptaibol family. In this work, electron paramagnetic resonance and circular dichroism spectroscopies were applied to study the interaction of synthetic ampullosporin A and three spin-labeled analogs with small unilamellar vesicles and bicelles. Zwitterionic vesicles were used to investigate the conformation and the penetration depth of the peptide at room temperature. Bicelles were employed in combination with EPR spectroscopy to study the order, dynamics, orientation, aggregation and the 3D-structure of the peptide at near physiological temperature. In the membrane, the peptide adopts a helical structure that changes in nature depending on the thickness of the membrane-mimetic system, from mostly α-helical in vesicles to a more elongated helix in bicelles, suggesting an increase in the 3_{10}-helical content. The orientation assumed by the peptide also shows a dependence on the membrane-mimetic system: in bicelles, ampullosporin A has a transmembrane orientation at a peptide-to-lipid (P : L) ratio of 1 : 100 and higher, while in vesicles it undergoes a transition from a parallel to a transmembrane orientation as a function of the P : L ratio. In bicelles, the peptide was found to be monomeric at a P : L ratio of 1 : 25 and lower. Overall, the comparison of the results obtained in the two membrane-mimetic systems showed that ampullosporin A has a rather flexible structure that readily adapts to the bilayer thickness.

1. Introduction

Peptaibiotics are members of a family of non-ribosomally synthesized hydrophobic peptides. Their primary structures are characterized by a high content of the nonproteinogenic α-amino acid α-aminoisobutyric acid (Aib), an acylated N-terminus and a C-terminal 1,2-amino alcohol.[1] According to the number of residues in the sequence they are classified into three groups: (i) short (from 4- to 10-mers), among which trichogin represents the prototype; (ii) medium-length (from 14- to 16-mers), a less investigated subgroup; and (iii) long (from 17- to 21-mers), with alamethicins as the most extensively studied family. It is generally accepted that they are membranolytic antibiotics but, while alamethicins have been shown to form voltage-dependent pores,[2] the detailed mechanism of action of short- and medium-length peptaibiotics is largely unknown.

Ampullosporin A, a medium-length peptaibol, was isolated from the mycelium of *Sepedonium ampullosporum* together with a mixture of less populated congeners, all bearing an N-terminal acetyl(Ac)-aromatic amino acid and a C-terminal leucinol (Lol) 1,2-amino alcohol.[3] Although ampullosporins display moderate antibacterial and antifungal activities,[3] other interesting biochemical and biophysical properties have been documented.[3–10] The sequence of ampullosporin A, the most abundant isoform (Table 1), is characterized by a triplet of consecutive C^{α}-tetrasubstituted Aib residues at positions 8–10 and a very high percentage (close to 50%) of Aib residues that are responsible for its remarkable resistance to proteolysis.[11] The peptide can cause leakage in liposomes[12] and an increase of conductance in planar membranes,[4,13] which have been associated with the pore-forming activity. The crystal structure of ampullosporin A shows a right-handed helix, with a predominant α-helical content at the N-terminus and a more disordered C-terminus.[14] The helix is bent near the Gln^{11} residue, even though the structure lacks prolines: the distance between the first α-carbon and the last one is 2.2 nm. As can be appreciated in the α-helical wheel representation shown below, (Fig. 1), the peptide has a large hydrophobic sector (~280°) and a small hydrophilic face characterized by three Gln residues that are polar, but uncharged, at physiological pH.

Despite this peptaibiotic being formed by about 50% achiral (Aib) residues, the shape and intensity of the circular dichroism (CD) curves in several organic solvents and detergent micelles

[a] *Dipartimento di Scienze Chimiche, Università degli Studi di Padova, 35131 Padova, Italy. E-mail: marina.gobbo@unipd.it, annalisa.maniero@unipd.it*
[b] *Dipartimento di Scienza dei Materiali, Università degli Studi di Milano Bicocca, 20126, Milano, Italy*

† Electronic supplementary information (ESI) available: Additional details of the spectral simulations, the penetration depth experiments and the orientation efficiency. See DOI: 10.1039/c5cp04136h

Table 1 Sequences of ampullosporin A (Amp) and the spin-labeled analogs employed in this study. The Aib-to-TOAC substitutions are shown in bold

Peptide	Sequence
Amp	Ac-Trp-Ala-**Aib**-Aib-Leu-Aib-Gln-Aib-Aib-Aib-Gln-Leu-**Aib**-Gln-Lol
AmpT3	Ac-Trp-Ala-**TOAC**-Aib-Leu-Aib-Gln-Aib-Aib-Aib-Gln-Leu-**Aib**-Gln-Lol
AmpT13	Ac-Trp-Ala-**Aib**-Aib-Leu-Aib-Gln-Aib-Aib-Aib-Gln-Leu-**TOAC**-Gln-Lol
AmpT3,13	Ac-Trp-Ala-**TOAC**-Aib-Leu-Aib-Gln-Aib-Aib-Aib-Gln-Leu-**TOAC**-Gln-Lol

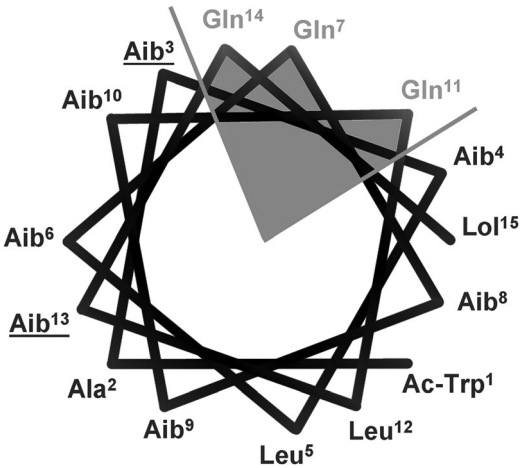

Fig. 1 α-Helical wheel representation of ampullosporin A. In gray the hydrophilic sector of the peptide (~80°) made of three Gln residues. Underlined are Aib[3] and Aib[13], the two positions that were chosen to insert the TOAC spin label.

point to a significant right-handed helicity and, in particular, to a high population of α-helical conformers.[12,15] The high helical content found in the crystal structure was recently observed in frozen methanol solution using electron paramagnetic resonance (EPR) spectroscopy.[12] The ability of the peptide to adopt an amphipathic helical structure in a membrane-mimicking environment can be related to its membrane-modifying properties. More detailed information about the mechanism of membrane permeabilization of ampullosporin A was undertaken by fluorescence quenching and solid-state NMR spectroscopies. These studies showed that the peptide adopts a parallel or transmembrane orientation depending on the bilayer thickness.[16,17]

Spin-labeling EPR spectroscopy is a well-proven technique for studying the interactions of peptides, proteins and other molecules with various kinds of lipid membranes, from liposomes to extracted cell membranes, providing a great amount of information on the solute and on its molecular environment.[18] In particular, EPR can precisely determine the insertion depth of a solute relative to the plane of the phosphate groups of the bilayer, comparing the data for the solute to those for a "molecular ruler" (*i.e.* a series of phospholipids spin-labeled at different positions of their lipid tails).[19] EPR can also provide information on the orientation of the solutes in the membrane when the membranes can be macroscopically oriented:[20–22] among these systems,

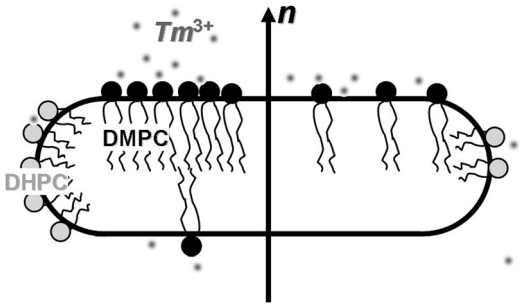

Fig. 2 Schematic representation of a bicelle. The cartoon shows the long chain phospholipids (DMPC), the short-chain phospholipids (DHPC), and the lanthanide ions (Tm^{3+}) used to align the membrane normal (*n*) parallel to an external magnetic field. For the abbreviations, see Experimental section.

bicelles (Fig. 2) are the best for magnetic spectroscopies since they form oriented phases in the magnetic field of the spectrometer at physiological temperature and without the need of a solid support.[23,24] Additionally, since bicelles form extremely viscous solutions, they can be used for the determination of distances between two paramagnetic probes in the range 0.4–2.5 nm from continuous-wave EPR (CW-EPR) spectra at physiological temperature.[22] Since peptides are diamagnetic, a paramagnetic label must be introduced in the molecule to use EPR spectroscopy. For peptaibiotics, one obvious choice is the nitroxide-containing α-amino acid 4-amino-1-oxyl-2,2,6,6-tetramethylpiperidine-4-carboxylic acid (TOAC, Scheme 1), which belongs to the family of conformationally constrained, helicogenic, C^{α}-tetrasubstituted α-amino-acids, with 3D-structural propensities strictly comparable to those of Aib.[25,26] Thus, TOAC exhibits a quite restricted mobility and its dynamics reflects directly that of the peptide backbone, a great advantage over other spin-labels such as the very flexible MTSSL, (1-oxyl-2,2,5,5-tetramethylpyrroline-3-methyl) methanethiosulfonate covalently linked to Cys (Scheme 1), commonly used for proteins. For all these reasons, TOAC has been largely exploited to study the biological properties of peptides.[27]

In this work, we studied the interaction of ampullosporin A and three spin-labeled analogs (Table 1) with zwitterionic membranes. Besides the bis-labeled AmpT3,13 analog,[12] two new

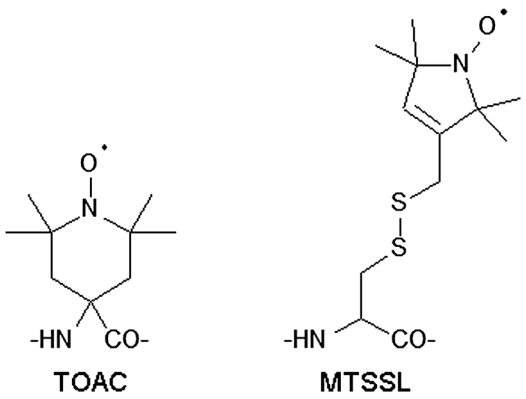

Scheme 1 Chemical structures of the TOAC and MTSSL spin labels.

analogs were prepared in which the TOAC label replaces the Aib residue at position 3 or 13 (AmpT3 and AmpT13). EPR spectroscopy was used to determine, at two peptide to lipid ratios (P : L), the insertion depth of the spin-labeled analogs in liposomes, while peptide conformation, orientation, dynamics, and aggregation properties were investigated in bicelles. For comparison, the conformational preferences of the peptides in organic solvents and in liposomes were examined by CD spectroscopy.

2. Experimental

2.1 Materials

Fmoc-TOAC-OH (Fmoc, fluorenyl-9-methyloxycarbonyl) and Fmoc-Aib-F were synthesized as reported previously.[25] *H*-L-Lol-2-chlorotrityl resin (200–400 mesh, loading 0.43 mmol g^{-1} resin) was purchased from Iris Biotech (Marktredwitz, Germany). Fmoc-amino acids were supplied by Novabiochem (Merck Biosciences, La Jolla, CA), and all other amino acid derivatives and reagents for peptide synthesis by Sigma-Aldrich (St. Louis, MO). 2-(1*H*-7-Aza-1,2,3-benzotriazol-1-yl)-1,1,3,3-tetramethyluronium hexafluorophosphate (HATU) was purchased from PE Biosystems (Warrington, UK). 1-Hydroxy-1,2,3-benzotriazole (HOBt) and 2-(1*H*-1,2,3-benzotriazol-1-yl)-1,1,3,3-tetramethyluronium hexafluorophosphate (HBTU) were Acros-Janssen (Geel, Belgium) products. 1,2-Dihexanoyl-*sn-glycero*-3-phosphocholine (DHPC), 1,2-dimyristoyl-*sn-glycero*-3-phosphocholine (DMPC), 1-palmitoyl-2-oleoyl-*sn-glycero*-3-phospho(tempo)choline (TempoPC), 1-palmitoyl-2-stearoyl-(*n*-doxyl)-*sn-glycero*-3-phosphocholine (*n*DPC, with *n* equal to 5, 7, 10, 12, or 14) and 1-palmitoyl-2-oleoyl-*sn-glycero*-3-phosphocholine (POPC) were purchased from Avanti Polar Lipids (Alabaster, AL, USA) as chloroform solutions. Methanol, 99.9%, spectrophotometric grade, [4-(2-hydroxyethyl)-1-piperazinyl]-ethanesulfonic acid (HEPES) and the lanthanide salts $TmCl_3{\cdot}6H_2O$ and $DyCl_3{\cdot}6H_2O$ were purchased from Sigma-Aldrich. A 50 mM, pH 7.0, HEPES buffer solution was prepared to be used for liposomes and bicelle preparations, and for the stock solutions of Tm^{3+} and Dy^{3+}.

2.2 HPLC and MS analyses

Analytical HPLC separations were carried out on a Dionex (Sunnyvale, CA) Summit dual-gradient HPLC apparatus, equipped with a four-channel UV-Vis detector, using a Vydac C_{18} (250 × 4.6 mm, 5 μm, flow rate at 1.5 mL min^{-1}) from W. R. Grace (Columbia, MD). To prepare the mobile phase, deionized water was further purified using a MilliQ reagent grade water system from Millipore (Bedford, MA). The eluants A (aqueous 0.1% trifluoroacetic acid, TFA) and B (90% aqueous CH_3CN containing 0.1% TFA) were employed for the preparation of binary gradients. Analyses were carried out using a linear gradient from 35 to 90% B in 30 min. Semi-preparative HPLC was carried out on a Shimadzu (Kyoto, Japan) series LC-6A chromatographic apparatus, equipped with two independent pump units, an UV-Vis detector, and a Vydac C_{18} column (250 × 22 mm, 10 μm, flow rate at 15 mL min^{-1}). Elutions were performed with the same mobile phases described above, without TFA as a modifier, using a linear gradient from 65 to 95% B in 20 min. Mass spectrometry (MS) analyses were carried out on a Mariner API-ToF workstation (PerSeptive Biosystems, Framingham, MA), operating in the positive mode.

2.3 Peptide synthesis

The synthesis of the two new labeled ampullosporin A analogs, AmpT3 and AmpT13, was performed by the solid-phase peptide synthesis methodology as previously described.[12] The crude peptides (55–58% yield) were purified by semi-preparative HPLC and characterized by analytical HPLC and ESI-MS.

[TOAC^3]Ampullosporin A (AmpT3): yield 3.5 mg (17%); analytical HPLC: t_R 25.1 min; ESI-MS (*m*/*z*): calcd for $C_{83}H_{138}N_{20}O_{20}$ $[M + H]^+$ 1735.04, found 1735.12.

[TOAC^{13}]Ampullosporin A (AmpT13): yield 0.7 mg (2%); analytical HPLC: t_R 23.6 min; ESI-MS (*m*/*z*): calcd for $C_{83}H_{138}N_{20}O_{20}$ $[M + H]^+$ 1735.04, found 1735.04.

2.4 CD spectroscopy in liposomes

The small unilamellar vesicles (SUV) used in this study were prepared from POPC. The lipids were dissolved in chloroform and a homogeneous lipid film was obtained by drying the solution under a gentle dry nitrogen stream. The film was left overnight under vacuum in a desiccator to remove any trace of the solvent. The following day the film was resuspended in buffer (see above) to obtain a lipid concentration of about 15 mM. SUV in the 30–50 nm diameter range were prepared by sonication: the lipid suspension was immersed in a water bath and sonicated until the solution started to clear. Vesicle dimensions were checked during preparation by dynamic light scattering using a NICOMP Model 370 Submicron Particle Sizer. Vesicles were used immediately after preparation.

The peptide was incorporated into the liposomes by adding the proper amount of methanol stock solution into an empty Eppendorf tube. Methanol was then evaporated under a gentle stream of nitrogen. The peptide was resuspended in a small amount of buffer and sonicated for 3 minutes. Lastly, a proper amount of POPC SUV solution was added in order to obtain a final POPC concentration of 10 mM. The concentration of the peptide stock solutions was about 1 mM, as determined by quantitative UV absorption measurements (ε_{Trp} = 6170 M^{-1} cm^{-1} at 282 nm). CD spectra were recorded at 293 K using a Jasco (Tokyo, Japan) model J-715 spectropolarimeter, equipped with a Haake thermostat (Thermo Fisher Scientific, Waltham, MA), averaging 8 scans. Baselines were corrected by subtracting the liposome contribution. Cylindrical, fused quartz cells of 0.2 or 0.1 mm path length (Hellma, Müllheim, Germany) were employed. The data are expressed in terms of $[\theta]_R$, the mean residue ellipticity (deg cm^2 $dmol^{-1}$).

2.5 EPR power saturation experiments in liposomes

Power saturation experiments were performed in POPC liposomes prepared in the same way as those used for CD experiments. The peptides were incorporated into liposomes as follows: a methanol solution of the peptide was evaporated in an Eppendorf tube. The pre-formed liposomes were added and the tube was repeatedly vortexed. The solution was then sonicated for 3 min. The EPR

experiments were performed using a Bruker ESP380 spectrometer operating at the X-band (~9.5 GHz), equipped with a room-temperature dielectric resonator, ER4123D. The microwave frequency was measured using a frequency counter, HP5342A. All spectra were obtained using the following parameters: a modulation amplitude of 0.16 mT; a modulation frequency of 100 kHz; a time constant of 41 ms; a conversion time of 82 ms; a scan width of 1.25 mT; 512 points; a temperature of 298 K. The microwave power was ramped down automatically from 95 mW to 0.05 mW (the attenuation ramp in dB units was 2.0, 4.0, 6.0, 8.0, 10.0, 12.0, 14.0, 16.0, 18.0, 20.0, 25.0, 30.0, 35.0). The spectra at each power were averaged 3 times. The experimental protocol for the insertion depth measurements is as follows: approximately 5 μL of the sample were loaded into a gas-permeable TPX capillary (L&M EPR Supplies, Inc., Milwaukee, WI, USA) and 3 saturation experiments were performed. The first experiment was done on the sample in equilibrium with air to saturate the membrane with oxygen. The second experiment was performed on the same sample after de-oxygenation under a dry nitrogen flow for 20 min. The third experiment was carried out on a new sample to which NiEDDA was added to a final concentration of 50 mM; the sample was then de-oxygenated as above. All experiments were performed at least in duplicate. The power saturation data were obtained using a home-written program in Matlab that calculates the peak-to-peak amplitudes of the central line of the spectra. The saturation curves were obtained by plotting the amplitude data *vs.* the microwave power, and fitted using the standard equation:[19] $y = A \cdot p_{1/2} \cdot [1 + (2^{1/h} - 1) \cdot x/p_{1/2}]^{-h}$, where $p_{1/2}$ is the saturation parameter, namely the power where the first derivative amplitude is reduced to half of its unsaturated value, h is the homogeneity parameter, indicating the homogeneity of saturation of the resonance line (ranging between $h = 1.5$ for a fully homogeneous line and $h = 0.5$ for a fully inhomogeneous line), and A is a scaling factor that accounts for the absolute signal intensity. The dimensionless immersion depth parameter (Φ) can be directly calculated from the ratio of the $p_{1/2}$ parameters obtained from the fitting of the three experiments described above:

$$\Phi = \ln \frac{p_{1/2}^{\text{oxygen}} - p_{1/2}^{\text{nitrogen}}}{p_{1/2}^{\text{NiEDDA}} - p_{1/2}^{\text{nitrogen}}}.$$

The values of Φ for the spin labeled lipids were recently published.[28] The Φ parameter can be used to assess the distance from the membrane surface of a solute (R) provided a calibration curve is calculated:[29,30] from our data we find $R/\text{nm} = 0.358 \cdot \Phi + 0.615$ (see the ESI† for details).

2.6 EPR experiments in bicelles

The chloroform solutions of the phospholipids and a methanol solution of ampullosporin A were mixed in a glass test tube. Except when otherwise noted, samples with AmpT3 or AmpT13 were diamagnetically diluted using Amp to a final labeling percentage of 17%: this procedure was done to avoid any concentration-dependent lineshape broadening. Samples at different peptide concentrations were prepared by keeping the lipid content constant and varying the amount of peptide to obtain the desired P : L ratio (the P : L ratios reported in this work refer to DMPC only). The final lipid composition of the solution was: 11.2 μmol DMPC, 3.1 μmol DHPC; the q = [DMPC]/[DHPC] ratio was therefore ~3.6. A thick film, containing the lipids and the peptide, was produced by the evaporation of the solvent under a stream of dry nitrogen gas, then the film was dried under vacuum overnight. The following day the film was scratched off the glass tube and placed into an Eppendorf tube, then 33 μL of buffer were added, obtaining a 25% (w/w) lipid concentration. The resulting suspension was vortexed until it appeared homogeneous. The sample was then placed in a bath sonicator that was filled with an ice/water mixture and sonicated for 30 min. Finally, the solution was subjected to 4 freeze/thaw cycles: 30 min in a 328 K water bath were followed by a quick freeze in liquid nitrogen; vortexing of the sample at each step was performed to ensure perfect homogeneity. The procedure yielded a clear, viscous, stock of bicelles with the peptide incorporated into the bilayers. The EPR samples were prepared as follows: 15 μL of bicelle stock were added to 10 μL of buffer for isotropic samples (*i.e.*, not macroscopically oriented), or, for oriented samples, to 10 μL of buffered solution of Tm^{3+} or Dy^{3+} (corresponding to a final $[Ln^{3+}]/[DHPC]$ ratio of 0.9). The resulting solution was transferred to a 1 mm inner diameter EPR quartz tube. The final concentration of the phospholipids was 17% (w/w). Given the experimental conditions (lipid concentration, q ratio, temperature), the bicelles used in this work are not ideal disks, but rather stacks of almost planar phospholipid bilayers dotted with DHPC pores and separated by buffer regions ~15 nm wide.[31] A literature procedure[23] was used to obtain aligned samples: the sample tube was placed at room temperature (~298 K) in the EPR cavity and the magnetic field was set to 800 mT; then, the temperature was slowly raised to 318 K and subsequently lowered to the temperature of choice, 308 K (35 °C). The magnetic field was set to be ~350 mT and the spectrum was recorded immediately: the loss of order in the sample during the measurement time (~40 s) is negligible as a result of the high viscosity of the bicelle solution which prevents lipid reorientation. For each sample, the experiments were repeated with Tm^{3+} or Dy^{3+} as dopants, to align the membrane normal parallel or perpendicular to the external magnetic field. EPR spectra of the peptide in bicelles were recorded using a Bruker ER200D spectrometer operating at the X-band (~9.5 GHz), equipped with a rectangular cavity, ER4102ST, fitted with a cryostat, and a variable-temperature controller, Bruker ER4111VT; the microwave frequency was measured by a frequency counter, HP5342A. All spectra were obtained using the following parameters: a microwave power of 2.1 mW; a modulation amplitude of 0.16 mT; a modulation frequency of 100 kHz; a time constant of 20 ms; a conversion time of 41 ms; a scan width of 15 mT; 1024 points; a temperature of 308 K; all spectra were obtained in a single scan.

The spectra of the singly labeled peptides AmpT3 and AmpT13 were simulated with a program based on the stochastic Liouville equation,[32] that is extensively used to simulate EPR spectra of nitroxides.[33–40] The simulation method relies on several reference

systems, the relative orientation of which is defined by different sets of Euler angles.[32] The principal values of the $\boldsymbol{g}$ and ^{14}N hyperfine ($\boldsymbol{A}$) tensors of the TOAC label were obtained from the literature.[35,41] The orientations of the principal diffusion axes relative to the $\boldsymbol{g}$ tensor reference frame (Ω_D) were estimated from the crystal structure. The principal values of the diffusion tensor ($\boldsymbol{D}$), the order parameter of the peptide (S), and the orientation of the magnetic field relative to the average long diffusion axis (Ψ) were extracted from the simulation.

The interspin distances, intramolecular for the doubly labeled peptide AmpT3,13, and intermolecular for the singly labeled peptide AmpT3, were obtained from the CW-EPR spectra in isotropic bicelles. The spectra were analyzed for dipolar broadening, obtaining the interspin distance distributions through the convolution methodology,[42] using a program previously described[43] that was kindly provided by prof. H. S. Mchaourab, Vanderbilt University, Nashville (TN). AmpT3,13 was diamagnetically diluted with Amp (17% of labeled peptides) at a 1 : 100 P : L ratio. The experiments on AmpT3 were performed at different P : L ratios and different labeling percentages (17%, 33%, 66%). The spectra of AmpT3 and AmpT13 with 17% of labeled peptides were used in the convolution analysis as reference spectra because they are not affected by dipolar broadening. In this work, we performed the convolution analysis of the spectra obtained at near-physiological temperature (308 K). While in fluid solutions the dipolar interaction is in principle partially averaged, it is still possible to analyze the dipolar broadening with reasonable precision, even at physiological temperature, in highly viscous media.[44,45] The interspin distance for the doubly labeled peptide AmpT3,13 (and those for AmpT3 and AmpT13 as references) was obtained also in POPC SUV: the SUV were the same used for CD spectroscopy and the conditions of the EPR experiments were identical to those in bicelles except for temperature (150 K) and the addition of glycerol as a cryoprotectant (37% v/v).

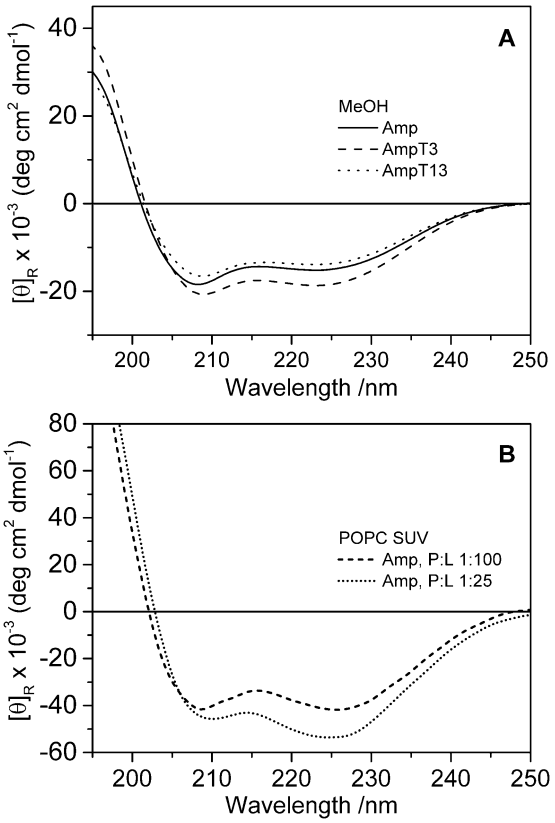

Fig. 3 Ampullosporin conformation in methanol and in POPC SUV. (A) CD spectra of ampullosporin A and its TOAC analogs in methanol. (B) CD spectra of ampullosporin A in POPC SUV at P : L 1 : 100 and 1 : 25 (POPC concentration is 10 mM).

3. Results

3.1 CD spectroscopy

We initially investigated the preferred conformations of ampullosporin A and its [TOAC] analogs in methanol solution. As illustrated in Fig. 3A, all CD spectra show two pronounced negative maxima near 225 and 208 nm (associated with the n $\rightarrow \pi^*$ transition and the parallel component of the split $\pi \rightarrow \pi^*$ transition of the peptide chromophore, respectively) followed by a positive maximum at approximately 195 nm ($\pi \rightarrow \pi^*$ perpendicular component). This pattern can be attributed to mostly right-handed helical peptides[46,47] with a largely prevailing α-helix population, as can be estimated from the ellipticity ratio $R = [\Theta]_{222}/[\Theta]_{208}$. This ratio has been reported[48–50] to be <0.35 for a prevailing 3_{10}-helix population[51–53] and >0.70 for a prevailing α-helix population. Under our experimental conditions, we found $R = 0.82$ for Amp, $R = 0.91$ for AmpT3, and $R = 0.85$ for AmpT13. These values are comparable to $R = 0.82$[12,15] published for ampullosporin A and unambiguously indicate a predominant α-helix 3D-structural type. The CD spectra of ampullosporin A in POPC SUV at two P : L ratios (Fig. 3B) show that in a phospholipid membrane both the α-helical population ($R > 1$ for both P : L ratios) and the overall helical content of the peptide (considering the ellipticity at 222 nm)[10] increase.

3.2 EPR spectroscopy

3.2.1 Insertion depth in liposomes. The insertion depth of ampullosporin A in POPC liposomes at different P : L ratios at room temperature was determined by power saturation experiments.[19] In Fig. 4 we report the power saturation curves of the two diamagnetically diluted, singly-labeled peptides (AmpT3, top and AmpT13, bottom) at P : L 1 : 100 and 1 : 25. The fitting curves were obtained according to the equation reported in the Experimental part. The penetration depth parameters Φ for the spin-labeled lipids acting as a "molecular ruler"[28] and for the peptides are reported in Table 2.

At a P : L ratio of 1 : 100, the TOAC label of AmpT3 is fully water exposed with a penetration depth lower than that of TempoPC, where the nitroxide is located in the lipid headgroup. The label in AmpT13 has a higher penetration depth, positioned at the level of the 5th–7th carbon atom of the lipids, just below the phosphate groups. At a 1 : 25 P : L ratio, the penetration depth of both analogs increases significantly, with

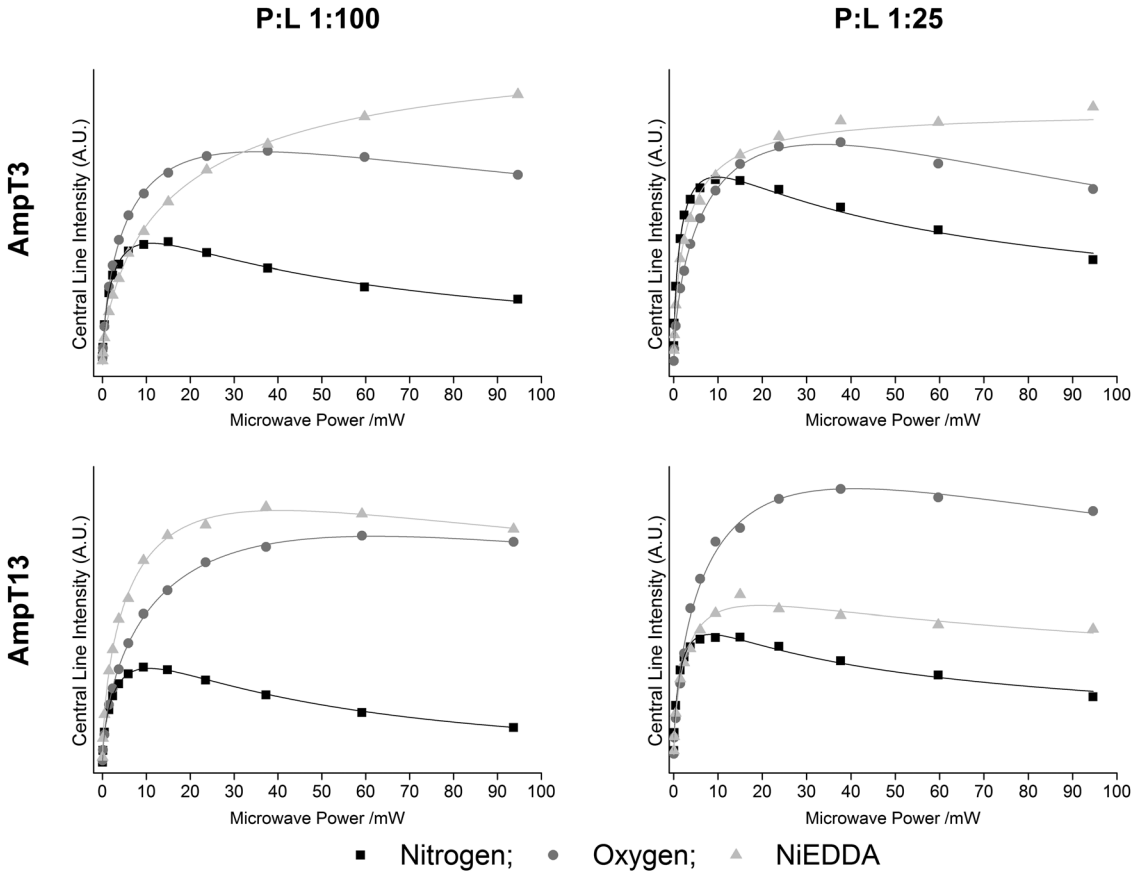

Fig. 4 Ampullosporin A penetration depth in liposomes. Power saturation data (dots) and the fitting curves (lines) for AmpT3 (top) and AmpT13 (bottom) in POPC liposomes. The symbols indicate the different sample conditions: black squares, sample purged with nitrogen; gray dots, sample in equilibrium with air (oxygen); light gray triangles, sample with 50 mM NiEDDA and purged with nitrogen. The experiments were performed at room temperature (298 K) at P : L 1 : 100 (left) and P : L 1 : 25 (right).

Table 2 Penetration depth parameter (Φ) of the reference spin labels (SL)[28] and of AmpT3 and AmpT13 in POPC liposomes obtained at room temperature. The distance from the membrane surface (R, in nm) of the two peptides is also reported. The Φ values reported have been obtained as the average of the results of two experiments (see the ESI for the results of the individual experiments)

SL	Φ	Peptide	P : L	Φ	R/nm
TempoPC	-0.1^a	AmpT3	P : L 1 : 100	−1.5	0.08
5DPC	1.4^b		P : L 1 : 25	1.2	1.02
7DPC	1.2^b				
10DPC	2.1	AmpT13	P : L 1 : 100	0.65	0.85
12DPC	2.4		P : L 1 : 25	1.7	1.22
14DPC	3.0				

[a] Repeated experiments with TempoPC showed a large variability in Φ, but the value is always below 0.3; this value has been redetermined after the publication of ref. 28. [b] An inversion in the linear trend was found also in the original work.[19]

the label of AmpT3 located at the level of the 5th–7th carbon atom of the lipids and that of AmpT13 close to the 10th carbon.

3.2.2 Peptide orientation and dynamics in bicelles. The magnetic, orientational, and motional parameters of ampullosporin A were determined in isotropic (*i.e.* without macroscopic alignment) and oriented bicelles at a P : L of 1 : 100 and at 308 K. The spectra and simulations of diamagnetically diluted AmpT3 and AmpT13 are shown in Fig. 5. The spectra in isotropic bicelles have been simulated using the MOMD approach.[32] The parameters we used for spectra simulations are reported in Table 3. The EPR spectra recorded in isotropic bicelles, with magnetic field parallel to the membrane normal n ($B_0 \| n$, Fig. 5B and E), and with magnetic field perpendicular to n ($B_0 \perp n$, Fig. 5C and F), are all different, as expected for a peptide adopting a well-defined orientation in the membrane. The bicelles in the presence of Amp at a P : L of 1 : 100 are well aligned as shown in the ESI.† However, a complete alignment of the bicelles does not imply that membrane-bound peptides, or parts of them, achieve the same degree of order, since the heterogeneity of the secondary structure or the backbone dynamics could lower their order. Indeed, while AmpT3 shows well-aligned spectra (Fig. 5B is very different from Fig. 5C), AmpT13 is much more disordered (Fig. 5E is similar to Fig. 5F). This aspect will be discussed below and in the Discussion section.

We simulated the spectra of each analog in isotropic bicelles and at $B_0 \| n$ and $B_0 \perp n$ with a single set of parameters. This approach ensures a good reliability of the simulations. The magnetic parameters of the TOAC label were taken from the

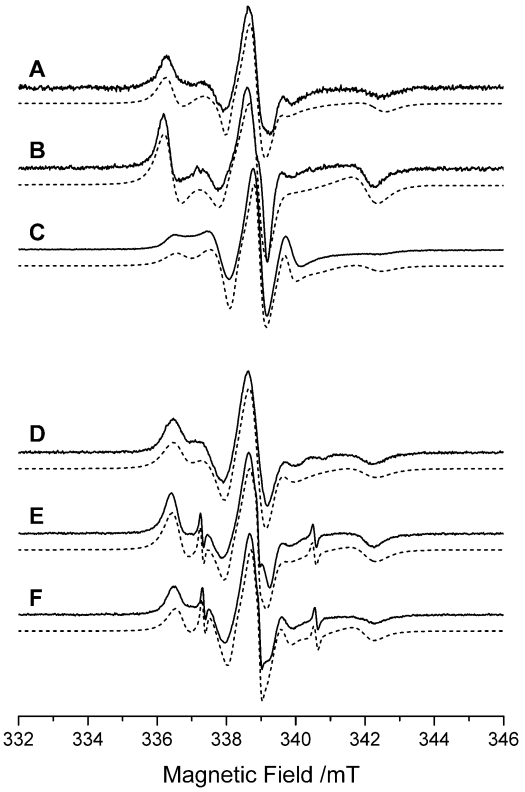

Fig. 5 Ampullosporin A motion and orientation in DMPC/DHPC bicelles. EPR spectra are those of AmpT3 (A–C) and AmpT13 (D–F). Spectra are taken in isotropic bicelles (A and D) and in oriented bicelles recorded with the magnetic field parallel (B and E) and perpendicular (C and F) to the membrane normal. Spectral simulations are shown in dashed lines. Temperature 308 K, P : L 1 : 100, peptides diamagnetically diluted at 17% labeling percentage.

Table 3 Parameters used for the fitting of the spectra of AmpT3 and AmpT13 in bicelles at all P : L ratios: $\boldsymbol{g}$ and hyperfine ($\boldsymbol{A}$) tensors, diffusion tensor ($\boldsymbol{D}$), angles between the magnetic and the diffusion frame (Ω_D), angle between the diffusion frames and the membrane normal (Ψ), order parameter (S). $\boldsymbol{A}_{zz}$, $\boldsymbol{D}$, Ψ, and S were obtained from spectral fitting

		$\boldsymbol{g}^a$	$\boldsymbol{A}^a$/mT	$\boldsymbol{D}_\parallel$/ 10^6 s^{-1}	$\boldsymbol{D}_\perp$/ 10^6 s^{-1}	$\Omega_D{}^b$			Ψ^c	S
						α	β	γ		
AmpT3	x	2.0096	0.56	79	10	0°	13°	46°	0°	0.165
	y	2.0064	0.56							
	z	2.0027	3.55							
AmpT13	x	2.0096	0.56	79	10	0°	30°	90°	0°	0.09
	y	2.0064	0.56							
	z	2.0027	3.35							

[a] $\boldsymbol{g}$ and $\boldsymbol{A}$ tensor principal values are taken from ref. 35. The values of the $\boldsymbol{A}_{zz}$ hyperfine component depend strongly on the polarity of the environment and have been varied to fit the spectra. [b] For an axial diffusion tensor the angle α is irrelevant.[32] [c] The error estimate is $\sim 10°$; we show the dependence of the fitting on Ψ in the ESI.

literature,[35] with the exception of the largest component of the hyperfine coupling tensor ($\boldsymbol{A}_{zz}$) that was adjusted to better fit the spectra. The $\boldsymbol{A}_{zz}$ component is the most sensitive to the polarity of the surroundings, with larger values observed for a polar environment. The larger $\boldsymbol{A}_{zz}$ value of AmpT3, compared to that of AmpT13, suggests that in bicelles the former is more water exposed than the latter. The oriented spectra of AmpT13 show a small contribution, amounting to less than 1% of the total spins, arising from the free spin-label (the three sharp lines in Fig. 5E and F).

The spectral simulations require the knowledge of the orientation of the TOAC moieties relative to the principal diffusion axis of the peptide. This information can be obtained from the spectral fitting or, when available, estimated from the crystal structure of the peptide. In this work, the Euler angles (Ω_D) relating the principal directions of the magnetic tensors ($\boldsymbol{g}$ and $\boldsymbol{A}$) of each TOAC label to the principal directions of the diffusion tensor ($\boldsymbol{D}$) were estimated from the crystal structure of ampullosporin A.[14] The estimate was made considering that the TOAC piperidine label usually adopts a twisted boat conformation[54] and that for helical peptides the main diffusion axis corresponds to the average helical axis. Under these assumptions, the spectral fitting provided the principal values of the diffusion tensor, showing that the peptide undergoes an anisotropic axial motion, with a much faster rotation about the helical axis than perpendicular to it ($\boldsymbol{D}_\parallel > \boldsymbol{D}_\perp$).

The main advantage of oriented bicelles lies in the possibility of determining the orientation of solutes in the membrane. From the simulations we obtained that the ampullosporin A helix adopts a transmembrane orientation in bicelles ($\Psi = 0° \pm 10°$) corresponding to an average helical axis parallel to the membrane normal. Additionally, we recorded the EPR spectra of AmpT3 at P : L 1 : 25 (data not shown): these are identical to the spectra reported in Fig. 5, confirming that in bicelles ampullosporin A maintains a transmembrane orientation, at least to P : L 1 : 100.

The order parameter (S) of AmpT13 is lower than that of AmpT3. This result suggests a greater conformation heterogeneity for the C-terminal part of the peptide in the membrane. This feature was also observed in the crystal structure.[14]

3.2.3 Conformational study in membranes. We investigated the secondary structure of ampullosporin A in bicelles at physiological temperature by measuring the interspin distance between the two TOAC labels of the doubly labeled peptide, AmpT3,13, previously synthesized in our laboratory.[12] The experiment was performed also in SUV of POPC in frozen solution (150 K). The spectra of AmpT3,13 (Fig. 6B in bicelles and Fig. 6D in SUV) were analyzed by the convolution methodology,[42] using the average of the spectra of the singly labeled analogs AmpT3 and AmpT13 ("Sum of Singles", Fig. 6A in bicelles and Fig. 6C in SUV) as the non-broadened spectra. Spectra were recorded in isotropic bicelles (*i.e.*, not macroscopically oriented), or in frozen solution of POPC SUV with glycerol added as a cryoprotectant. The experiments in SUV were performed at low temperature since at room temperature there was partial averaging of the dipolar interaction that impaired the spectral analysis. The peptides were diamagnetically diluted at 17% labeling percentage to ensure the absence of broadening arising from intermolecular spin–spin interactions. The convolution analysis gives the distance distribution curve shown in Fig. 6, bottom. The Gaussian distance distribution curve in bicelles (r_{max} = 1.94 nm and half width at half height Δ_{hh} = 0.06 nm) shows an average distance that is about 0.2 nm larger than the one we previously obtained in

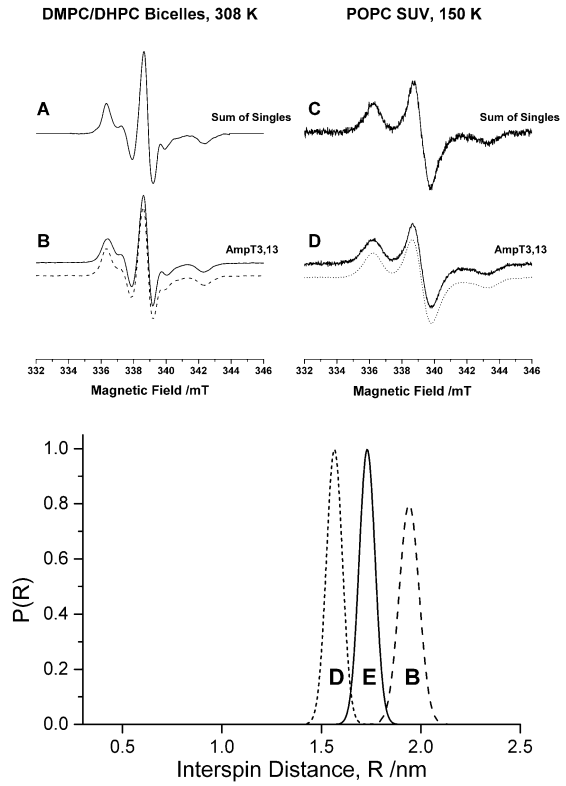

Fig. 6 Ampullosporin A conformation in isotropic DMPC/DHPC bicelles, 308 K (A and B), and in POPC SUV, 150 K (C and D). Top, EPR spectra resulting from the sum of the experimental spectra of AmpT3 and AmpT13 (A and C), and of AmpT3,13 (B and D). Simulations of AmpT3,13 are shown in dashed/dotted lines. Bottom, distance distribution curves for AmpT3,13 in bicelles (B), in SUV (D) and, for comparison, in methanol at 77 K (E), the latter obtained from analysis of the CW-EPR spectra.[12] P : L 1 : 100, peptides diamagnetically diluted at 17% labeling percentage.

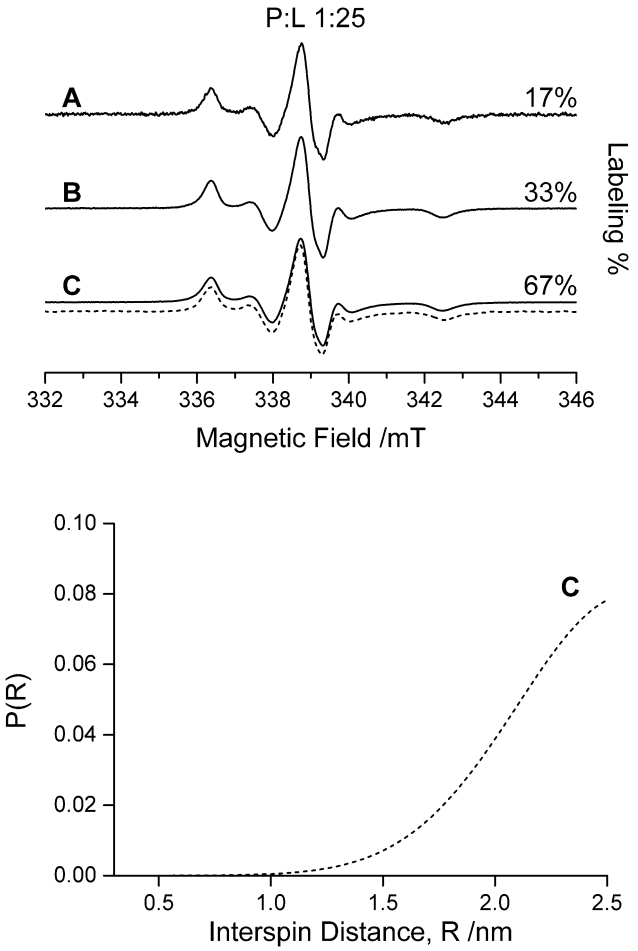

Fig. 7 Ampullosporin A aggregation in isotropic DMPC/DHPC bicelles. Top, experimental EPR spectra of AmpT3 diamagnetically diluted with Amp at increasing labeling percentages: (A) 17% labeling, (B) 33% labeling, (C) 67% labeling. The simulation obtained by the convolution procedure is reported for spectrum (C) in a dashed line. Temperature 308 K, P : L 1 : 25. Bottom, distance distribution curve for spectrum C.

methanol at 77 K (r_{max} = 1.73 nm and Δ_{hh} = 0.05 nm)[12] and considerably larger than the one obtained in SUV (r_{max} = 1.56 nm and Δ_{hh} = 0.05 nm). The interspin distance in SUV is remarkably similar to the one we estimated from the crystal structure (~1.6 nm, obtained by modeling the TOAC residues into the crystal structure and taking the inter-nitroxide distance[9]). The distance distribution widths in all environments are comparably narrow, supporting the view that almost the totality of the peptide adopts a well-defined structure in each environment.

3.2.4 Peptide aggregation in bicelles. We investigated the aggregation propensity of ampullosporin A in membranes as a function of the P : L ratio using AmpT3. We studied only AmpT3 and not AmpT13 since in the latter the spin label is inserted in a less structured region of the peptide, as seen from the lower order parameter (Table 3). Therefore, AmpT13 is less likely to be involved in a specific peptide–peptide interface. We recorded the EPR spectra in isotropic bicelles at different P : L ratios (1 : 100 and 1 : 25) and different labeling percentages (AmpT3/Amp: 17%/83%, 33%/67%, and 67%/33%), and analyzed the spectra for the presence of line broadening induced by intermolecular dipolar spin–spin interactions. We observed no line broadening at P : L 1 : 100 at all labeling percentages (data not shown). Fig. 7, top, shows the spectra obtained at P : L 1 : 25: no line broadening was observed at 17% and 33% labeling ratios (Fig. 7A and B), while a very minor broadening is present in the spectrum at 67% labeling (Fig. 7C). This spectrum was examined by the convolution methodology[42] using the spectrum of AmpT3 at P : L 1 : 100 and 17% labeling as the non-broadened spectrum (Fig. 6A). The simulation is shown in Fig. 7C (dashed line) and the Gaussian interspin distance distribution curve in Fig. 7, bottom (r_{max} = 2.6 nm and Δ_{hh} = 0.6 nm). The average distance is compatible with the one expected for a homogeneous distribution of transmembrane peptide monomers (~3 nm). This estimate was made considering the average diameter for a peptide helix (1.1 nm)[55] and the area per DMPC lipid (~60 Å^2).[56] We conclude that in bicelles ampullosporin A does not aggregate into stable, well-defined structures up to P : L 1 : 25.

4. Discussion

In this work, we studied ampullosporin A in two different model membrane systems to explore different aspects of the

peptide–membrane interaction. Small unilamellar vesicles of POPC allowed us to determine the overall secondary structure of the peptaibiotic using EPR and CD spectroscopies and the insertion depth of spin-labeled analogs as a function of the P : L ratio using EPR. We took advantage of the DMPC/DHPC bicelles to obtain detailed information on the secondary structure, dynamics, orientation and aggregation, using EPR. All experiments were performed either at physiological temperature or at room temperature, with membranes in solution in their liquid crystalline (fluid) phase, with the exception of the interspin distance determination in SUV, which was performed at 150 K.

The CD spectra show that ampullosporin A adopts a helical structure in methanol with a predominance of the α-helix over the 3_{10}-helix. The α-helical content further increases in SUV (Fig. 3). Comparable results are obtained in frozen solution using EPR for AmpT3,13: the average interspin distance decreases from 1.73 nm methanol[12] to 1.56 nm in SUV (Fig. 6). In bicelles, the interspin distance obtained at physiological temperature is longer (1.94 nm) and closer to the one expected for an ideal 3_{10}-helix (1.9 nm).[51–53] These results suggest that the peptide adopts a slightly different conformation in the two membrane systems, predominantly α-helical in SUV of POPC and more elongated, likely with a higher 3_{10}-helical character, in DMPC bicelles. Previously, also solid-state NMR data suggested that the secondary structure of ampullosporin A in thin PC membranes (di-C12:0-PC and di-C10:0-PC) encompasses a high degree of 3_{10}-helical structures.[17] A change in conformation depending on the environment is not surprising since it is known that the peptide secondary structure has an intrinsic flexibility, and the energy difference between the two helical conformations is small for Aib-containing peptides.[14,53]

The orientation adopted by the peptide helix relative to the membrane surface as a function of the P : L ratio is different in the two membrane systems. The orientation in SUV was determined from the penetration depth of the two singly labeled analogs. To clarify the topology of the peptide in the membrane, we calculated the distance from the membrane surface (R) of the peptides (see the ESI† for details): the R values, reported in Table 1, were then compared with the experimental bilayer thickness of POPC (3.91 nm at 30 °C).[56] The results are schematically summarized in Fig. 8.

At P : L 1 : 100, both TOAC labels have a very low penetration depth. The data are consistent with a parallel orientation of the ampullosporin A helix (Fig. 8A) in which TOAC at position 3 is fully exposed to the water phase while TOAC at position 13 lies just below the polar headgroup region. This orientation is energetically favorable since it exposes the hydrophilic sector (Fig. 1) towards the water phase, while keeping the hydrophobic Trp residue buried in the membrane. A parallel orientation is in agreement with the one previously suggested for ampullosporin A on the basis of fluorescence quenching experiments (large unilamellar vesicles of egg PC, pH 7.4, P : L ≤ 140) and the calculation of the peptide "amphipathic moment".[16] Moreover, solid-state NMR spectra of POPC deposited on cover glasses (pH 7.5) showed that ampullosporin A lies parallel to the membrane surface at P : L 1 : 100, while the orientation of the peptide is not well defined at P : L 1 : 10.[17]

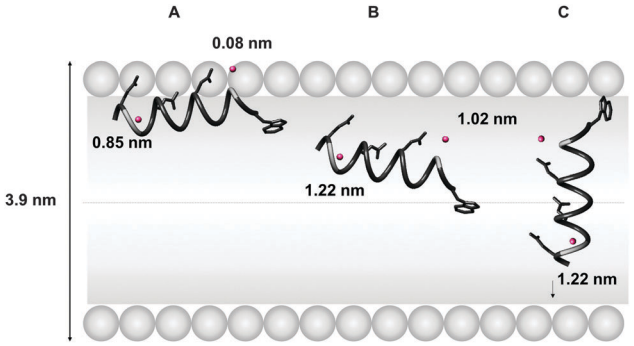

Fig. 8 In-scale cartoon of the penetration depths of ampullosporin A analogs in a POPC bilayer. The peptides are illustrated as ideal α-helices in the ribbon representation. The nitrogen atoms of the TOAC labels are shown as dots (purple in the online version). The Gln and Trp side chains are shown explicitly in stick representation. The numbers represent the distance from the membrane surface (R) of the TOAC nitrogen atoms. Model (A) describes the peptide topology at P : L ratio 1 : 100. Models (B) and (C) describe two possible interpretations of the topology at P : L ratio 1 : 25. In model (C), the penetration depth of AmpT13 is measured from the bottom membrane leaflet.

At P : L 1 : 25, our saturation experiments gave a much higher penetration depth for both labeling positions. This finding can be explained either by a parallel insertion of the peptide deep in the membrane core (Fig. 8B) or by a transmembrane insertion (Fig. 8C). In the second hypothesis, the penetration depths correspond to the TOAC[3] residue being located below the polar headgroup region in one membrane leaflet and the TOAC[13] residue being located around the middle of the other leaflet. We favor the latter hypothesis in which ampullosporin A changes its orientation from parallel to transmembrane in a concentration-dependent way: indeed, this is a common behavior for hydrophobic peptides, and has been associated with their antimicrobial mechanism of action.[57] In this transmembrane orientation the peptide would bury the C-terminal part, while Trp[1] remains preferentially located just below the polar headgroup region. The anchoring effect of Trp residues when located at the polar–apolar interface has been previously recognized.[58] The preferential insertion of the C-terminus found in this work is not a common feature for peptaibiotics. Zervamicin, which has an N-terminal Trp residue like ampullosporin A, has been suggested to bury either ends, the N-terminus according to fluorescence/modelling data[16] and molecular dynamics,[59] or the C-terminus according to an EPR study.[60] Antiamoebin, which has a Phe residue at the N-terminus and a phenylalaninol at the C-terminus, has been found to preferentially insert into the bilayer the fully hydrophobic N-terminal part of the peptide.[16,61,62] Alamethicin, one of the most studied peptaibiotics, is believed to first insert the N-terminus, keeping the charged Glu residue at the C-terminus towards the water phase.[63]

In bicelles, ampullosporin A adopts a transmembrane orientation at P : L ratios 1 : 100 and higher. However, the order parameters (S) of the TOAC residues, obtained from the spectral simulations, are low. This finding indicates that the peptide is not strongly anchored to the membrane surfaces as found for alamethicin.[22] The order parameter for the C-terminus is

remarkably low, but, since we achieved a good spectral simulation using a single diffusion tensor for both TOAC labels, we suggest that the lower order parameter of TOAC[13] arises from some conformational heterogeneity of the C-terminus and not from the much faster dynamics that would be observed in the presence of significant helical fraying. Moreover, the narrow intramolecular interspin distance distribution displayed by AmpT3,13 also confirms that the C-terminus remains folded (otherwise we would have observed a much broader distribution).

The differences in the peptide structure and orientation between SUV and bicelles could be tied to the different hydrophobic thicknesses of the two membranes. The hydrophobic thickness is 2.88 nm for POPC and 2.57 nm for DMPC, at 30 °C,[56] because of the different lengths and unsaturation degrees of the lipid tails (16 : 0–18 : 1 for POPC; 14 : 0–14 : 0 for DMPC). Indeed, a change from a parallel to a transmembrane orientation as a function of the bilayer thickness was observed previously for ampullosporin A in PC bilayers deposited on cover glasses.[17] The condition of perfect match between the length of the hydrophobic region of a transmembrane peptide and the membrane hydrophobic thickness is energetically favorable. Any mismatch in the two lengths (termed "hydrophobic mismatch") can be minimized by local membrane deformations (thinning or expansion), changes in peptide conformation and/or helical tilting.[64–68] We suggest that the stable transmembrane insertion in bicelles is a result of the hydrophobic mismatch minimization that is reached by the elongation of the helix from its mainly α-helical structure in SUV to a prevalently 3_{10} structure in bicelles. In the crystal structure, as the distance between the α-carbons of the first and the last amino acid is 2.2 nm, the peptide is 0.35 nm shorter than the hydrophobic thickness of DMPC. The negative hydrophobic mismatch that would be present if the peptide adopts in DMPC the same structure found in the crystal is then strongly reduced considering the elongation by 0.34 nm found in the AmpT3,13 analog in bicelles. In contrast, in POPC SUV the peptide is too short to minimize the hydrophobic mismatch. Then, in the POPC membrane ampullosporin A adopts its preferred α-helical conformation and the parallel orientation is stabilized by the exposure of the hydrophilic sector to the aqueous solution. Above a critical concentration, the peptaibiotic can switch to a transmembrane orientation, even if it does not fully span the bilayer.

A transmembrane orientation is usually tied to the mechanism of action of hydrophobic peptides. It has been speculated that the membrane depolarization induced by alamethicin and ampullosporin A would depend on the same mechanism of action, namely the formation of barrel-stave pores.[2,4,13] However, while this mechanism has been proven for alamethicin, which is able to fully span the bacterial membranes, it is still unclear whether it could be extended to shorter peptaibiotics like ampullosporin A or trichogin GA IV.[1] As for the former peptaibiotic, we did not observe any aggregation in bicelles up to P : L 1 : 25; in contrast, alamethicin showed unequivocal signs of aggregation at a P : L 1 : 50.[22] We can speculate that ampullosporin A, in contrast to alamethicin, cannot strongly anchor to the membrane surfaces (see the low order parameters discussed earlier in the text) and is more prone to laterally diffuse in the membrane, thus reducing the extent of the formation of stable aggregates. Therefore, the membrane depolarization induced by ampullosporin A might originate either from transient aggregates and/or from stable pores formed only by a small fraction of peptides. In fact, peptide aggregation might not even be needed to explain the observed membrane depolarization, as molecular dynamics studies have shown that even one or two peptides are enough to produce membrane permeability through local disruption of the membrane structure.[69,70]

5. Conclusions

We used CD and EPR spectroscopies to study the conformation, orientation, dynamics and the aggregation propensity of ampullosporin A and its spin-labeled analogs in zwitterionic SUV and bicelles.

We found that the peptide orientation and the helical structure change in the two membrane systems. We rationalized this behavior in terms of the minimization of the hydrophobic mismatch in the two systems having different thicknesses. In methanol and in POPC SUV, where the peptide is too short to fully span the bilayer, it adopts its preferred, mostly α-helical, structure. In the thinner DMPC/DHPC bicelles, to minimize the hydrophobic mismatch, the peptide structure elongates, suggesting a prevailing 3_{10}-helical content. The structural differences are mirrored in the orientation adopted by ampullosporin A in the two systems. In vesicles, we suggest that the peptide would change its orientation as a function of the P : L ratio: at low peptide concentration it locates parallel to the membrane surface, exposing its hydrophilic sector to the aqueous solution, while at higher concentrations it adopts a transmembrane orientation. In bicelles, ampullosporin A keeps a transmembrane orientation at a P : L ratio 1 : 100 and higher, stabilized by the good match between the peptide length and the bilayer thickness. In addition, we detected no aggregation in bicelles because the peptide was found to be monomeric at a P : L ratio 1 : 25 and lower.

Overall, the comparison of the data obtained in the two membrane-mimetic systems showed that ampullosporin A has a rather flexible structure that readily adapts to the bilayer thickness.

Acknowledgements

We thank Dr Barbara Biondi for ESI-MS spectra. This work was supported by Fondazione CARIPARO (Progetti Eccellenza 2011/2012) and MIUR (PRIN 2010–2011, prot. 2010NRREPL).

References

1 *Peptaibiotics*, ed. C. Toniolo and H. Brückner, Wiley-VCH Verlag GmbH & Co, 2009.
2 B. Leitgeb, A. Szekeres, L. Manczinger, C. Vagvolgyi and L. Kredics, *Chem. Biodiversity*, 2007, **4**, 1027–1051.

3 M. Ritzau, S. Heinze, K. Dornberger, A. Berg, W. Fleck, B. Schlegel, A. Hartl and U. Grafe, *J. Antibiot.*, 1997, **50**, 722–728.
4 P. A. Grigoriev, A. Berg, R. Schlegel and U. Grafe, *Bioelectrochem. Bioenerg.*, 1997, **44**, 155–158.
5 J. Engelberth, T. Koch, F. Kuhnemann and W. Boland, *Angew. Chem., Int. Ed.*, 2000, **39**, 1860–1862.
6 H. J. Krugel, A. Becker, A. Polten, G. Grecksch, R. Singh, A. Berg, C. Seidenbecher and H. P. Saluz, *J. Neurochem.*, 2004, **90**, 137.
7 H. Krugel, A. Becker, A. Polten, G. Grecksch, R. Singh, A. Berg, C. Seidenbecher and H. P. Saluz, *J. Neurochem.*, 2006, **97**, 74–81.
8 I. Berek, A. Becker, H. Schroder, A. Hartl, V. Hollt and G. Grecksch, *Behav. Brain Res.*, 2009, **203**, 232–239.
9 S. Rippa, H. Adenier, M. Derbaly and L. Beven, *Chem. Biodiversity*, 2007, **4**, 1360–1373.
10 S. Rippa, M. Eid, F. Formaggio, C. Toniolo and L. Beven, *ChemBioChem*, 2010, **11**, 2042–2049.
11 H. H. Nguyen, D. Imhof, M. Kronen, B. Schlegel, A. Hartl, U. Grafe, L. Gera and S. Reissmann, *J. Med. Chem.*, 2002, **45**, 2781–2787.
12 A. D. Milov, Y. D. Tsvetkov, M. Bortolus, A. L. Maniero, M. Gobbo, C. Toniolo and F. Formaggio, *Biopolymers*, 2014, **102**, 40–48.
13 P. A. Grigoriev, M. Kronen, B. Schlegel, A. Hartl and U. Grafe, *Bioelectrochemistry*, 2002, **57**, 119–121.
14 M. Kronen, H. Gorls, H. H. Nguyen, S. Reissmann, M. Bohl, J. Suhnel and U. Grafe, *J. Pept. Sci.*, 2003, **9**, 729–744.
15 H. H. Nguyen, D. Imhof, M. Kronen, U. Grafe and S. Reissmann, *J. Pept. Sci.*, 2003, **9**, 714–728.
16 T. N. Kropacheva, E. S. Salnikov, H. H. Nguyen, S. Reissmann, Z. A. Yakimenko, A. A. Tagaev, T. V. Ovchinnikova and J. Raap, *Biochim. Biophys. Acta, Biomembr.*, 2005, **1715**, 6–18.
17 E. S. Salnikov, H. Friedrich, X. Li, P. Bertani, S. Reissmann, C. Hertweck, J. D. J. O'Neil, J. Raap and B. Bechinger, *Biophys. J.*, 2009, **96**, 86–100.
18 *Spin Labeling The Next Millennium*, ed. L. J. Berliner, Plenum Press, New York, 1998.
19 C. Altenbach, D. A. Greenhalgh, H. G. Khorana and W. L. Hubbell, *Proc. Natl. Acad. Sci. U. S. A.*, 1994, **91**, 1667–1671.
20 D. J. Mayo, J. J. Inbaraj, N. Subbaraman, S. M. Grosser, C. A. Chan and G. A. Lorigan, *J. Am. Chem. Soc.*, 2008, **130**, 9656–9657.
21 M. Bortolus, G. Parisio, A. L. Maniero and A. Ferrarini, *Langmuir*, 2011, **27**, 12560–12568.
22 M. Bortolus, M. De Zotti, F. Formaggio and A. L. Maniero, *Biochim. Biophys. Acta, Biomembr.*, 2013, **1828**, 2620–2627.
23 T. B. Cardon, E. K. Tiburu and G. A. Lorigan, *J. Magn. Reson.*, 2003, **161**, 77–90.
24 U. H. N. Durr, R. Soong and A. Ramamoorthy, *Prog. Nucl. Magn. Reson. Spectrosc.*, 2013, **69**, 1–22.
25 R. Marchetto, S. Schreier and C. R. Nakaie, *J. Am. Chem. Soc.*, 1993, **115**, 11042–11043.
26 C. Toniolo, M. Crisma and F. Formaggio, *Biopolymers*, 1998, **47**, 153–158.
27 S. Schreier, J. Bozelli, Jr., N. Marín, R. F. Vieira and C. Nakaie, *Biophys. Rev.*, 2012, **4**, 45–66.
28 G. Mobbili, E. Crucianelli, A. Barbon, M. Marcaccio, M. Pisani, A. Dalzini, E. Ussano, M. Bortolus, P. Stipa and P. Astolfi, *RSC Adv.*, 2015, **5**, 98955–98966, DOI: 10.1039/C5RA18963B.
29 C. S. Klug, W. Y. Su and J. B. Feix, *Biochemistry*, 1997, **36**, 13027–13033.
30 L. A. Dalton, J. O. McIntyre and S. Fleischer, *Biochemistry*, 1987, **26**, 2117–2130.
31 M. P. Nieh, C. J. Glinka, S. Krueger, R. S. Prosser and J. Katsaras, *Langmuir*, 2001, **17**, 2629–2638.
32 D. E. Budil, S. Lee, S. Saxena and J. H. Freed, *J. Magn. Reson., Ser. A*, 1996, **120**, 155–189.
33 Z. C. Liang, Y. Lou, J. H. Freed, L. Columbus and W. L. Hubbell, *J. Phys. Chem. B*, 2004, **108**, 17649–17659.
34 B. M. Kroncke, P. S. Horanyi and L. Columbus, *Biochemistry*, 2010, **49**, 10045–10060.
35 J. J. Inbaraj, T. B. Cardon, M. Laryukhin, S. M. Grosser and G. A. Lorigan, *J. Am. Chem. Soc.*, 2006, **128**, 9549–9554.
36 D. J. Xu, R. H. Crepeau, C. K. Ober and J. H. Freed, *J. Phys. Chem.*, 1996, **100**, 15873–15885.
37 L. Hoffman, R. A. Stein, R. J. Colbran and H. S. Mchaourab, *EMBO J.*, 2011, **30**, 1251–1262.
38 J. P. Barnes, Z. C. Liang, H. S. Mchaourab, J. H. Freed and W. L. Hubbell, *Biophys. J.*, 1999, **76**, 3298–3306.
39 M. Bortolus, P. Centomo, M. Zecca, A. Sassi, K. Jerabek, A. L. Maniero and B. Corain, *Chem. – Eur. J.*, 2012, **18**, 4706–4713.
40 M. Bortolus, A. Dalzini, C. Toniolo, K. S. Hahm and A. L. Maniero, *J. Pept. Sci.*, 2014, **20**, 517–525.
41 D. Kurad, G. Jeschke and D. Marsh, *Appl. Magn. Reson.*, 2001, **21**, 469–481.
42 M. D. Rabenstein and Y. K. Shin, *Proc. Natl. Acad. Sci. U. S. A.*, 1995, **92**, 8239–8243.
43 M. Bortolus, F. Tombolato, I. Tessari, M. Bisaglia, S. Mammi, L. Bubacco, A. Ferrarini and A. L. Maniero, *J. Am. Chem. Soc.*, 2008, **130**, 6690–6691.
44 C. Altenbach, K. J. Oh, R. J. Trabanino, K. Hideg and W. L. Hubbell, *Biochemistry*, 2001, **40**, 15471–15482.
45 N. Alexander, M. Bortolus, A. Al-Mestarihi, H. Mchaourab and J. Meiler, *Structure*, 2008, **16**, 181–195.
46 S. Beychok, in *Poly-α-Amino-Acids: Protein Models for Conformational Studies*, ed. G. D. Fasman, Dekker, New York, 1967, pp. 293–337.
47 M. Goodman and C. Toniolo, *Biopolymers*, 1968, **6**, 1673–1689.
48 M. C. Manning and R. W. Woody, *Biopolymers*, 1991, **31**, 569–586.
49 C. Toniolo, A. Polese, F. Formaggio, M. Crisma and J. Kamphuis, *J. Am. Chem. Soc.*, 1996, **118**, 2744–2745.
50 F. Formaggio, M. Crisma, P. Rossi, P. Scrimin, B. Kaptein, Q. B. Broxterman, J. Kamphuis and C. Toniolo, *Chem. – Eur. J.*, 2000, **6**, 4498–4504.
51 C. Toniolo and E. Benedetti, *Trends Biochem. Sci.*, 1991, **16**, 350–353.

52 E. Benedetti, B. Di Blasio, V. Pavone, C. Pedone, C. Toniolo and M. Crisma, *Biopolymers*, 1992, **32**, 453–456.
53 K. A. Bolin and G. L. Millhauser, *Acc. Chem. Res.*, 1999, **32**, 1027–1033.
54 J. L. FlippenAnderson, C. George, G. Valle, E. Valente, A. Bianco, F. Formaggio, M. Crisma and C. Toniolo, *Int. J. Pept. Protein Res.*, 1996, **47**, 231–238.
55 K. He, S. J. Ludtke, H. W. Huang and D. L. Worcester, *Biochemistry*, 1995, **34**, 15614–15618.
56 N. Kucerka, M. P. Nieh and J. Katsaras, *Biochim. Biophys. Acta, Biomembr.*, 2011, **1808**, 2761–2771.
57 H. W. Huang, *Biochim. Biophys. Acta, Biomembr.*, 2006, **1758**, 1292–1302.
58 M. R. R. de Planque, B. B. Bonev, J. A. A. Demmers, D. V. Greathouse, R. E. Koeppe, F. Separovic, A. Watts and J. A. Killian, *Biochemistry*, 2003, **42**, 5341–5348.
59 O. V. Levtsova, M. Y. Antonov, T. V. Naumenkova and O. S. Sokolova, *Comput. Biol. Chem.*, 2011, **35**, 34–39.
60 A. D. Milov, R. I. Samoilova, A. A. Shubin, E. Y. Gorbunova, L. G. Mustaeva, T. V. Ovchinnikova, J. Raap and Y. D. Tsvetkov, *Appl. Magn. Reson.*, 2010, **38**, 75–84.
61 Z. O. Shenkarev, A. S. Paramonov, E. N. Lyukmanova, A. K. Gizatullina, A. V. Zhuravleva, A. A. Tagaev, Z. A. Yakimenko, I. N. Telezhinskaya, M. P. Kirpichnikov, T. V. Ovchinnikova and A. S. Arseniev, *Chem. Biodiversity*, 2013, **10**, 838–863.
62 E. N. Lyukmanova, Z. O. Shenkarev, A. S. Paramonov, A. G. Sobol, T. V. Ovchinnikova, V. V. Chupin, M. P. Kirpichnikov, M. J. J. Blommers and A. S. Arseniev, *J. Am. Chem. Soc.*, 2008, **130**, 2140–2141.
63 B. Bechinger, *J. Membr. Biol.*, 1997, **156**, 197–211.
64 B. Bechinger, D. A. Skladnev, A. Ogrel, X. Li, E. V. Rogozhkina, T. V. Ovchinnikova, J. D. J. O'Neil and J. Raap, *Biochemistry*, 2001, **40**, 9428–9437.
65 E. S. Salnikov, A. J. Mason and B. Bechinger, *Biochimie*, 2009, **91**, 734–743.
66 T. Kim and W. Im, *Biophys. J.*, 2010, **99**, 175–183.
67 Y. Gofman, T. Haliloglu and N. Ben-Tal, *J. Chem. Theory Comput.*, 2012, **8**, 2896–2904.
68 U. Harzer and B. Bechinger, *Biochemistry*, 2000, **39**, 13106–13114.
69 G. Bocchinfuso, A. Palleschi, B. Orioni, G. Grande, F. Formaggio, C. Toniolo, Y. Park, K. S. Hahm and L. Stella, *J. Pept. Sci.*, 2009, **15**, 550–558.
70 D. Sengupta, H. Leontiadou, A. E. Mark and S. J. Marrink, *Biochim. Biophys. Acta, Biomembr.*, 2008, **1778**, 2308–2317.

